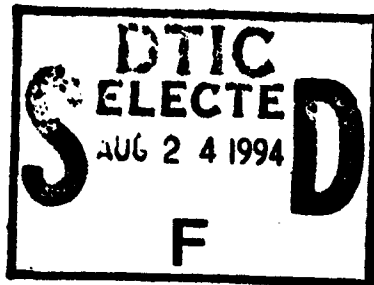


AD-A283 656



NAVAL POSTGRADUATE SCHOOL
Monterey, California

1



THESIS

INTERACTION , BURSTING AND CONTROL OF VORTICES OF
A CROPPED DOUBLE-DELTA WING AT HIGH
ANGLE OF ATTACK

by

Abdullah M. ALKHOZAM

March, 1994

Thesis Advisor:
CO-Advisor:

S.K.Hebbar
M.F.Platzer

Approved for public release; distribution is unlimited.

94-26911



2248

94 8 23 078

REPORT DOCUMENTATION PAGE

Form Approved OMB No. 0704

Public reporting burden for this collection of information is estimated to average 1 hour per response, including the time for reviewing instruction, searching existing data sources, gathering and maintaining the data needed, and completing and reviewing the collection of information. Send comments regarding this burden estimate or any other aspect of this collection of information, including suggestions for reducing this burden, to Washington headquarters Services, Directorate for Information Operations and Reports, 1215 Jefferson Davis Highway, Suite 1204, Arlington, VA 22202-4302, and to the Office of Management and Budget, Paperwork Reduction Project (0704-0188) Washington DC 20503.

1. AGENCY USE ONLY (Leave blank)	2. REPORT DATE March 1994	3. REPORT TYPE AND DATES COVERED Master's Thesis	
4. TITLE AND SUBTITLE INTERACTION , BURSTING AND CONTROL OF VORTICES OF A CROPPED DOUBLE-DELTA WING AT HIGH ANGLE OF ATTACK		5. FUNDING NUMBERS	
6. AUTHOR(S) Abdullah M. Alkhozam		8. PERFORMING ORGANIZATION REPORT NUMBER	
7. PERFORMING ORGANIZATION NAME(S) AND ADDRESS(ES) Naval Postgraduate School Monterey CA 93943-5000		10. SPONSORING/MONITORING AGENCY REPORT NUMBER	
9. SPONSORING/MONITORING AGENCY NAME(S) AND ADDRESS(ES)		10. SPONSORING/MONITORING AGENCY REPORT NUMBER	
11. SUPPLEMENTARY NOTES The views expressed in this thesis are those of the author and do not reflect the official policy or position of the Department of Defense or the U.S. Government.			
12a. DISTRIBUTION/AVAILABILITY STATEMENT Approved for public release; distribution is unlimited.		12b. DISTRIBUTION CODE A*	
13. ABSTRACT (maximum 200 words) A flow visualization study of the vortical flow over a cropped double-delta wing model with sharp leading edges and its three derivatives with small geometric modifications (fillets) at the strake wing junction was conducted in the Naval Postgraduate School water tunnel using the dye-injection technique. The fillets increased the wing area of the baseline model by 1%. The main focus of this study was to evaluate the effect of fillets on vortex core trajectories , interactions and breakdown on the leeward surface at high angle of attack (AOA) with zero sideslip angle. Comparison of test results for different fillet shapes indicates delay in both vortex interaction and breakdown at high AOA , particularly for the diamond fillet shapes. The vortex breakdown data implies lift augmentation for both static and dynamic case, with the static data correlating well with recently published numerical data.			
14. SUBJECT TERMS High angle-of-attack aerodynamics, effect of fillets on vortex core trajectories, interaction and breakdown , flow visualization by dye-injection technique, static and dynamic water tunnel studies on double-delta wings .		15. NUMBER OF PAGES 224	
		16. PRICE CODE	
17. SECURITY CLASSIFICATION OF REPORT Unclassified	18. SECURITY CLASSIFICATION OF THIS PAGE Unclassified	19. SECURITY CLASSIFICATION OF ABSTRACT Unclassified	20. LIMITATION OF ABSTRACT UL

NSN 7540-01-280-5500

Standard Form 298 (Rev. 2-89)

Prescribed by ANSI Std. Z39-18

Approved for public release; distribution is unlimited.

Interaction , Bursting and Dynamic Control of Vortices of a Cropped
Double-Delta Wing at High Angle of Attack

by

Abdullah M. Alkhozam
1st Lieutenant, Kuwait Air Force
B.S., Embry-Riddle Aeronautical University, Daytona Beach, Florida, 1987

Submitted in partial fulfillment
of the requirements for the degree of

MASTER OF SCIENCE IN AERONAUTICAL ENGINEERING

from the


NAVAL POSTGRADUATE SCHOOL

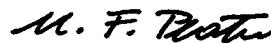
March 1994

Author:

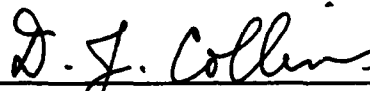

Abdullah M. Alkhozam

Approved by:


S.K. Hebbar, Thesis Advisor


M.F. Platzer, Co-Advisor

M.F. Platzer, Co-Advisor


D.J. Collins, Chairman

D. Collins, Chairman

Department of Aeronautics and Astronautics

ABSTRACT

A flow visualization study of the vortex flow over a cropped double-delta wing model with sharp leading edges and its three derivatives with small geometric modifications (fillets) at the strake wing junction was conducted in the Naval Postgraduate School water tunnel using the dye-injection technique. The fillets increased the wing area of the baseline model by 1%. The main focus of this study was to evaluate the effect of fillets on vortex core trajectories, interactions and breakdown on the leeward surface at high angles of attack (AOA) with a sideslip angle. Comparison of test results for different fillet shapes indicates delay in both vortex interaction and breakdown at high AOA, particularly for the diamond fillet shape. The vortex breakdown data implies lift augmentation for both static and dynamic case, with the static data correlating well with recently published numerical data.

Accession For		
NTIS	CRA&I	<input checked="" type="checkbox"/>
DTIC	TAB	<input type="checkbox"/>
Unannounced		<input type="checkbox"/>
Justification		
By		
Distribution /		
Availability Codes		
Dist	Avail and/or Special	
A-1		

TABLE OF CONTENTS

I. INTRODUCTION	1
A. HISTORY	1
B. AERODYNAMICS OF DELTA & DOUBLE-DELTA WINGS	4
C. FILLET AERODYNAMICS	9
II. EXPERIMENTAL APPARATUS	12
A. THE NPS WATER TUNNEL	12
B. DOUBLE-DELTA WING MODELS	14
C. DYE TUBE INSTALLATION	16
D. MODEL MOUNTING	19
III. EXPERIMENTAL PROCEDURE	21
A. EXPERIMENTAL PROGRAM	21
B. REDUCED PITCH RATE	22
C. DATA ACQUISITION AND REDUCTION	23
D. METHOD OF PHOTOGRAPHY AND VIDEO RECORDING	24

IV. RESULTS AND DISCUSSION	27
A. EFFECT OF AOA ON VORTEX CORE TRAJECTORIES AND VORTEX INTERACTION	28
1. Vortex Core Trajectories	28
2. Vortex Interaction	29
3. Effect of Fillet Shapes on the Interaction of the Strake and Fillet Vortex Core Trajectories	31
B. STATIC AND DYNAMIC EFFECTS OF AOA ON STRAKE VORTEX CORE BREAKDOWN	33
1. Static Condition	33
2. Dynamic Condition	34
3. Effect of Fillet Shapes on Strake Vortex Breakdown	35
V. CONCLUSIONS	37
LIST OF REFERENCES	40
APPENDIX A. EXPERIMENTAL RESULTS (TABLES)	42
APPENDIX B. EXPERIMENTAL RESULTS (PHOTOGRAPHS)	85
APPENDIX C. EXPERIMENTAL RESULTS (GRAPHS)	131
INITIAL DISTRIBUTION LIST	217

ACKNOWLEDGMENT

This thesis was a part of a research program on double-delta wings supported by the Naval Air Warfare Center/Aircraft Division, Warminster, Pennsylvania . My gratitude goes to my thesis advisor , Professor S.K. Hebbar, and co-advisor Professor M.F. Platzler , for their guidance, teaching, encouragment and patience throughout the course of this project. I would like to thank the many people at the Naval Postgraduate School who provided the services and expertise necessary to accomplish this research. In particular :

Mr. Pat Hickey , Aeronautics lab.

Mr. Ron Ramaker , Aeronautics model shop

Mr. Jack King , Aeronautics Lab

Mr. Tony Cricelli , Computer System Manager

Mr. Andy Sarakon and Mr. Mitch Nichols , Photo Lab.

Mr. Frank Cardoza and Mr. Harry Thomas , Video Lab

I. INTRODUCTION

A. HISTORY

In 1935 Busemann proposed the use of sweepback to reduce drag at supersonic speeds. By 1939 Betz had shown that sweepback could be used to delay the onset of compressibility problems arising from local regions of supersonic flow terminating in shock waves, though practical applications were not long in following. In the early 1940s, notably the German Me 163 Komet tailless rocket fighter appeared with sweep along with the more conventional twin-turbojet Me 262 that had a sweepback of 18.5 deg. While it was the first high speed aircraft not to have the forward weight concentration of piston engine, it turned out to be tail-heavy and in order to restore the balance between the lift and mass centers the wing outboard of the engine nacelles was swept back [Ref.1]. After WWII the allied occupation forces' research team found vast quantities of evidence of sweepback wing designs which showed just how advanced German thinking was. Immediately in USSR Mikoyan

and Gurevich designed the first swept-back fast fighter (Fig.1) in 1946 and received a Stalin prize (First Class) for "New Work in Aircraft Construction" in 1952 [Ref.2]. In 1951 Sweden was the first European nation to introduce the Saab-29 swept-wing and its derivative for research, the Saab-210 Draken (Fig.2). The same year the XF-92A was introduced in the USA with a delta wing (Fig. 3).

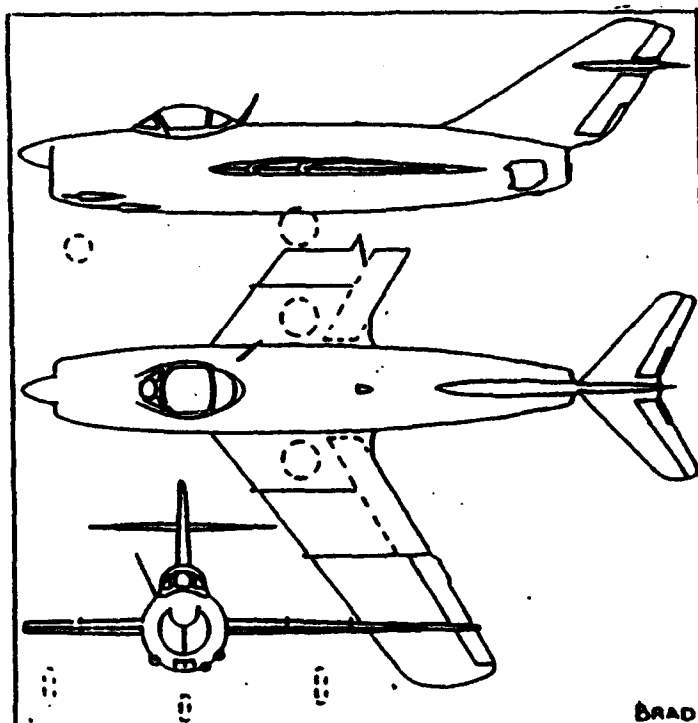


Fig. 1 The MIG-15 All-weather Fighter

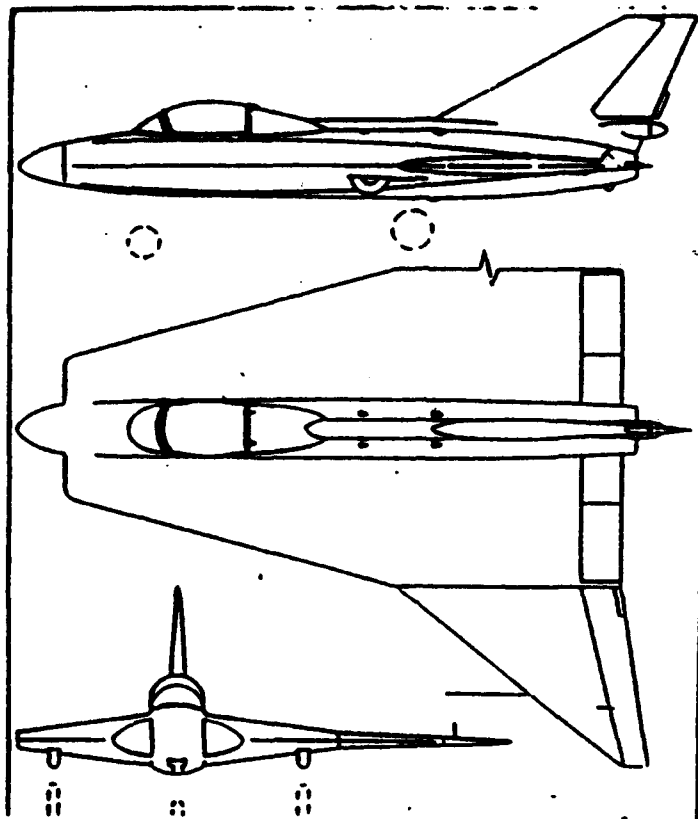


Fig.2 The Saab-210 Draken Delta-Wing

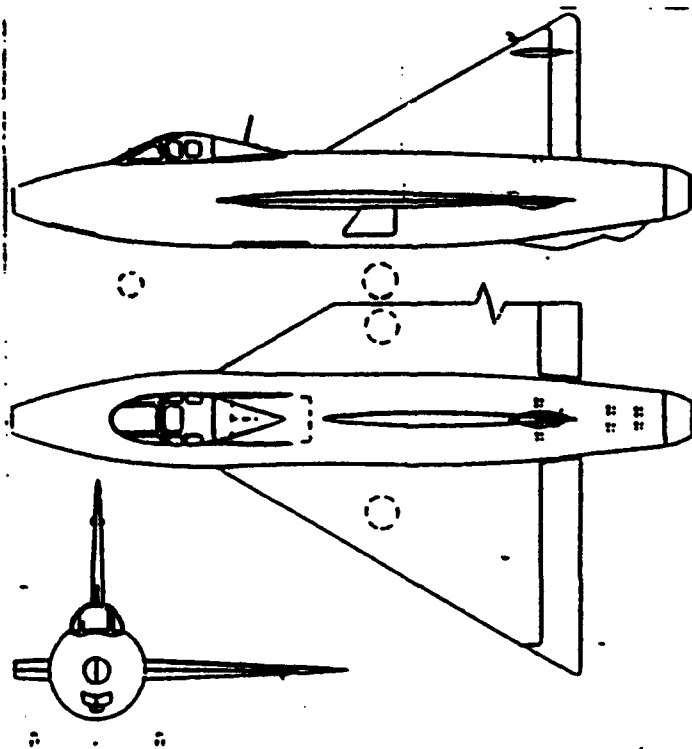


Fig. 3 The Convair XF-92 Delta-Wing

B) AERODYNAMICS OF DELTA & DOUBLE-DELTA WINGS

The advantage of a single-delta-wing design is that the leading edge vortex flows are effective in reducing prestall buffet levels to give a more gradual loss of lift above the angle of attack (AOA) for maximum lift coefficient but the design leads to low wing loading and poor maneuverability [Ref.1]. The design of a modern light weight fighter that can cruise supersonically, maneuver transonically and has a post-stall capability requires additional, highly swept area ahead of the main wing called strake or leading edge extension (LEX)[Refs.3 and 4]. The growing interest in high AOA maneuver has refocussed the attention of the research community, NASA and the aircraft industry to conduct a High-Alpha Technology Program (HATP) for improving and providing new concepts for vortex control of future modern fighter aircraft. This has led to the McDonnell Douglas F/A-18E/F upgraded from the F/A-18C/D (Figs.4 & 5) and the Russian Sukhoi Su-27 (Fig-6).

The basic aerodynamic phenomenon of a delta wing includes formation of leading edge vortices, their development and subsequent breakdown (burst) [Ref.5].

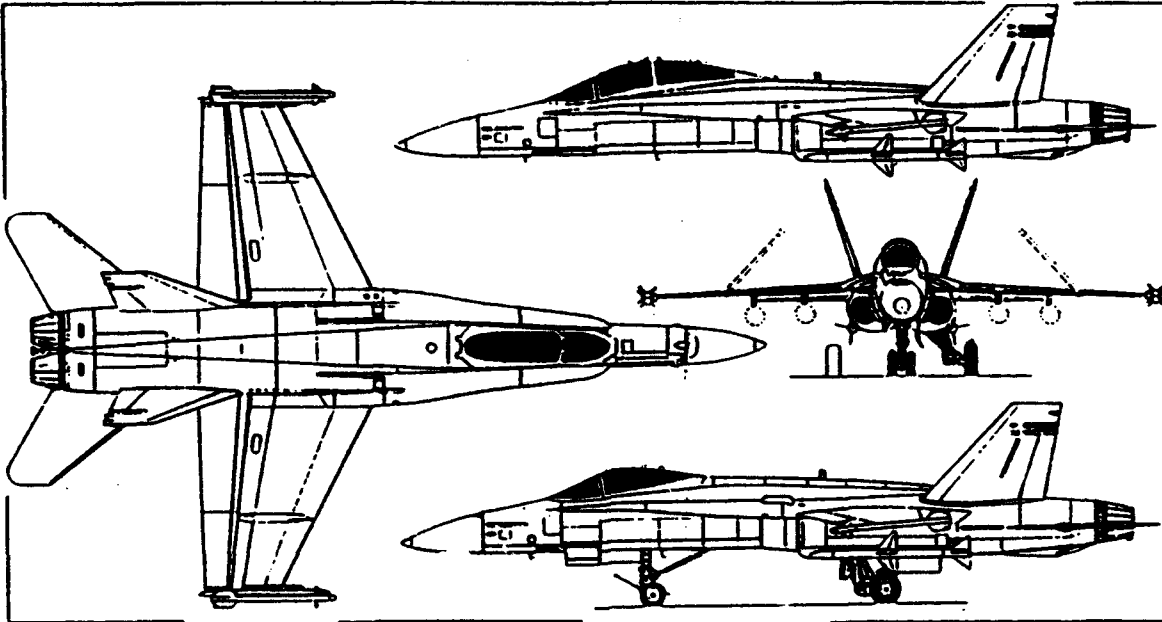


Fig. 4 McDonnell Douglas F/A-18C/D

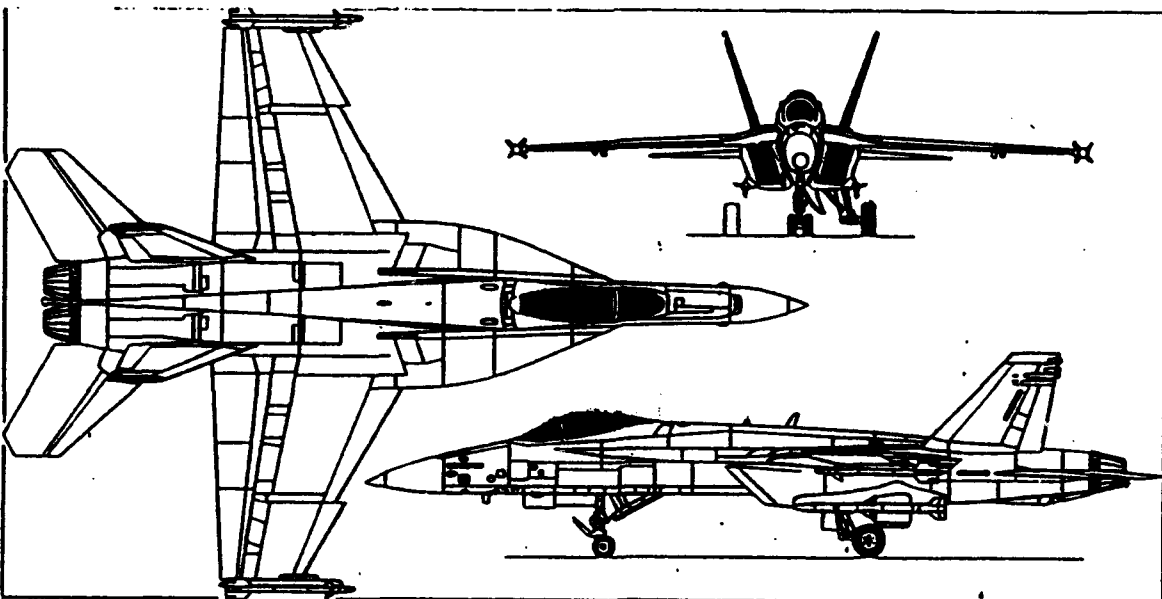


Fig. 5 McDonnell Douglas F/A-18E/F

Generally two symmetric leading edge vortices are generated on wings with sweep angles greater than 45 deg as the wing pitches up (Fig.7) ; these vortices cause the flow over the upper surface to accelerate producing extra lift called vortex lift . At high AOA , the core flow of the vortex suddenly stagnates and expands in size . This phenomenon is called vortex breakdown or bursting whose location is affected by wing sweep, AOA and the leading edge shape [Ref.6].

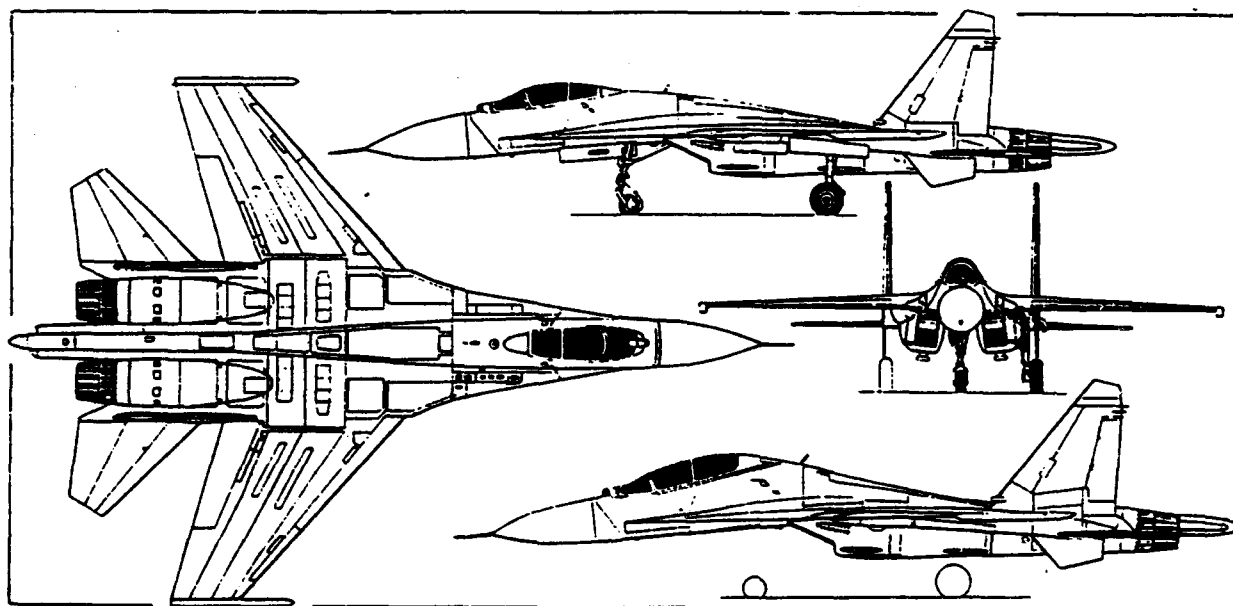


Fig. 6 Sukhoi Su-27

A combination of a strake and a wing gives a double-delta-wing configuration whose geometric characteristics are similar to a delta wing but for a discontinuity (kink) in its leading edge . The flow over a double-delta wing is very similar to that over a delta wing, but much more complicated. At high AOA the vortical structure over a double-delta wing consists of a strake vortex generated at the apex and a wing vortex generated at the kink (Fig.8). At low AOA , the interaction of these vortices leads to their coiling-up (intertwining). At high AOA , one of the vortices (usually the strake vortex) bursts even before the interaction and triggers the bursting of the other. The vortex burst phenomenon is influenced by various factors similar to those in the case of a single-delta wing. When a strake is added to a delta wing it not only increases the lifting area of the wing, but also creates its own leading edge vortices which help to stabilize the flow field over the main wing.

A review of experimental data for delta wings under both steady and unsteady conditions appears in [Ref.5]. Recent studies on double-delta wings have generally focussed

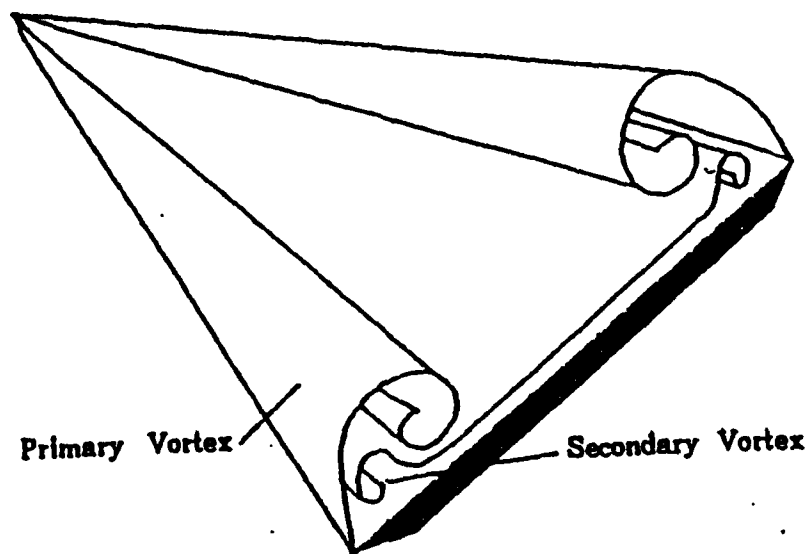


Fig. 7 Typical Vortex Structure over a Delta Wing at High AOA

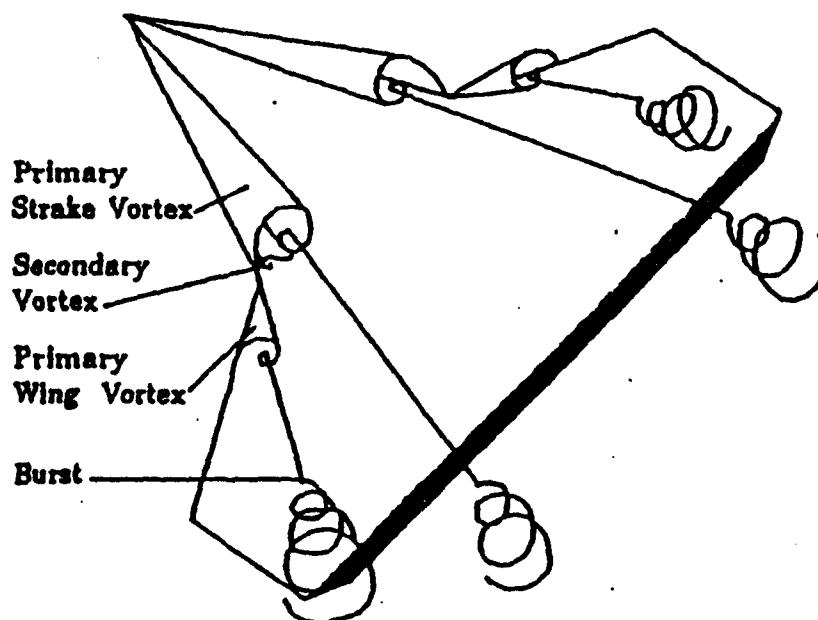


Fig. 8 Typical Vortex Structure over a Cropped Double-Delta Wing at High AOA.

attention on static conditions of the model, with emphasis on understanding the complicated phenomena of vortex interaction and bursting. Thompson [Ref.7] reported an extensive water tunnel flow visualization study on a family of double-delta wings. A water tunnel investigation on the coiling-up of vortices on a double-delta wing appears in [Ref.8]. Wind tunnel studies of vortical flows over double-delta wings have been reported by Olsen and Nelson [Ref.9], Graves, et al.[Ref.10], and Grismer, et al.[Ref.11]. The data available on double-delta wings in dynamic motion is extremely limited. The water tunnel flow visualization data reported recently by Hebbar , et al.[Ref.4] is the first of its kind for a double-delta wing model in pitching motion.

C) FILLET AERODYNAMICS

The vortical flow dominates the lift at high angle of AOA. One of the current active reseach areas in high AOA aerodynamics is the control of flow through vortex manipulation to enhance the aircraft maneuverability. Both pneumatic and mechanical devices are being investigated as

candidates for vortex manipulation. A number of studies have been reported in the literature that deal with vortex management for control purposes. A recent numerical study by Kern [Ref.12] on vortex flow control through small geometry modifications (fillets) at the strake/wing junction of a cropped double-delta wing suggested that the use of fillets could enhance the lift by 13.6% at low AOA and 17.9% at high AOA with a slight improvement in lift-to-drag ratio. It even suggested that the fillets may be good candidates for roll control devices. Thus, pending further studies and experimental verification, the concept of flow control by small deployable fillets at the junction of a double-delta wing appears promising.

The present investigation was undertaken to better understand the physics of vortical flows over sharp-edged double-delta wings, with and without juncture fillets. It consisted of extensive flow visualization studies in the Naval Postgraduate School (NPS) water tunnel facility with dye-injection technique and focussed on vortex core trajectories, interaction and breakdown on the leeward surface at high AOA. The models included a 76/40 deg cropped

double-delta wing baseline model and its three derivatives with small geometry modifications (fillets) at the junction of the strake and wing leading edges. The model and fillet geometries were identical to the ones used by Kern [Ref.12].

II. EXPERIMENTAL APPARATUS

A. THE NPS WATER TUNNEL

The experiments were conducted in the Naval Postgraduate School flow visualization water tunnel facility [Ref.13]. This water tunnel was the first one designed by Eidetics International, Inc., Torrance, California, and installed at NPS in late 1988. Figure 9 depicts the layout of the water tunnel. It is a closed circuit facility for studying a wide range of aerodynamic and fluid dynamic phenomena. Its key design features are high flow quality and horizontal orientation. The latter feature facilitates model access, and enables the model to be readily changed without emptying the water tunnel. The facility is operated as a continuous flow channel, and the water level is adjusted to be approximately 2 inches below the top of the test section . The top cover is removable for easy access to the model while the water tunnel is operating. The test section of the water tunnel is 15 inches wide, 20 inches high, and 60 inches long and it is

constructed of glass to allow simultaneous viewing of the model flow field from the bottom, from both sides and from the rear. Viewing from the rear is specially advantageous when studying flow structures in the cross-flow plane. There is enough space below the bottom of the test section for convenient viewing and for setting up still photography and videotape recording. The test section flow velocity is variable from 0 up to 1.0 ft/sec. The level of the flow quality over the range of test section velocities is as follows:

Turbulence intensity level	=< 1.0% RMS
Velocity uniformity	=< +/-2.0%
Mean flow angularity	=< +/-1.0deg (pitch & yaw angle)

Six canisters filled with water-soluble food coloring are used for flow visualization. Each canister has a routed line to the model support system. A compressor and a pressure regulator are used for pressurization and controlling the pressure level in the canisters. The pressurized system helps in regulating the dye emission and blowing air out of the dye lines going to the model.

The model support system is designed for high angle-of-attack aerodynamic research studies. The model is usually mounted upside down in the test section (Fig.10). The model support system utilizes a C-strut to vary the pitch travel up to 50 deg between the limits of -10 deg and 110 deg , and a turntable to provide yaw variations up to +/-20 deg. The model attitude control system consists of two servo motors which provide independent control of model pitch and yaw , each motor having a high/low rate switch.

B. DOUBLE-DELTA WING MODELS

Four different shapes of double-delta wing models were used in this investigation : a baseline model and its three derivatives. The baseline model shown in figure 11 was constructed of 0.25-inch-thick plexiglass and consisted of a 76 deg-swept strake and a 40 deg swept wing, both with sharp, 20 deg bevelled leading edges and flat top surfaces. It had a centerline chord of 9.375 inches a span of 9.5 inches, and a planform area of 39.9 square inches. The three derivatives of the baseline model were also constructed by incorporating small geometry modifications (fillets) at the

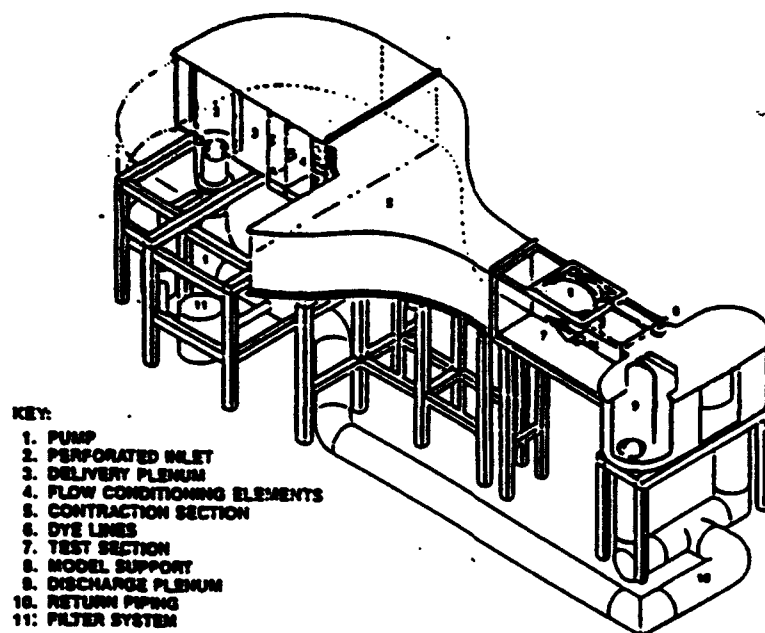


Fig. 9 The NPS Flow Visualization Water Tunnel Facility

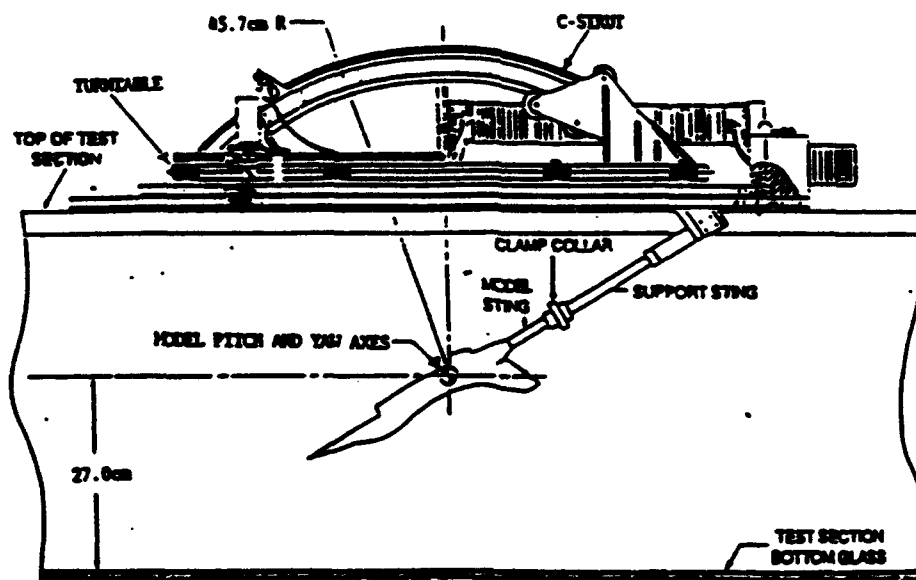


Fig 10 Model Support System of the NPS Water Tunnel

intersection (juncture or kink) of the strake and wing leading edges. Each fillet increases the planform area of the baseline model by nearly 1% . The fillet dimensions are identical to the ones used by Kern[Ref.12] and are shown in figure 12. The vortex burst location was easily identifiable with the help of grid lines marked on the upper surface of the models.

C. DYE TUBE INSTALLATION

The dye tubes consisted of small brass tubes installed on the bottom surface of the wing. Both the location of the dye injection and the injection rate were crucial to obtain a good flow visualization of the model flow field. Figure 13 shows two different positions of the dye tube. In position 1 the dye tube is shown installed on the bottom surface of the wing with the tip sitting squarely on the flat surface below the apex. This location was found to yield satisfactory results. In position 2 the dye tube is shown installed as in the previous position but the tip was pushed a little bit forward. This position was found less satisfactory at high AOA as the dye stream lines looked more like a wide band and

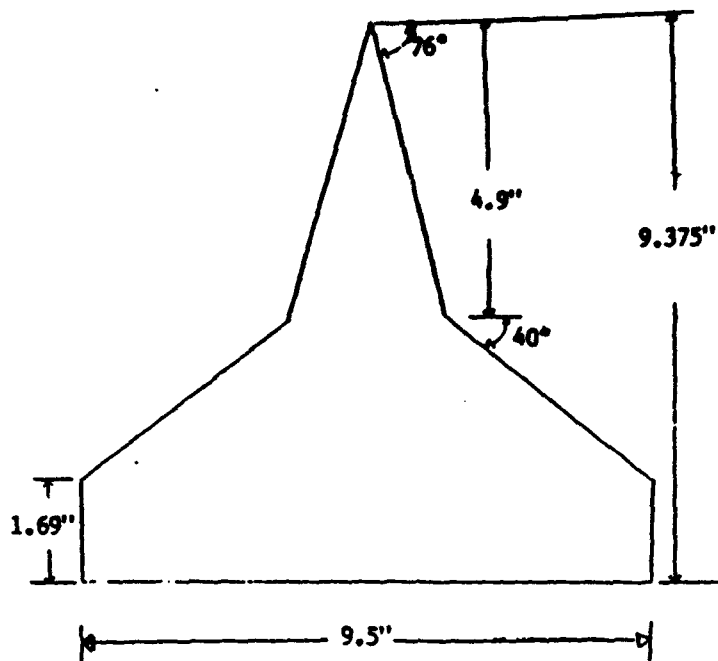


Fig.11 The Baseline Double - Delta Wing Model with Sharp Bevelled Leading Edges and Flat Top Surface

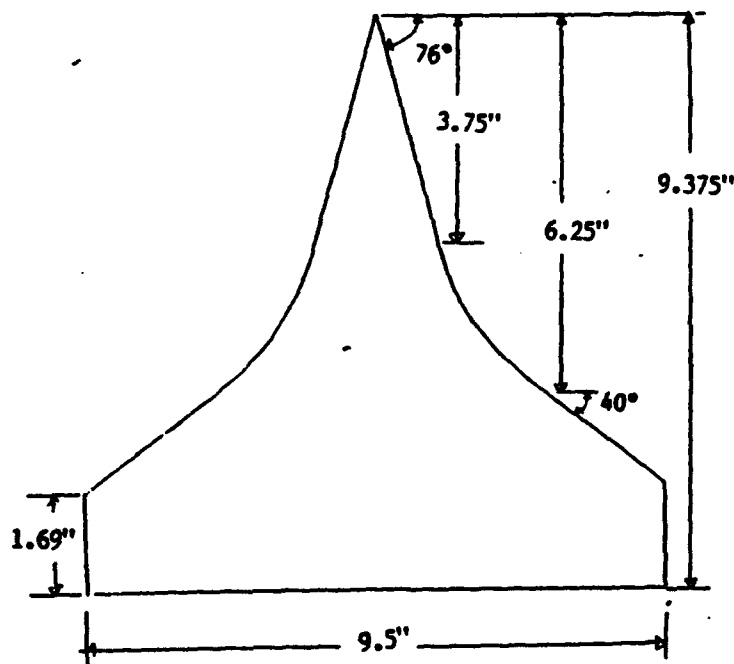


Fig.12 The Double - Delta Wing Models with Different Juncture Fillets, a) Parabolic

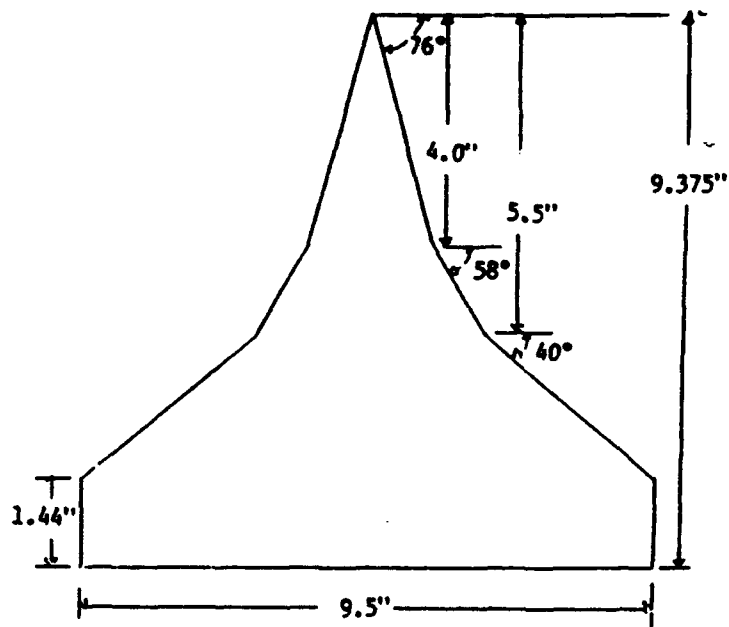


Fig.12 The Double - Delta Wing Models with Different Juncture Fillets, b) Linear

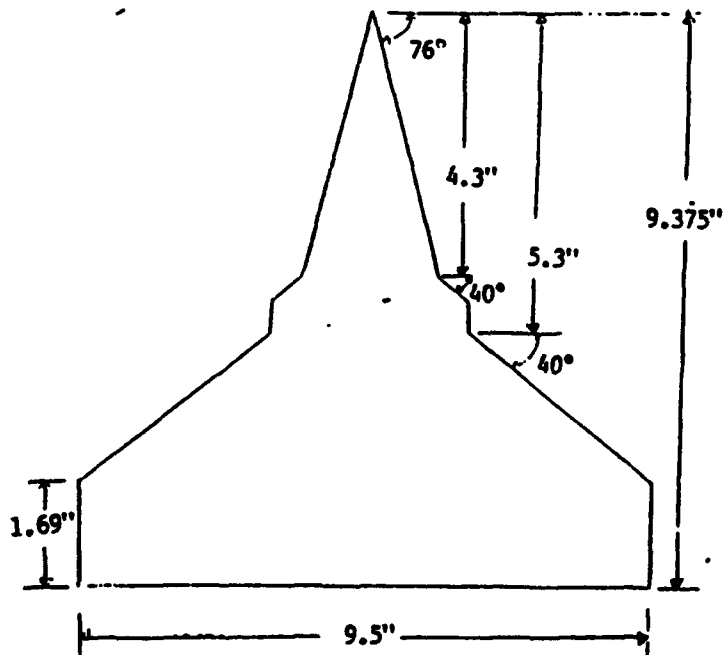


Fig.12 The Double - Delta Wing Models with Different Juncture Fillets, c) Diamond

not a concentrated well defined vortex core. Different color dyes were selected for different locations. Table 1 shows the dye locations for each model in percent of centerline chord.

TABLE 1 DYE LOCATIONS (% OF THE CHORD)

Dye location	BASELINE	LINEAR	PARABOLIC	DIAMOND
apex	5.3%	5.3%	5.3%	5.3%
beginning of fillet	52.3% *	42.7%	40.0%	46.0%
end of fillet	52.3% *	58.7%	66.7%	56.5%

* This represents the tip location of the dye tube used for visualizing wing vortex

D. MODEL MOUNTING

To have a good symmetry of the vortex core and the vortex burst , it is very important to mount the model horizontally in the water tunnel with zero pitch , zero yaw and zero roll. Details of model mounting are given in [Ref.14]. The model sting was secured to the sting holder of the model support system and then introduced into the test section . The centerline of the model was aligned with the

freestream (tunnel centerline) for ensuring zero pitch angle. To assure zero yaw the model apex was set at equal distance from either sidewall of the test section. To assure zero roll angle the left and right wing tips were located at the same height from the bottom of the test section . The model pitch axis was located 5.25 inches aft of the apex (56% of the centerline chord).

III. EXPERIMENTAL PROCEDURE

A. EXPERIMENTAL PROGRAM

The goal of this investigation was to evaluate the effect of fillets on vortex core trajectories , interactions and breakdown on the leeward surface of a cropped-double-delta wing at high angles of attack with zero sideslip angle. The experimental program consisted of flow visualization of the models with zero sideslip in static condition and during dynamic maneuver with AOA varying from 0 to 50 deg (simple pitch-up motion) and 50 to 0 deg (simple pitch-down motion). The dye-flow visualization of the model in both topview and sideview during static and dynamic conditions was documented by using still picture photography and videotape recording. The flow velocity in the water tunnel was kept nearly constant at 0.25 ft/sec that corresponded to a nominal Reynolds number of 24161/ft (18876 based on the centerline chord) .

B. REDUCED PITCH RATE

In reality aircraft encounter unsteadiness under all operating conditions whether due to input dynamic motion (e.g., pitch up/down) or natural disturbances (e.g., windshear, gusts). Therefore it is essential to understand the stability of an aircraft operating in these environments and its response to flow unsteadiness. The appropriate non-dimensional parameter characterizing the response to flow unsteadiness during pitching motions is the reduced pitch rate, k given by:

$$k = \frac{\dot{\alpha} L}{2V}$$

where,

k = reduced pitch rate, nondimensional

$\dot{\alpha}$ = pitch rate , rad/sec

L = characteristic length of the model, ft

V = free stream velocity ft/sec

The model pitch rate during the dynamic motion was ± 3.85 deg/sec . This corresponds to a reduced pitch rate of ± 0.1 based on the centerline chord .

C. DATA ACQUISITION AND REDUCTION

Data acquisition consisted of using two video cameras and two 35mm cameras simultaneously to record the sideview and topview of the vortical flow field of the strake and the fillet vortex cores for the four models at different AOA.

The data reduction consisted of :

1. Measuring the vortex core locations in X-direction(along the model centerline from the apex), Y-direction (outboard from the model centerline) and Z-direction (perpendicular to, and away from the surface), and plotting vortex core trajectories at different AOAs for static conditions.
2. Measuring the burst location of the strake vortex and plotting it as a function of AOA for static and dynamic conditions.

The measurements were made on both sides of the model centerline using the apex as a reference point . The vortex core locations and the burst locations were visually determined from the videotape/photographs with utmost care

and nondimensionalized using the centerline chord length .

In the case of the strake vortex both the core locations and the burst locations were determined , whereas only the core locations were determined for the juncture vortex (of the baseline model) and the vortices shed at the beginning and the end of the fillet region of other models. There may be some degree of imprecision in the data due to the difficulty in locating the burst point, particularly at high AOAs during dynamic motion . In addition , during the static segment of the experiment the vortex burst location for any model at any AOA fluctuated up to ± 0.75 inches (about $\pm 8\%$ of the centerline chord). For a discussion on the quality of the NPS water tunnel burst data, see Hebbar et al.[Ref.15] . The vortex core coordinates and the burst locations are listed in Appendix A.

D. METHOD OF PHOTOGRAPHY AND VIDEO RECORDING

The equipment used for the data acquisition consisted of two 35mm automatic cameras, one U-matic Sony video camera, one Panasonic video camera, 3 Smith-Victor 600- watt photographic lights , and a fixed flood light

installed below the test section . For the sideview photographs two of the lights were placed at a distance of 3 feet at 45 deg angle from the test section , and the third one was placed 90 deg at the back of the test section . Figure 14 illustrates the lighting set-up for both sideview and topview (top surface of the model).

A Minolta 5000i Maxima camera was used for the sideview using 35mm B&W Kodak ASA-400 film. It was focussed manually at the model one time only. A Nikon 2050 camera was placed at the bottom of the test section for the topview and it was focussed manually one time only with the model pitched at 25 deg. It was operated with 35mm B&W Kodak ASA-1600 film using a remote shutter . The Sony video camera was placed at the bottom of the test section whereas the Panasonic video camera was placed at the side for the sideview . Both sideview and topview of the model photographs and videos were taken simultaneously at angles of attack of 5, 10, 16, 20, 22.5, 26, 30, 35, 40, 45 and 50 deg. During the dynamic pitching of the model , the fixed flood light was operated (switched on & off) each time the model reached the desired

pitch angle to help identify the instantaneous pitch angle during subsequent playback of the videotape for data reduction.

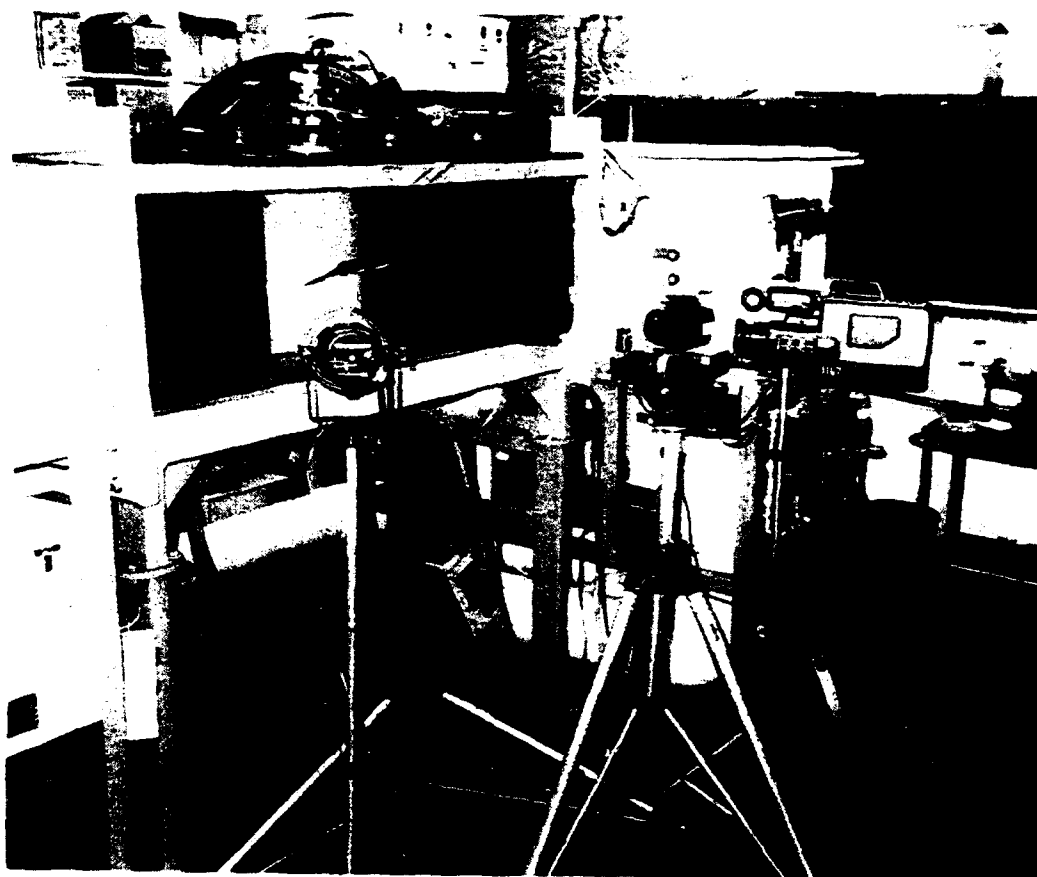


Fig.14 Video camera , 35-mm camera and lighting setup of the experiment

IV. RESULTS AND DISCUSSION

A large amount of flow visualization data has been collected during the course of the investigation using several rolls of 35mm black and white film and videotape recording both in sideview and topview . The reduced data will be quantitatively analyzed in two parts . The first part deals with the effects of AOA on vortex core trajectories and vortex interactions for static conditions with zero sideslip . The second part deals with the effects of AOA on the breakdown (bursting) response of the strake vortex during static and dynamic (pitching) conditions with zero sideslip.

The experimental data on vortex core trajectory and bursting is tabulated in Appendix A (Tables 2-59). Several selected photographs are presented in Appendix B (Figures 15-59) to highlight the flow phenomena and the effect of fillets. Each figure shows two views of the flow field , one in the sideview and the other in the topview (taken from below the test section of the water tunnel) . Note that the AOA reading in these photographs is not necessarily the true

AOA because the sideview camera was not always focussed exactly at the model centerline . The true AOA was read off the AOA indicator on the tunnel control box . The vortex trajectory plots and the vortex burst plots derived from the videotape recordings are included in Appendix C (Figures 60-144).

A. EFFECTS OF AOA ON VORTEX CORE TRAJECTORIES AND VORTEX INTERACTION

The following discussion refers to vortex trajectory plots obtained from the static flow visualization data and shown in Appendix C.

1. Vortex Core Trajectories

Individual vortex core trajectories for various AOAs are shown in Figs. 60-63 for the baseline model , Figs. 76-81 for the linear-fillet model , Figs. 95-100 for the parabolic-fillet model, and Figs. 114-119 for the diamond-fillet model. The strake vortex core trajectories for all the models are shown in Figs. 133-138 ,for AOAs of 10,20 & 30 deg, respectively.

Figures 133-135 represent the strake vortex core location in Y-direction (outboard from the model centerline). At 10 deg AOA the strake vortex core of the baseline model is closer to the model centerline than those of the filleted models . As the angle of attack increases from 10 to 30 deg the vortex cores move inboard for all the models . However, the inboard movement of the vortex core is delayed for the diamond-fillet model as the AOA is increased.

Figures 136-138 represent the strake vortex core location in Z-direction (perpendicular to, and away from the model surface) . The vortex core trajectory in the Z-direction behaves non-monotonically for the linear- and the parabolic-fillet models at 10 deg AOA . The vortex core trajectory of the baseline model is farthest away from the surface and the vortex core of the diamond-fillet model is the nearest one to the surface .

2. Vortex Interaction

Vortex interaction can be studied with the help of combined trajectory plots shown in Figs. 64-73 for the baseline model, Figs. 82-91 for the linear-fillet model,

Figs. 101-110 for the parabolic-fillet model, and Figs. 120-129 for the diamond-fillet model .

Figures 120-124 represent the interaction of the strake and the fillet vortex cores in the spanwise direction as a function of the centerline chord (x/c) for different angles of attack . At 10 deg AOA the strake vortex core interacts with the beginning-of-the-fillet vortex core at 55% of centerline chord (x/c) and 10% outboard from the model centerline (y/c) , and it interacts with the end-of-the-fillet vortex core at 70% (x/c) and 15% (y/c) . At 20 deg AOA the strake vortex core interacts with the beginning of the fillet vortex core at 52.5% (x/c) and 8.5% (y/c) , and it interacts with the end-of-the-fillet vortex core at 65% (x/c) and 12.5% (y/c) . Note that at 30 deg AOA there is no interaction as the fillet vortices are already burst and there is only the strake vortex core present. It is thus seen that as the angle of attack increases the interaction moves upstream and inboard . Similar interaction behavior can also be seen in the case of other models .

Figures 117-119 represent the strake, beginning-of-fillet and end-of-fillet vortex core locations in Z-

direction (perpendicular to , and away from the model surface) for the diamond-fillet model . From figure 117 it is seen that as the AOA increases the vortex core trajectory moves away from the surface but the trend is reversed at 30 deg . The beginning-and-the-end-of-the fillet vortex cores behave monotonically . Similar trends are observed with other models as well.

3. Effect of Fillet Shapes on the Interaction of the Strake and Fillet Vortex Core Trajectories

It must be noted that the vortex core shed from a sharp leading edge and its burst location are usually assumed to be relatively insensitive to Reynolds number . But the interaction between the strake vortex and the wing (or fillet) vortex is found to be a function of Reynolds number [Ref. 7] .

At 10 deg AOA both the strake and the fillet vortex cores are already well developed over the diamond-fillet model and coiled-up around each other (Fig. 120). The strake vortex core is nearly conical over the strake portion of the wing [Ref. 10] . It is drawn outboard by the fillet vortices

whereas the fillet vortices are drawn away from the wing leading edge by the strake vortex . As the AOA increases to 20 deg , the coiling-up of the vortices occurs earlier . At 22.5 deg AOA there is no interaction between the strake vortex and the-end-of-fillet vortex , however the strake vortex is interacting with the-beginning-of-fillet vortex and the interaction moves further upstream . At 30 deg AOA there is no vortex interaction at all . The fillet vortices burst at their origin and the strake vortex bursts ahead of the fillet location.

Examination of the vortex interaction for all the models clearly indicates the mutual induction effect the strake and fillet vortex cores have on each other . The strake vortex induces an upward and an inboard movement of the fillets vortices ; conversely , the fillets vortices induce a downward and outboard movement of the strake vortex . The interaction of the vortex cores leads to their intertwining (coiling around each other) , and as the angle of attack increases , the interaction moves upstream until the AOA is large enough to cause the bursting of the strake vortex

(even before the interaction) and subsequent destabilization of the fillet vortices.

B. STATIC AND DYNAMIC EFFECTS OF AOA ON STRAKE VORTEX CORE BREAKDOWN

A few general observations are appropriate here . The strake vortex core breakdown was not visible over the model surface at low $AOA < 10$ deg because it occurred in the wake behind the trailing edge . It was also not easy to measure it at very high $AOA > 40$ deg. Note that the non-visualization of the wing and fillet vortices was deliberate and intended to facilitate identification of strake vortex burst location (Figs. 15-19, 27-31, 38-42, and 49-53).

1. Static Condition

Figures 74, 92, 111 and 130 (Appendix C) represent the flow-visualization data for the baseline, linear-, parabolic- and diamond-fillet models respectively, showing the strake vortex burst location along the model centerline from the apex (X_b/c) as a function of AOA . The figures show the fluctuation of the burst location up to ± 0.75 inch (about $\pm 8\%$ of the centerline chord). As the AOA increases from

0 deg the vortical flowfield develops over the upper surface of the wing . At 10 deg AOA the strake vortex core is well developed and it is seen to burst just around the trailing edge . As the AOA increases the burst location moves upstream and approaches the apex at 50 deg AOA.

2. Dynamic Condition

Figures 139-142 represent the flow visualization data during simple pitch-up motion (0 - 50 deg) and simple pitch-down motion (50 - 0 deg) of the baseline, linear-, parabolic- and diamond-fillet models, respectively . These figures show streamwise burst location of the strake vortex (X_b/c) as a function of the instantaneous AOA . Also shown here for comparison are burst location plots for the static case . These figures show clearly the effect of pitching motion namely the vortex burst lag . During the pitch-down motion , the strake vortex bursting occurs earlier relative to static condition resulting in a vortex system which is equivalent to a static system at an increased angle of attack . During the pitch-up motion the strake vortex bursting occurs at a point further downstream than would occur for pitch-down motion and static case . The vortex

burst response observed here is similar to the one observed by Hebbar et al. [Ref. 4] , Olsen and Nelson [Ref. 9] . and by Magness et al. [Ref. 16] for simple-delta wings .

3. Effect of Fillet Shapes on Strake Vortex Breakdown

Figure 143 compares the strake vortex burst location plots for the static condition of different fillet shapes with that for the baseline model . These plots represent the strake vortex core bursting in X-direction (along the model centerline measured from the apex) as a function of angle of attack . It should be noted here that there was some experimental uncertainty associated with the data reduction. While no definite trend in the vortex burst response of parabolic-fillet and linear-fillet models relative to the baseline model is detectable over the AOA range tested , the results indicate a clear trend in the vortex burst delay for the diamond-fillet shape [Ref. 17]. This vortex burst delay improves the flowfield structure over the wing surface and will therefore enhance the lift. This data correlates well with the numerical prediction of Kern [Ref. 12], verifying the concept of flow control by fillets for the static condition .

Figure 144 compares the strake vortex burst location plots for the dynamic condition (pitch-up and pitch-down) of different fillet shapes with that for the baseline model . A close examination indicates that during the pitch-up and pitch-down motions the strake vortex bursting is delayed for the diamond -fillet model . This trend is identical to the result discussed earlier for the static case. The dynamic data therefore implies possible lift augmentation with diamond-fillet shape during pitching maneuvers to enhance the controllability and performance of the aircraft.

V. CONCLUSIONS

A flow visualization investigation of the vortical flow over a cropped double-delta wing model with sharp leading edges and its three derivatives with small geometric modifications (fillets) at the strake wing junction , was conducted in the NPS water tunnel using the dye-injection technique . The primary focus of this investigations was to evaluate the effect of fillets on vortex core trajectories , interactions and breakdown over the model surface at high AOA with zero sideslip angle . The following conclusions are drawn from the results of the experimental investigations :

1. The mutual induction effect of strake and fillet vortex cores on each other leads to their intertwining (i.e. coiling around each other) . With increasing AOA , the interaction point moves upstream , inboard , and upward but only until the AOA is large enough to cause the bursting of the strake vortex even before the interaction could begin.

2. The data suggests vortex interaction delay associated with the diamond-filletlet model . Compared to other models , the strake vortex core trajectory of the diamond-filletlet model remains closest to the model surface and farthest from the centerline at high AOA .
3. A comparison of static test results for different fillet shapes indicates a clear improvement in vortex burst delay for the diamond-filletlet model over the baseline model , thus correlating well with the recently published numerical data of Kern [Ref. 12] and supporting the concept of flow control by fillets.
4. The strake vortex burst location plots with and without the fillets show the usual vortex burst lag associated with the dynamic motion . They clearly indicate the vortex burst delay associated with the diamond-filletlet model during both pitch-up and pitch-down maneuvers , thus extending the concept of flow control by fillets for enhanced maneuvering of fighter aircraft .

The following recommendations are made based on this investigation :

1. The investigation should be extended to include the effects of sideslip (yaw).
2. A quantitative investigation of the flowfield characteristics should be undertaken with a laser Doppler velocimetry (LDV) . The data may be used to correlate the present flow visualization data and computational data.
3. It is highly recommended to use other fillet shapes to study their suitability as flow control devices.
4. A wind tunnel investigation of these fillet shapes using a force balance is recommended to further assess quantitatively the suitability of the fillets as control devices .

LIST OF REFERENCES

1. Whitford, R. *Design for Air Combat*, Janes Publishing Company Ltd, London, 1987.
2. Janes all the world aircraft, 1953.
3. Bertin, John J. and Smith, Michael L., *Aerodynamics for Engineers*, Prentice Hall, Second edition, 1989.
4. Hebbar S.K., Platzer M.F. and Li, F.H. "A Visualization study of the vortical flow over a double-delta wing in dynamic motion" AIAA 93-3425, Aug. 1993.
5. Lee, M., and Ho, C.-M., "Vortex Dynamics of Delta Wings," In: *Lecture Notes in Engineering*, Vol. 46, *Frontiers in Experimental Fluid Mechanics* (ed. M. Gad-el-Hak), pp. 365-427, Springer Verlag, 1989.
6. Walters, M.W., "flow field of Bursting Vortices over moderately Swept Delta Wing," HTP-5 Workshop on Vortical Flow Breakdown and Structural Interactions, NASA Langley Research Center, Aug. 15-16, 1991.
7. Thompson, D.H., "Visualization of Vortex Flows around Wings with Highly Swept Leading Edges," 9th Australasian Fluid Mechanics Conference, Auckland, Dec. 1986.
8. Yu, F., Young, K. and Chang, R., "An Investigation on the coiling-up of Vortices on a Double-Delta Wing," AIAA 28th Aerospace Sciences Meeting, Reno, Nevada, Jan. 1990.
9. Olsen, P., and Nelson, R., "Vortex Interaction over Double-Delta Wings at High Angles of Attack," AIAA Paper 89-2191, July/Aug. 1989.
10. Graves, T.V., Nelson, R.C., Schwimley, S.L., and Ely, W.L., "Aerodynamic Performance of Strake Wing Configurations," In: *High-Angle-of-Attack Technology Vol. I*, NASA CP-3149, Part 1, pp. 173-204, May 1992.
11. Grismer, D.S., Nelson, R.C., and Ely, W.L., "An Experimental Study of Double-Delta Wings in Sideslip," AIAA Paper 91-3308, Sept. 1991.
12. Kern, S.B., "vortex Flow Control using Fillets on a Double-Delta Wing," *Journal of Aircraft*, Vol. 30, No. 6, Nov/Dec. 1993, P. 818. Also see AIAA paper 92-0411.

13. User's Manual, Flow Visualization Water Tunnel Operation Manual for Model 1520, Eidetic International, Inc., Torrance, California, 1988. (prepared for Naval Post Graduate School, Monterey, California).
14. Cavazos, O.V., *A Flow Visualization Study of Lex Generated Vortices on a Scale Model of an F/A-18 Fighter Aircraft at High Angle of Attack*, Master's thesis, Naval Post Graduate School, Monterey, California, June 1990.
15. Hebbar, S.K., Platzer, M.F., Park, .N., and Cavazos, O.V., "A Dynamic Flow Visualization Study of a Two-Percent F/A-18 Fighter Aircraft Model at High Angle of Attack," In : *High-Angle-of-Attack Technology*, Vol.I, NASA CP-3149, Part 3, pp.1025-1037, May 1992.
16. Magness, R.D. and Rockwell, D., "Control of Leading Edge Vortices on a Delta Wing ", AIAA paper 89-0900, March 1989.
17. S.K. Hebbar, M.F. Platzer, A. Alkhozam "Investigation into the effects of juncture fillets on the vortical flow over a cropped, double-delta wing " AIAA paper 94-0626, 32nd Aerospace Sciences Meeting & Exhibit, Jan 10-13, 1994, Reno, NV.

APPENDIX A EXPERIMENTAL RESULTS (TABLES)

TABLES (2 - 59)

TABLE 2 Strake vortex core trajectory over the baseline model in % chord length , AOA = 10 deg.

No.	X/C	Y/C	Z/C
1	10	1.33	1.33
2	15	2.67	1.33
3	20	3.33	1.6
4	25	4.0	2.13
5	35	5.33	2.4
6	40	6.67	2.67
7	50	8.0	2.93
8	60	10.0	3.2
9	65	11.33	3.73
10	70	12.67	4.0
11	75	14.67	5.33
12	80	16.0	5.87
13	85	18.67	6.67
14	90	20.67	6.75
15	93	22	6.93

TABLE 3 Strake vortex core trajectory over the baseline model in % chord length , AOA = 16 deg.

No.	X/C	Y/C	Z/C
1	10	1.33	1.33
2	15	2.67	1.33
3	20	3.33	1.6
4	25	4.0	2.13
5	30	4.67	2.67
6	35	5.33	2.67
7	40	6.67	3.0
8	45	7.33	4.0
9	50	8.0	4.0
10	55	9.0	5.0
11	60	9.5	5.33
12	65	10.5	6.0
13	70	11.33	6.67
14	75	12.67	6.67
15	80	14	7.0

TABLE 4 Strake vortex core trajectory over the baseline model in % chord length , AOA = 20 deg.

No.	X/C	Y/C	Z/C
1	10	1.33	1.33
2	15	2.67	1.33
3	20	3.33	1.75
4	22.5	3.67	2.0
5	25	4.0	2.5
6	28	4.0	2.75
7	30	4.67	3.0
8	33	5.33	3.25
9	37	6.0	3.375
10	40	6.33	3.5
11	45	6.67	4.75
12	50	7.33	6.0
13	53	8.0	6.25
14	57	8.67	6.5
15	60	9.0	7.0

TABLE 5 Strake vortex core trajectory over the baseline model in % chord length , AOA = 22.5 deg.

No.	X/C	Y/C	Z/C
1	10	1.33	1.33
2	15	2.67	1.33
3	20	3.33	1.75
4	22.5	3.67	2.1
5	25	4.0	2.67
6	27	4.0	3.0
7	30	4.67	3.125
8	32	5.33	3.25
9	36	6.0	3.375
10	40	6.25	3.67
11	42	6.5	4.5
12	44	6.75	5.0
13	46	7.0	5.5
14	48	7.125	6.0
15	50	7.25	6.25

TABLE 6 Strake vortex core trajectory over the baseline model in % chord length , AOA = 30 deg.

No.	X/C	Y/C	Z/C
1	10	1.33	0.5
2	12	1.33	0.67
3	14	2.0	0.75
4	16	2.25	1.0
5	18	2.75	1.5
6	20	3.0	1.75
7	22.5	3.5	2.0
8	25	3.75	2.25
9	26	3.8	2.67
10	27	3.85	2.8
11	28	4.0	2.85
12	29	4.25	2.9
13	30	4.5	2.95
14	32	4.67	3.0
15	33	4.8	3.125

TABLE 7 Wing vortex core trajectory over the baseline model in % chord length , AOA = 10 deg.

No.	X/Y	Y/C	Z/C
1	53.3	14.67	1.33
2	55.0	14.5	1.33
3	56.0	14.0	2.13
4	58.0	12.67	4.267
5	60.0	12.0	5.33
6	62.0	11.33	6.4
7	64.0	10.67	8.53
8	66.0	10.0	9.6
9	68.0	10.67	10.67
10	70.0	12.0	8.53
11	72.0	13.33	6.4
12	75.0	17.33	2.13
13	77.0	21.33	1.33

TABLE 8 Wing vortex core trajectory over the baseline model
in % chord length , AOA = 16 deg.

No.	X/C	Y/C	Z/C
1	53.3	14.67	1.33
2	55.0	14.5	2.13
3	56.0	14.0	3.2
4	58.0	12.5	5.33
5	60.0	11.67	6.4
6	62.0	11.0	8.53
7	64.0	10.0	9.6
8	66.0	9.33	10.67
9	68.0	6.67	13.33
10	70.0	8.5	9.6
11	72.0	9.5	8.53

TABLE 9 Wing vortex core trajectory over the baseline model in % chord length , AOA = 20 deg.

No.	X/C	Y/C	Z/C
1	53.3	14.67	1.33
2	56.0	14.5	4.267
3	58.6	12.0	6.4
4	61.0	11.5	9.33
5	64.0	10.67	9.6
6	66.0	9.33	10.67

TABLE 10 Wing vortex core trajectory over the baseline model in % chord length , AOA = 22.5 deg.

No.	X/C	Y/C	Z/C
1	53.3	14.67	1.33
2	56.0	14.5	5.33
3	58.6	11.75	10.67
4	61.0	11.25	12.0
5	64.0	10.5	13.33
6	65.3	9.25	16.0

TABLE 11 Wing vortex core trajectory over the baseline model in % chord length , AOA = 30 deg

No.	X/C	Y/C	Z/C
1	53.5	14.67	1.33
2	54.7	14.375	5.33
3	56.0	12.5	9.33
4	57.3	11.5	10.67
5	58.6	11.0	12.0

TABLE 12 Strake vortex breakdown location over the baseline model in % chord length

AOA (deg)	X/C maximum	X/C minimum	X/C mean
10	94.0	92.7	93.3
16	85.3	80.0	82.0
20	69.3	64.0	66.0
22.5	58.7	50.7	53.0
26	53.3	37.3	48.0
30	45.3	29.3	37.0
35	34.7	18.6	27.0
40	24.0	16.0	20.0
45	18.6	13.3	16.0
50	10.7	5.3	8.0

TABLE 13 Wing vortex breakdown location over the baseline model in % chord length

AOA (deg)	X/C maximum	X/C minimum	X/C mean
16	90.7	85.3	88.0
20	85.3	74.7	80.0
22.5	80.0	73.0	77.3
26	61.3	56.0	58.7

TABLE 14 Strake vortex core trajectory over the linear-fillet model in % chord length , AOA = 10 deg.

No.	X/C	Y/C	Z/C
1	10	1.333	1.333
2	15	2.67	1.333
3	20	3.33	1.6
4	25	4.0	2.13
5	35	5.33	2.4
6	40	7.33	2.93
7	50	9.33	3.467
8	60	12.67	4.0
9	65	14.67	2.13
10	70	17.33	1.333
11	75	18.67	2.13
12	80	19.33	2.67
13	85	22.67	3.73
14	90	25.33	5.33
15	94	28.0	6.4

TABLE 15 Starke vortex core trajectory over the linear-fillet model in % chord length , AOA = 16 deg.

No.	X/C	Y/C	Z/C
1	10.0	1.33	1.333
2	20.0	3.33	1.6
3	25.0	4.0	2.13
4	30.0	4.67	2.67
5	35.0	5.33	2.93
6	40.0	6.7	3.04
7	45.0	8.0	3.2
8	50.0	9.33	3.73
9	55.0	10.67	4.267
10	60.0	12.0	3.2
11	65.0	13.33	2.67
12	70.0	14.67	3.73
13	75.0	17.33	4.8
14	80.0	18.67	6.4
15	85.33	20.0	7.46

TABLE 16 Strake vortex core trajectory over the linear-fillet model in % chord length , AOA = 20 deg.

No.	X/C	Y/C	Z/C
1	10	1.33	1.33
2	20	3.33	1.75
3	22.5	3.67	2.0
4	25	4.0	2.67
5	28	4.67	2.93
6	30	5.0	3.2
7	33	5.33	3.4
8	37	6.0	3.73
9	40	6.7	4.106
10	45	7.67	4.48
11	50	9.33	4.8
12	53	10.0	5.12
13	57	10.33	5.33
14	60	11.0	5.33
15	61.33	12.0	5.33

TABLE 17 Strake vortex core trajectory over the linear-fillet model in % chord length , AOA = 22.5 deg.

No.	X/C	Y/C	Z/C
1	10	1.33	1.33
2	15	2.67	1.33
3	20	3.33	1.75
4	22.5	3.67	2.13
5	25	4.0	2.67
6	27	4.0	2.99
7	30	4.67	3.125
8	32	5.33	3.2
9	34	5.67	3.2
10	36	6.0	3.47
11	40	6.7	3.73
12	42	7.33	4.27
13	44	8.0	4.533
14	46	8.33	4.8
15	50.67	9.33	4.8

TABLE 18 Strake vortex core trajectory over the linear-fillet model in % chord length , AOA = 30 deg.

No.	X/C	Y/C	Z/C
1	10	1.33	0.533
2	12	1.33	0.672
3	14	2.0	0.747
4	16	2.25	1.0
5	18	2.75	1.5
6	20	3.0	1.7
7	22.5	3.5	2.0
8	25	3.75	2.25
9	26	3.8	2.67
10	27	4.0	2.77
11	28	4.33	2.85
12	29	4.67	2.88
13	30	4.67	2.9
14	32	5.0	2.93
15	33	5.33	2.93

TABLE 19 Beginning-of-fillet vortex core trajectory over the linear-fillet model in % chord length , AOA = 10 deg.

No.	X/C	Y/C	Z/C
1	42.7	12.0	0.133
2	45.3	10.67	0.333
3	48	9.33	0.67
4	53.3	8.0	1.33
5	56	8.0	1.0
6	58.6	10.67	0.67
7	61	14.67	0.333
8	64	16.0	1.33
9	69.3	14.67	2.0
10	72	14.0	1.33
11	75	14.67	1.0
12	90	23.33	2.67
13	93.3	23.33	1.33

TABLE 20 Beginning-of-fillet vortex core trajectory over the linear-fillet model in % chord length , AOA = 16 deg.

No.	X/C	Y/C	Z/C
1	42.7	12.0	0.533
2	45.3	10.0	1.333
3	50	8.0	2.67
4	53.3	6.7	4.8
5	56	8.0	3.73
6	58.6	12.0	1.33
7	64	13.33	4.8
8	69.3	12.0	7.47
9	72	13.33	5.6
10	75	17.33	3.73
11	80	17.33	2.67

TABLE 21 Beginning-of-filletlet vortex core trajectory over the linear-filletlet model in % chord length , $\text{AOA} = 20 \text{ deg.}$

No.	X/C	Y/C	Z/X
1	42.7	12.0	0.533
2	45.3	10.0	4.0
3	50.0	7.33	7.47
4	53.3	6.0	4.27
5	58.6	6.0	2.67
6	61	13.33	3.2
7	64	14.67	3.2

TABLE 22 Beginning-of-filletlet vortex core trajectory over the linear-filletlet model in % chord length , $\text{AOA} 22.5 \text{ deg.}$

No.	X/C	Y/C	Z/C
1	42.7	12.0	0.533
2	45.3	10.0	4.27
3	48.0	8.0	8.0
4	50.0	6.7	5.07
5	53.3	5.33	2.133
6	56.0	5.33	2.133

TABLE 23 End-of-fillet vortex core trajectory over the linear-fillet model in % chord length , AOA =10 deg.

No.	X/C	Y/C	Z/C
1	58.6	14.67	5.33
2	64.0	14.67	2.67
3	69.3	24.0	3.733
4	75.0	25.33	4.0
5	80.0	26.7	2.133
6	85.3	26.7	5.33
7	90.6	26.7	3.2

TABLE 24 End-of-fillet vortex core trajectory over the linear-fillet model in % chord length , AOA = 16 deg.

No.	X/C	Y/C	Z/X
1	58.6	14.67	0.533
2	64.0	19.33	2.67
3	69.3	16.7	4.8
4	75.0	13.33	8.0
5	80.0	12.0	4.267

TABLE 25 End-of-fillet vortex core trajectory over the linear-fillet model in % chord length , AOA =20 deg.

No.	X/C	Y/C	Z/C
1	58.6	14.67	0.533
2	64.0	20.0	13.33
3	69.3	16.0	8.0

TABLE 26 End-of-fillet vortex core trajectory over the linear-fillet model in % chord length , AOA = 22.5 deg.

No.	X/C	Y/C	Z/C
1	58.6	14.67	0.533
2	61.3	14.67	5.33

TABLE 27 Strake vortex breakdown location over the linear-fillet model in % chord length

AOA (deg)	X/C maximum	X/C minimum	X/C mean
10	98.67	93.33	96.0
16	93.33	88.0	90.0
20	69.33	61.33	65.0
22.5	61.33	50.67	56.0
26	50.67	34.67	43.0
30	37.33	32.0	34.7
35	32.0	21.3	26.7
40	24.0	18.67	21.3
45	18.67	13.33	16.0
50	12.0	9.33	10.6

TABLE 28 Beginning-of-fillet vortex breakdown location over the linear-fillet model in % chord length

AOA (deg)	X/C maximum	X/C minimum	X/C mean
16	88.0	82.67	88.0
20	72.0	67.0	69.3
22.5	67.0	61.33	64.0
26	61.3	56.0	58.6

TABLE 29 End-of-fillet vortex breakdown location over the linear-fillet model in % chord length

AOA (deg)	X/C maximum	X/C minimum	X/C mean
10	98.7	93.3	96.0
16	88.0	77.33	82.7
20	77.33	72.0	74.7
22.5	67.0	61.3	64.0

TABLE 30 Strake vortex core trajectory over the parabolic-fillet model in % chord length , AOA = 10 deg.

No.	X/C	Y/C	Z/C
1	10	1.333	1.333
2	15	2.67	.333
3	20	3.33	1.6
4	25	4.0	2.13
5	35	5.33	2.4
6	40	7.33	2.93
7	50	9.33	3.467
8	60	11.33	3.733
9	65	13.33	4.0
10	70	16.0	4.267
11	75	18.67	5.33
12	80	21.33	6.7
13	85	21.33	5.33
14	90	22.67	4.0
15	95	24.0	2.67

TABLE 31 Strake vortex core trajectory over the parabolic-fillet model in % chord length , AOA = 16 deg.

No.	X/C	Y/C	Z/C
1	10	1.33	1.33
2	20	3.33	1.6
3	25	4.0	2.13
4	30	4.67	2.67
5	35	5.33	2.93
6	40	7.33	3.04
7	45	8.0	3.467
8	50	9.33	3.73
9	55	10.0	4.0
10	60	10.67	4.267
11	65	11.33	4.8
12	70	14.67	5.33
13	75	18.0	6.4
14	80	18.67	7.47
15	85.33	18.67	4.0

TABLE 32 Strake vortex core trajectory over the parabolic-fillet model in% chord length , AOA = 20 deg.

No.	X/C	Y/C	Z/C
1	10	1.33	1.33
2	20	3.33	1.75
3	22.5	3.67	2.0
4	25	4.0	2.67
5	28	4.67	2.93
6	30	5.0	3.2
7	33	5.33	3.41
8	37	6.0	3.63
9	40	7.33	4.05
10	45	8.0	4.267
11	50	8.67	4.48
12	53	9.33	4.693
13	57	10.0	4.91
14	60	10.0	5.12
15	61.33	10.67	5.33

TABLE 33 Strake vortex core trajectory over the parabolic-fillet model in % chord length , AOA = 22.5 deg.

No.	X/C	Y/C	Z/C
1	10	1.33	1.33
2	15	2.67	1.33
3	20	3.33	1.75
4	22.5	3.67	2.133
5	25	4.0	2.67
6	27	4.0	2.99
7	30	4.67	3.125
8	32	5.33	3.2
9	34	5.67	3.41
10	36	6.0	3.52
11	40	6.7	3.63
12	42	7.33	3.73
13	44	7.67	3.84
14	46	8.0	3.95
15	50.6	8.0	4.267

TABLE 34 Strake vortex core trajectory over the parabolic-fillet model in % chord length , AOA = 30 deg.

No.	X/C	Y/C	Z/C
1	10	1.33	0.533
2	12	1.33	0.672
3	14	2.0	0.747
4	16	2.25	1.0
5	18	2.75	1.493
6	20	3.0	1.706
7	22.5	3.5	2.0
8	25	3.75	2.25
9	26	3.8	2.67
10	27	4.0	2.8
11	28	4.33	2.848
12	29	4.67	2.88
13	30	4.67	2.9013

TABLE 35 Beginning-of-fillet vortex core trajectory over the parabolic-fillet model in % chord length , AOA = 10 deg.

No.	X/C	Y/C	Z/C
1	42.7	12.0	0.533
2	45.3	10.67	1.333
3	48	9.33	4.0
4	53.3	8.0	3.2
5	56	8.0	2.13
6	58.6	9.33	4.0
7	61	12.0	5.33
8	64	16.0	4.533
9	69.3	18.67	4.0
10	72	21.33	3.73
11	75	21.33	3.2
12	90	22.67	2.67
13	93.3	22.67	2.67

TABLE 36 Beginning-of-fillet vortex core trajectory over the parabolic-fillet model in % chord length , AOA = 16 deg.

No.	X/C	Y/C	Z/C
1	42.7	12.0	0.533
2	45.3	10.0	2.67
3	50	8.0	5.33
4	53.3	6.7	4.0
5	56	8.0	2.67
6	58.6	10.67	4.0
7	64	15.33	6.4
8	69.3	16.0	9.33
9	72	14.67	5.33
10	75	14.67	4.0
11	80	14.67	3.2

TABLE 37 Beginning-of-fillet vortex core trajectory over the parabolic-fillet model in % chord length , AOA = 20 deg.

No.	X/C	Y/C	Z/C
1	42.7	12.0	0.533
2	45.3	10.0	2.67
3	50	7.33	8.53
4	53.3	6.7	6.4
5	58.6	6.0	4.267
6	61	8.0	3.2
7	64	10.67	2.67

TABLE 38 Beginning-of-fillet vortex core trajectory over the parabolic-fillet model in % chord length , AOA = 22.5 deg.

No.	X/C	Y/C	Z/C
1	42.7	12.0	0.533
2	45.3	10.0	4.0
3	48	10.67	10.67
4	50	6.7	7.47
5	53.3	6.0	5.33
6	56	5.33	3.2

TABLE 39 End-of-fillet vortex core trajectory over the parabolic-fillet model in % chord length , AOA = 10 deg.

No.	X/C	Y/C	Z/C
1	67	29.33	0.533
2	69.3	28.67	3.2
3	72	28.0	8.0

TABLE 40 End-of-fillet vortex core trajectory over the parabolic-fillet model in % chord length , AOA = 16 deg.

No.	X/C	Y/C	Z/C
1	67	29.33	0.533
2	68	30.0	2.67
3	69.3	30.67	5.33

TABLE 41 Strake vortex breakdown location over the parabolic-fillet model in % chord length

AOA (deg)	X/C maximum	X/C minimum	X/C mean
16	90.67	85.33	88.0
20	69.33	64.0	67.0
22.5	61.33	50.67	56.0
26	53.33	42.67	48.0
30	37.33	26.7	32.0
35	32.0	21.33	26.7
40	24.0	13.33	18.67
45	21.33	10.67	16.0
50	14.67	12.0	13.33

TABLE 42 Beginning-of-fillet vortex breakdown location over the parabolic-fillet model in % chord length

AOA (deg)	X/C maximum	X/C minimum	X/C mean
16	88.0	82.67	85.33
20	77.33	67.0	72.0
22.5	69.33	58.67	64.0

TABLE 43 End-of-fillet vortex breakdown location over the parabolic-fillet model in % chord length

AOA (deg)	X/C maximum	X/C minimum	X/C mean
5	85.33	80.0	82.67
10	82.67	72.0	77.33
16	74.67	69.33	72.0

TABLE 44 Strake vortex core trajectory over the diamond-fillet model in % chord length , AOA = 10 deg.

No.	X/C	Y/C	Z/C
1	10	1.33	1.33
2	15	2.67	1.33
3	20	3.33	1.6
4	25	4.0	2.13
5	35	5.33	2.347
6	40	7.33	2.67
7	50	8.67	2.67
8	60	11.33	2.93
9	65	12.0	3.2
10	70	14.67	3.467
11	75	17.33	3.733
12	80	20.0	4.267
13	85	21.33	4.8
14	90	22.0	5.33
15	95	22.67	6.933

TABLE 45 Strake vortex core trajectory over the diamond-fillet model in % chord length , AOA = 16 deg.

No.	X/C	Y/C	Z/C
1	10	1.33	1.33
2	20	3.33	1.6
3	30	4.0	2.67
4	35	4.67	2.93
5	40	6.7	3.04
6	45	7.33	3.2
7	50	8.0	3.733
8	55	8.67	3.2
9	60	11.33	4.0
10	65	13.33	4.8
11	70	14.67	5.33
12	75	16.0	5.867
13	80	18.67	6.4
14	85.33	21.33	7.46
15	88	22.67	8.0

TABLE 46 Strake vortex core trajectory over the diamond-fillet model in % chord length , AOA = 20 deg.

No.	X/C	Y/C	Z/C
1	10	1.33	1.333
2	20	3.333	1.6
3	25	4.0	2.13
4	30	5.0	2.67
5	33	5.333	2.83
6	37	6.0	2.99
7	40	6.7	3.04
8	45	7.67	3.2
9	50	8.0	3.47
10	53	8.67	3.73
11	57	10.33	4.267
12	61.3	12.0	4.8
13	65	12.67	5.33
14	67	13.33	6.933

TABLE 47 Strake vortex core trajectory over the diamond-fillet model in % chord length , AOA =22.5 deg.

No.	X/C	Y/C	Z/C
1	10	1.33	1.33
2	15	2.67	1.33
3	20	3.33	1.75
4	25	4.0	2.67
5	30	4.67	3.125
6	37	6.0	3.47
7	40	6.7	3.73
8	45	7.33	4.267
9	50	7.67	4.8
10	53.3	8.0	5.33

TABLE 48 Strake vortex core trajectory over the diamond-fillet model in % chord length , AOA = 30 deg.

No.	X/C	Y/C	Z/C
1	10	1.33	0.533
2	12	1.33	0.672
3	14	2.0	0.747
4	16	2.25	1.0
5	18	2.75	1.5
6	20	3.0	1.71
7	25	3.75	2.25
8	27	4.0	2.8
9	32	5.0	2.933
10	35	5.33	2.933

TABLE 49 Beginning-of-fillet vortex core trajectory over the diamond-fillet model in % chord length , AOA = 10 deg.

No.	X/C	Y/C	Z/C
1	46.7	12.0	0.533
2	50	10.67	2.67
3	60	9.33	5.33
4	65	11.33	4.267
5	70	16.7	4.0
6	75	18.67	5.33
7	80	16.0	8.0
8	85	21.33	5.33
9	90	21.33	4.0
10	95	21.33	2.67

TABLE 50 Beginning-of-fillet vortex core trajectory over the diamond-fillet model in % chord length , AOA = 16 deg.

No.	X/C	Y/C	Z/C
1	46.7	12.0	0.533
2	50	9.33	2.67
3	53.3	8.0	4.8
4	56	7.33	6.93
5	58.6	6.7	5.867
6	64	13.33	4.0
7	69.3	16.0	5.33
8	72	14.67	9.1
9	75	14.67	5.867
10	77.3	14.67	3.2

TABLE 51 Beginning-of-fillet vortex core trajectory over the diamond-fillet model in % chord length , AOA = 20 deg.

No.	X/C	Y/C	Z/C
1	46.7	12.0	0.533
2	50	8.67	4.0
3	53.3	8.0	8.0
4	56	6.7	5.33
5	58.6	8.0	2.67
6	64	13.33	5.867
7	69.3	14.67	9.1
8	72	13.33	5.33
9	75	13.33	2.67

TABLE 52 Beginning-of-fillet vortex core trajectory over the diamond-fillet model in % chord length , AOA = 22.5 deg.

No.	X/C	Y/C	Z/C
1	46.7	12.0	0.533
2	50	8.0	2.67
3	53.3	6.7	6.933
4	56	6.0	10.67
5	58.6	6.7	8.0
6	61.3	9.33	5.33
7	64	10.67	2.67

TABLE 53 End-of-filletlet vortex core trajectory over the diamond-filletlet model in % chord length , AOA = 10 deg.

No.	X/C	Y/C	Z/C
1	57.3	17.33	0.533
2	58.6	18.67	2.67
3	64.0	16.0	5.33
4	69.3	14.67	4.0
5	72	16.0	3.467
6	75	17.33	2.67
7	80	24.0	3.733

TABLE 54 End-of-filletlet vortex core trajectory over the diamond-filletlet model in % chord length , AOA = 16 deg.

No.	X/C	Y/C	Z/C
1	57.3	17.33	0.533
2	58.6	16.0	2.67
3	61.3	16.0	5.333
4	64	14.67	6.4
5	67	14.67	8.0
6	69.3	13.33	5.333
7	72	14.67	4.0
8	75	16.0	5.333

TABLE 55 End-of-fillet vortex core trajectory over the diamond-fillet in % chord length , AOA = 20 deg.

No.	X/C	Y/C	Z/C
1	57.3	17.33	0.533
2	58.6	16.0	2.67
3	61.3	14.67	5.33
4	64	13.33	9.33
5	67	12.0	4.267
6	69.3	10.67	4.8

TABLE 56 End-of-fillet vortex core trajectory over the diamond-fillet model in % chord length , AOA= 22.5 deg.

No.	X/C	Y/C	Z/C
1	57.3	17.33	0.533
2	58.6	16.7	5.333

TABLE 57 Strake vortex breakdown location over the diamond-fillet model in % chord length

AOA (deg)	X/C maximum	X/C minimum	X/C mean
10	99	97.33	98.7
16	96	90.67	93.3
20	74.7	69.33	72.0
22.5	64.0	53.33	58.67
26	53.33	48.0	50.67
30	45.33	34.67	40.0
35	40.0	29.33	34.67
40	26.7	21.33	24.0
45	21.33	16.0	18.67
50	17.33	12.0	14.67

TABLE 58 Beginning-of-fillet vortex breakdown location over the diamond-fillet model in % chord length

AOA (deg)	X/C maximum	X/C minimum	X/C mean
10	99	97.33	98.7
16	88	82.67	85.33
20	82.67	77.33	80.0
22.5	69.33	64.0	67.0
26	50.67	48.0	49.33

TABLE 59 End-of-fillet vortex breakdown location over the diamond-fillet model in % chord length

AOA (deg)	X/C maximum	X/C minimum	X/C mean
5	97.33	94.67	96.0
10	88.0	82.67	85.33
16	82.67	77.33	80.0
20	74.7	69.33	72.0
22.5	62.67	60.0	61.33

APPENDIX B EXPERIMENTAL RESULTS (PHOTOGRAPHS)

FIGURES (15 - 59)

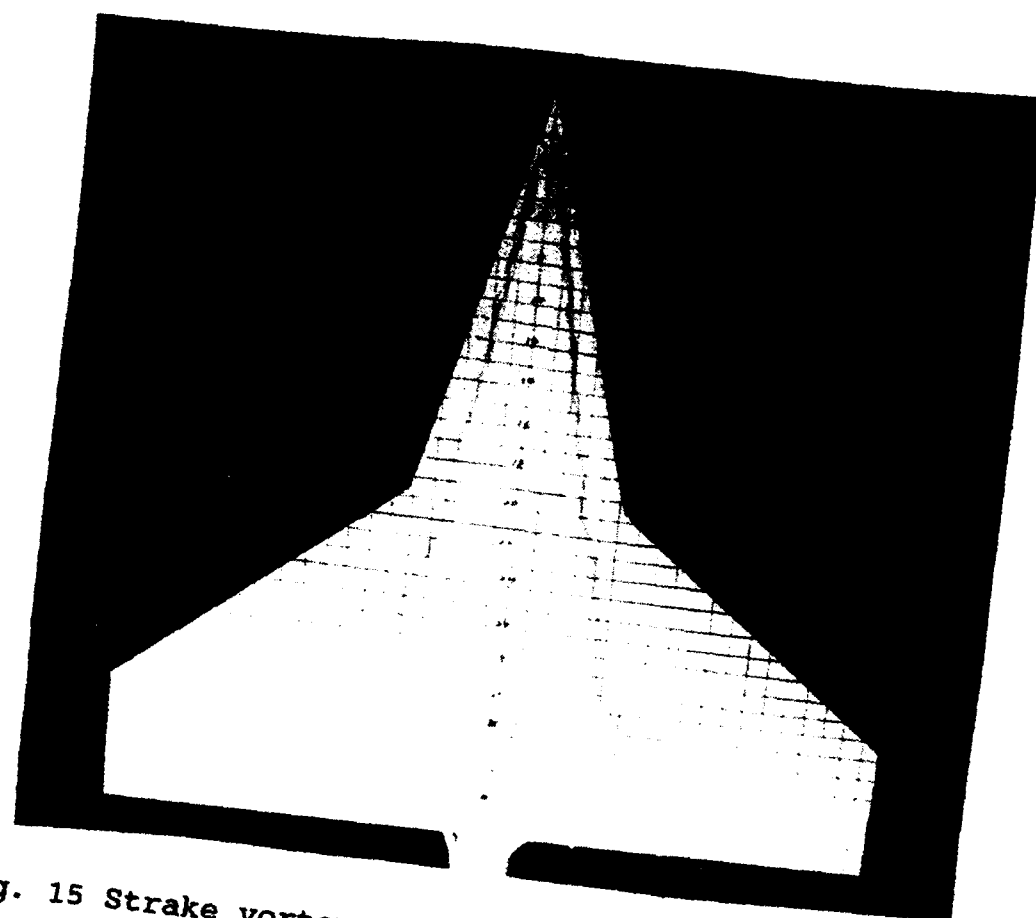
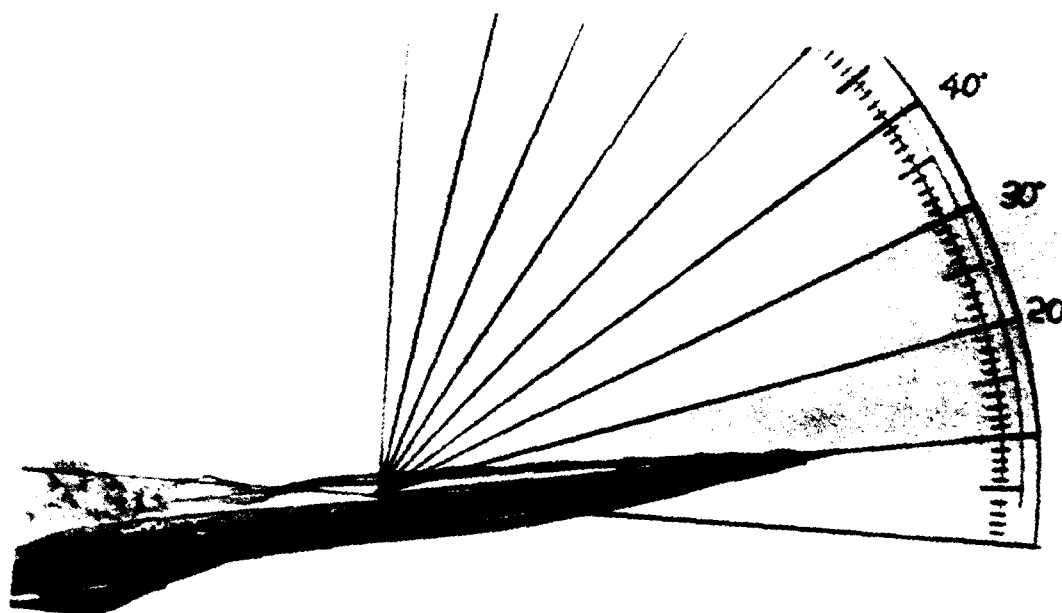


Fig. 15 Strake vortex , baseline model AOA = 16 deg

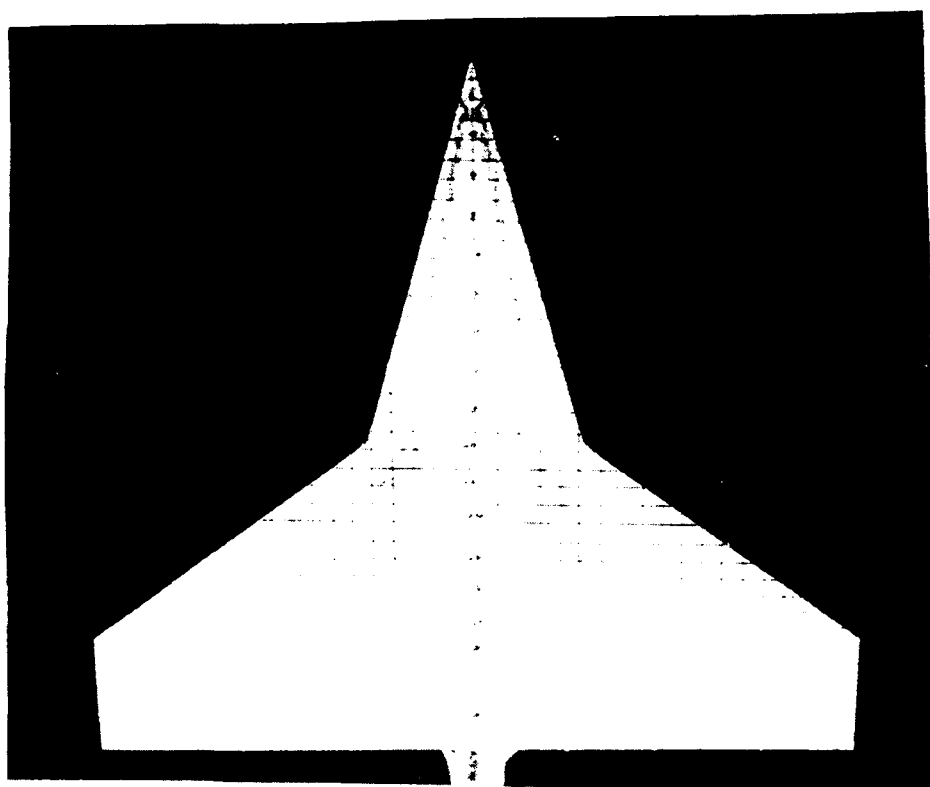
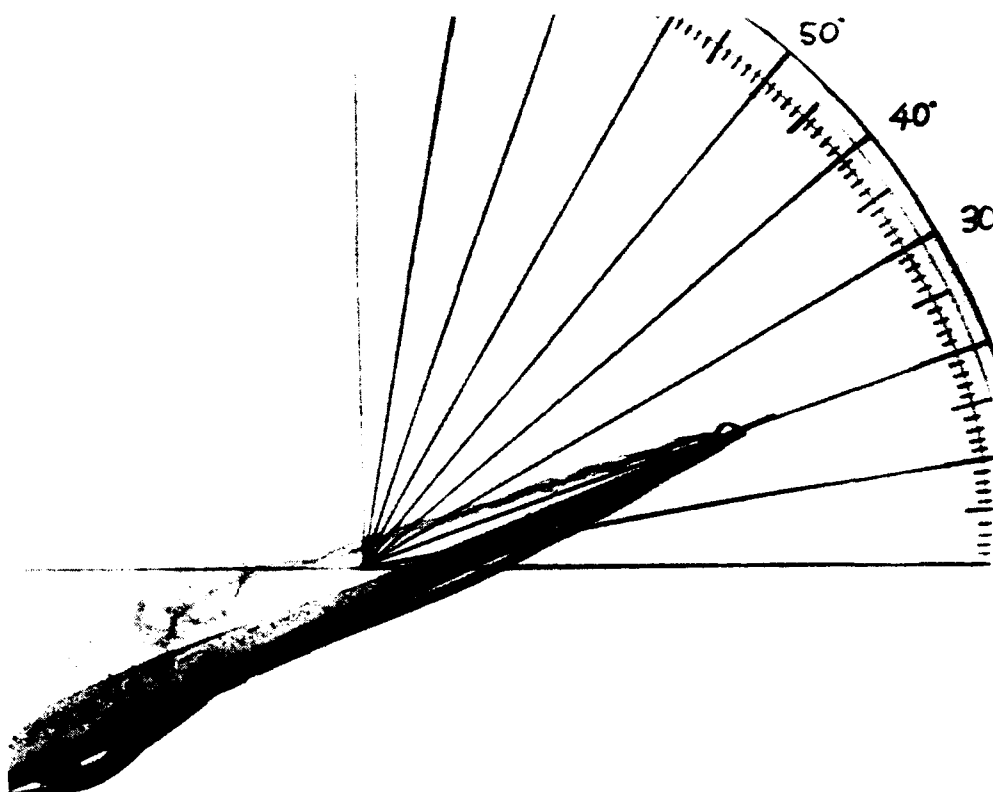


Fig. 16 Strake vortex , baseline model AOA = 22.5 deg

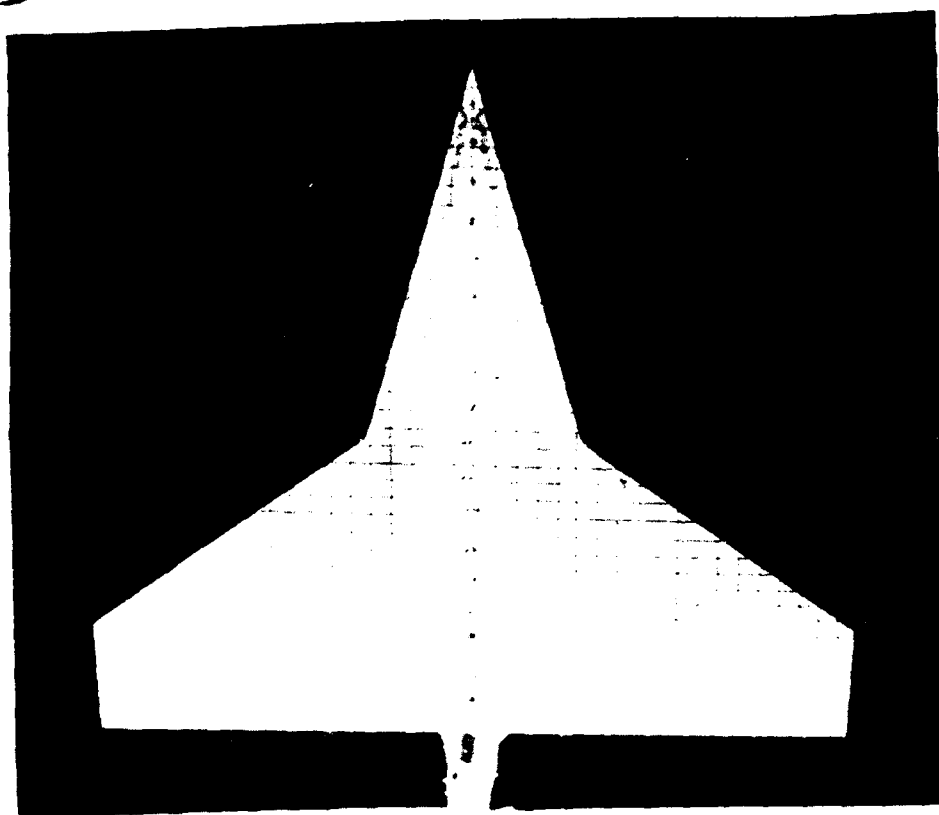
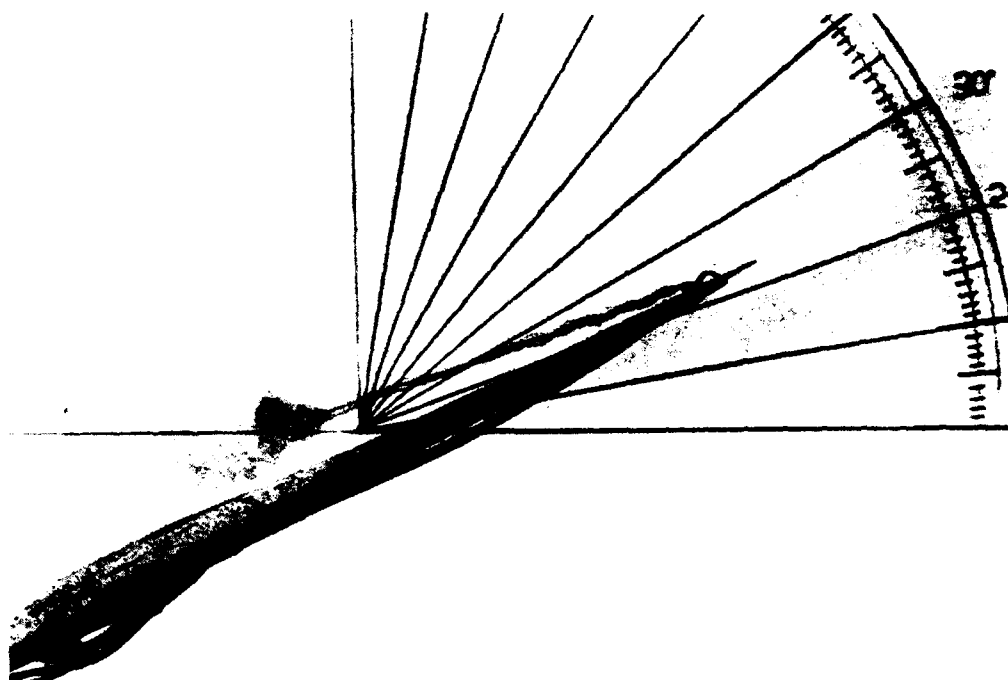


Fig. 17 Strake vortex , baseline model AOA = 26 deg

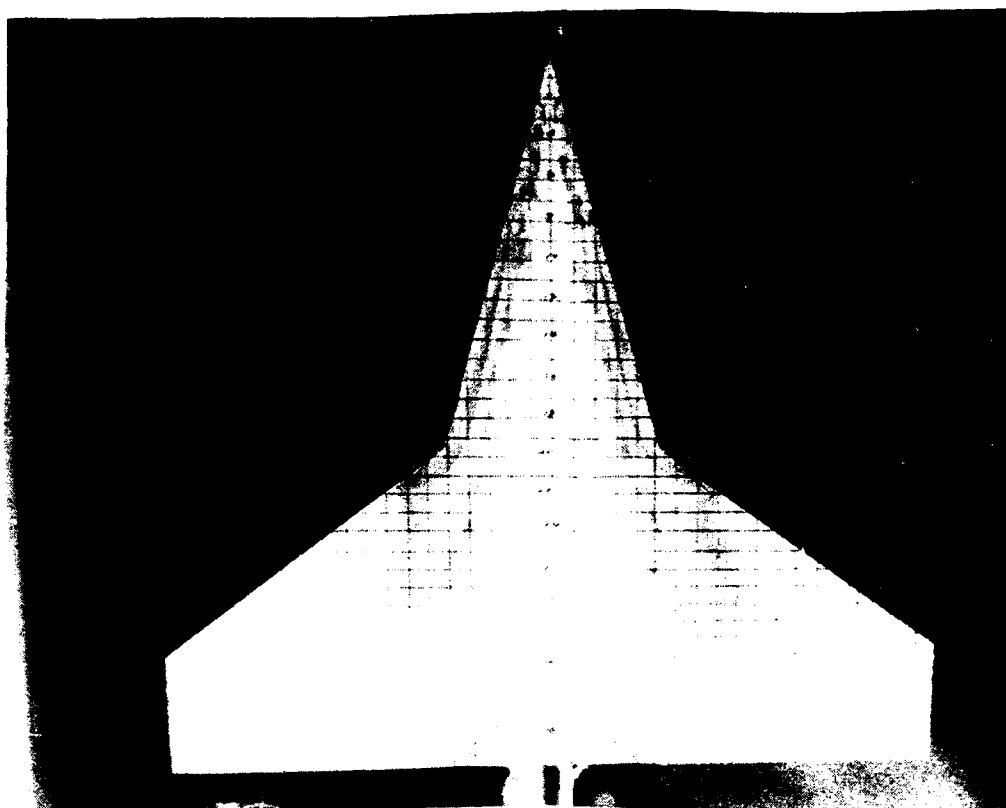
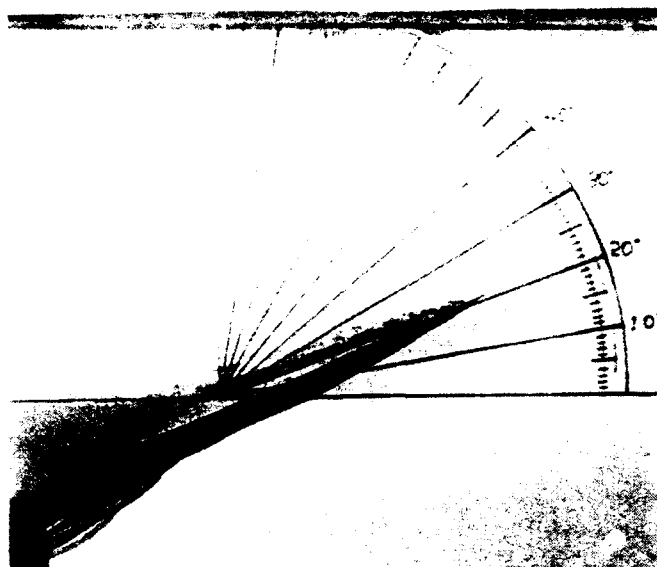


Fig. 18 Strake vortex , baseline model(dynamic, pitch-up)
AOA = 20 deg

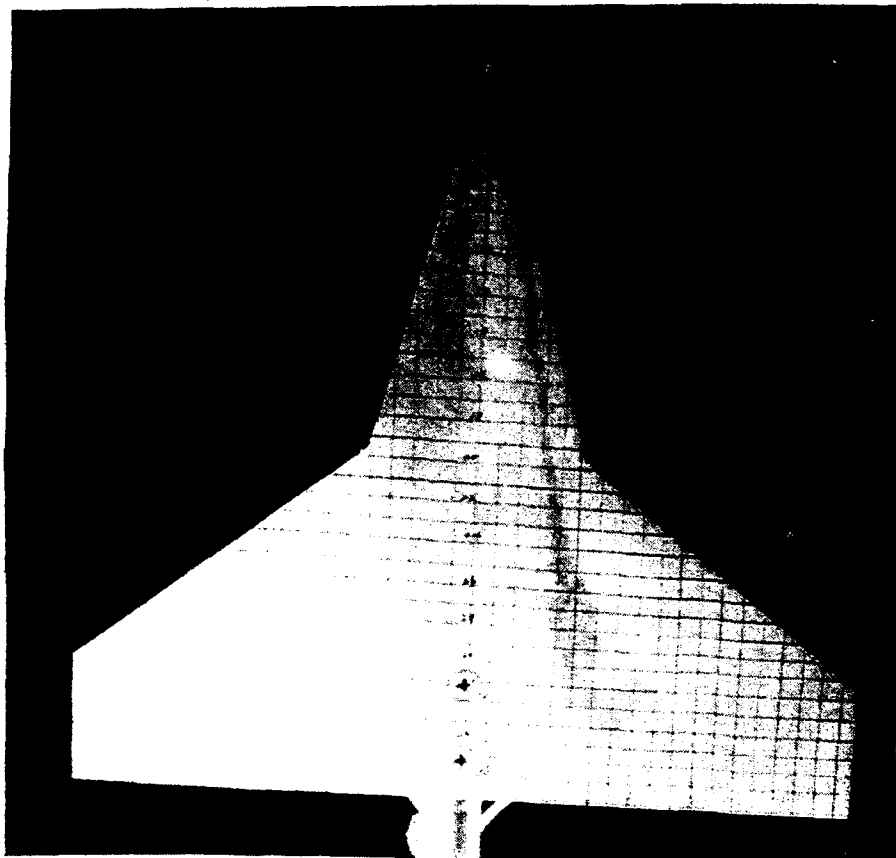
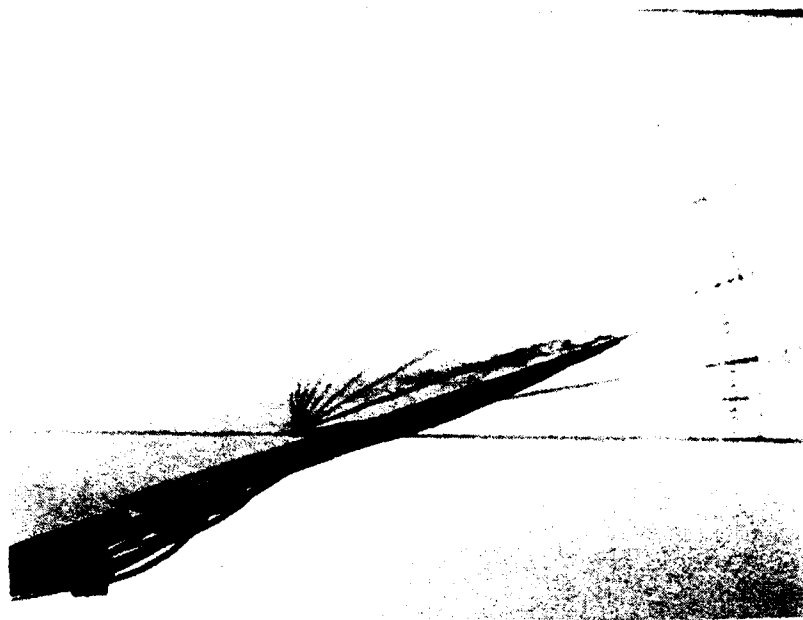


Fig. 19 Strake vortex , baseline model(dynamic, pitch-down)
AOA = 20 deg

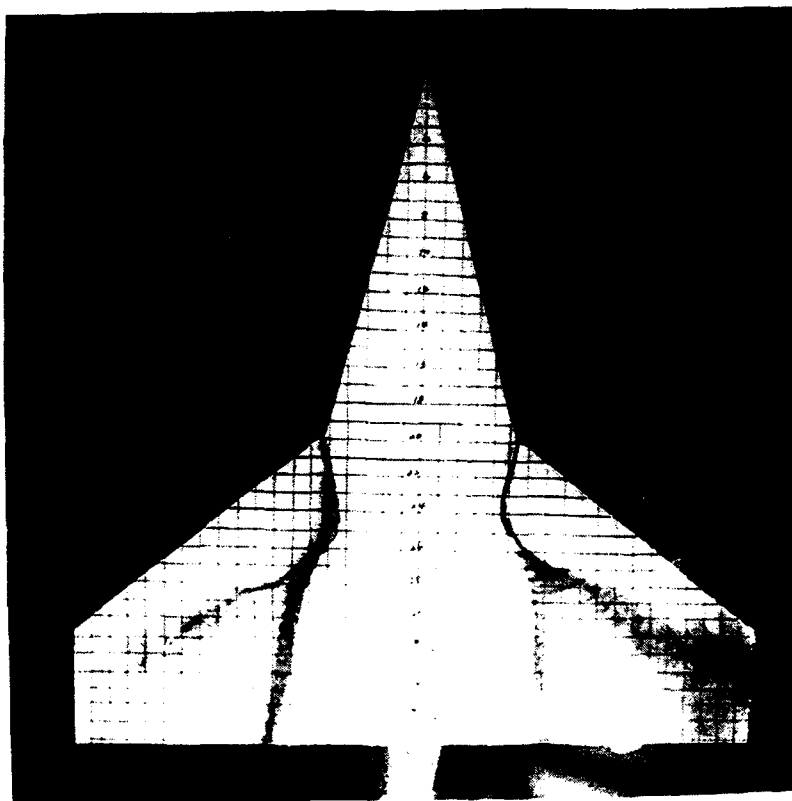
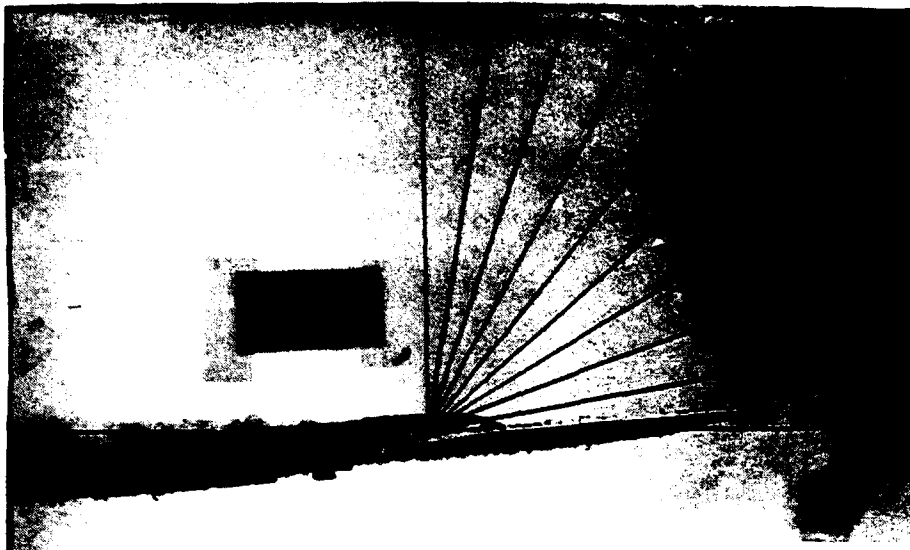


Fig. 20 Wing vortex , baseline model AOA = 5 deg

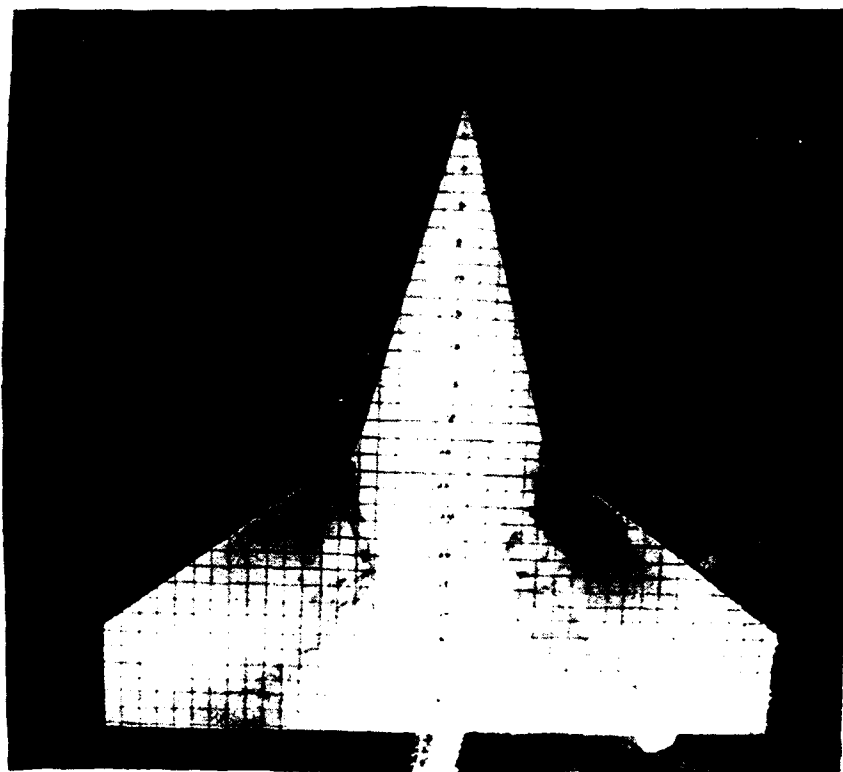


Fig. 21 Wing vortex , baseline model AOA = 20 deg

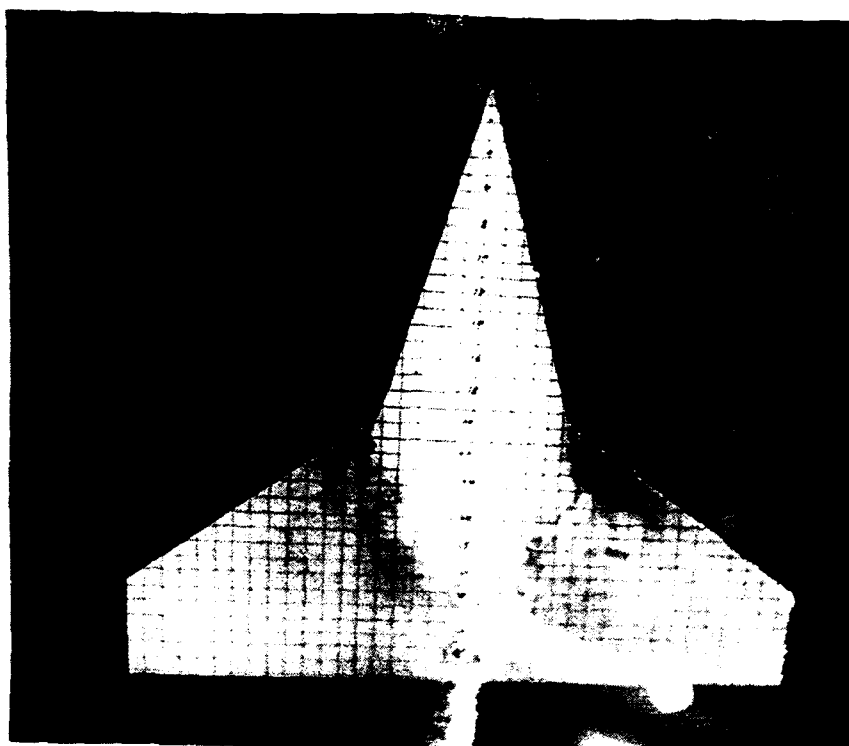
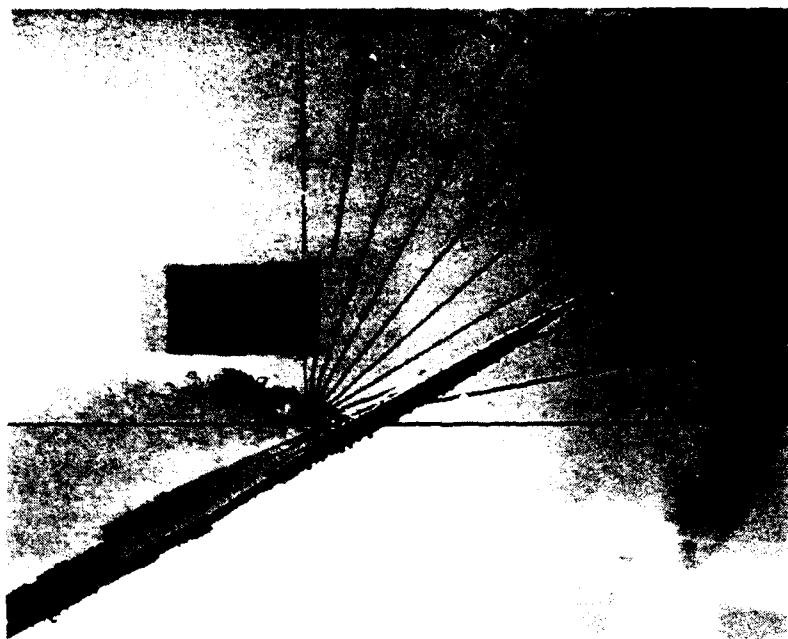


Fig. 22 Wing vortex , baseline model AOA = 26 deg

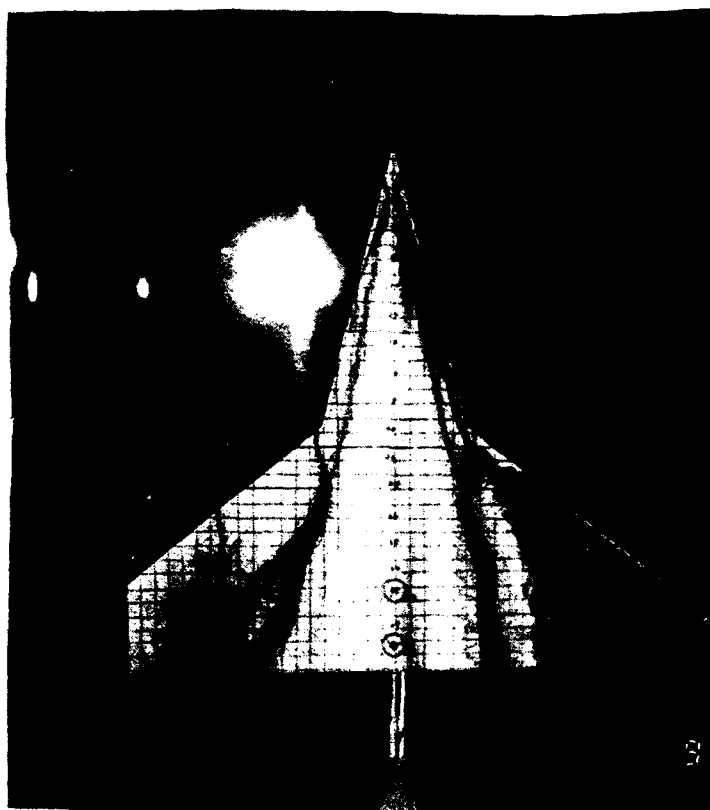
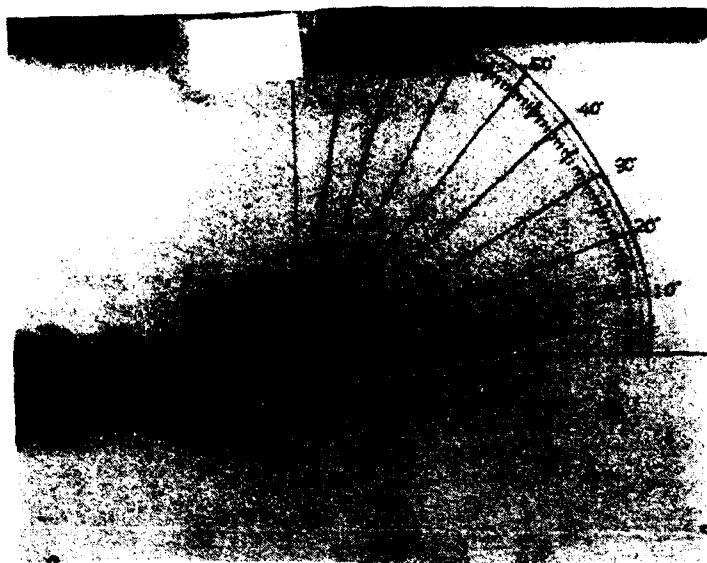


Fig. 23 Strake & Wing vortex , baseline model
AOA = 10 deg

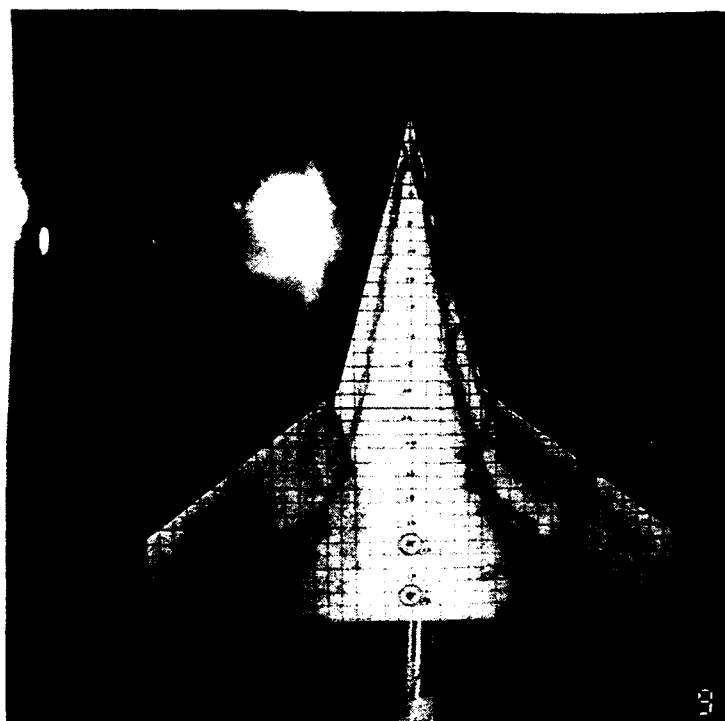
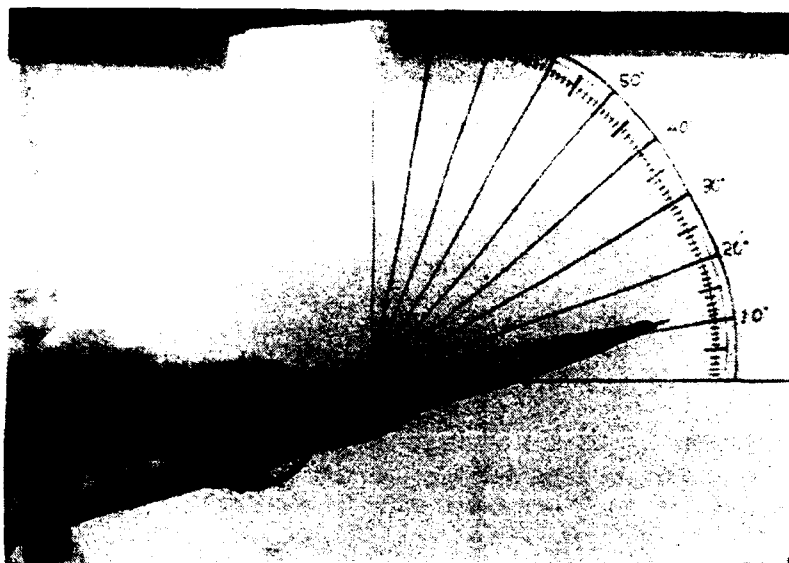


Fig. 24 Strake & Wing vortex , baseline model
AOA = 13 deg

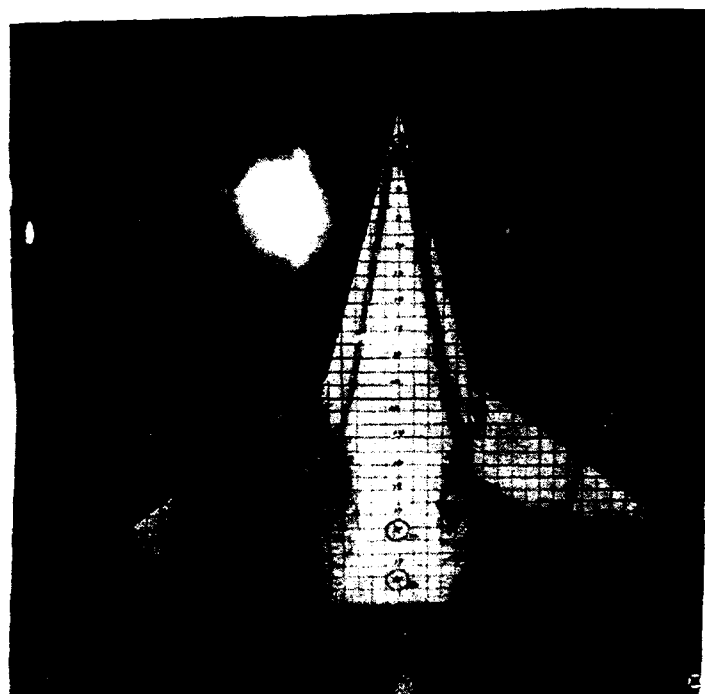
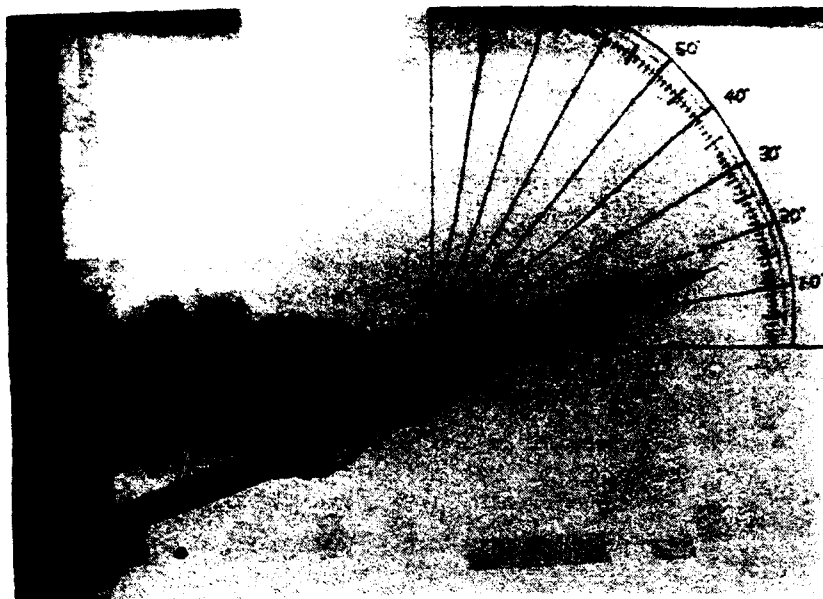


Fig. 25 Strake & Wing vortex , baseline model
AOA = 18 deg

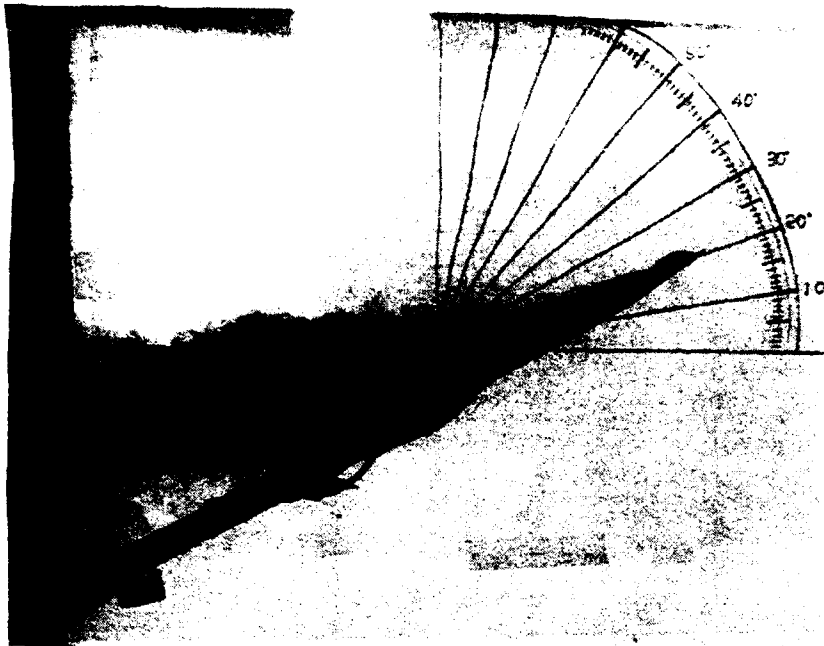


Fig. 26 Strake & Wing vortex , baseline model
AOA = 21 deg

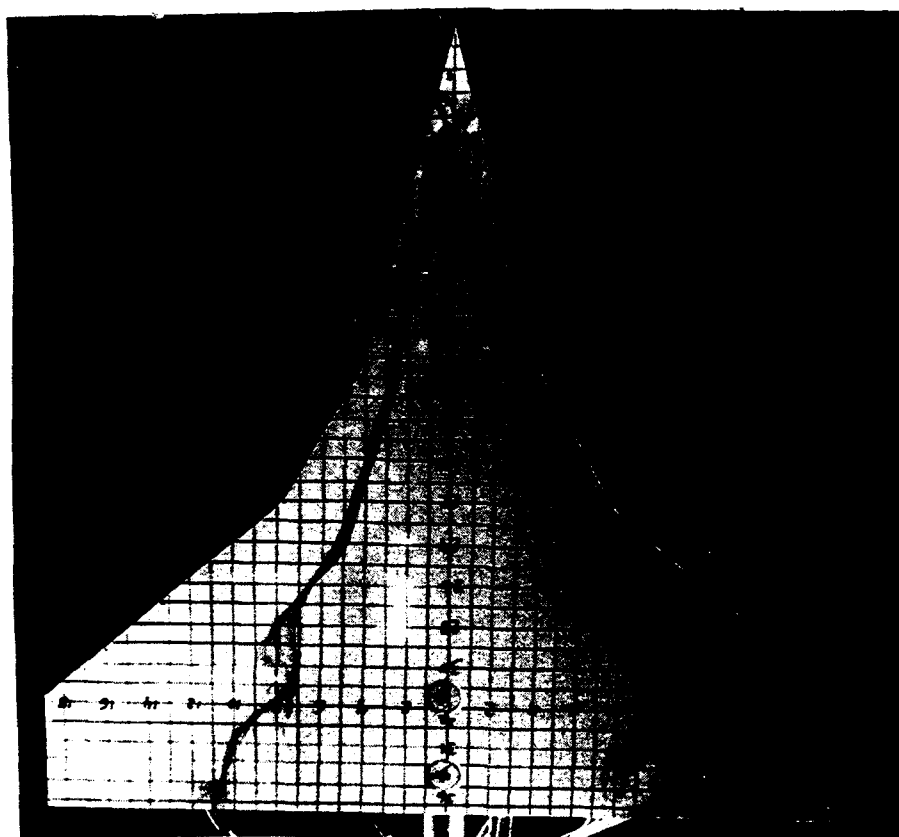
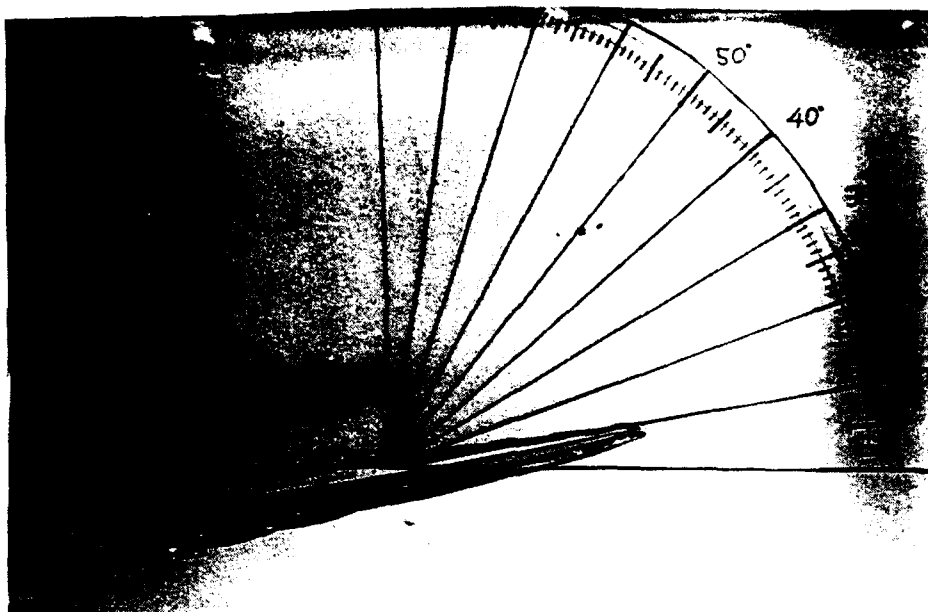


Fig. 27 Strake vortex , linear model AOA = 10 deg

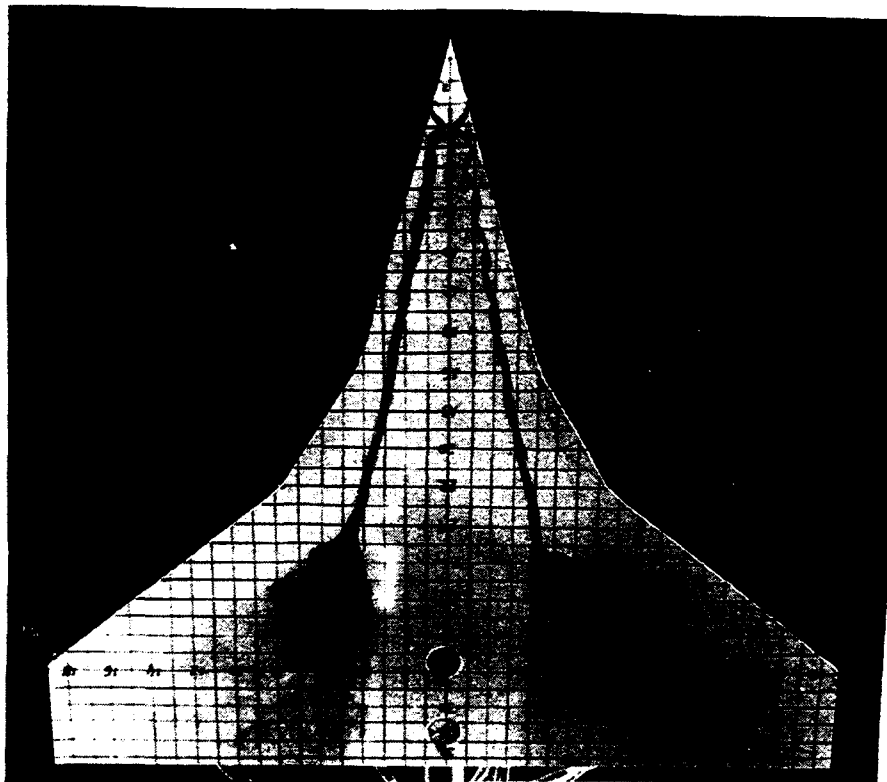
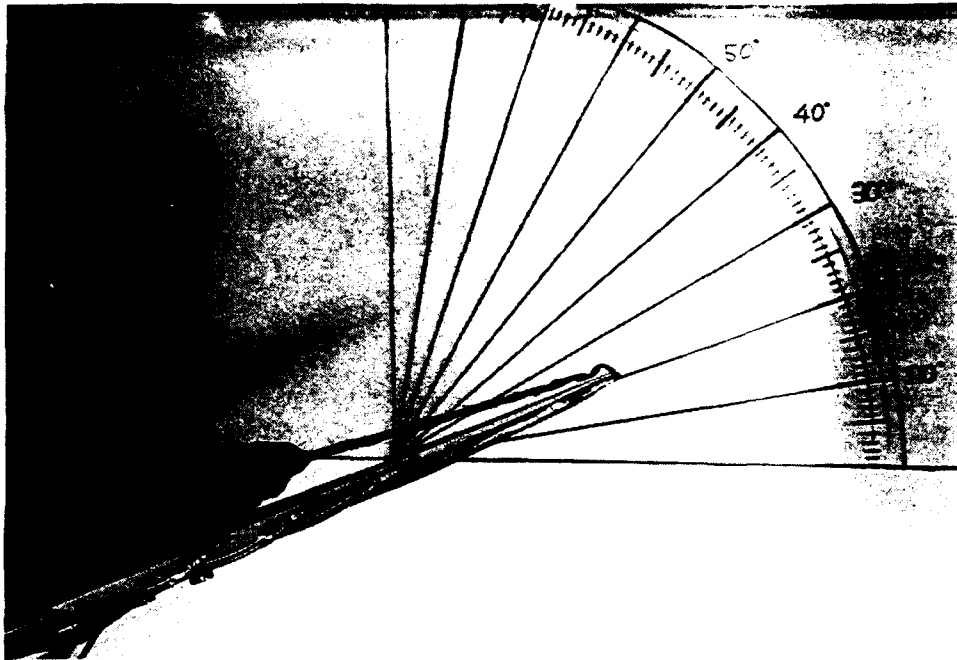


Fig. 28 Strake vortex , linear model AOA = 20 deg

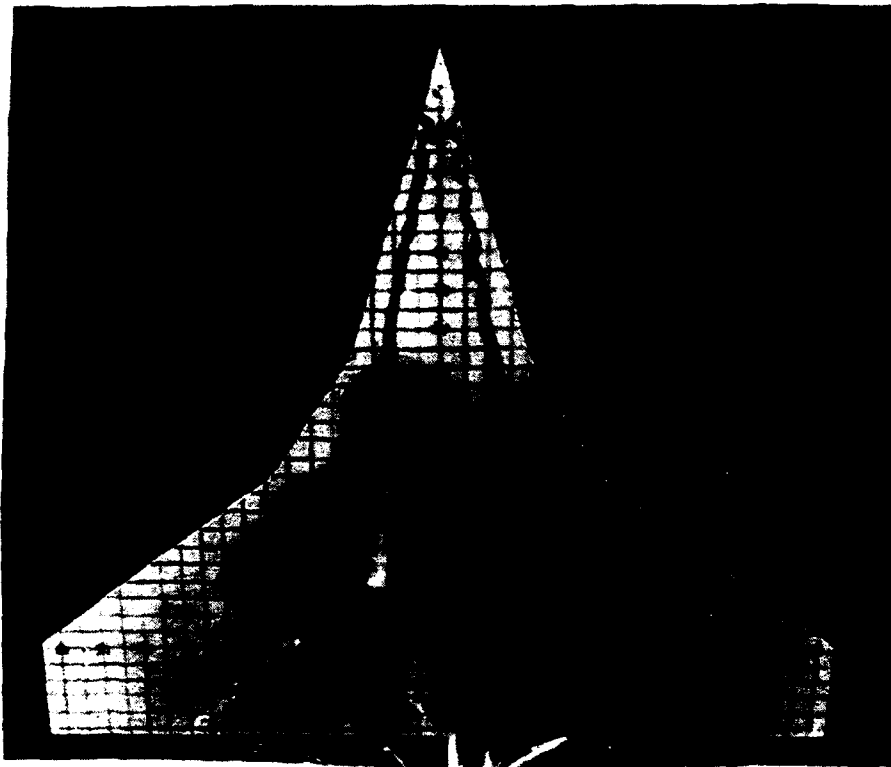
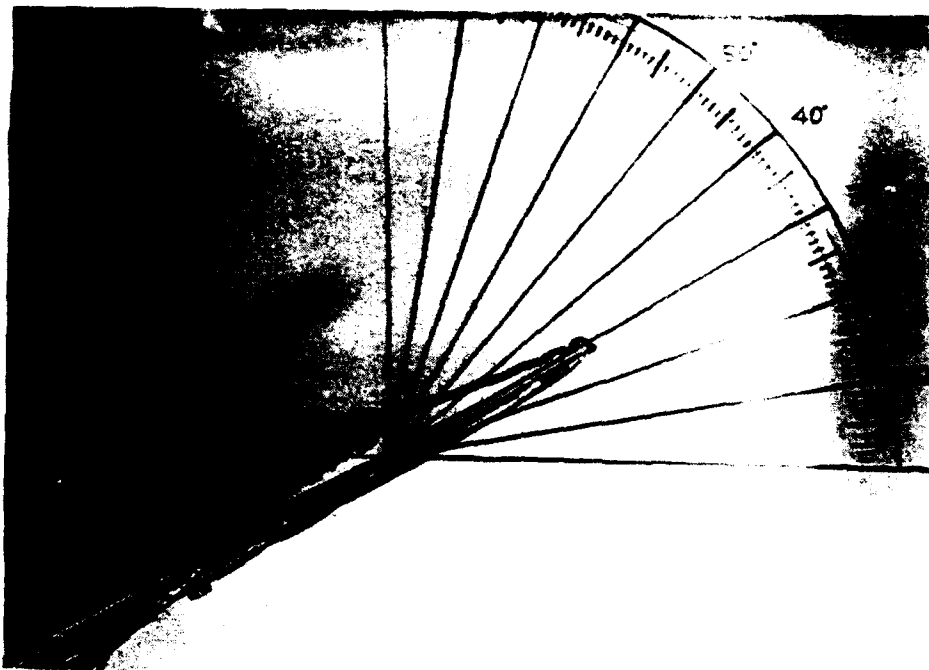


Fig. 29 Strake vortex , linear model AOA = 26 deg

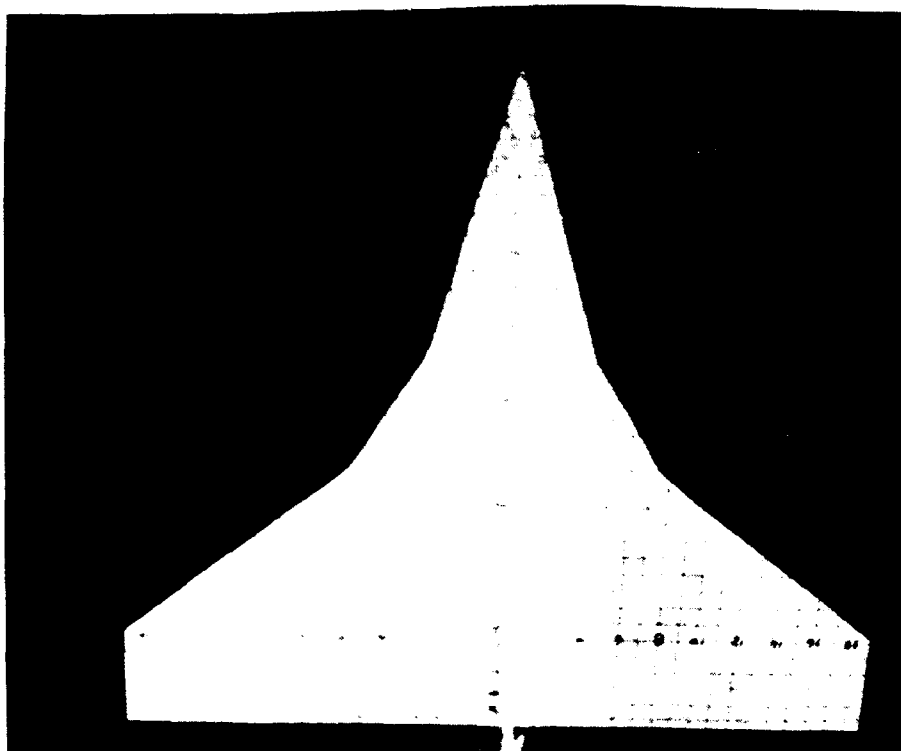
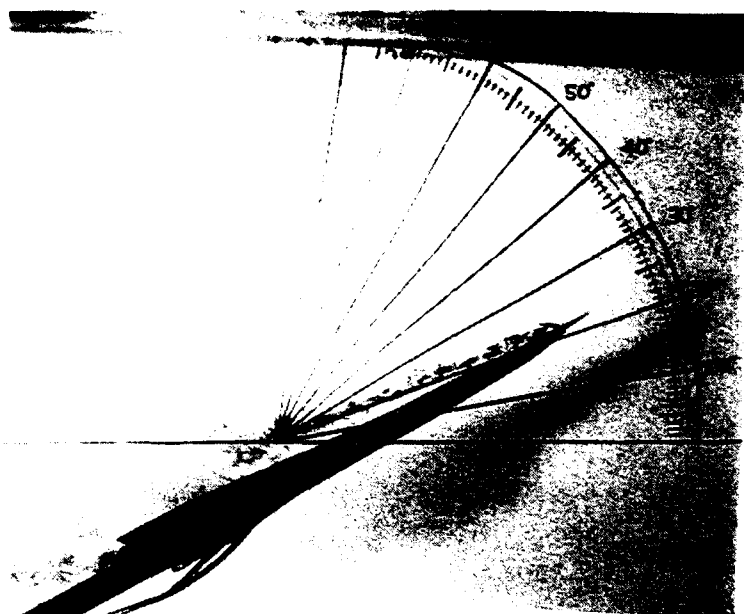


Fig. 30 Strake vortex , linear model (dynamic pitch-up)
AOA = 20 deg

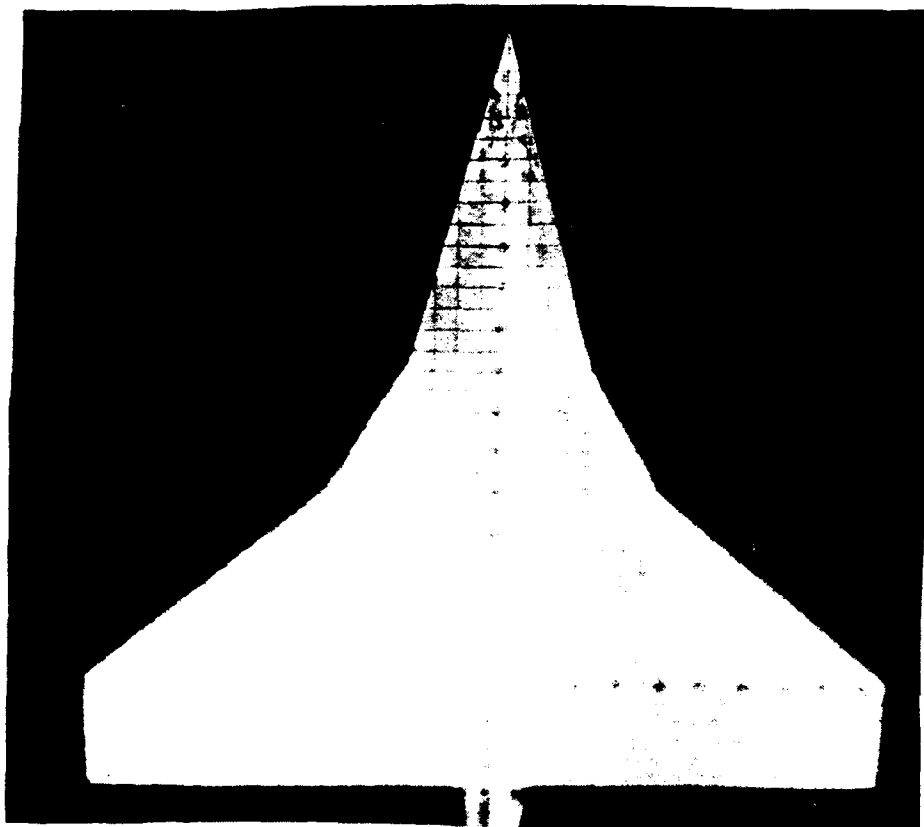
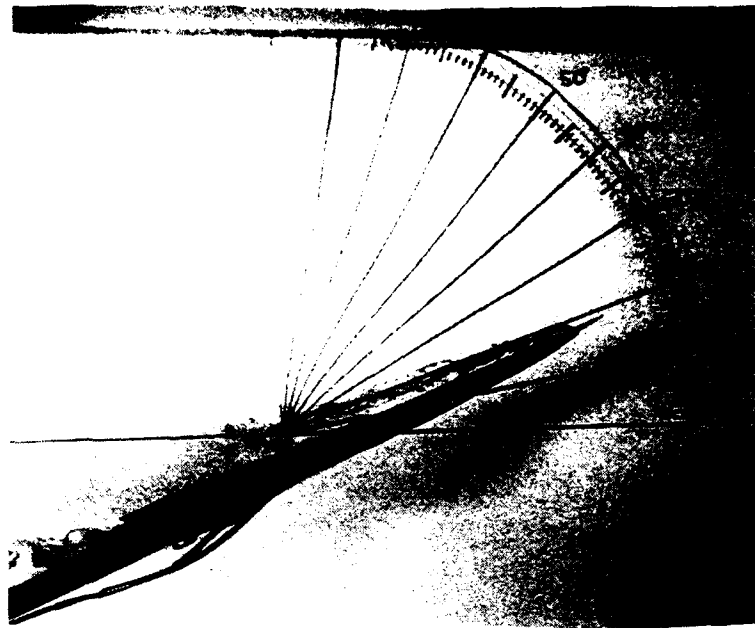


Fig. 31 Strake vortex , linear model (dynamic pitch-down)
AOA = 20 deg

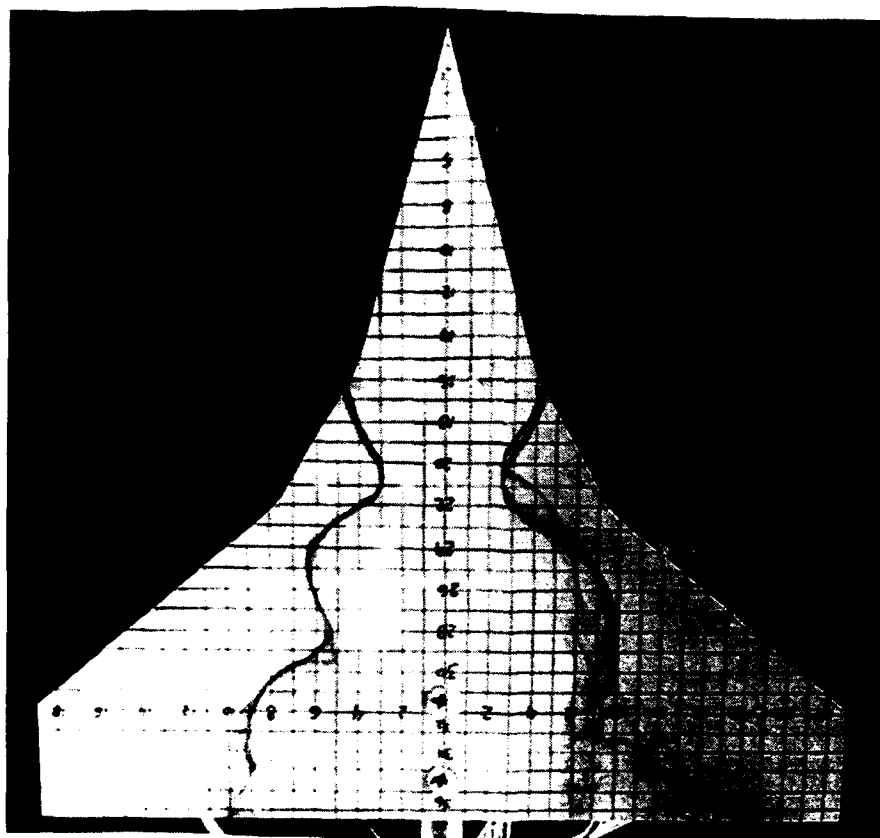
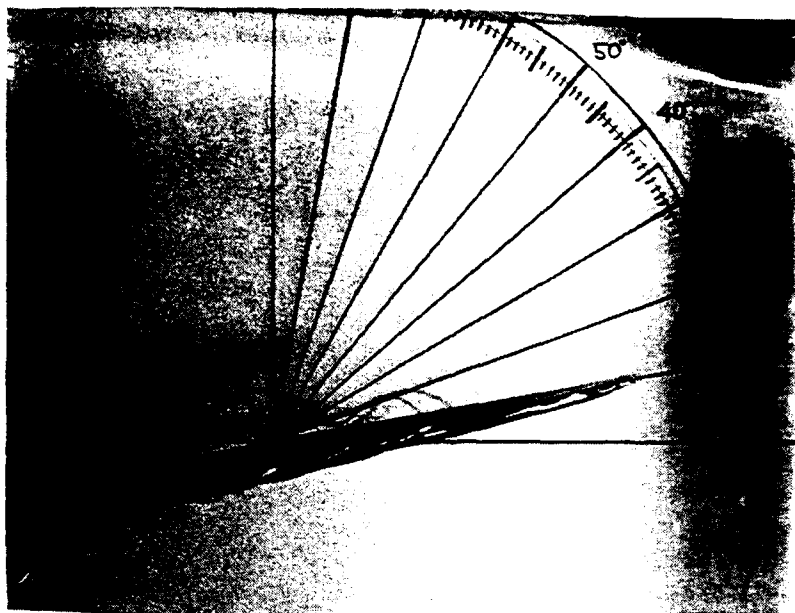


Fig. 32 Beginning-of-fillet vortex , linear model
AOA = 10 deg

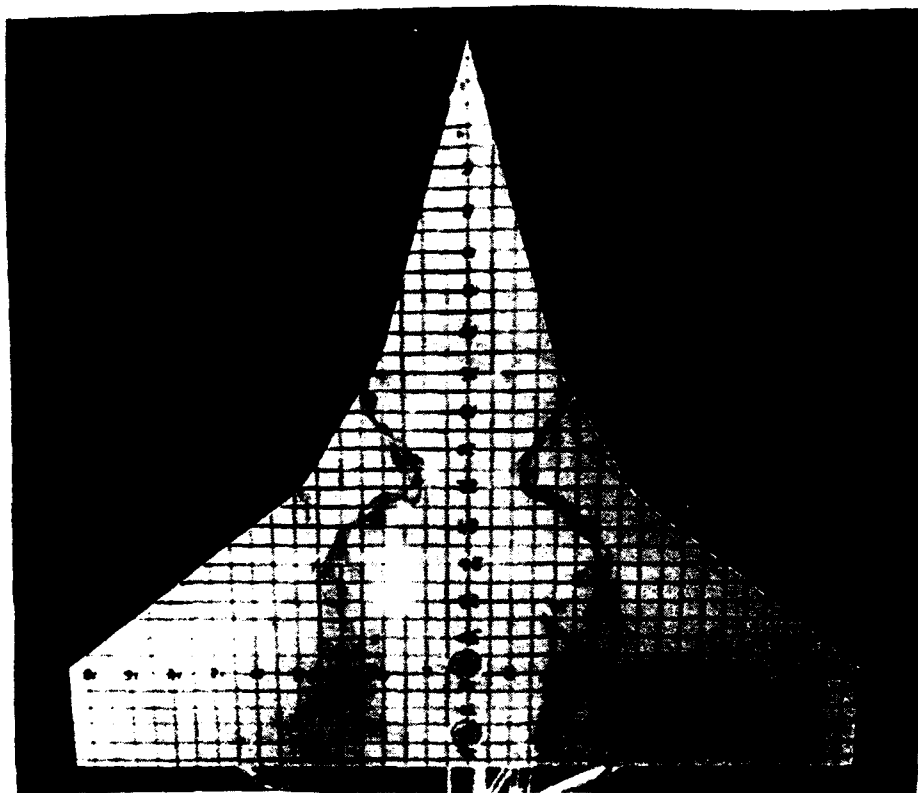
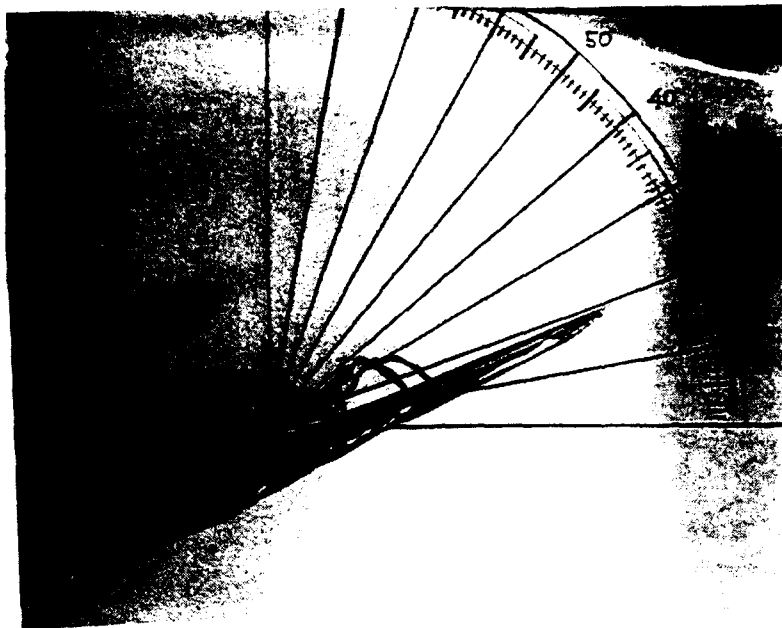


Fig. 33 Beginning-of-fillet vortex , linear model
 AOA = 20 deg

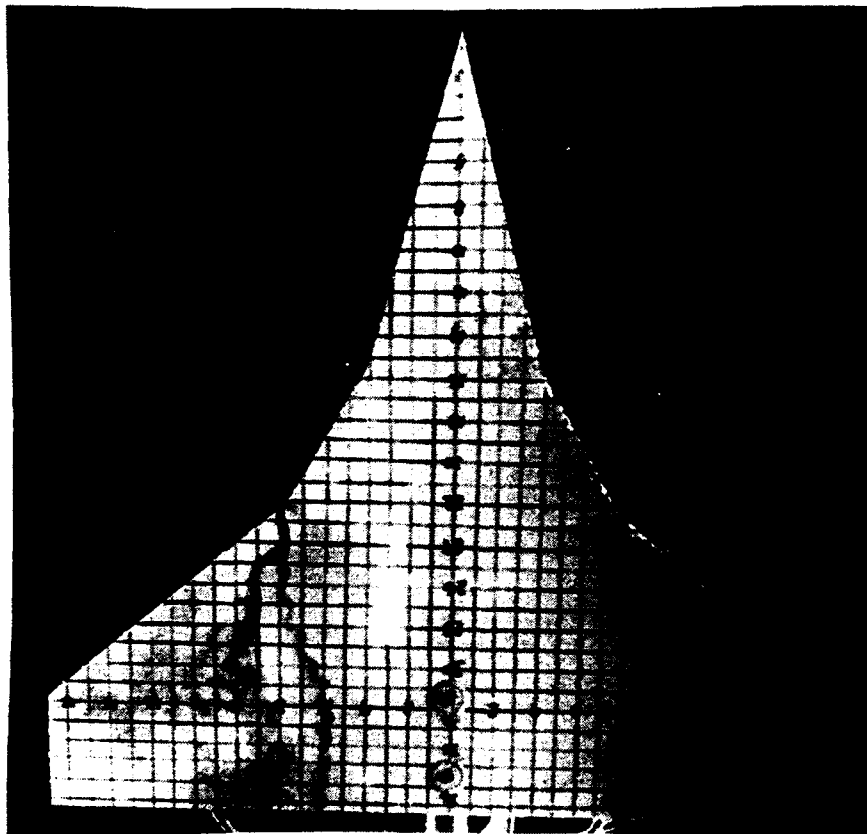
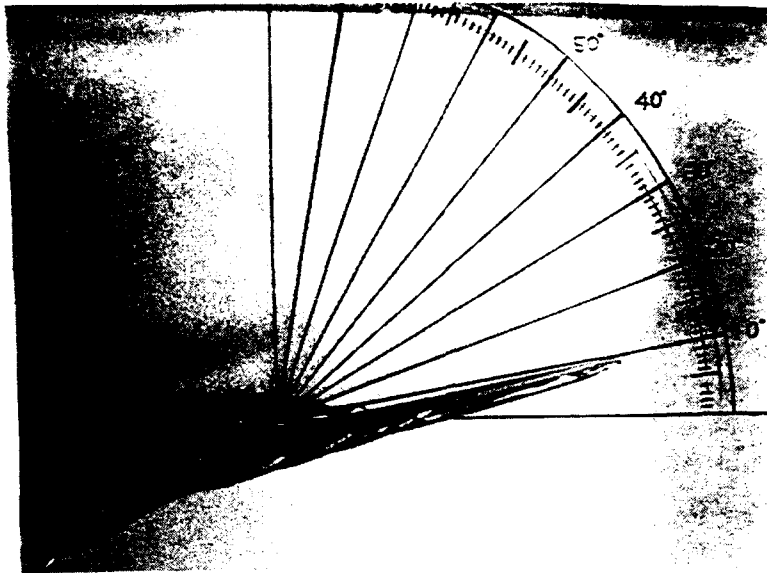


Fig. 34 End-of-fillet vortex , linear model AOA = 10 deg

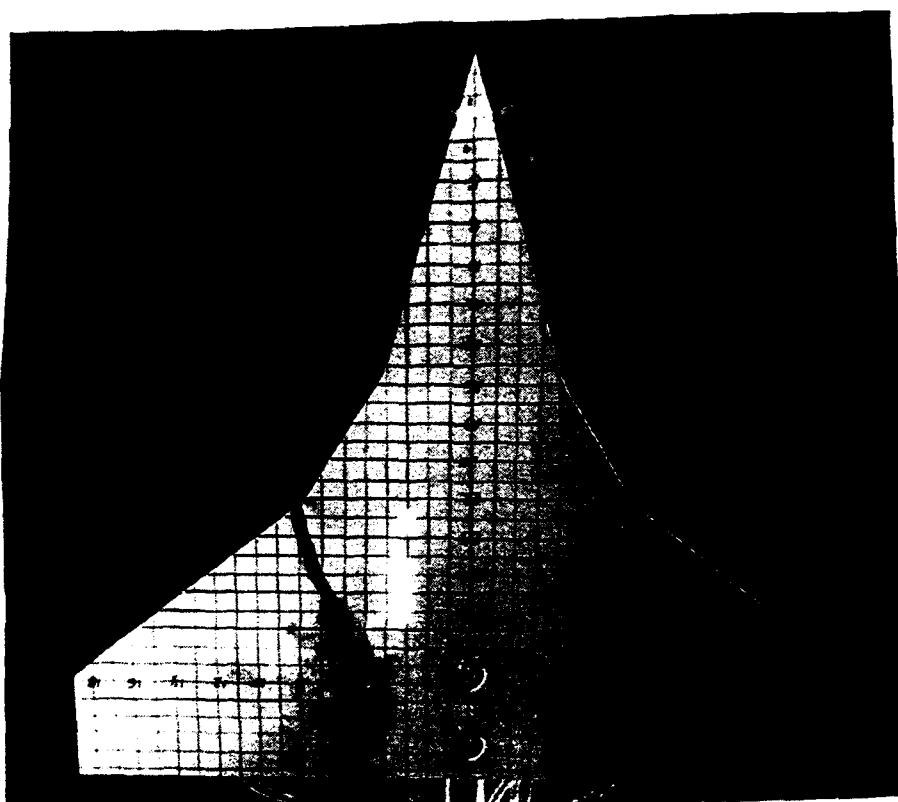
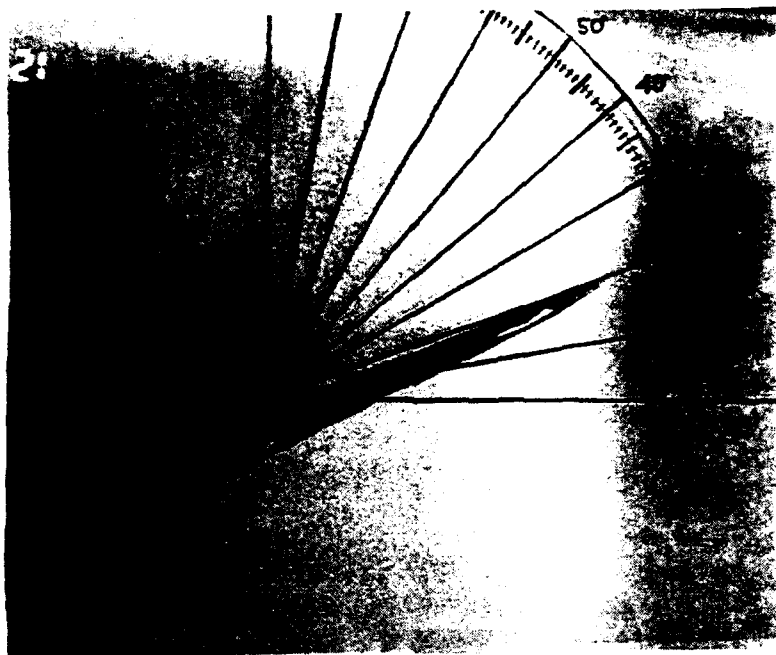


Fig. 35 End-of-fillet vortex , linear model AOA = 20 deg

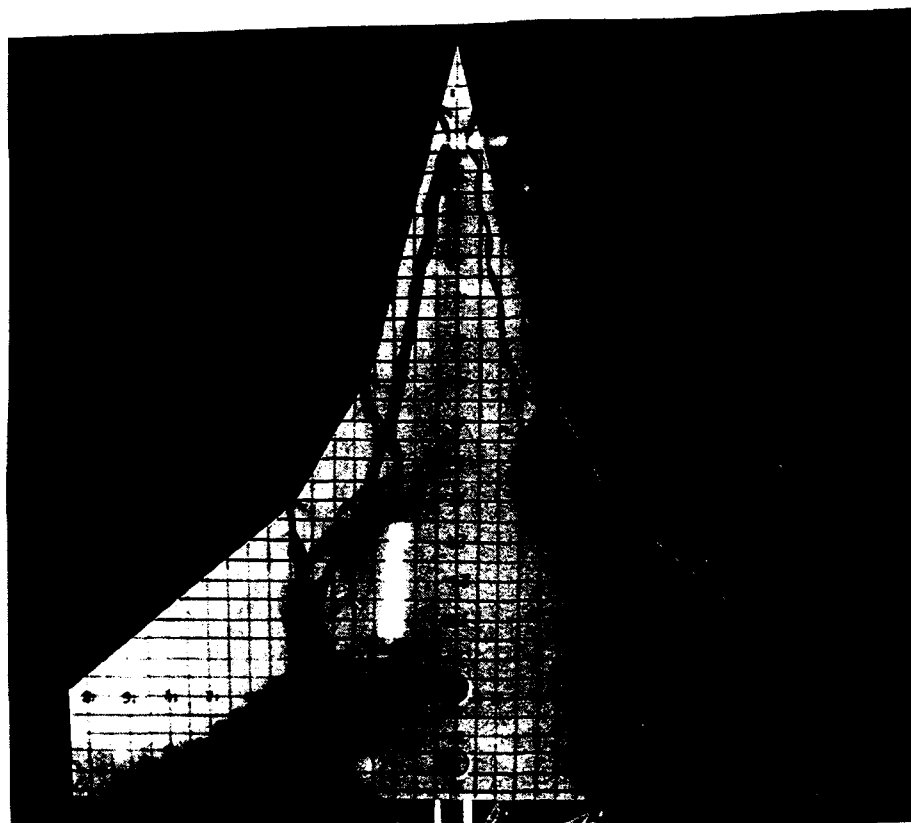
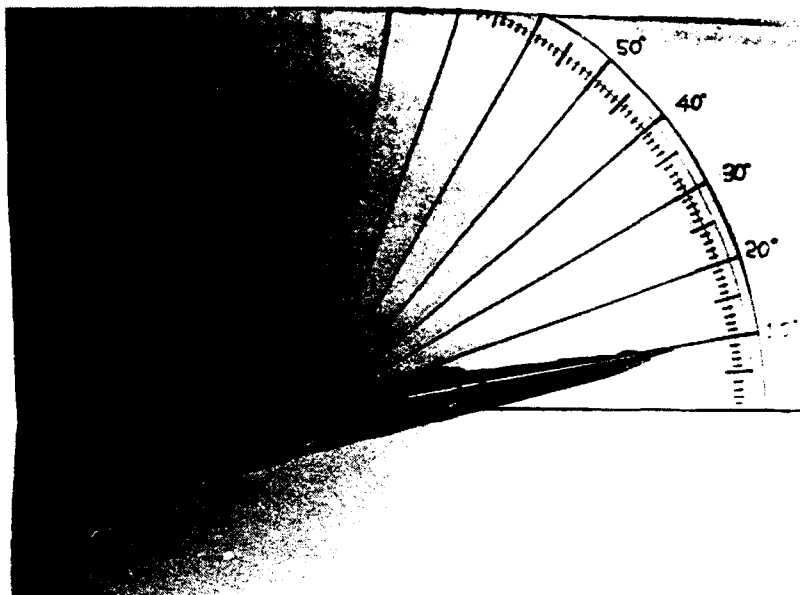


Fig. 36 Strake, beginning- and End-of-fillet vortices ,
linear model AOA = 10 deg

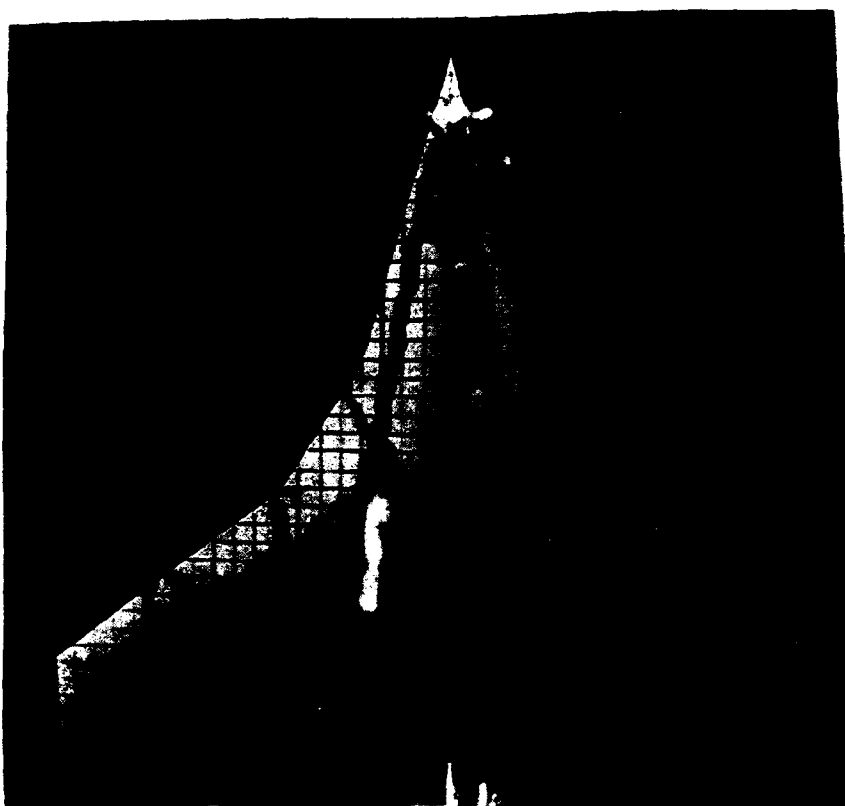
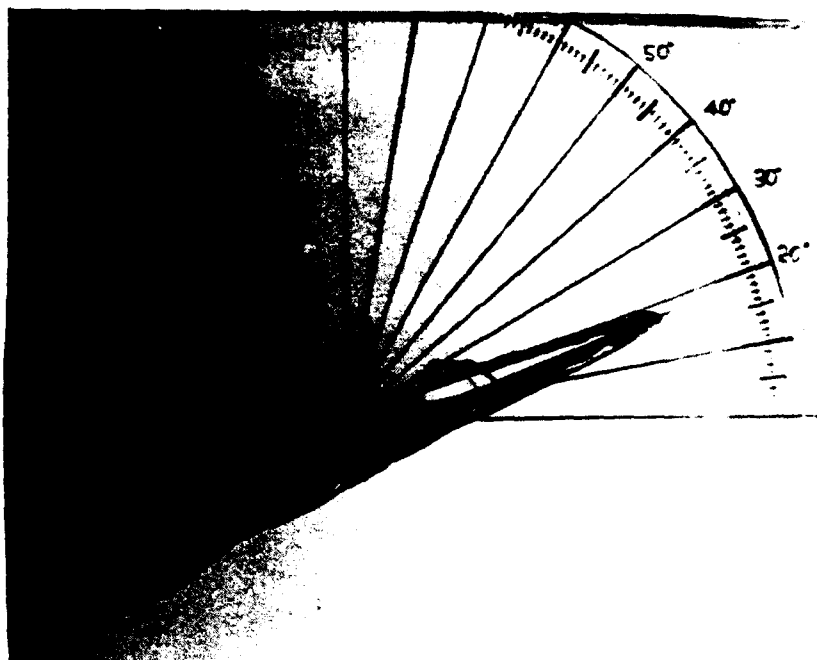


Fig. 37 Strake, beginning- and End-of-fillet vortices ,
linear model AOA = 20 deg

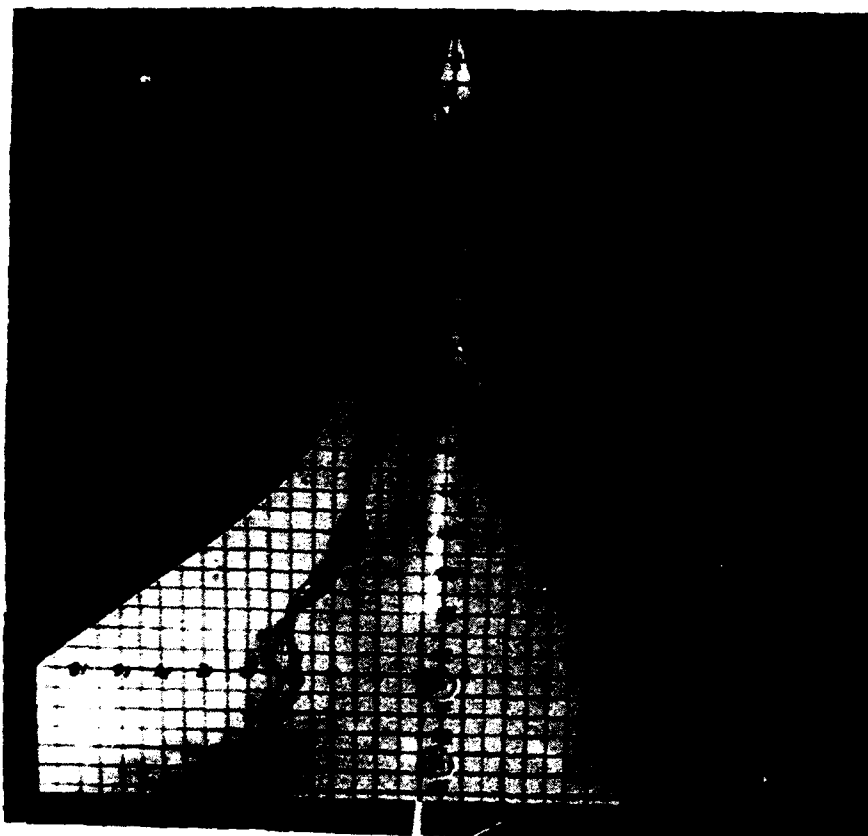
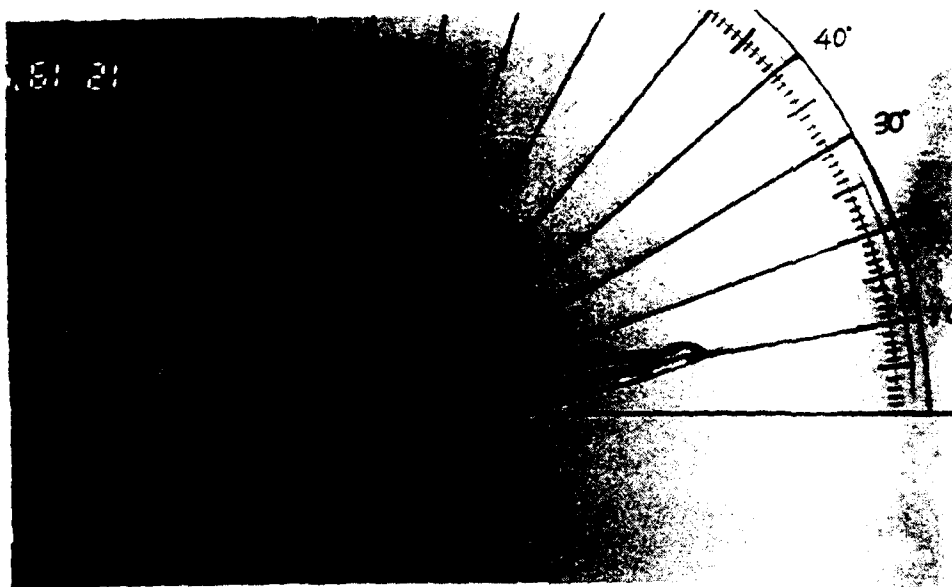


Fig. 38 Strake vortex , parabolic model AOA = 10 deg

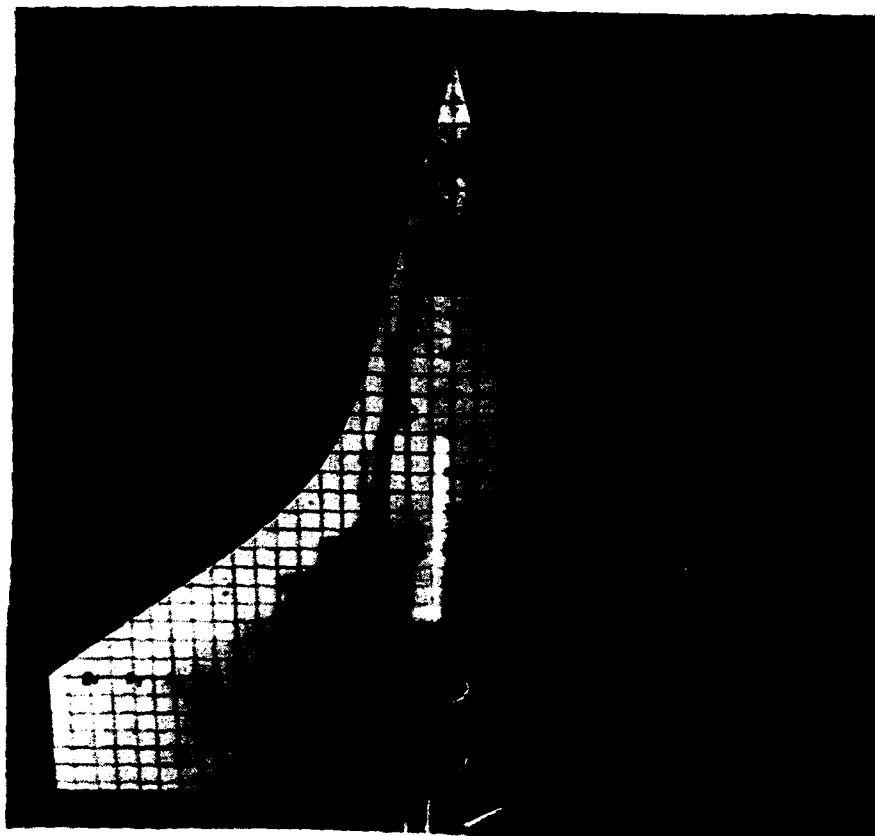
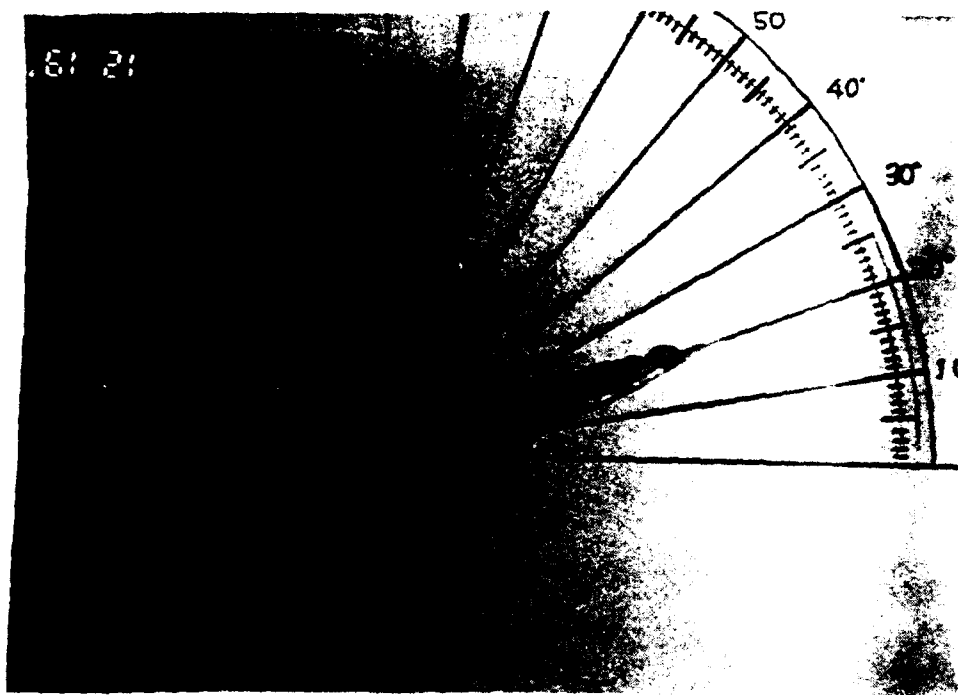


Fig. 39 Strake vortex , parabolic model AOA = 20 deg

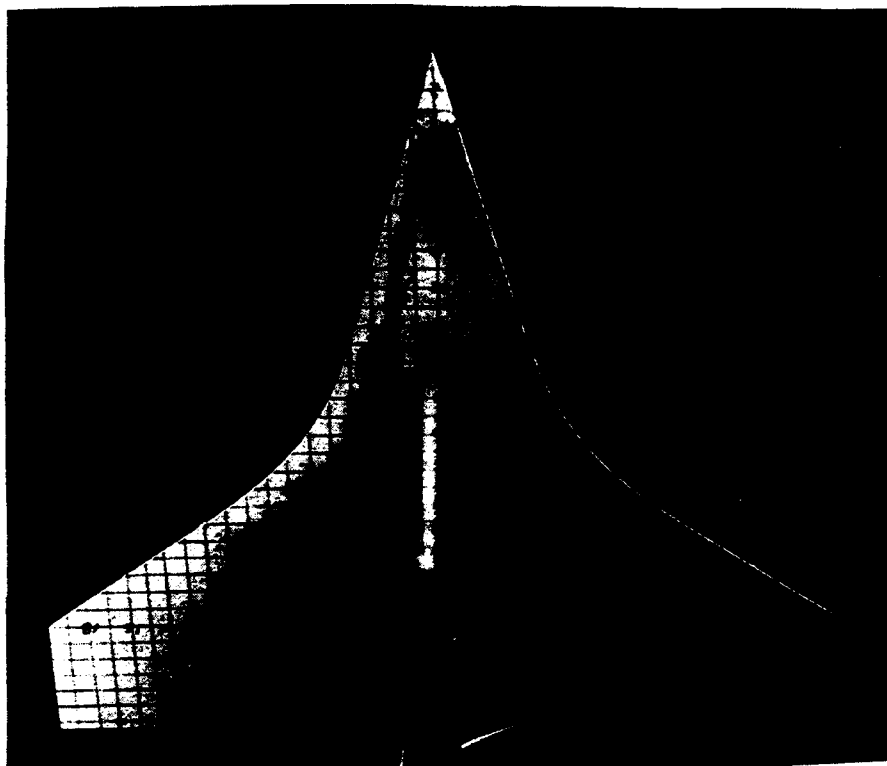
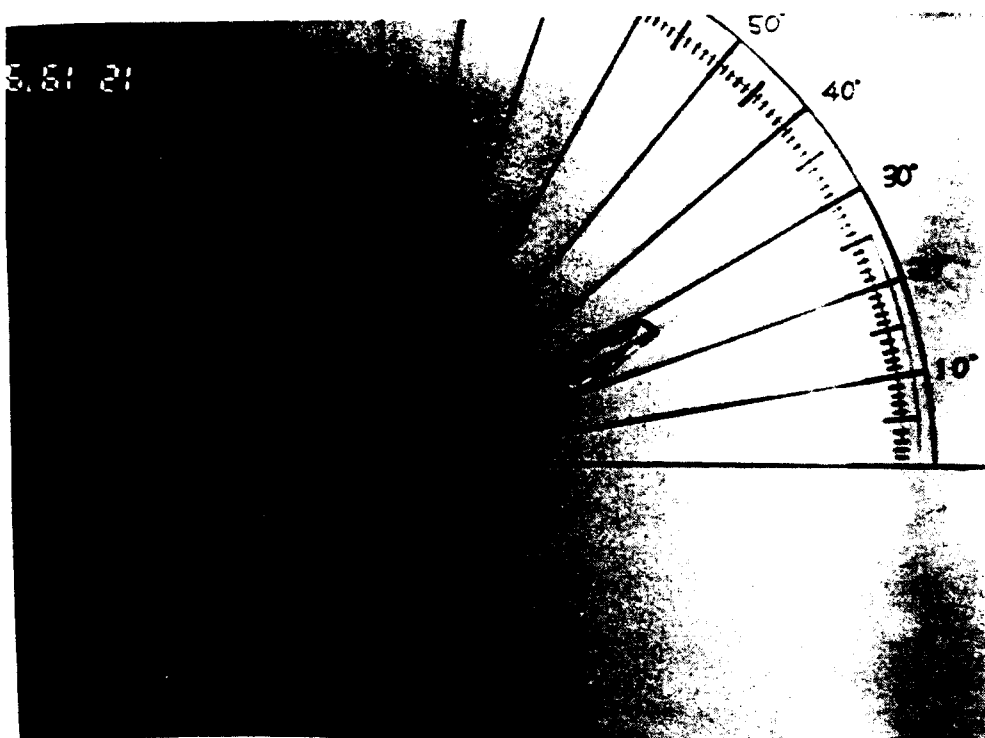


Fig. 40 Strake vortex , parabolic model AOA = 26 deg

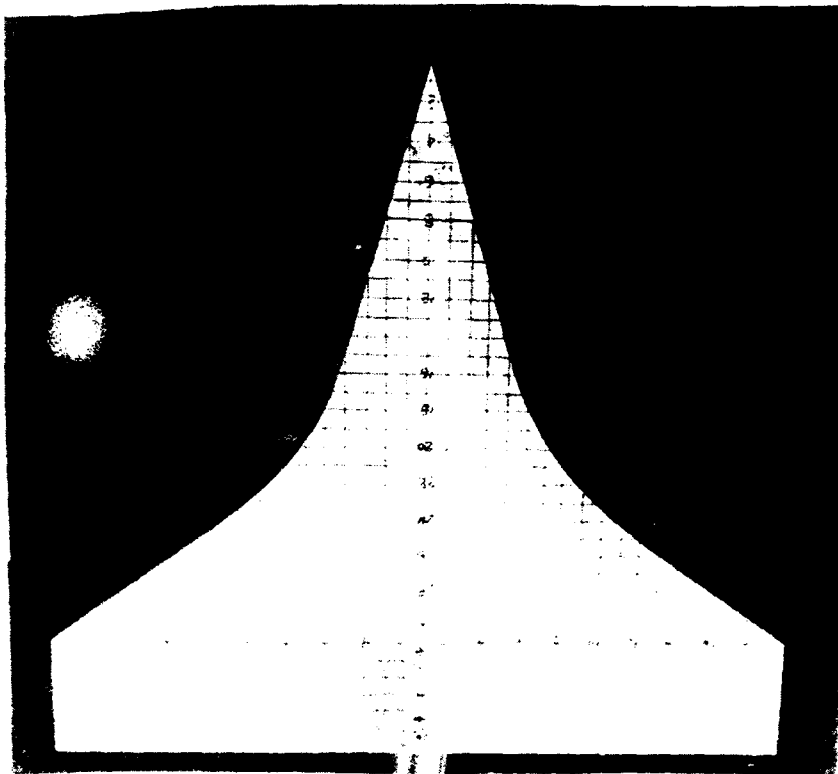
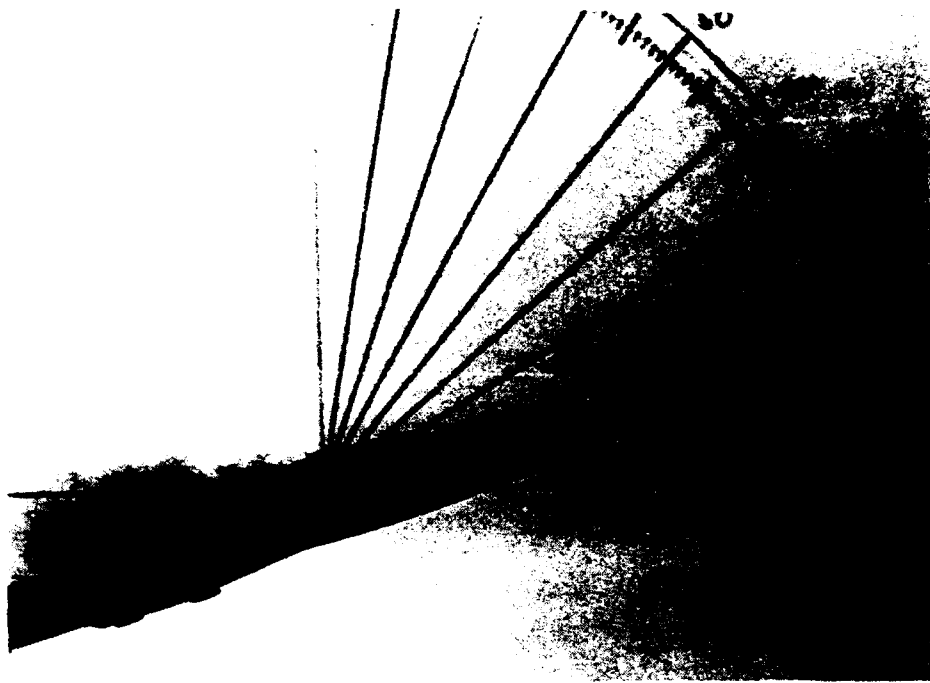


Fig. 41 Strake vortex , parabolic model (dynamic pitch-up)
AOA = 16 deg

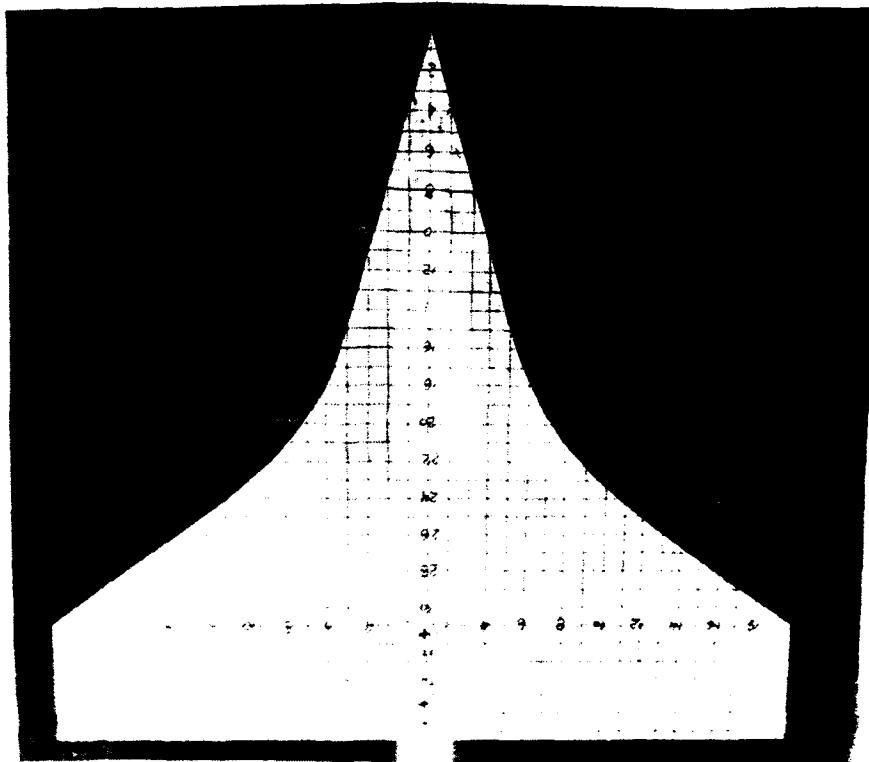
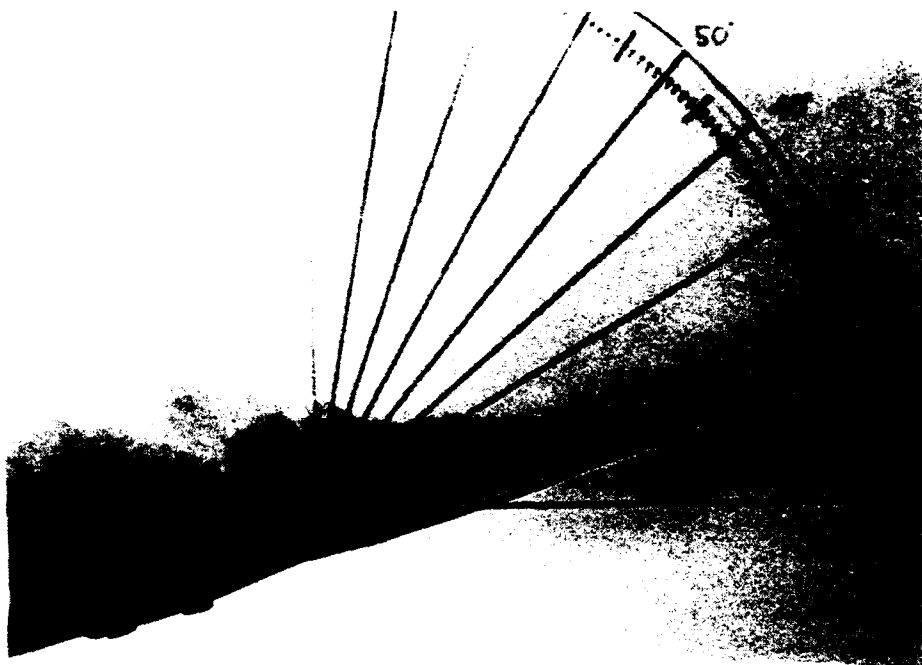


Fig. 42 Strake vortex , parabolic model (dynamic pitch-down)
AOA = 16 deg

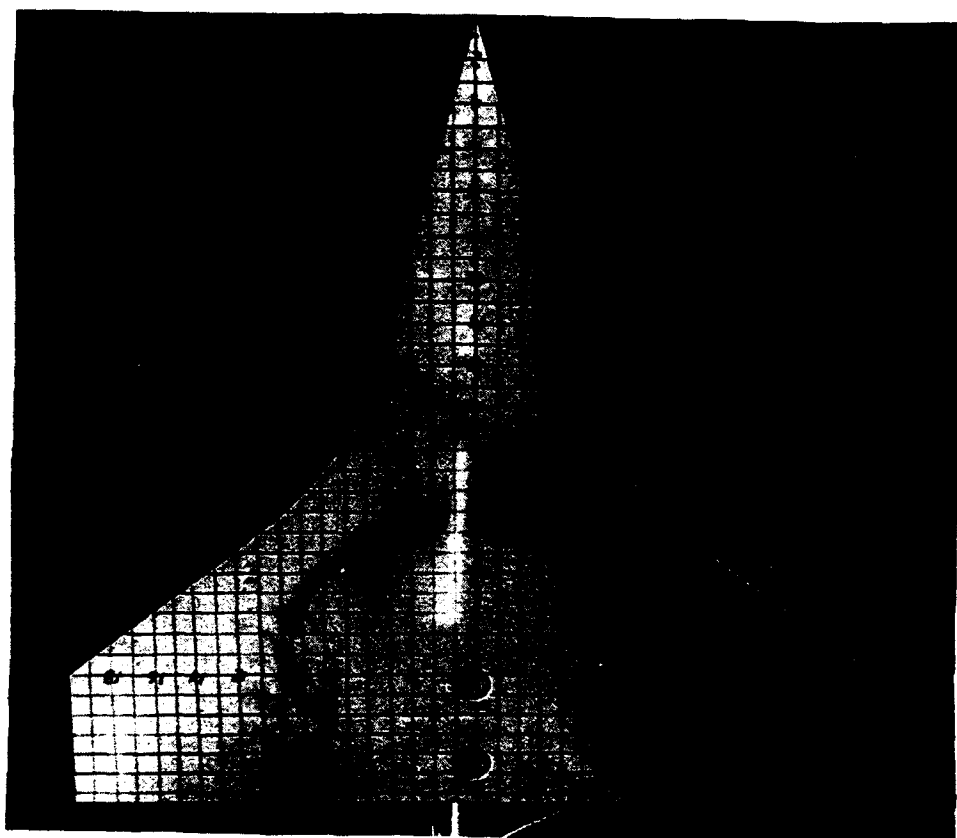
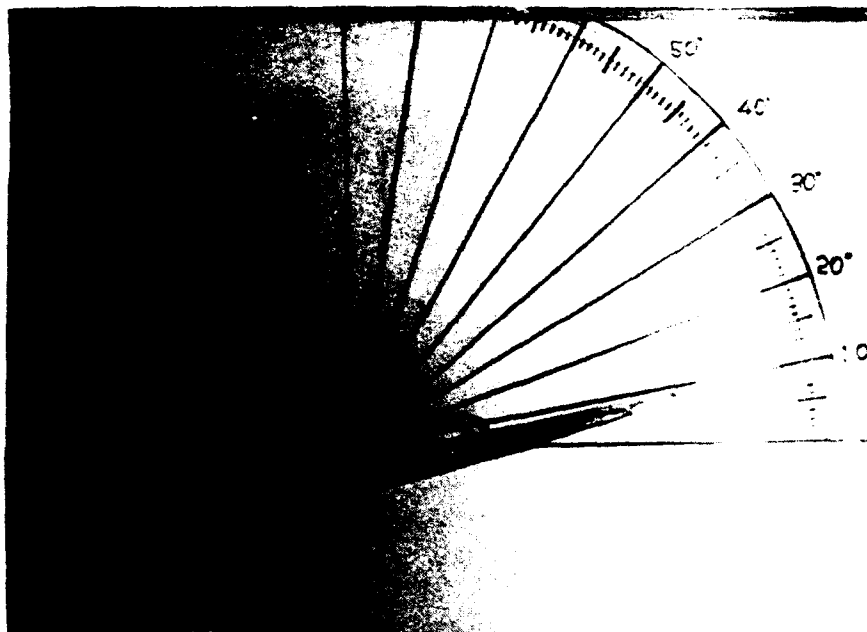


Fig. 43 Beginning-of-fillet vortex , parabolic model
AOA = 10 deg

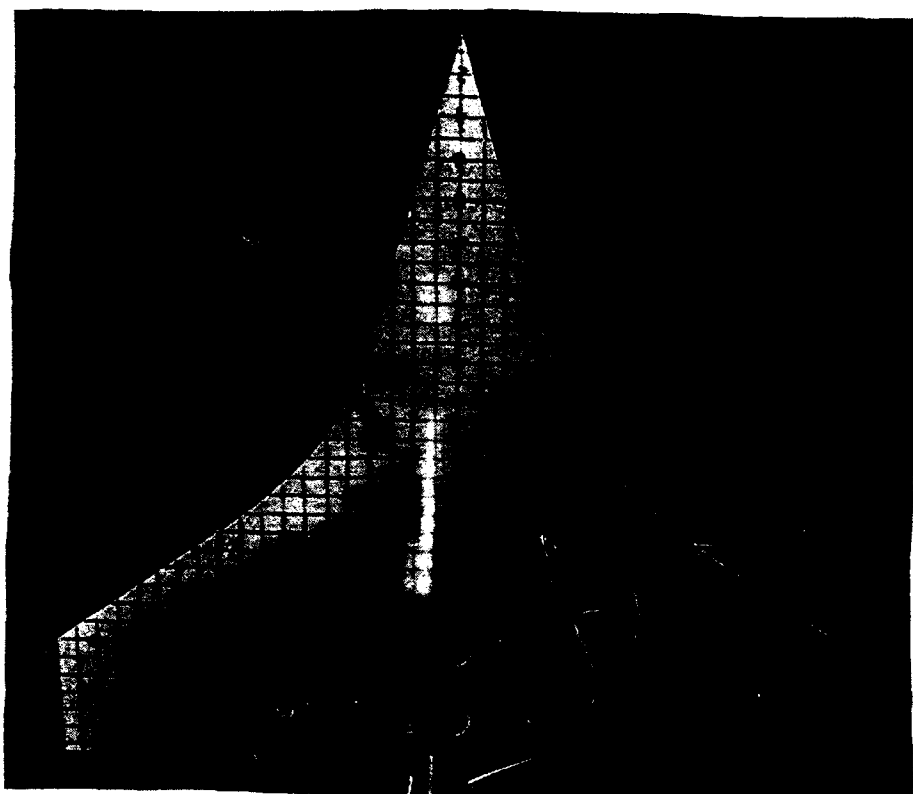
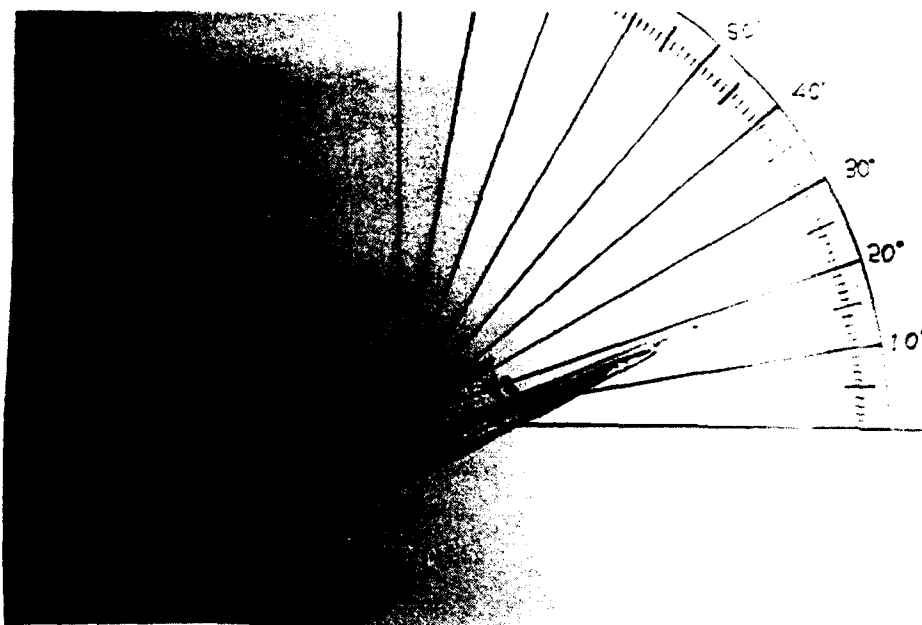


Fig. 44 Beginning-of-fillet vortex , parabolic model
AOA = 20 deg

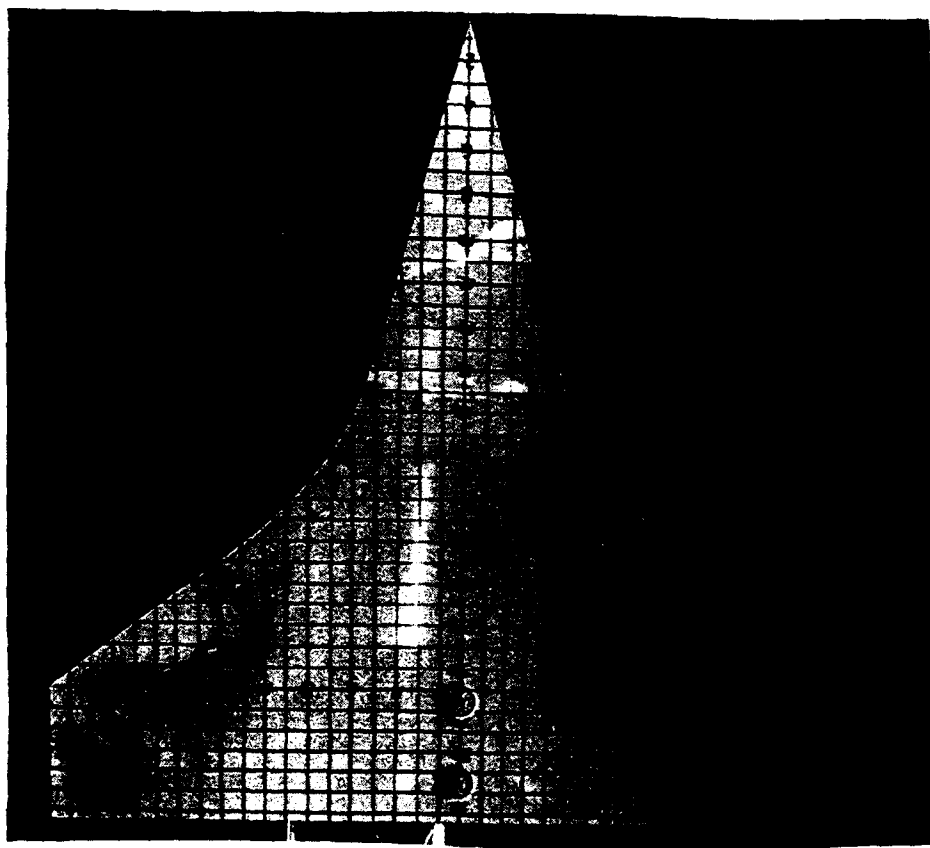
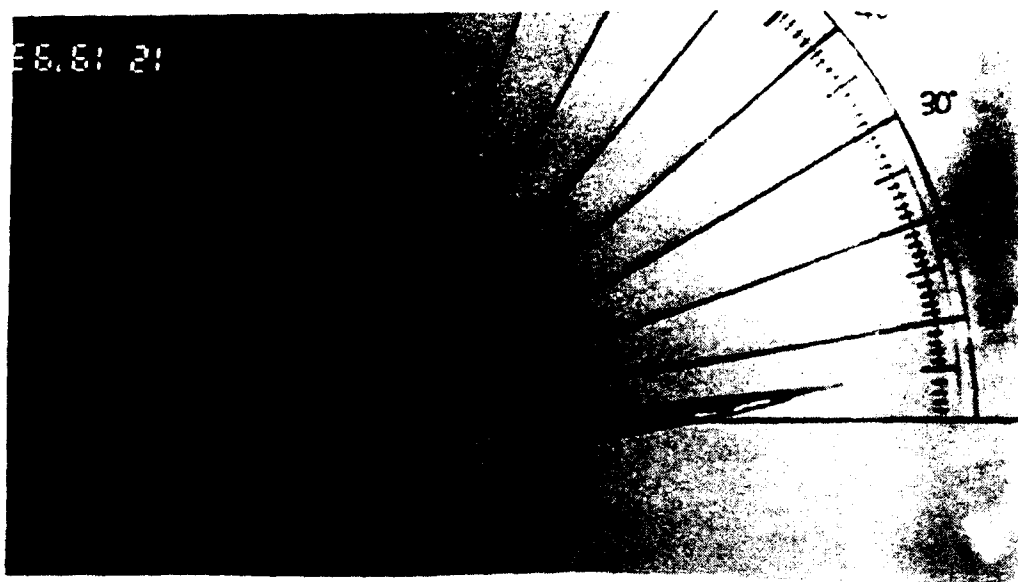


Fig. 45 End-of-fillet vortex , parabolic model AOA = 5 deg

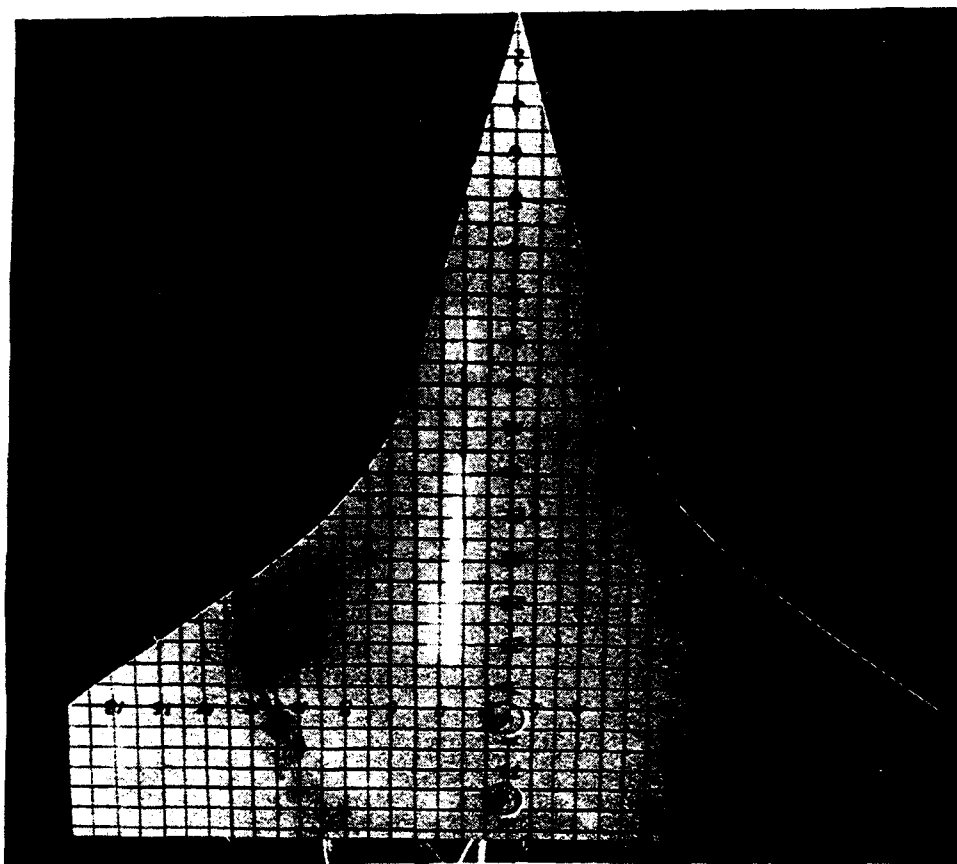


Fig. 46 End-of-fillet vortex , parabolic model AOA = 16 deg

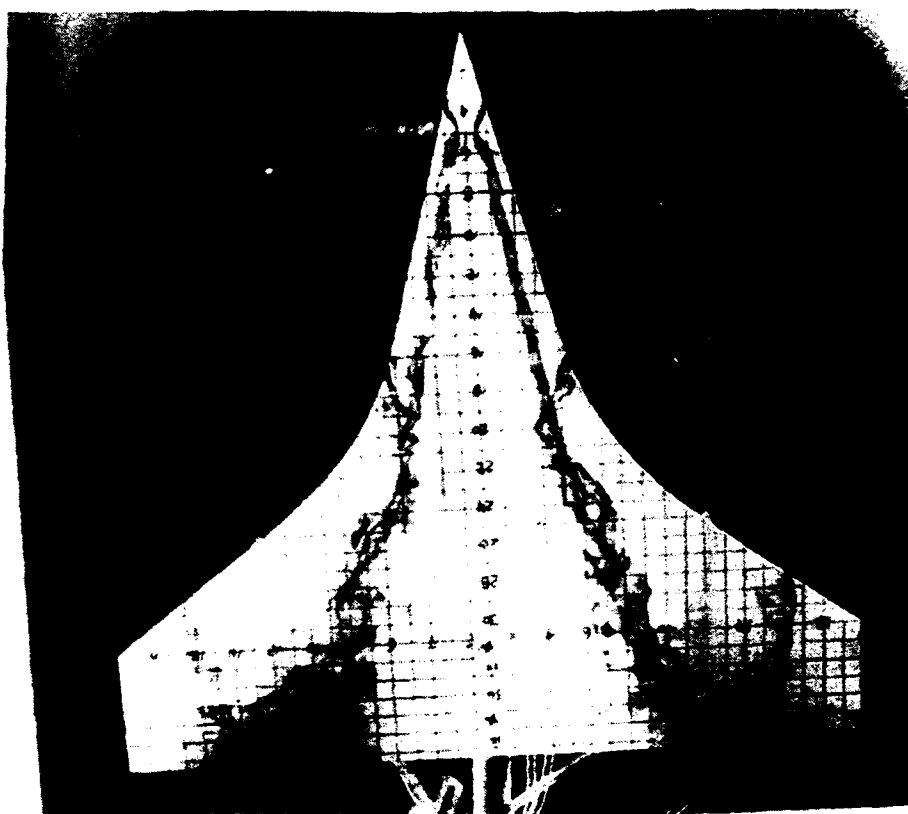
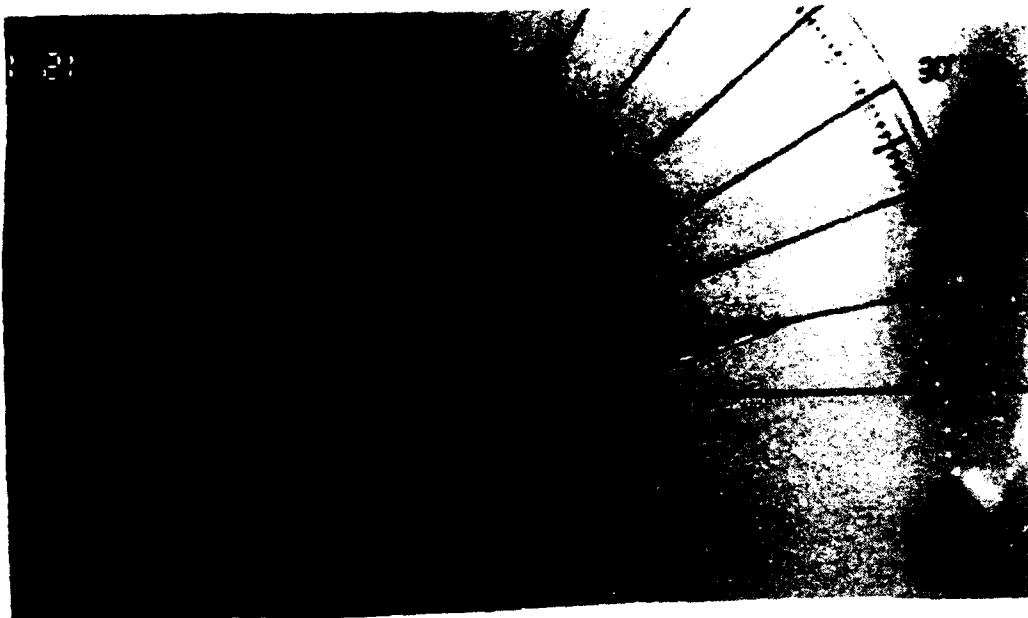


Fig. 47 Strake, beginning- and end-of-fillet vortices,
parabolic model AOA = 10 deg

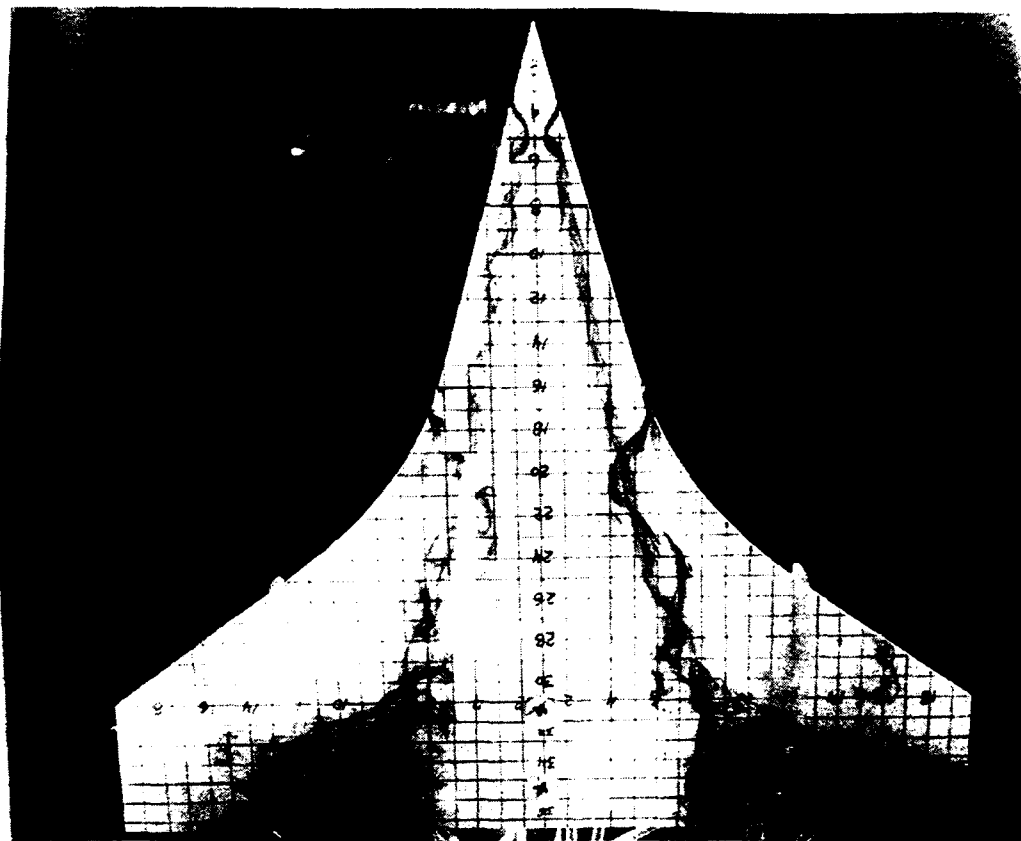
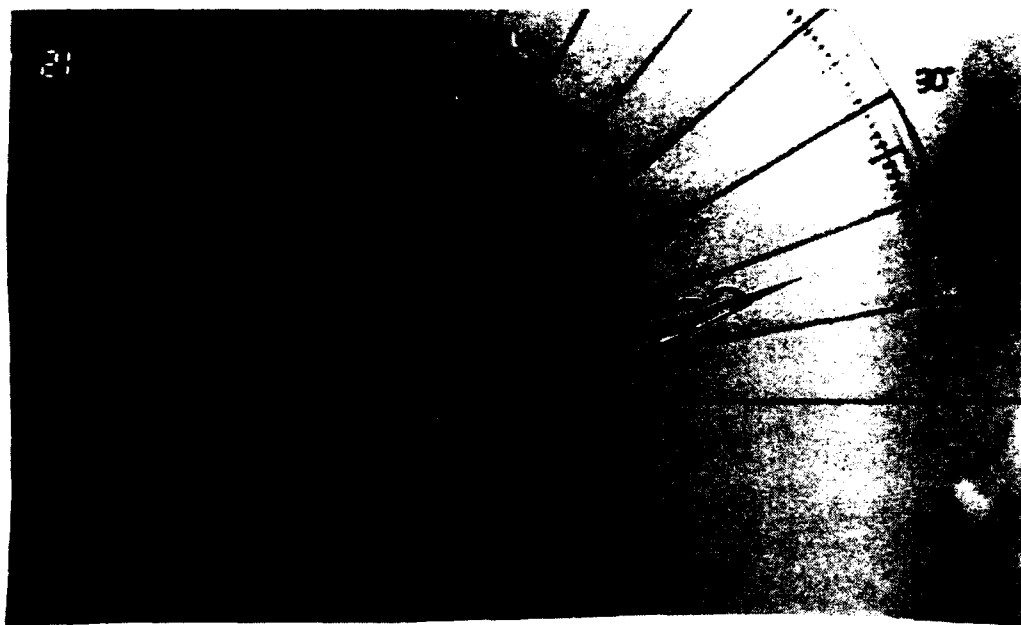


Fig. 48 Strake, beginning- and end-of-fillet vortices, parabolic model AOA = 16 deg

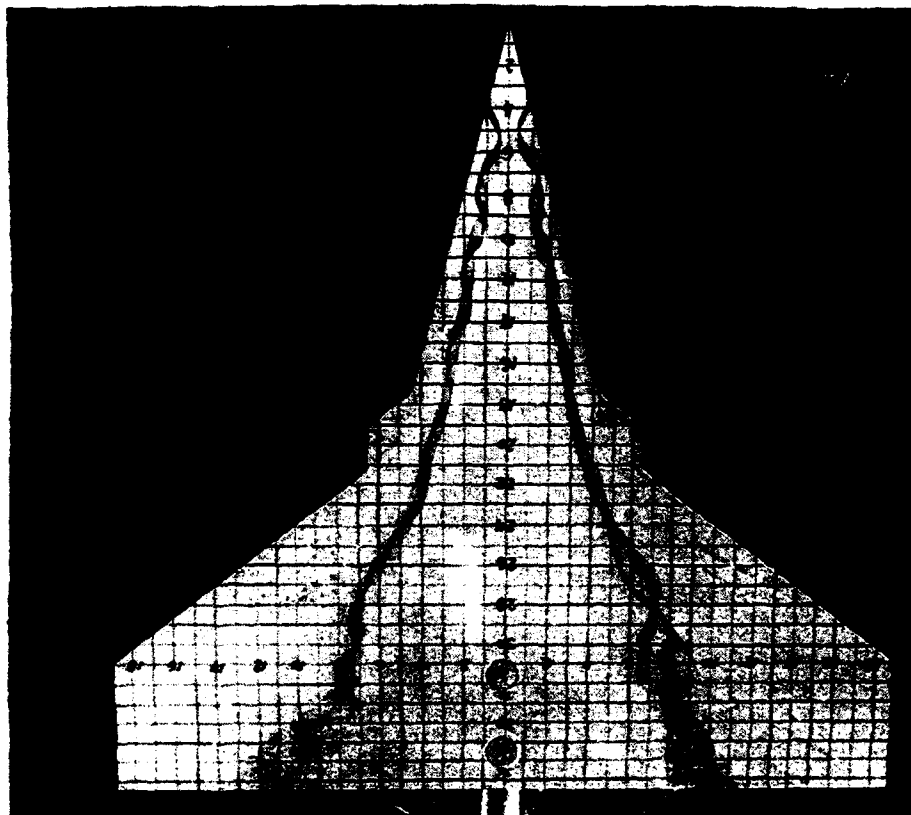
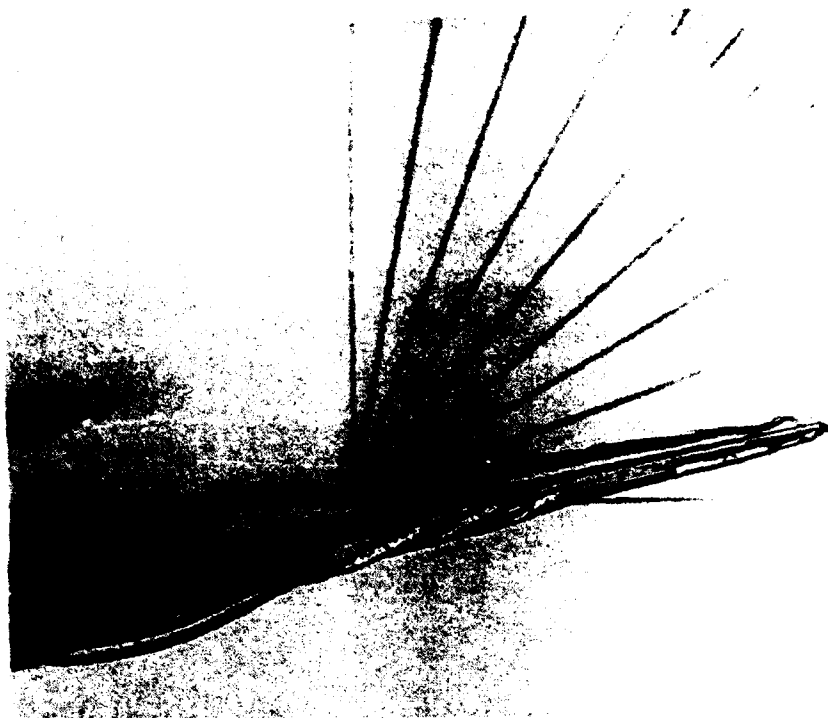


Fig. 49 Strake vortex , diamond model AOA = 10 deg

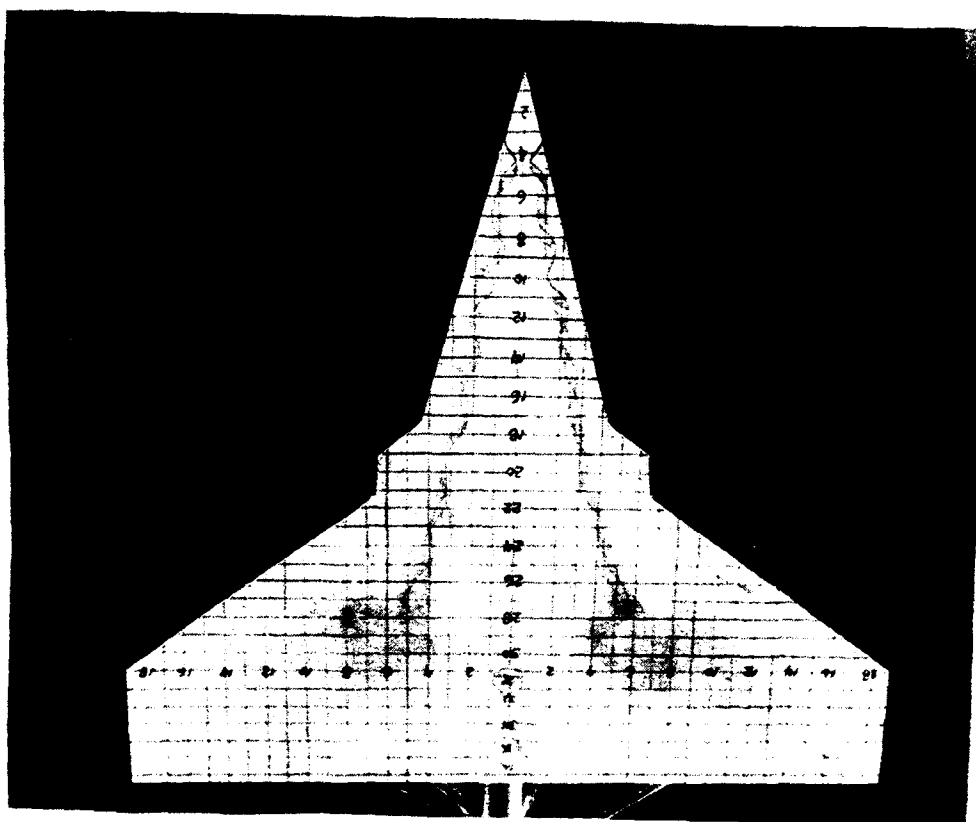
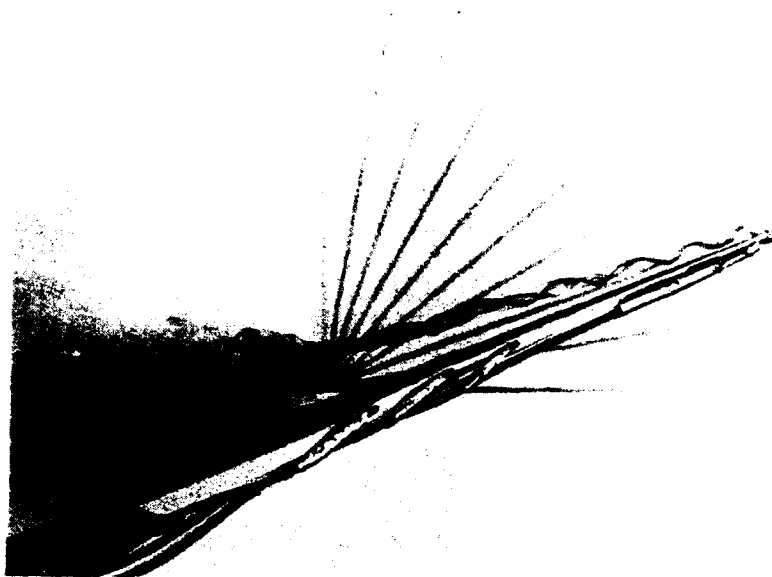


Fig. 50 Strake vortex , diamond model AOA = 20 deg

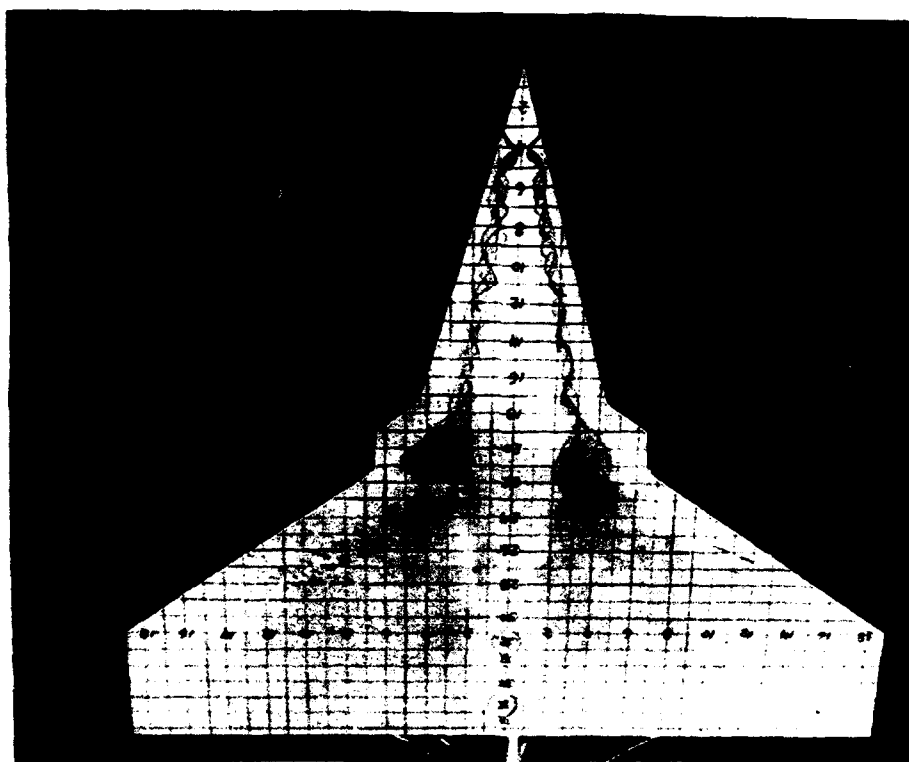


Fig. 51 Strake vortex , diamond model AOA = 26 deg

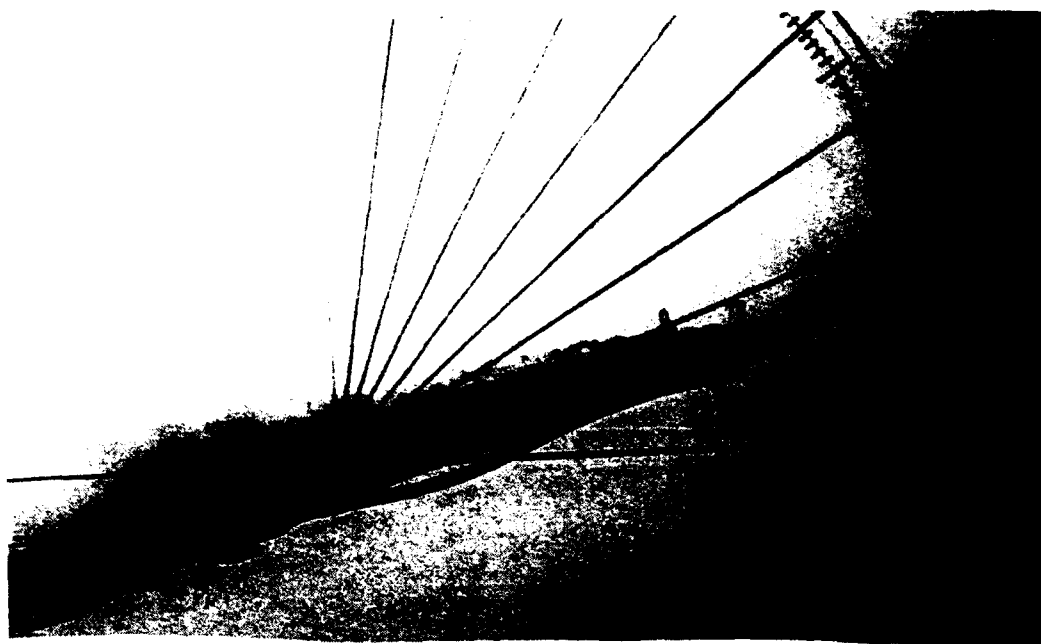


Fig. 52 Strake vortex , diamond model (dynamic pitch-up)
AOA = 16 deg

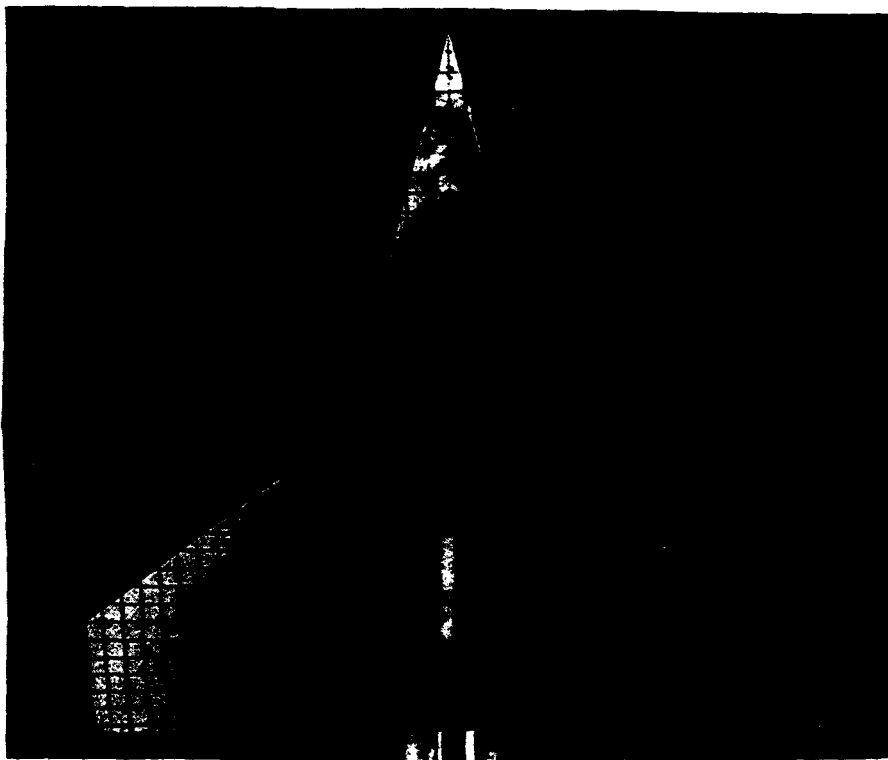
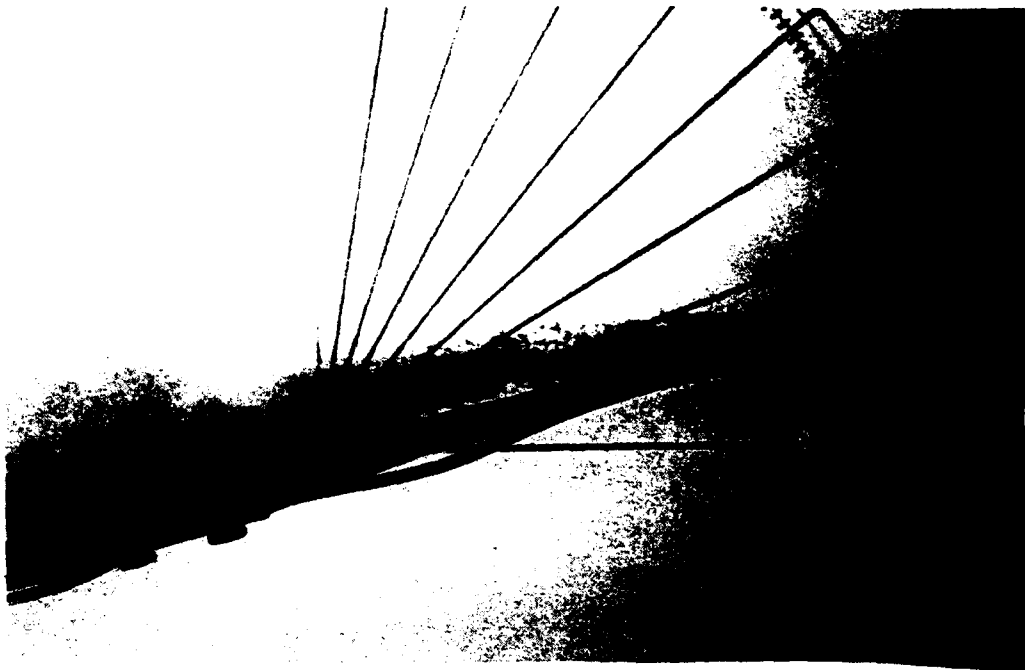


Fig. 53 Strake vortex , diamond model (dynamic pitch-down)
AOA = 16 deg

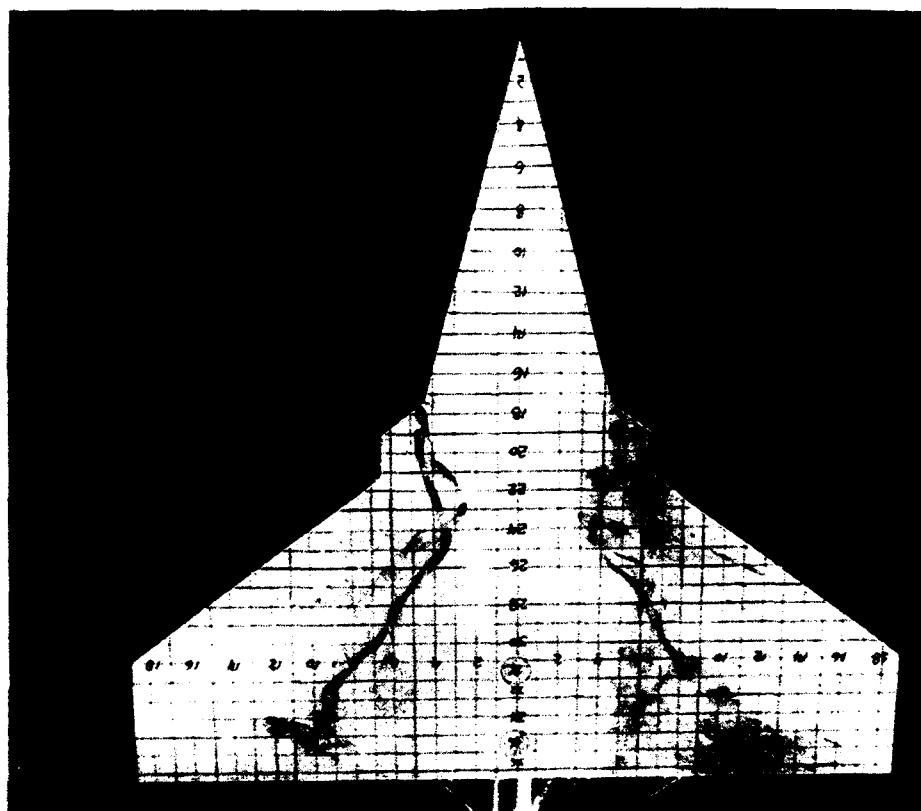
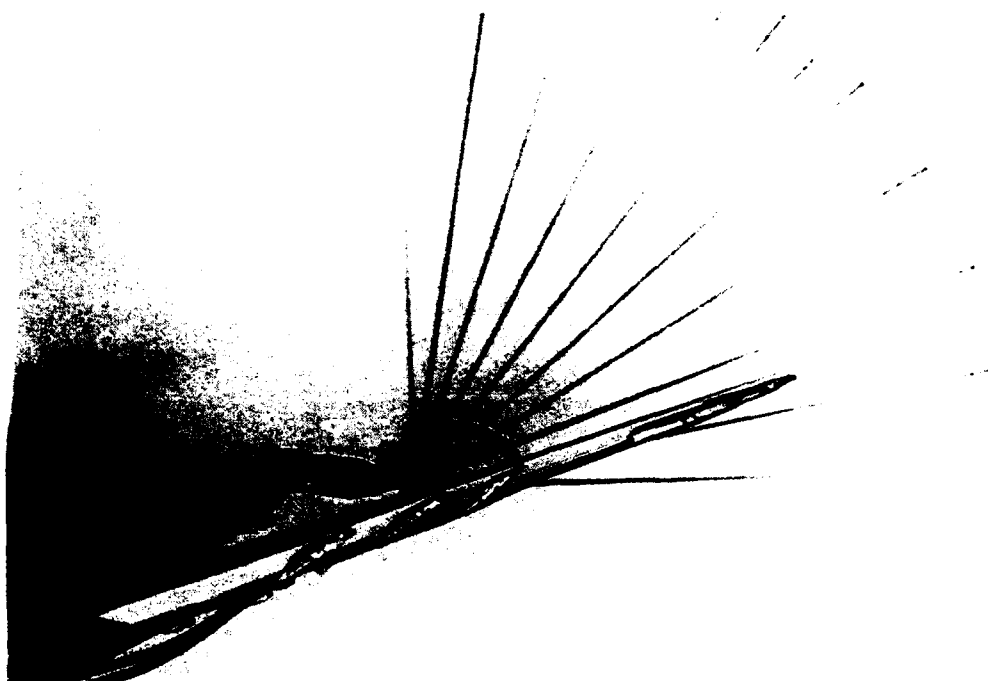


Fig. 54 Beginning-of-fillet vortex , diamond model
AOA = 16 deg

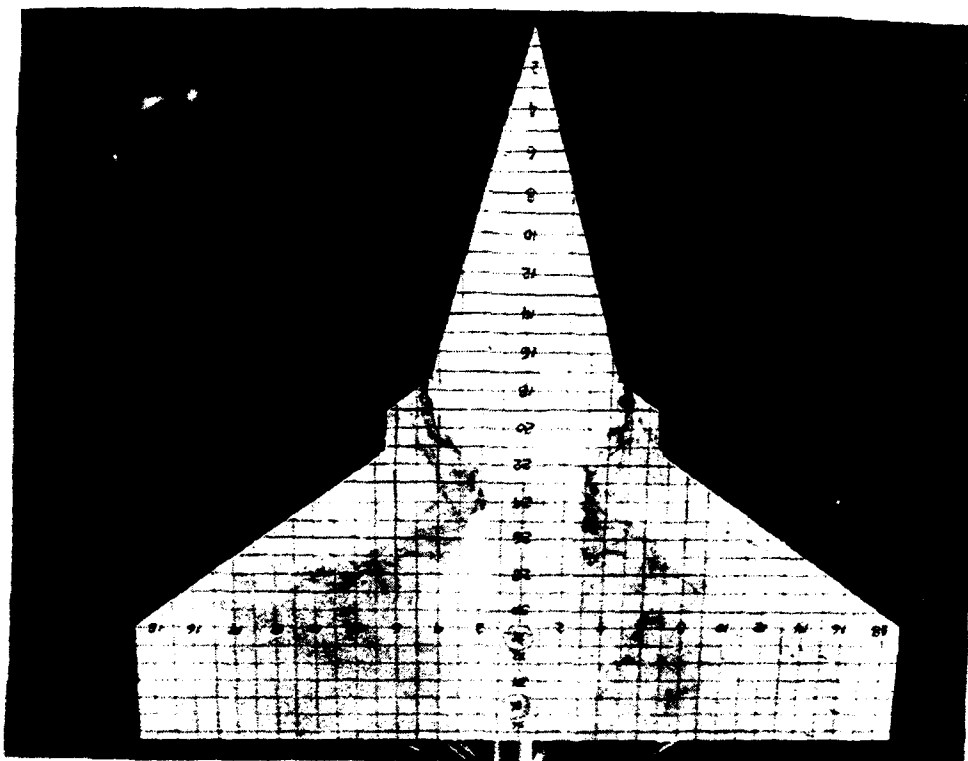
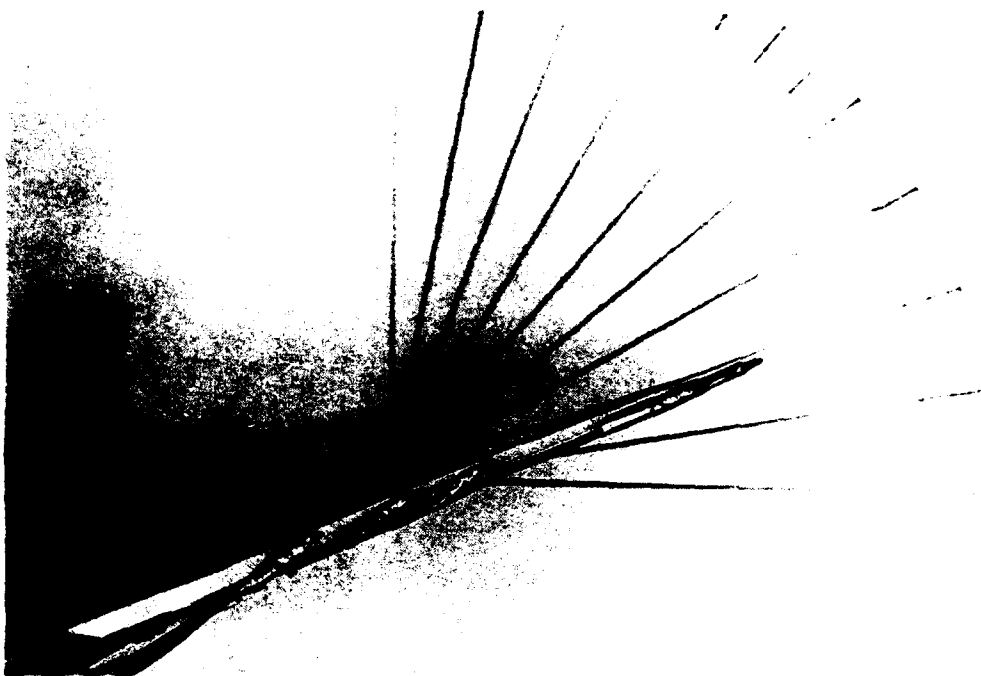


Fig. 55 Beginning-of-fillet vortex , diamond model
AOA = 20 deg

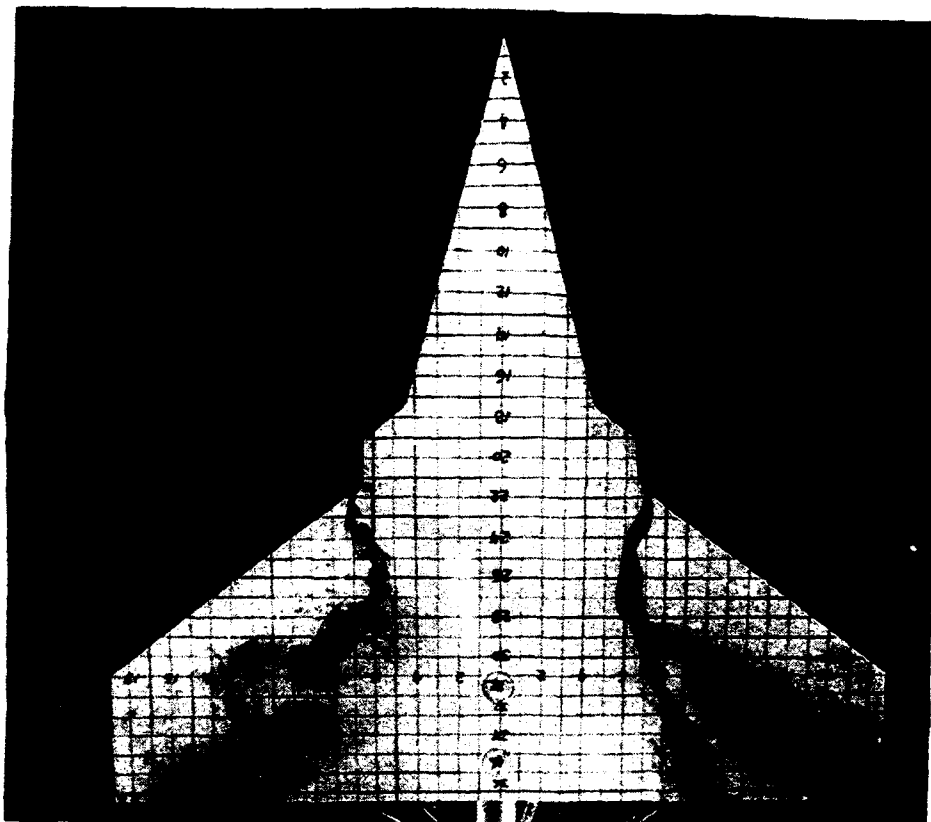
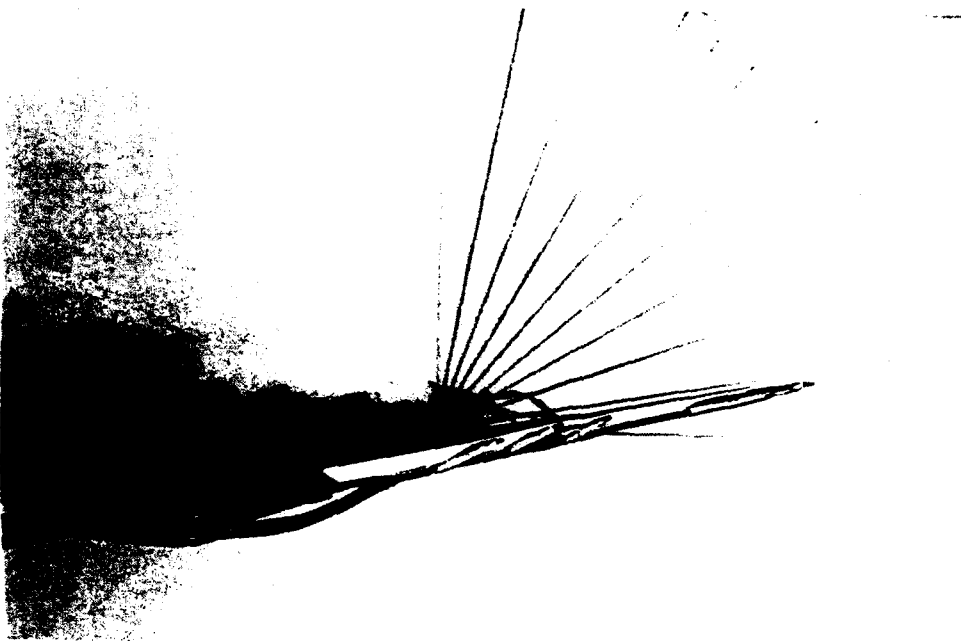


Fig. 56 End-of-fillet vortex , diamond model
AOA = 10 deg

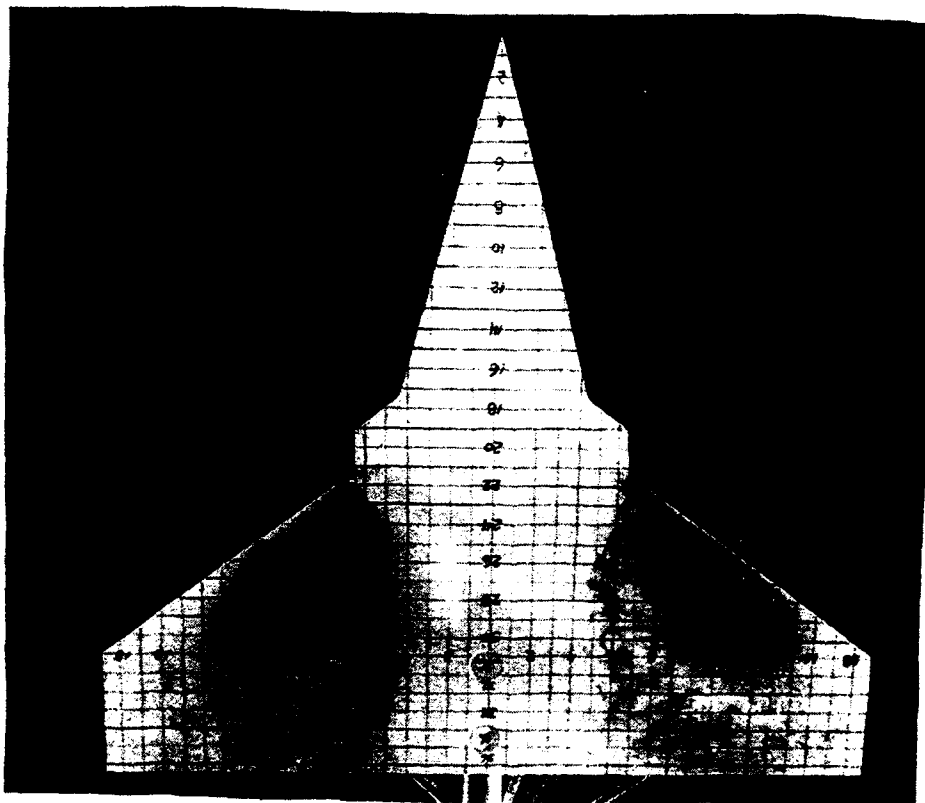
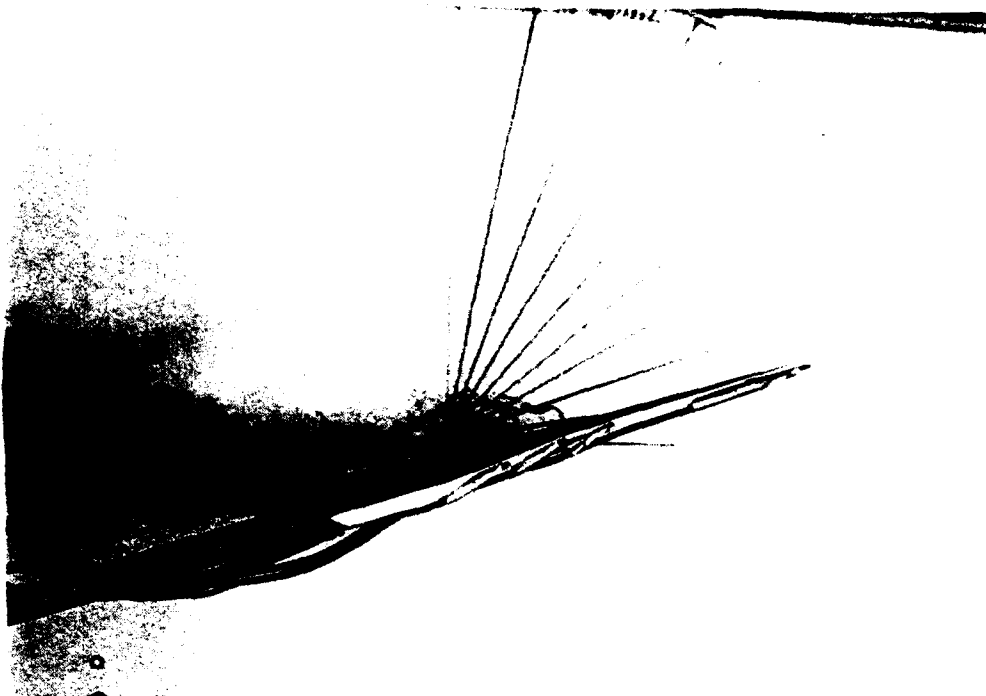


Fig. 57 End-of-fillet vortex , diamond model
AOA = 16 deg

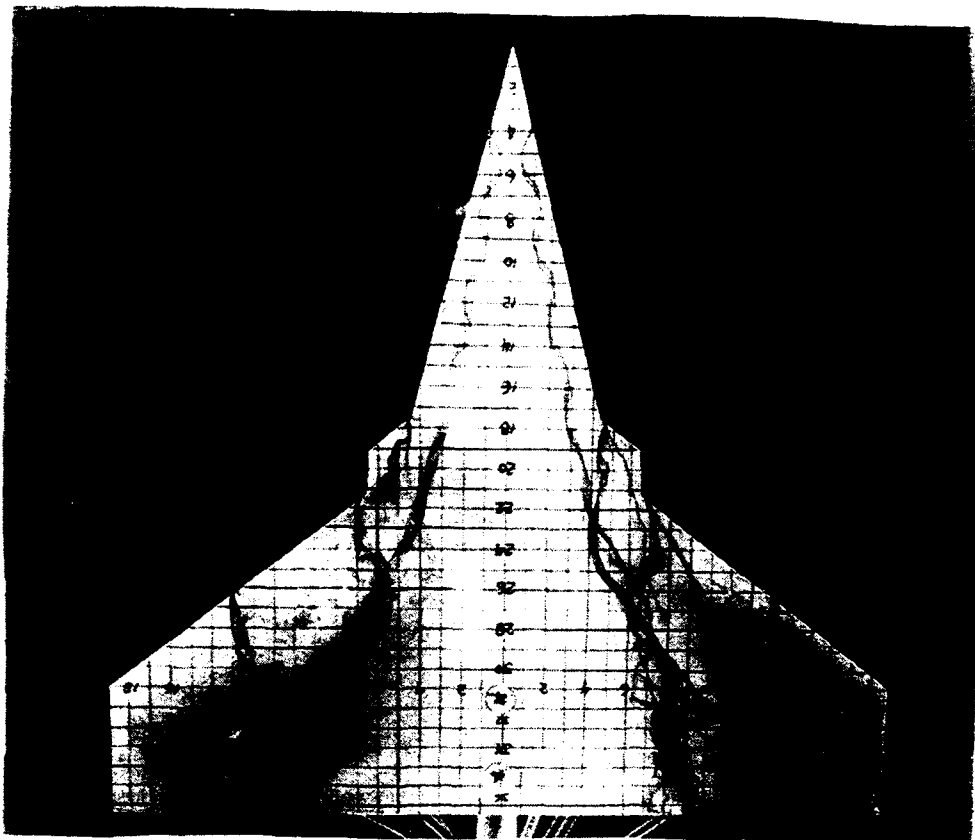
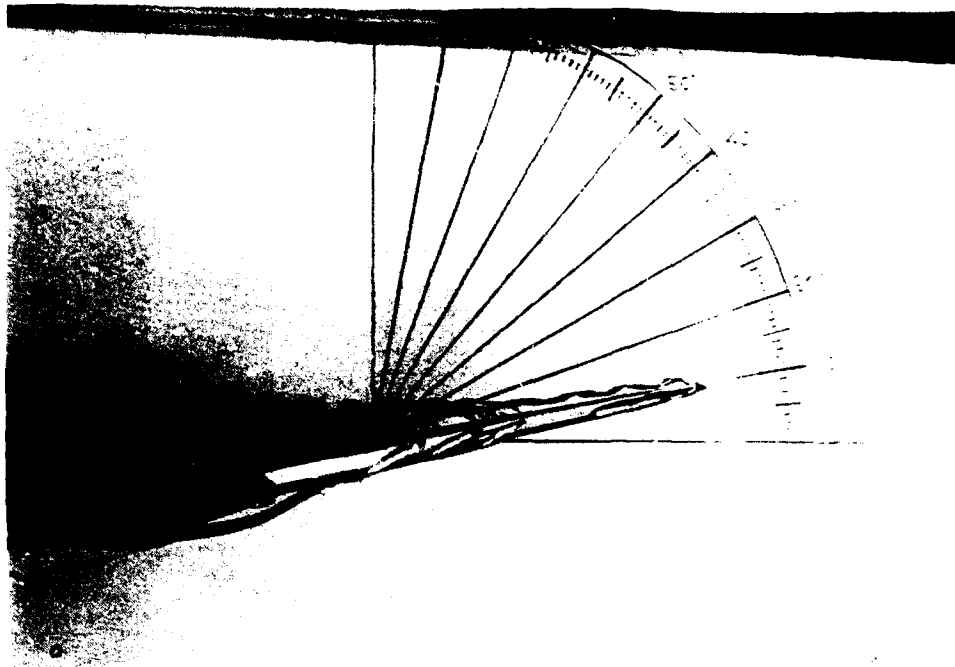


Fig. 58 Strake, beginning- and end-of-fillet vortices, diamond model AOA = 10 deg

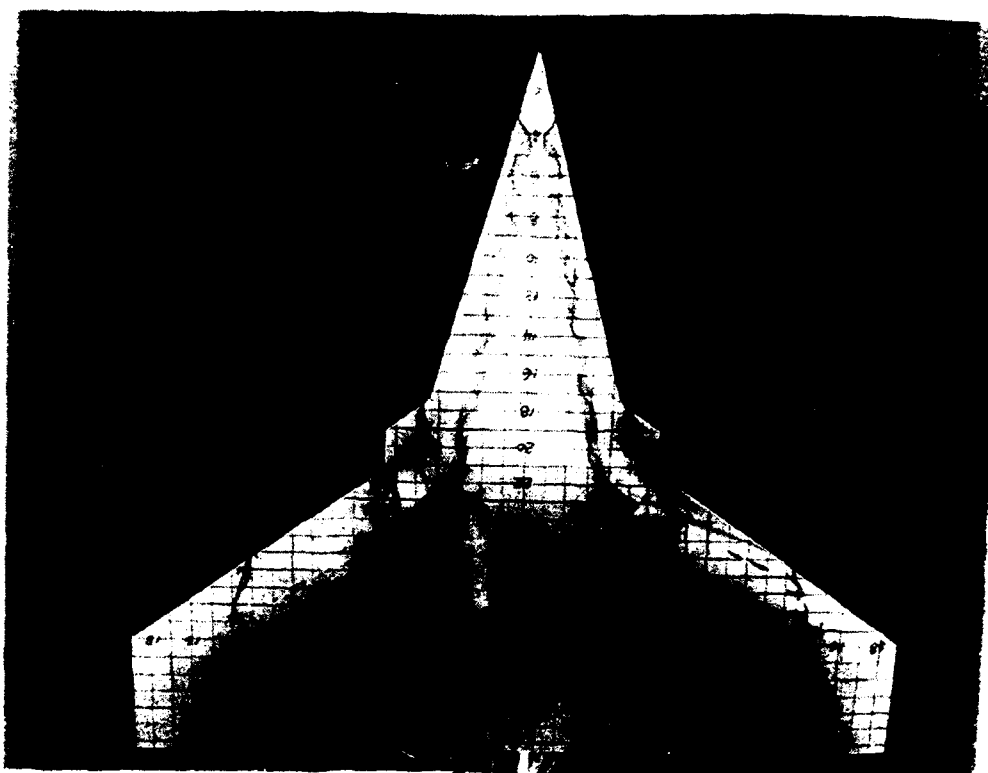
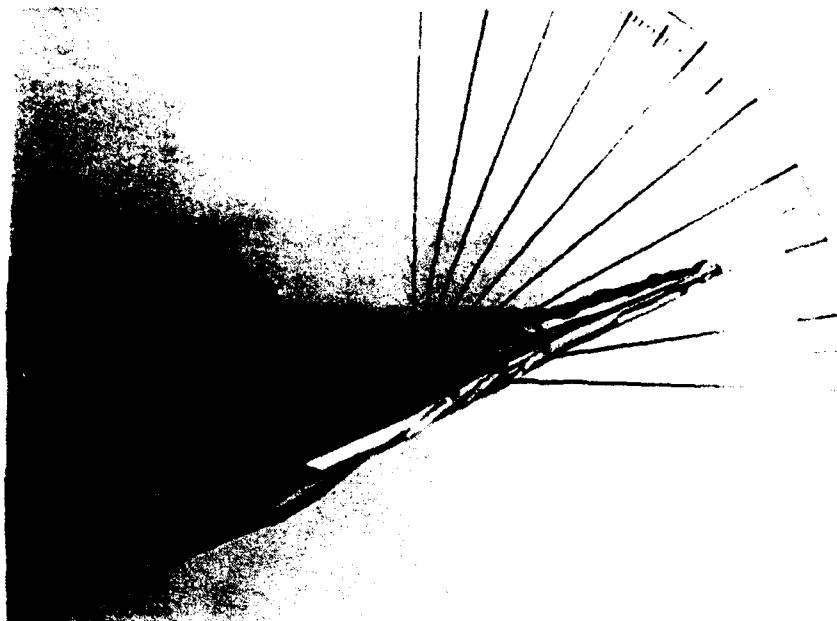


Fig. 59 Strake, beginning- and end-of-fillet vortices,
diamond model AOA = 22.5 deg

APPENDIX C EXPERIMENTAL RESULTS (GRAPHS)

FIGURES (60 - 144)

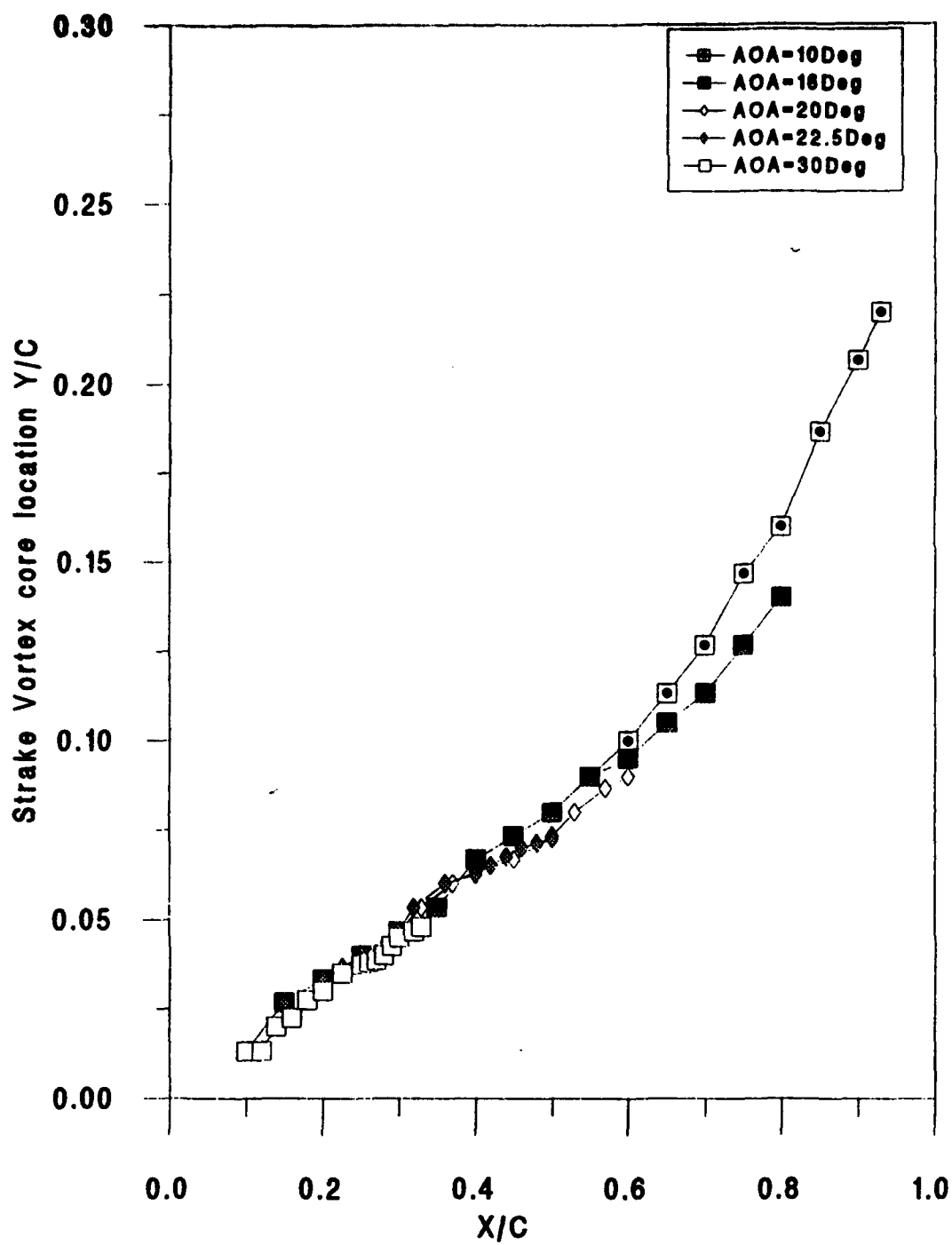


Fig.60 Vortex core location Y/C for baseline model

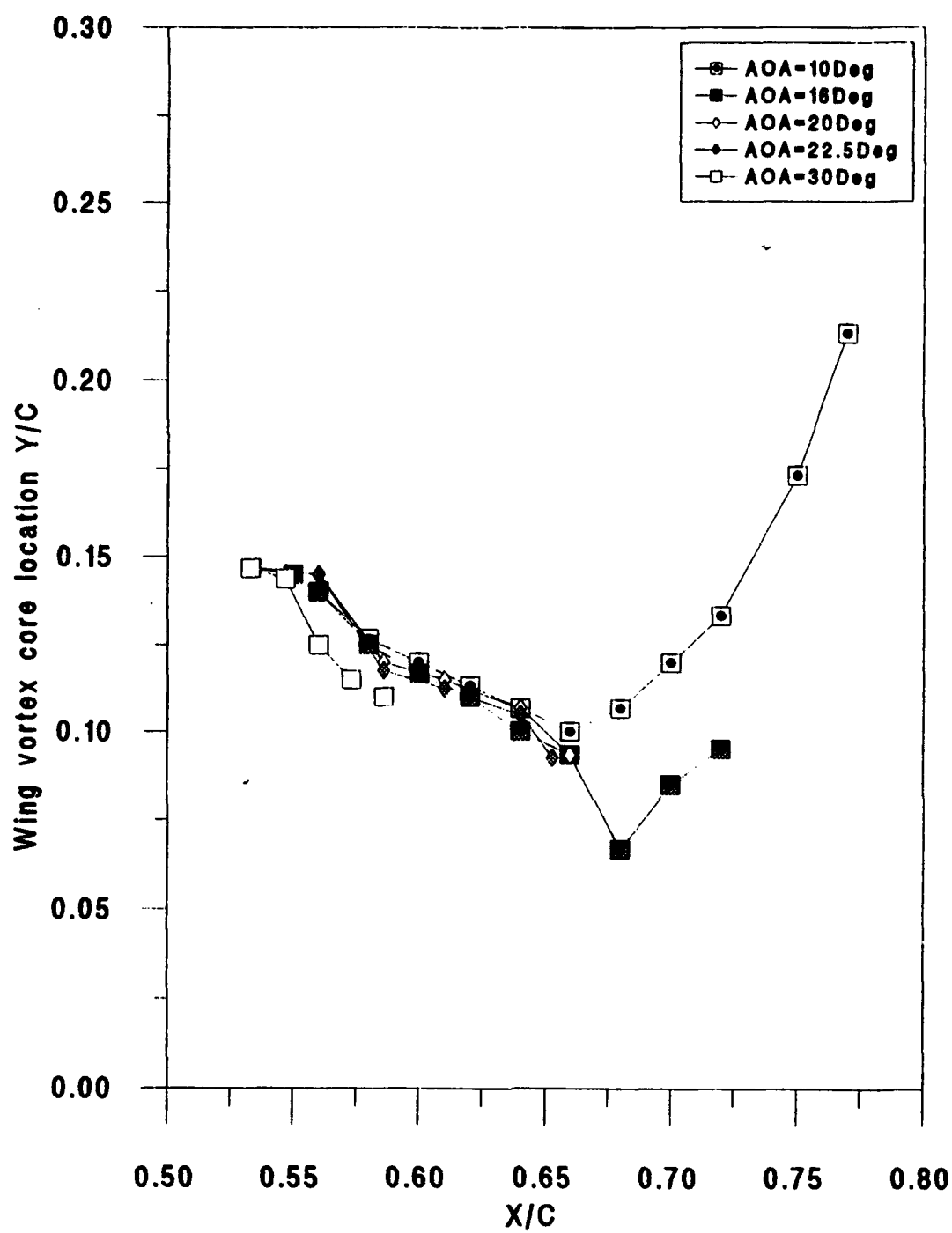


Fig. 61 Vortex core location Y/C for baseline model

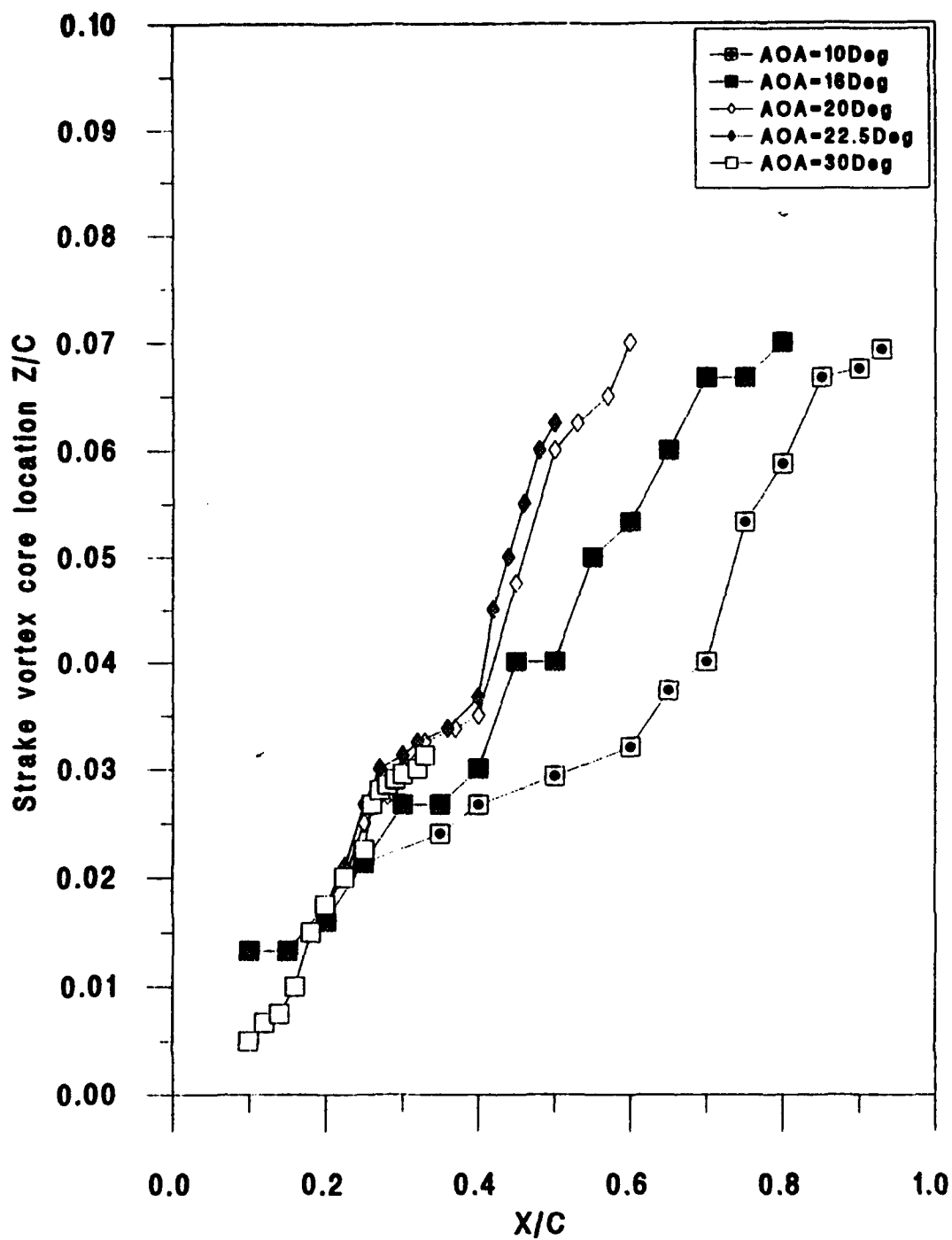


Fig. 62 Vortex core location Z/C for baseline model

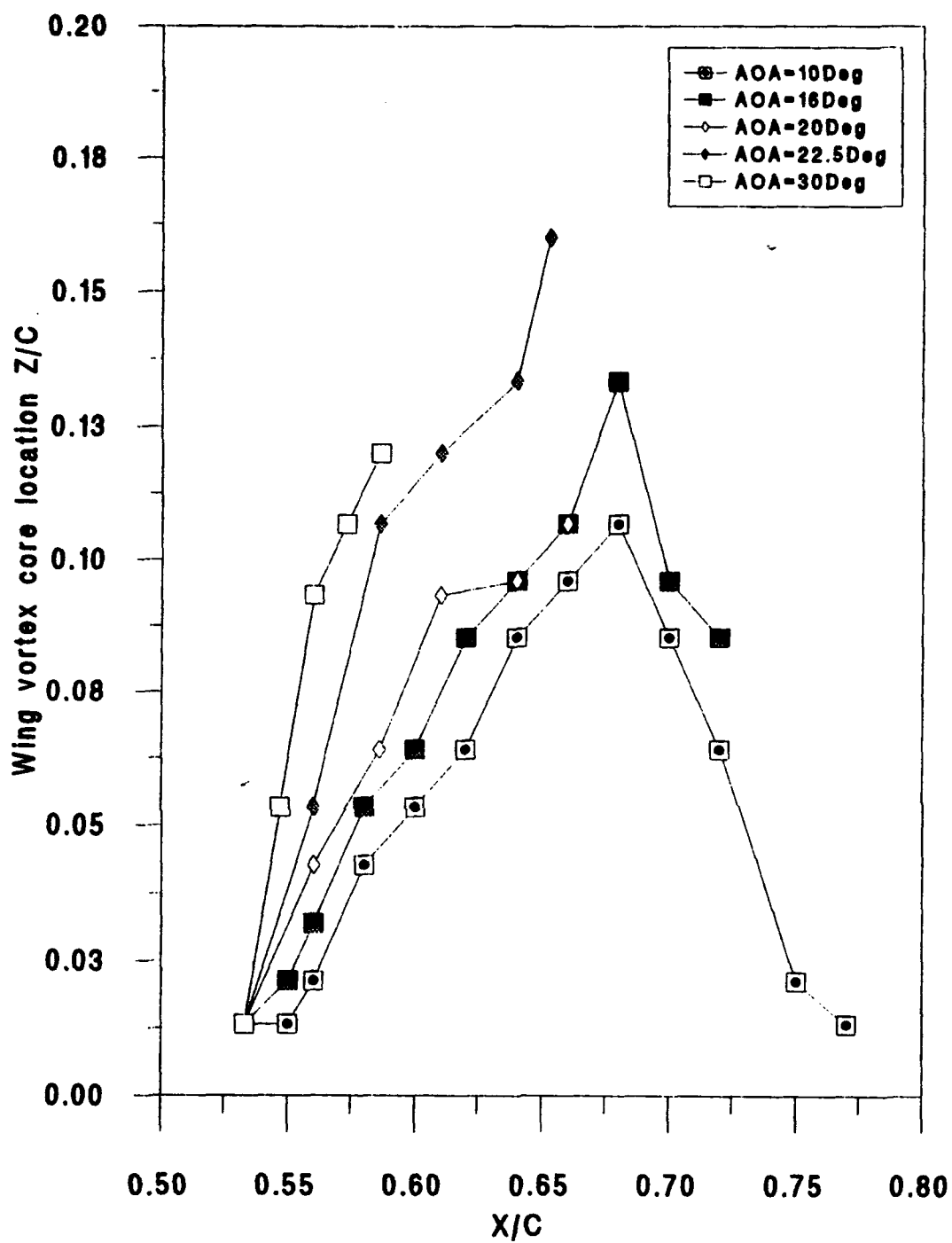


Fig. 63 Vortex core location Z/C for baseline model

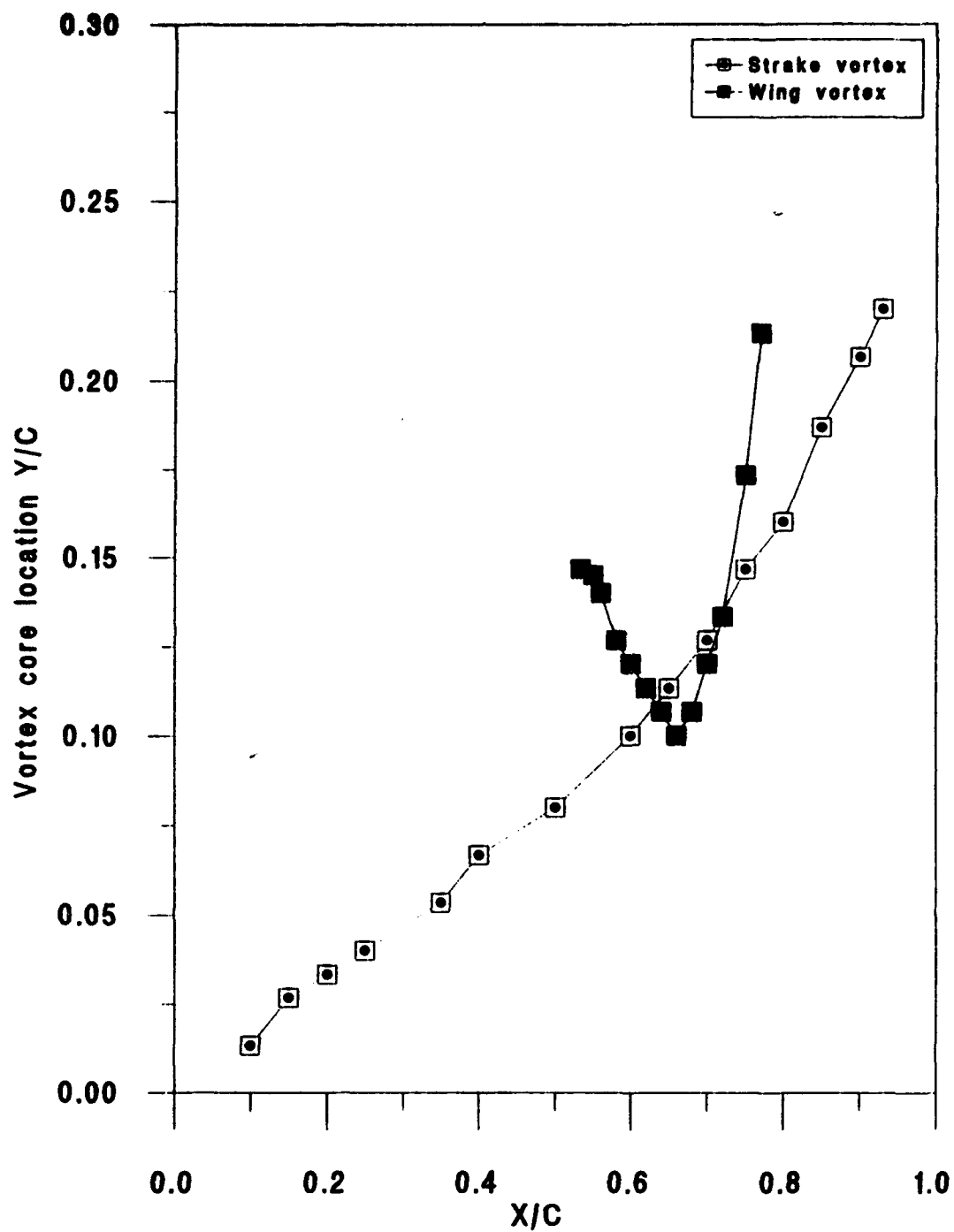


Fig. 64 Vortex core location Y/C for baseline model at $AOA = 10$ Deg.

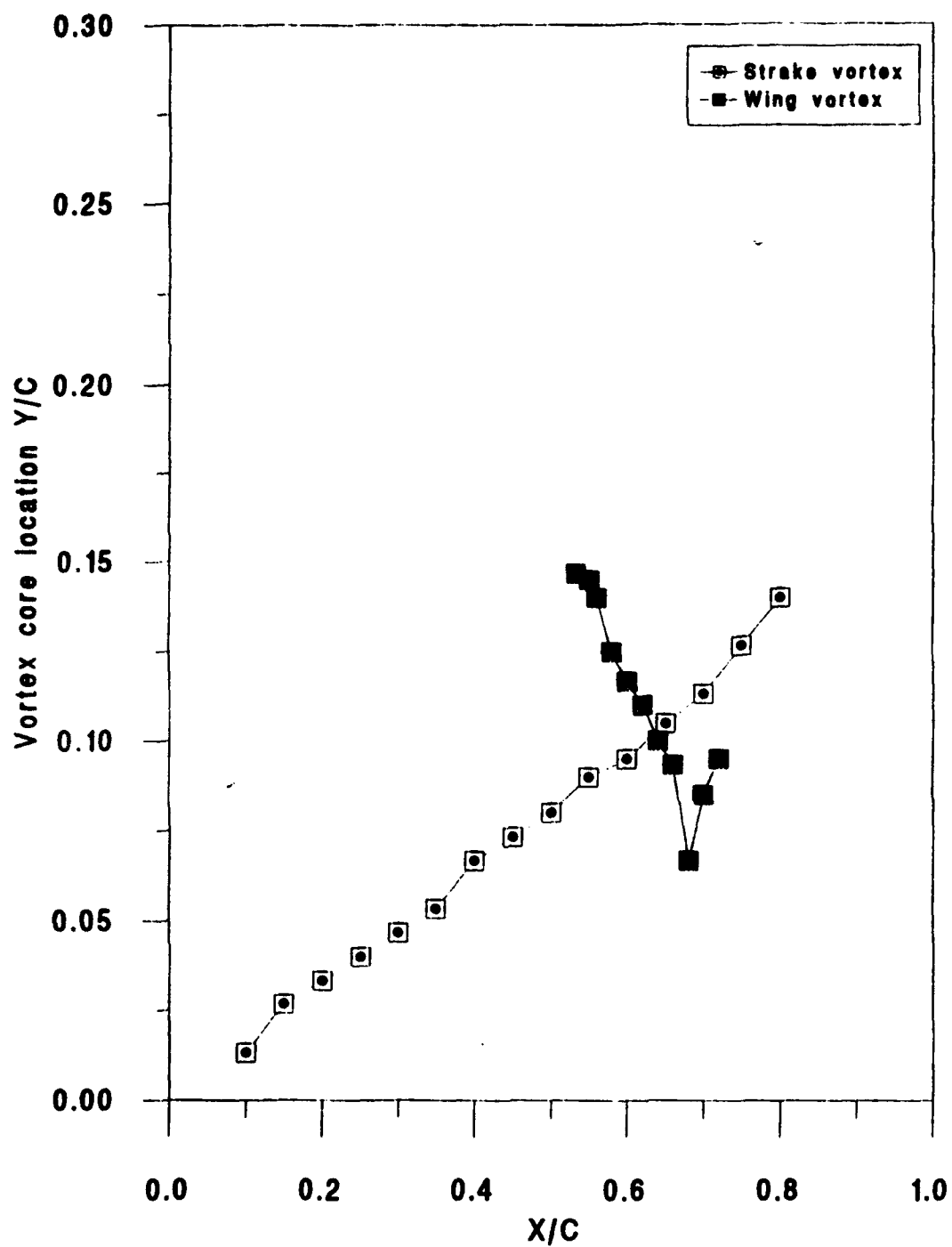


Fig. 65 vortex core location Y/C for baseline model at
AOA = 16 Deg.

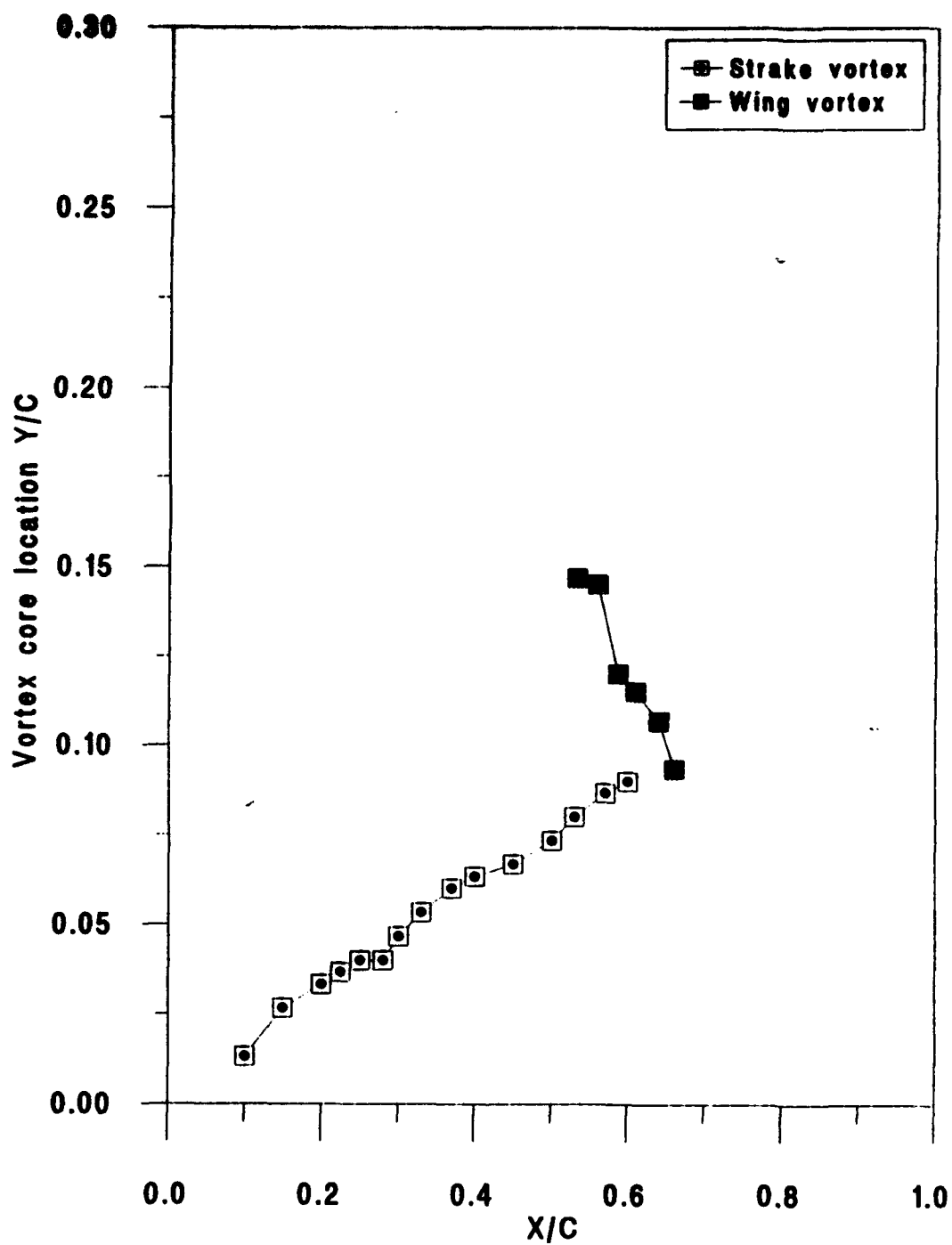


Fig. 66 Vortex core location Y/C for baseline model at AOA =20 Deg.

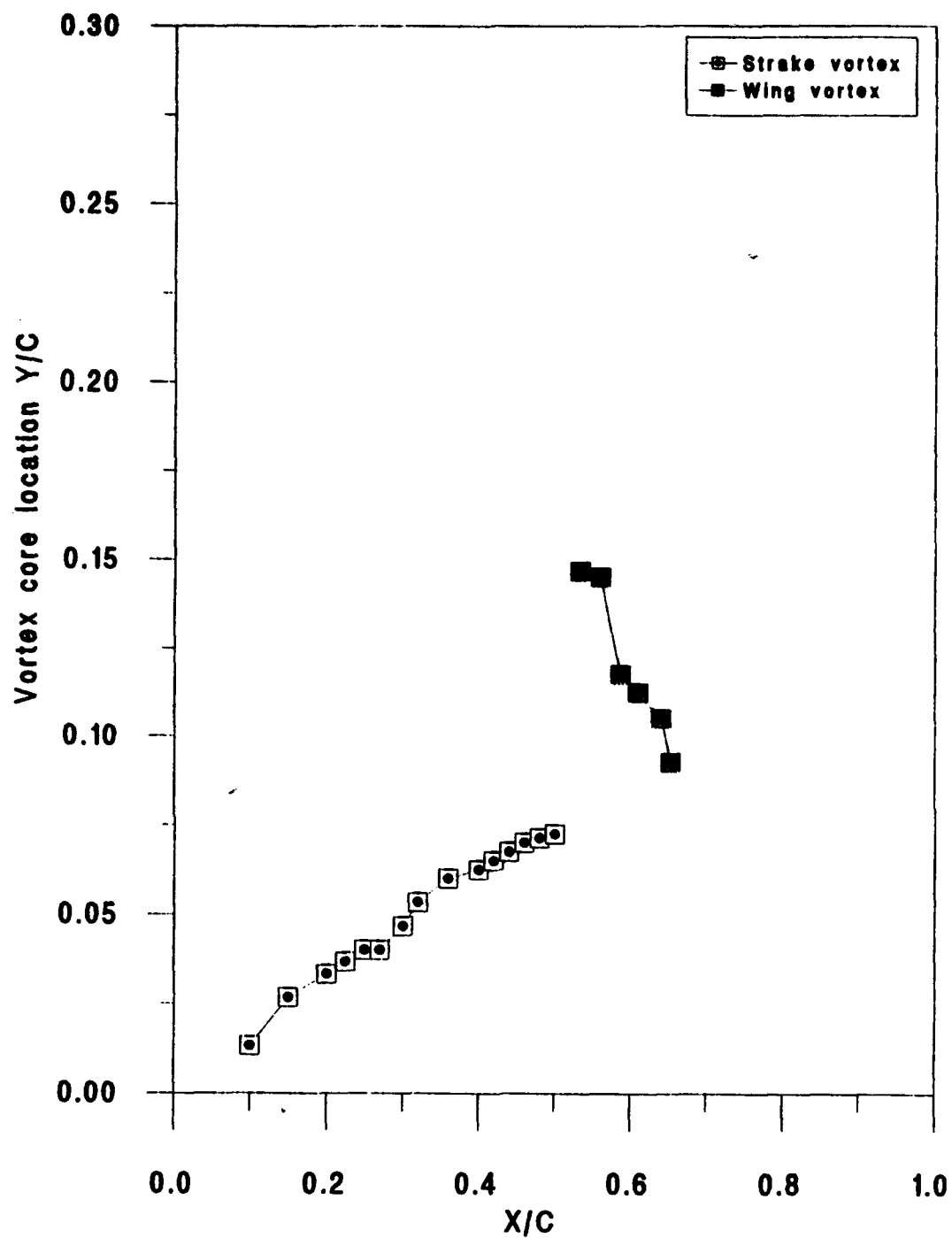


Fig. 67 Vortex core location Y/C for baseline model at $AOA = 22.5$ Deg.

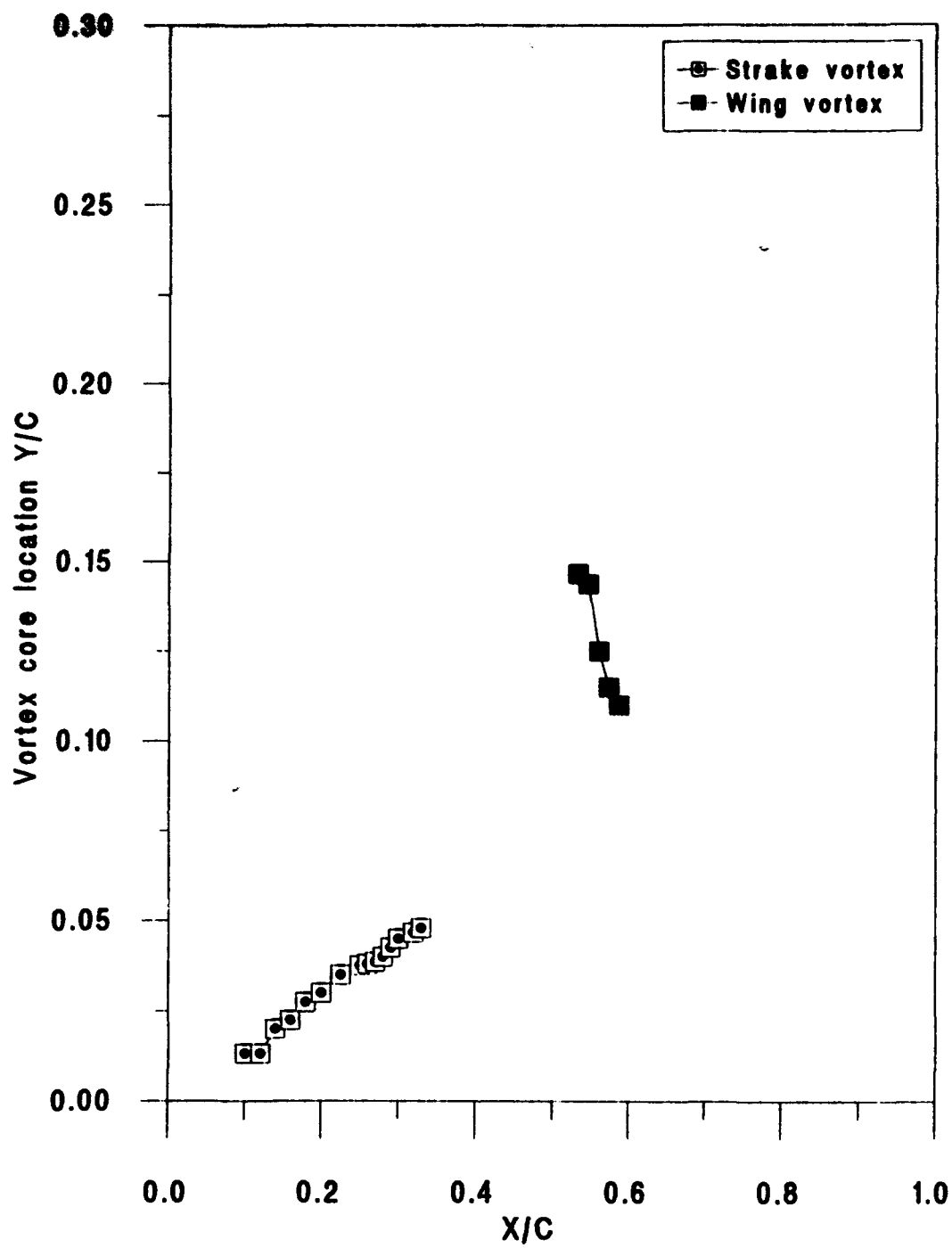


Fig. 68 Vortex core location Y/C for baseline model at $AOA = 30$ Deg.

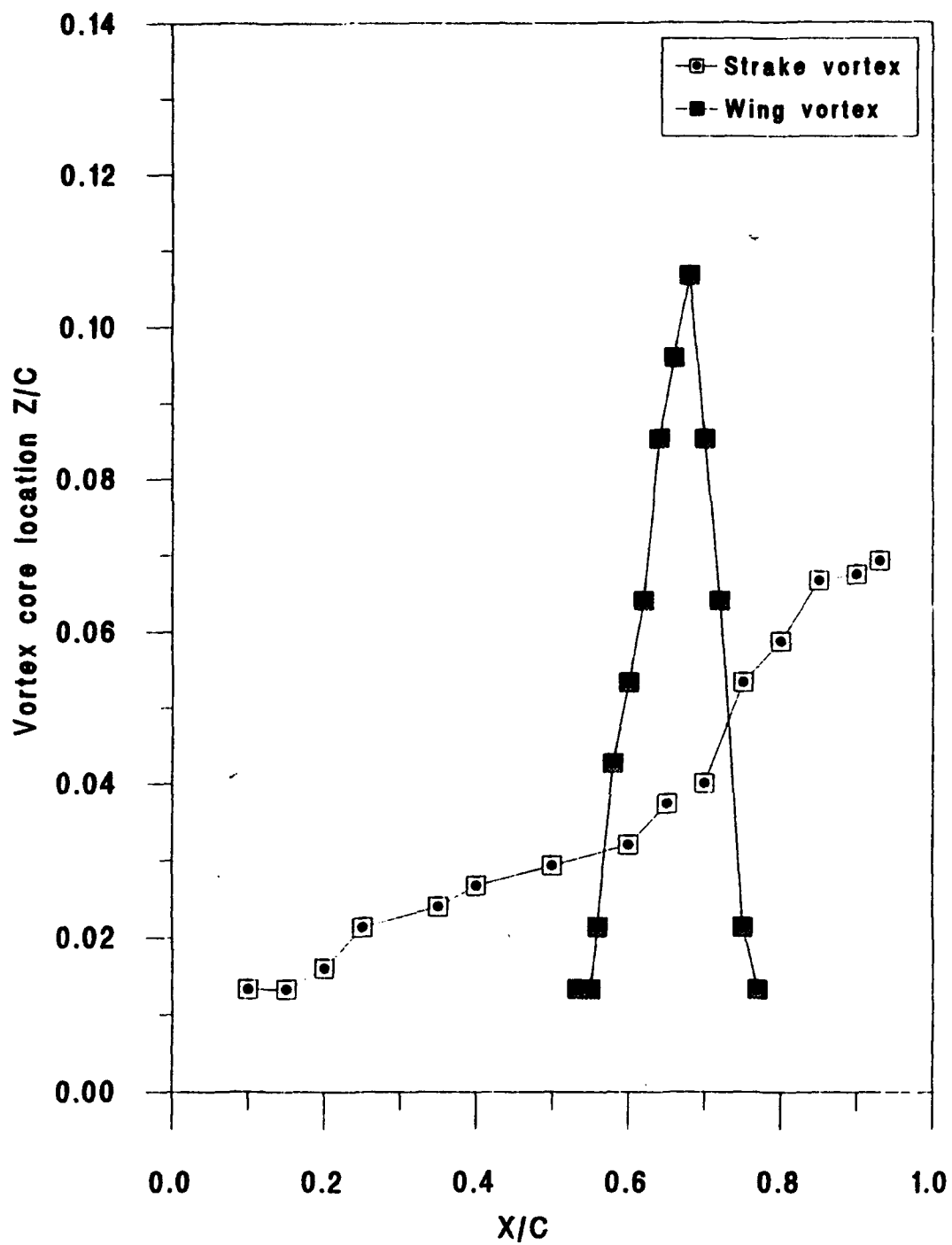


Fig. 69 Vortex core location Z/C for baseline model at AOA = 10 Deg.

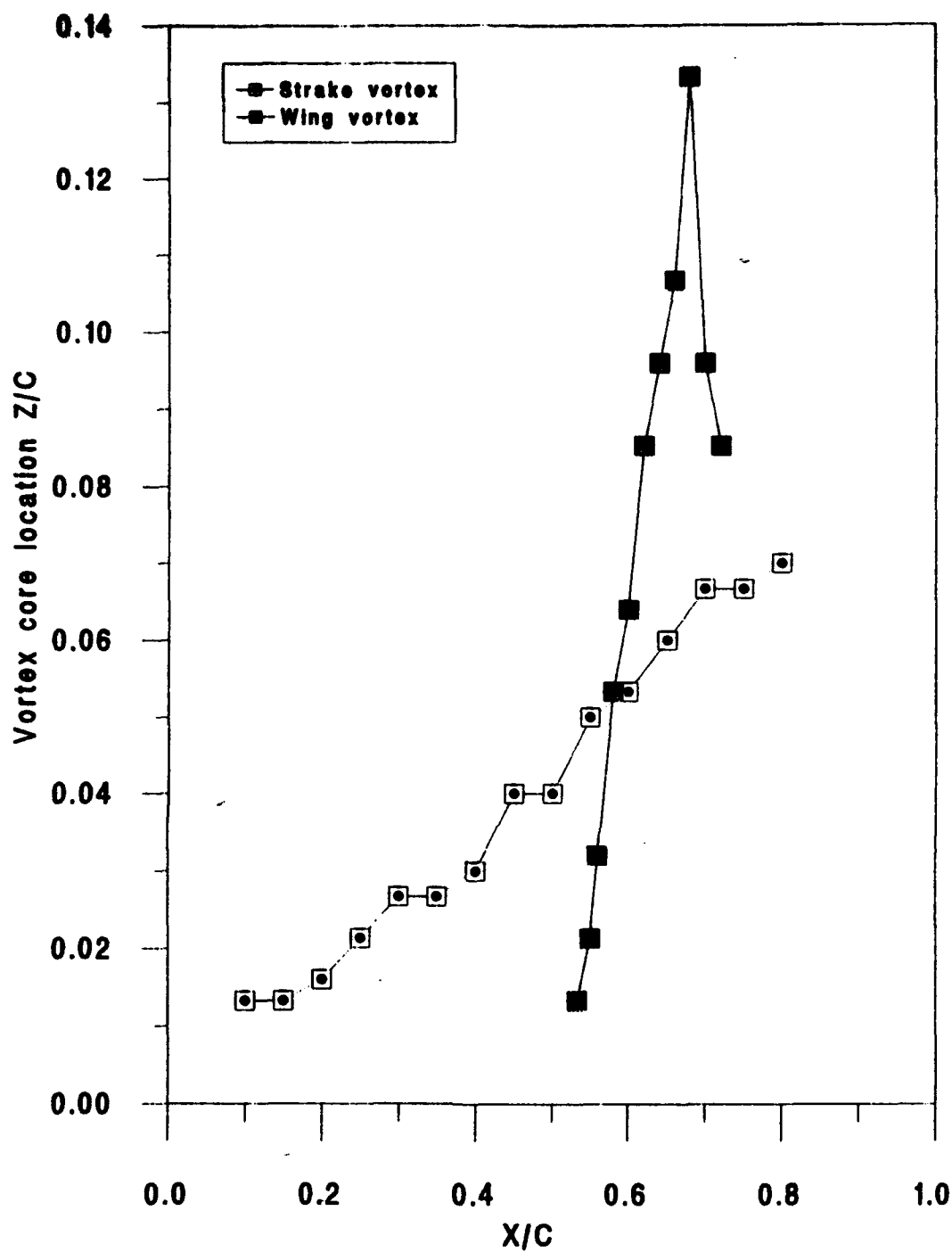


Fig. 70 Vortex core location Z/C for baseline model at
AOA = 16 Deg.

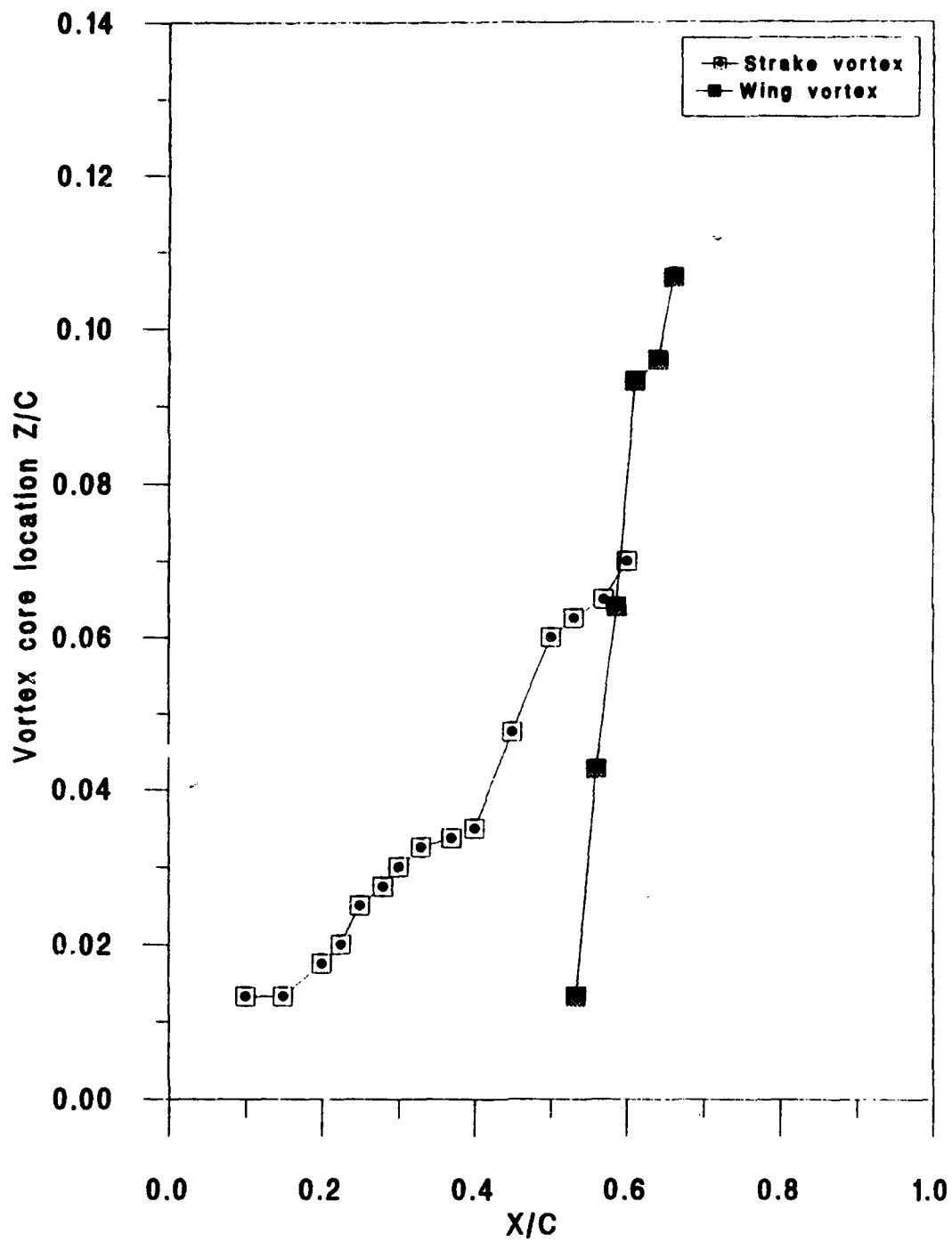


Fig. 71 Vortex core location Z/C for baseline model at AOA = 20 Deg.

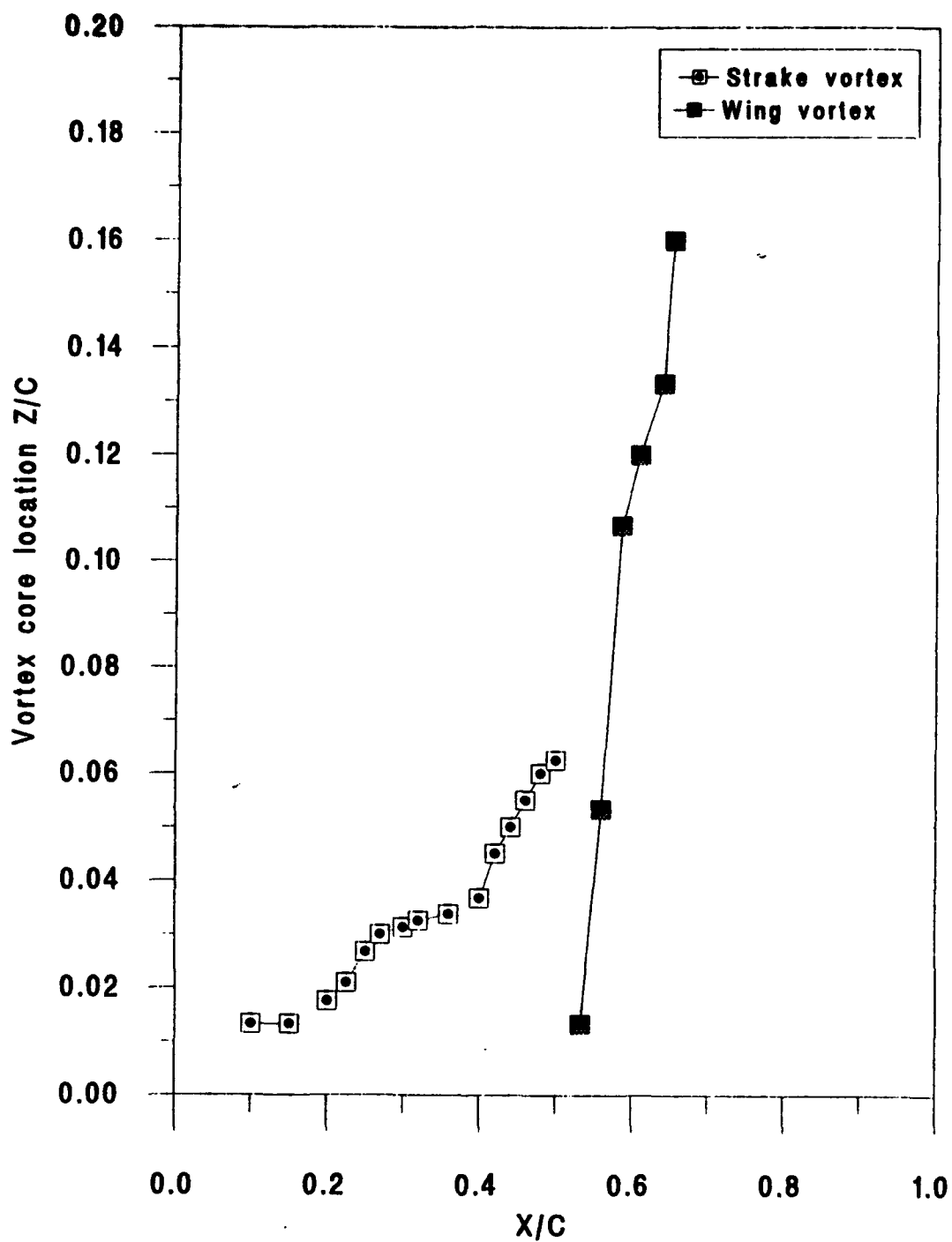


Fig. 72 Vortex core location Z/C for baseline model at AOA =22.5 Deg.

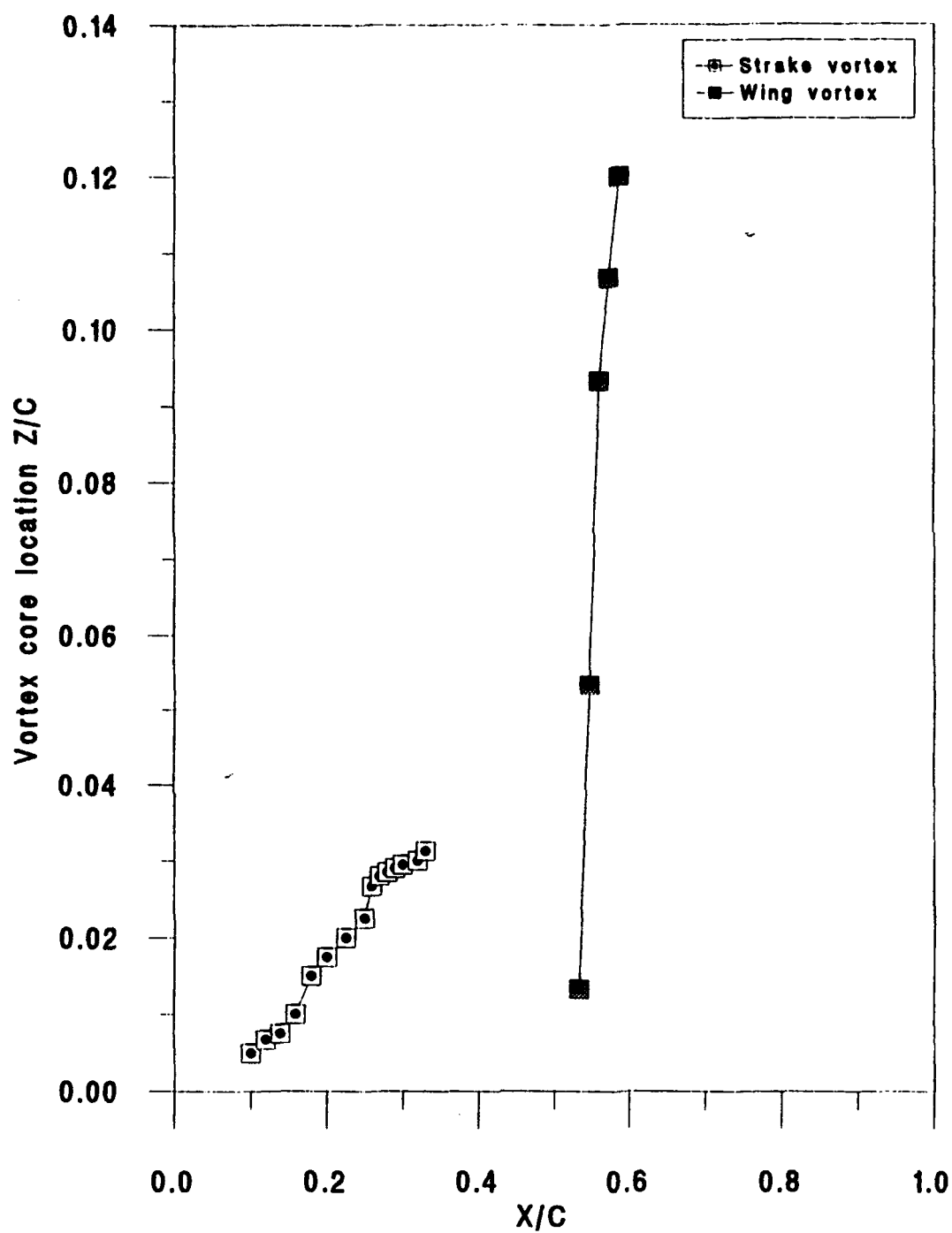


Fig. 73 Vortex core location Z/C for baseline model at AOA = 30 Deg.

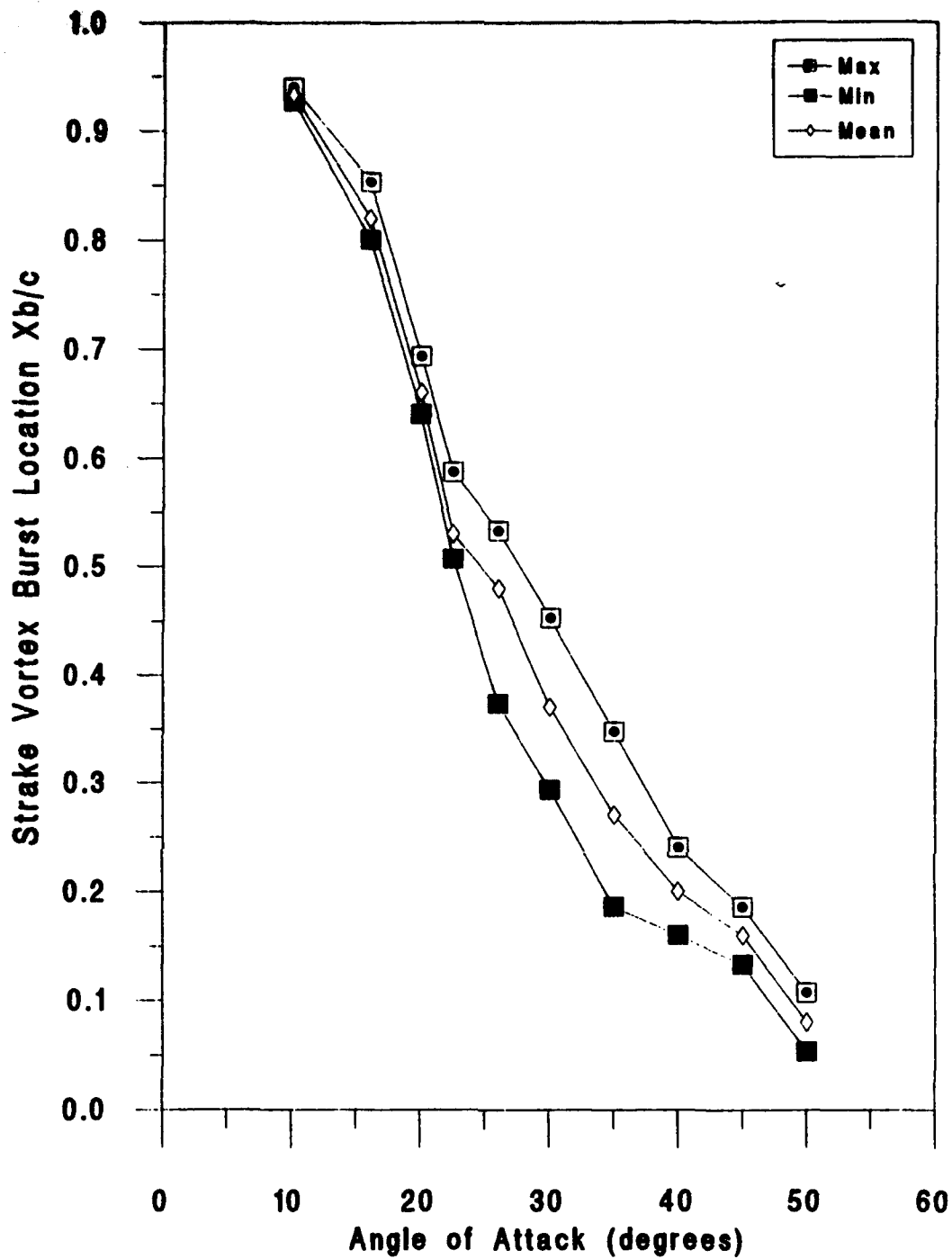


Fig. 74 vortex burst location Xb/c
(maximum, minimum & mean) for baseline model

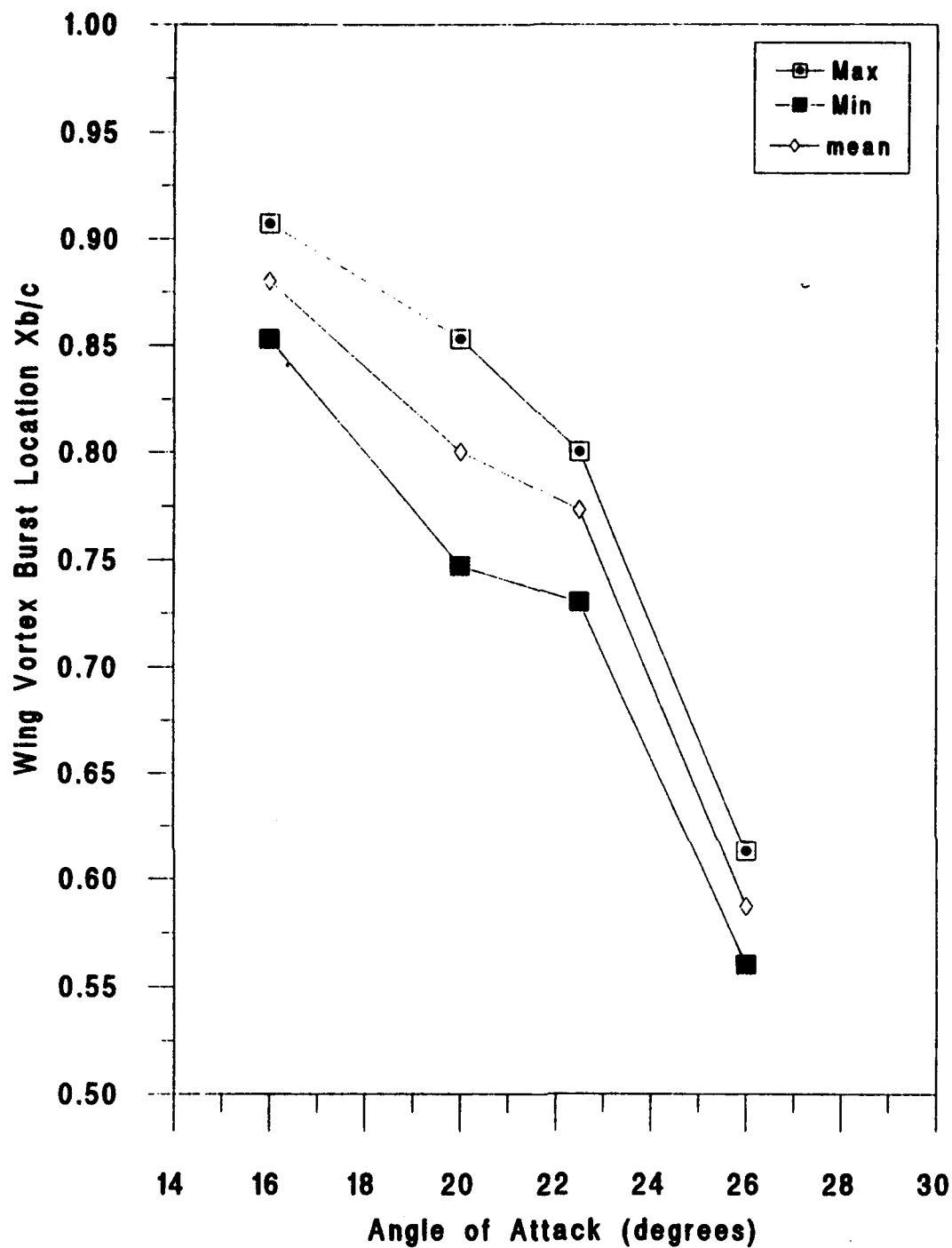


Fig. 75 Vortex burst location Xb/c
(maximum, minimum & mean) for baseline model

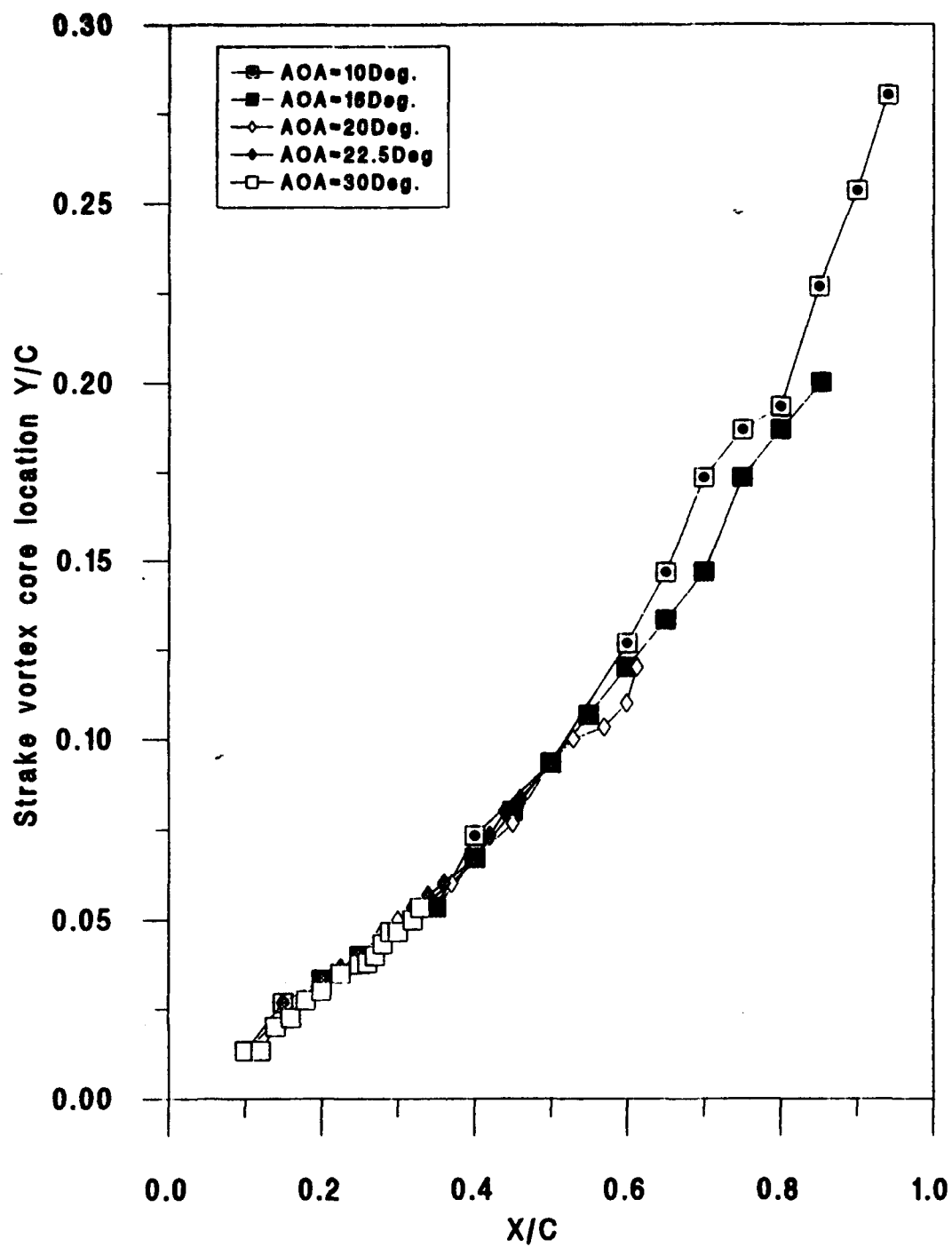


Fig. 76 Vortex core location Y/C for linear-fillet model

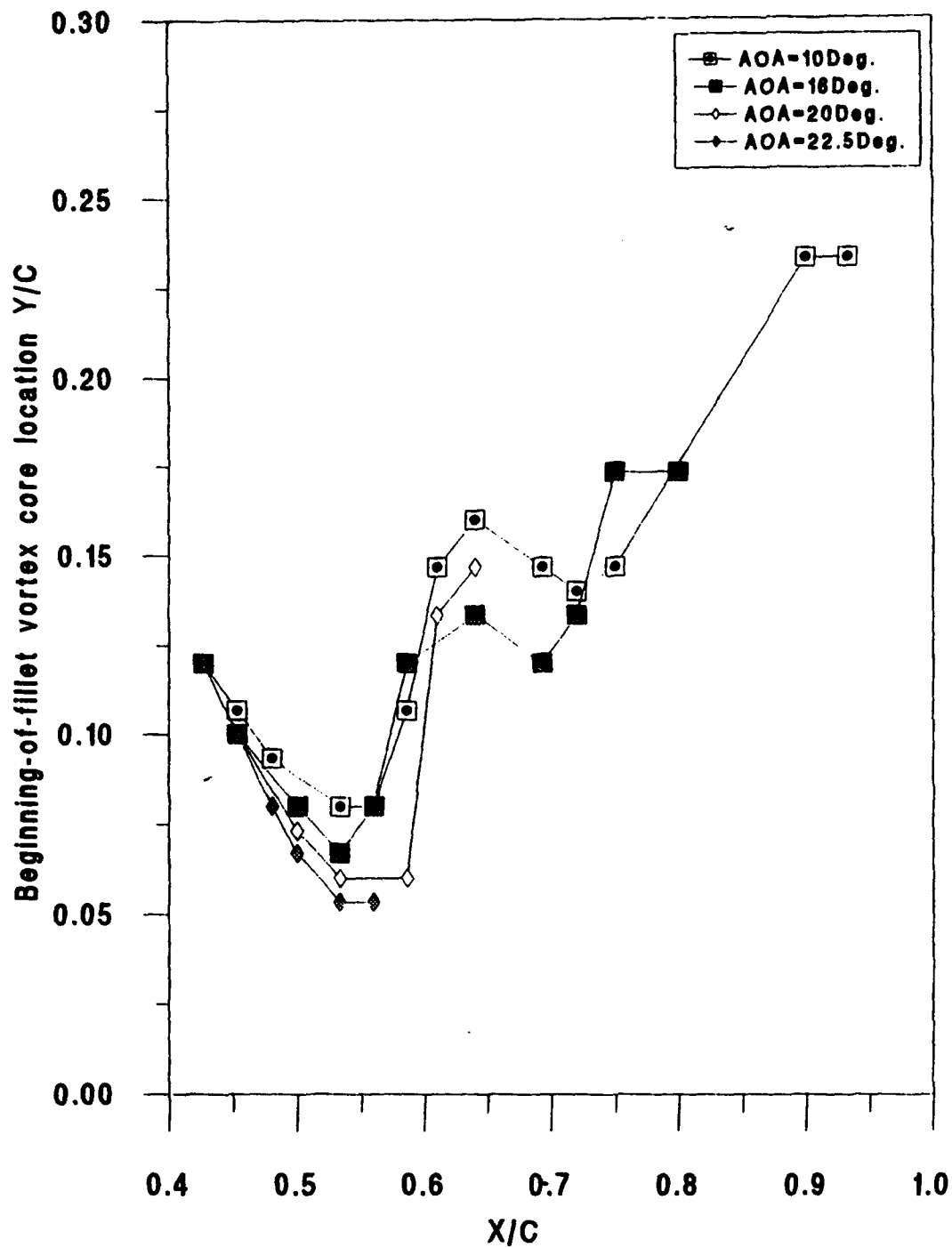


Fig. 77 Vortex core location Y/C for linear-fillet model

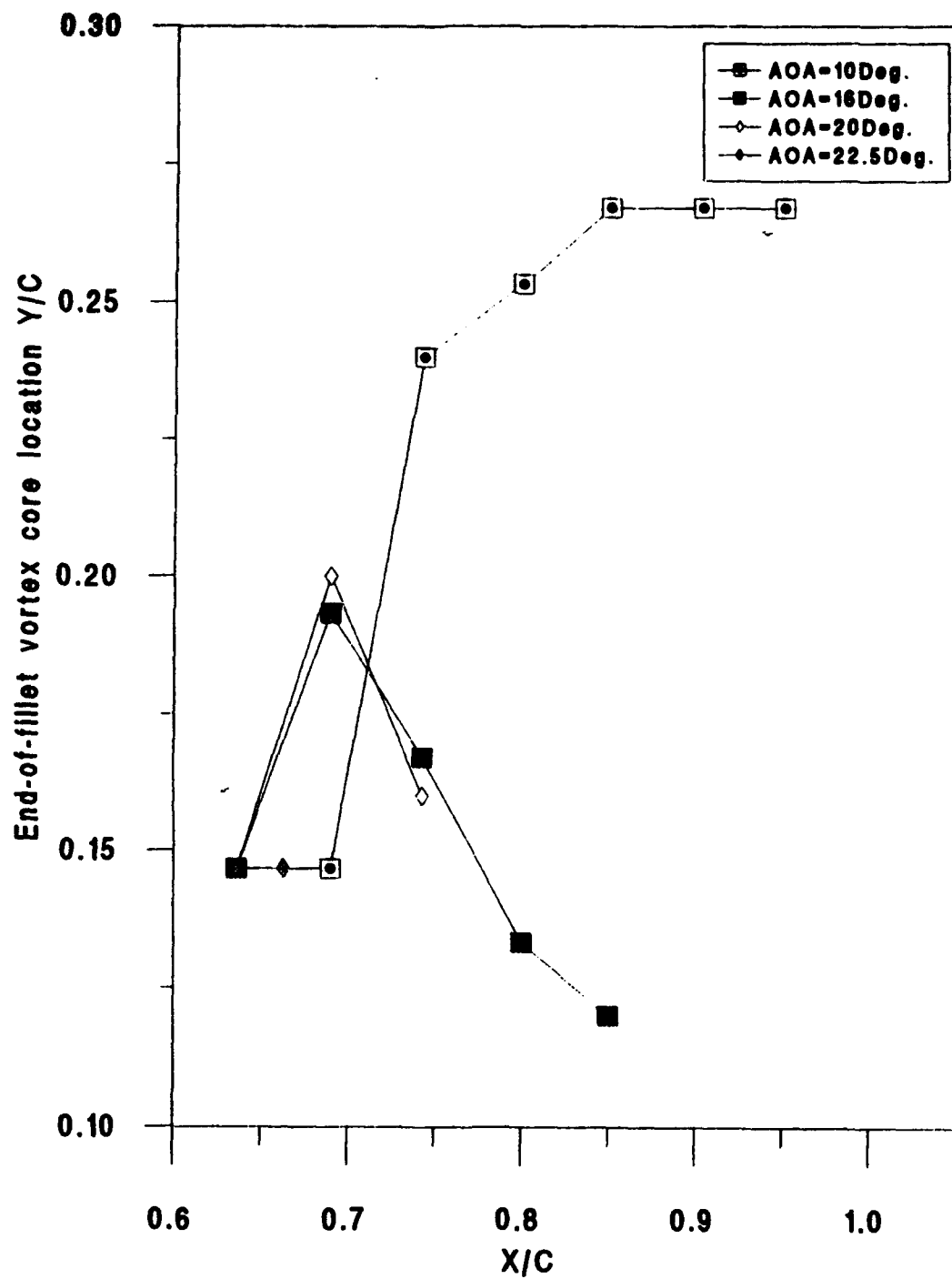


Fig. 78 Vortex core location Y/C for linear-fillet model

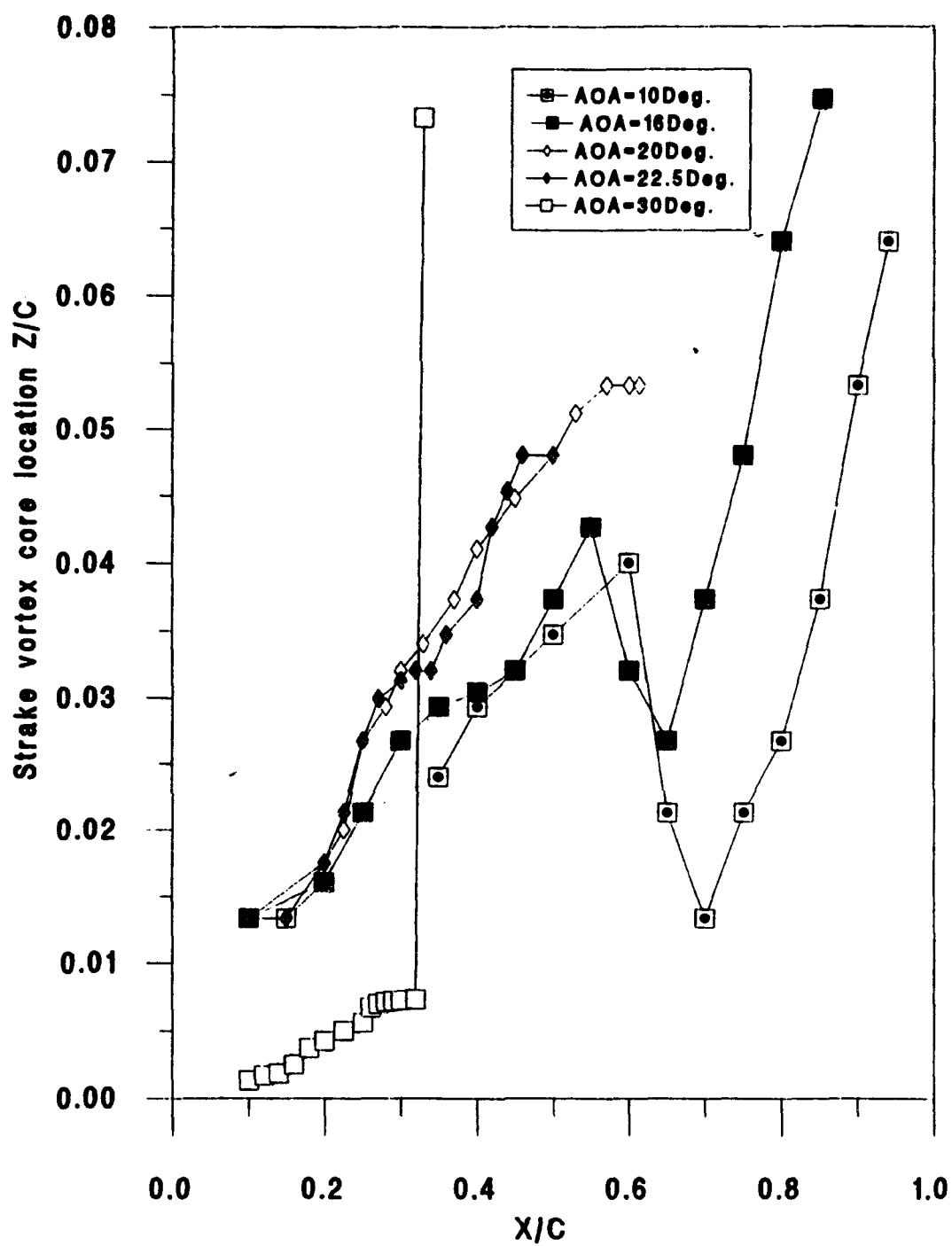


Fig. 79 Vortex core location Z/C for linear-fillet model

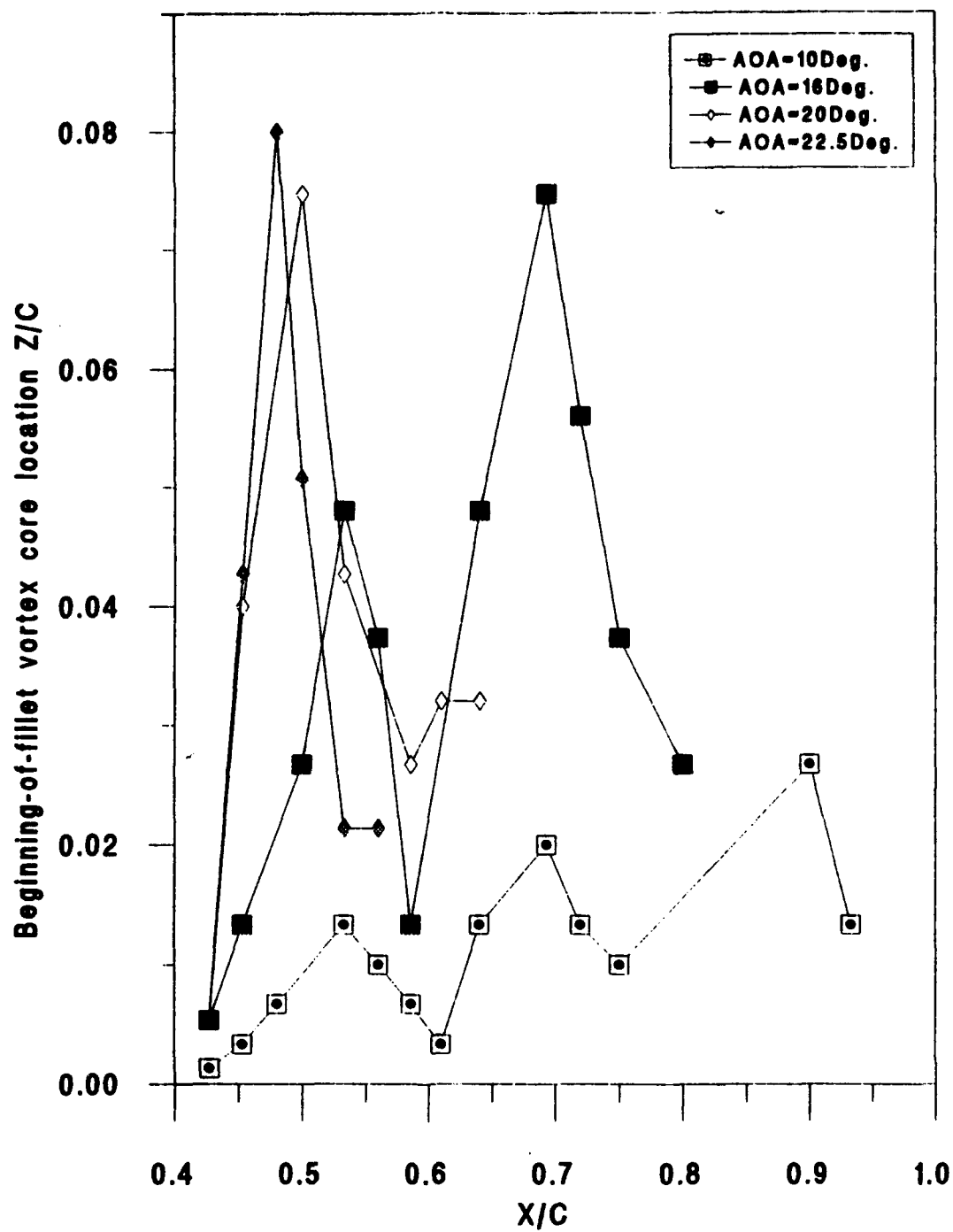


Fig. 80 Vortex core location Z/C for linear-fillet model

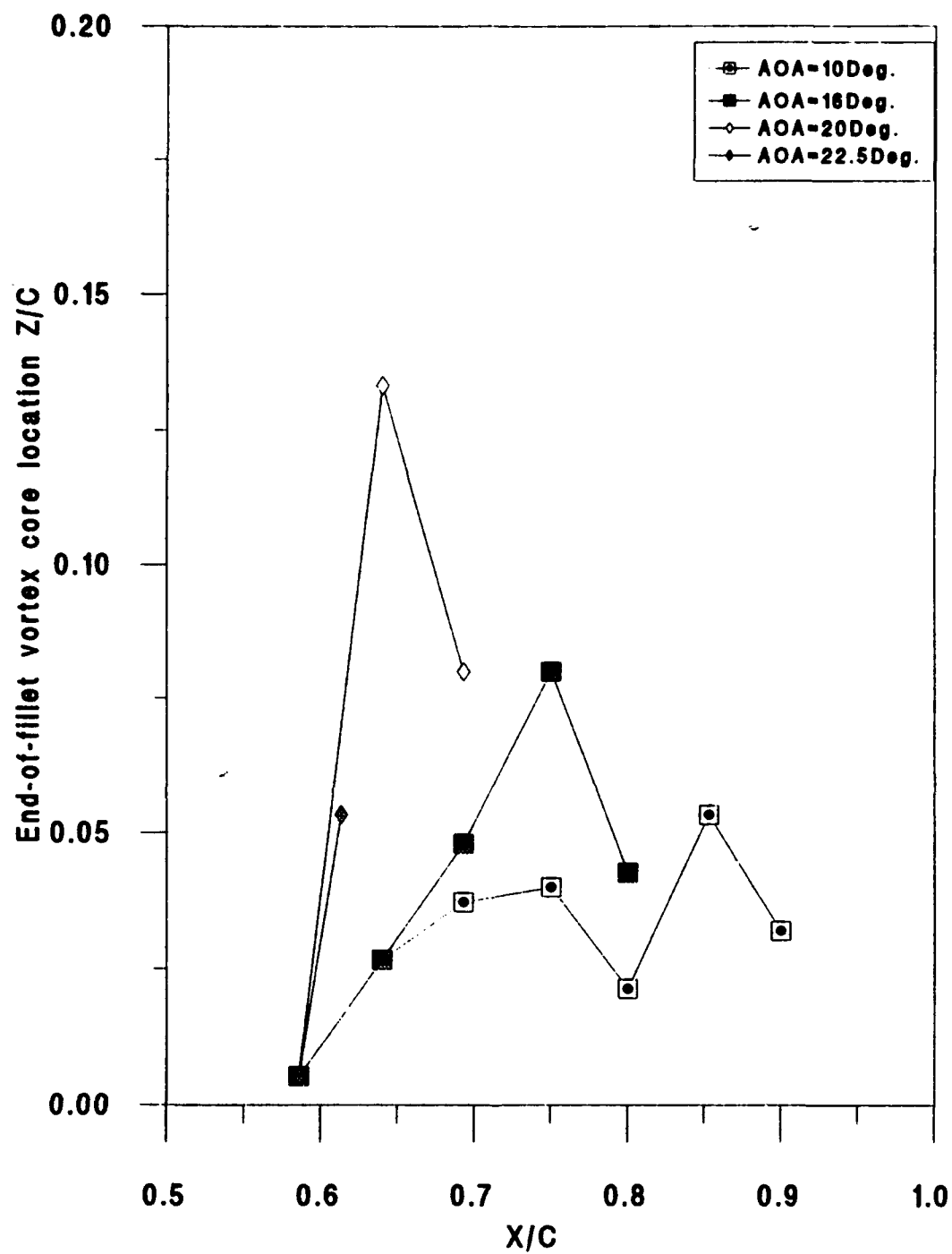


Fig. 81 Vortex core location Z/C for linear-fillet model

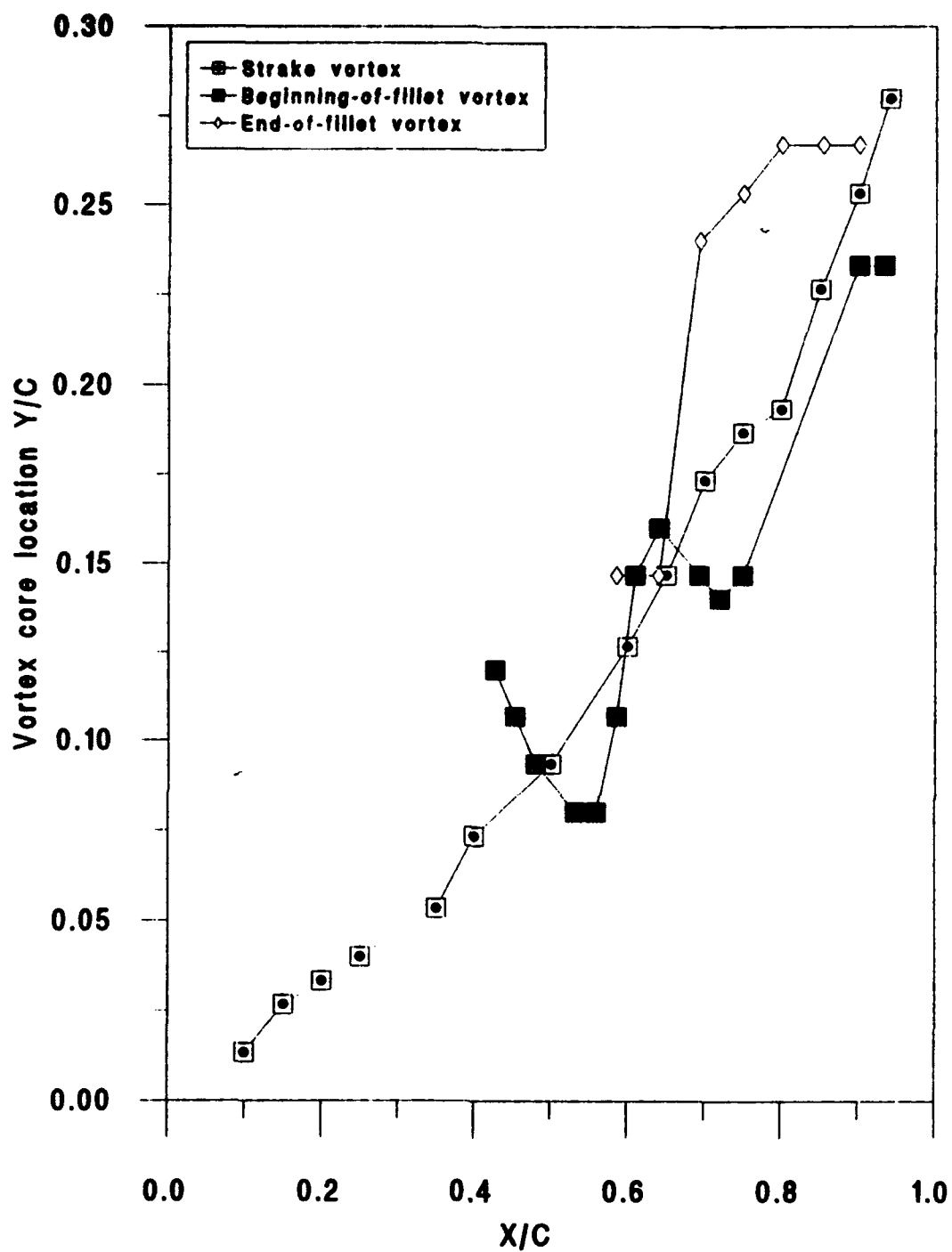


Fig. 82 Vortex core location Y/C for linear-fillet model at $AOA = 10$ Deg.

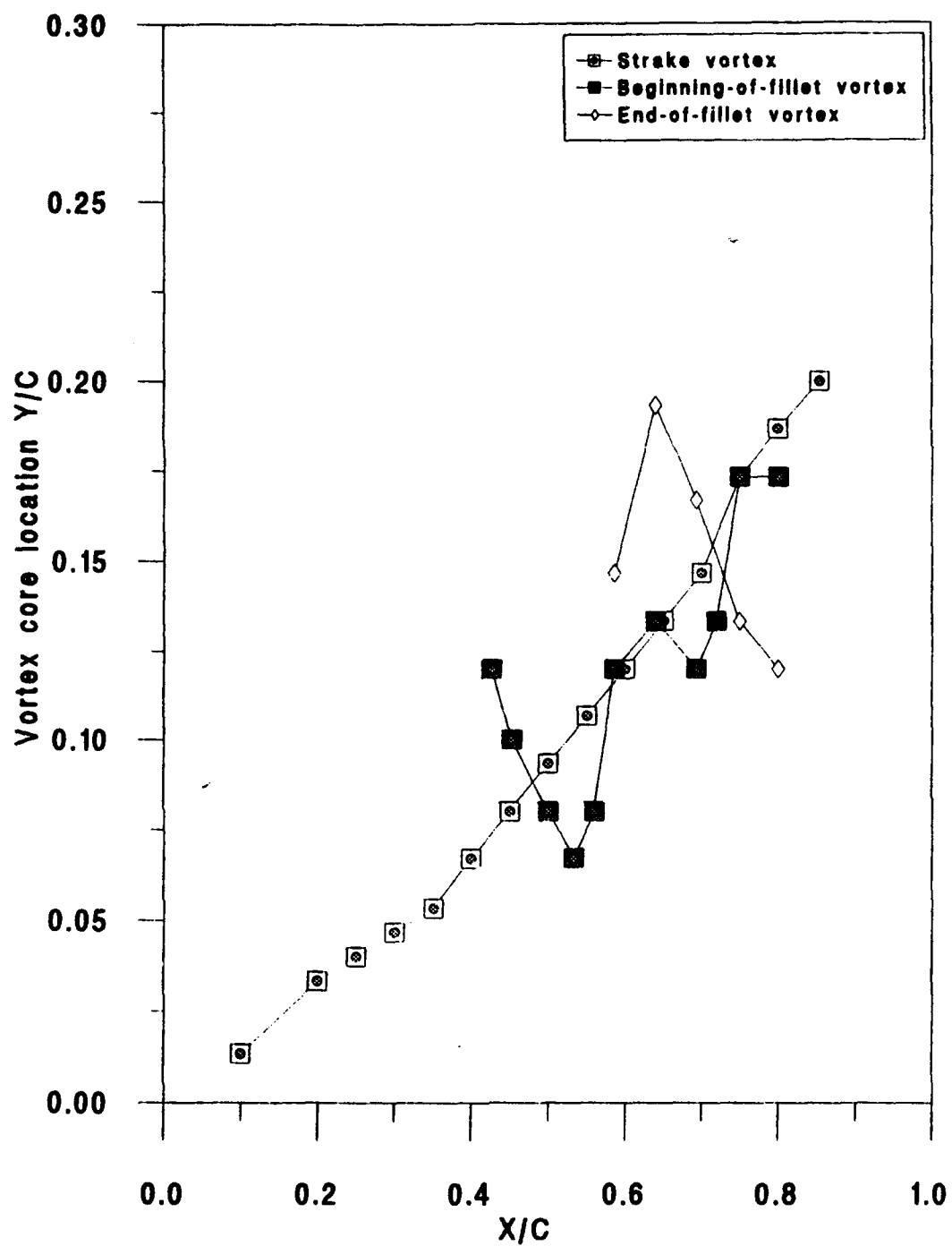


Fig. 83 Vortex core location for linear-fillet model at AOA= 16 Deg.

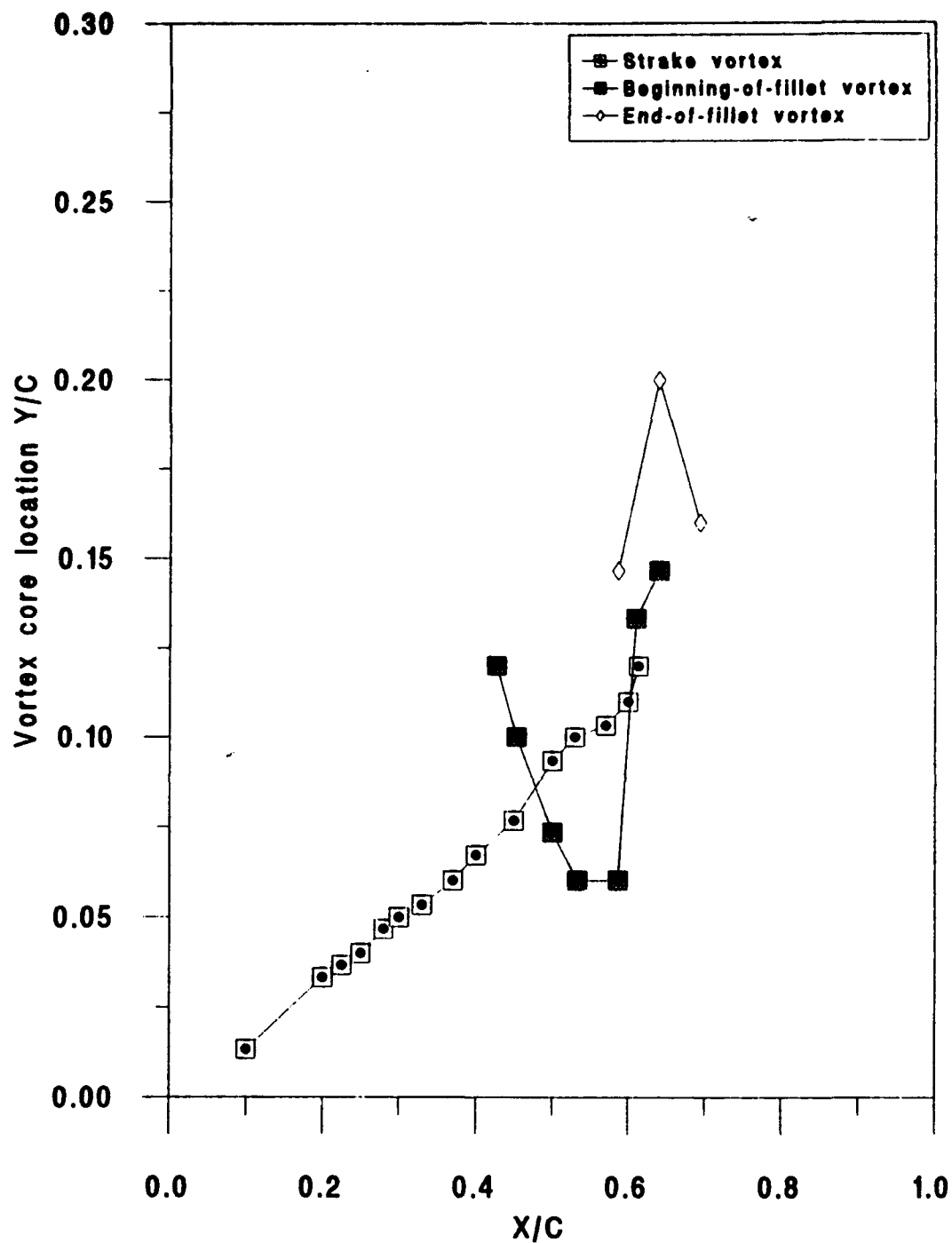


Fig. 84 Vortex core location Y/C for linear-fillet model at $AOA=20$ Deg.

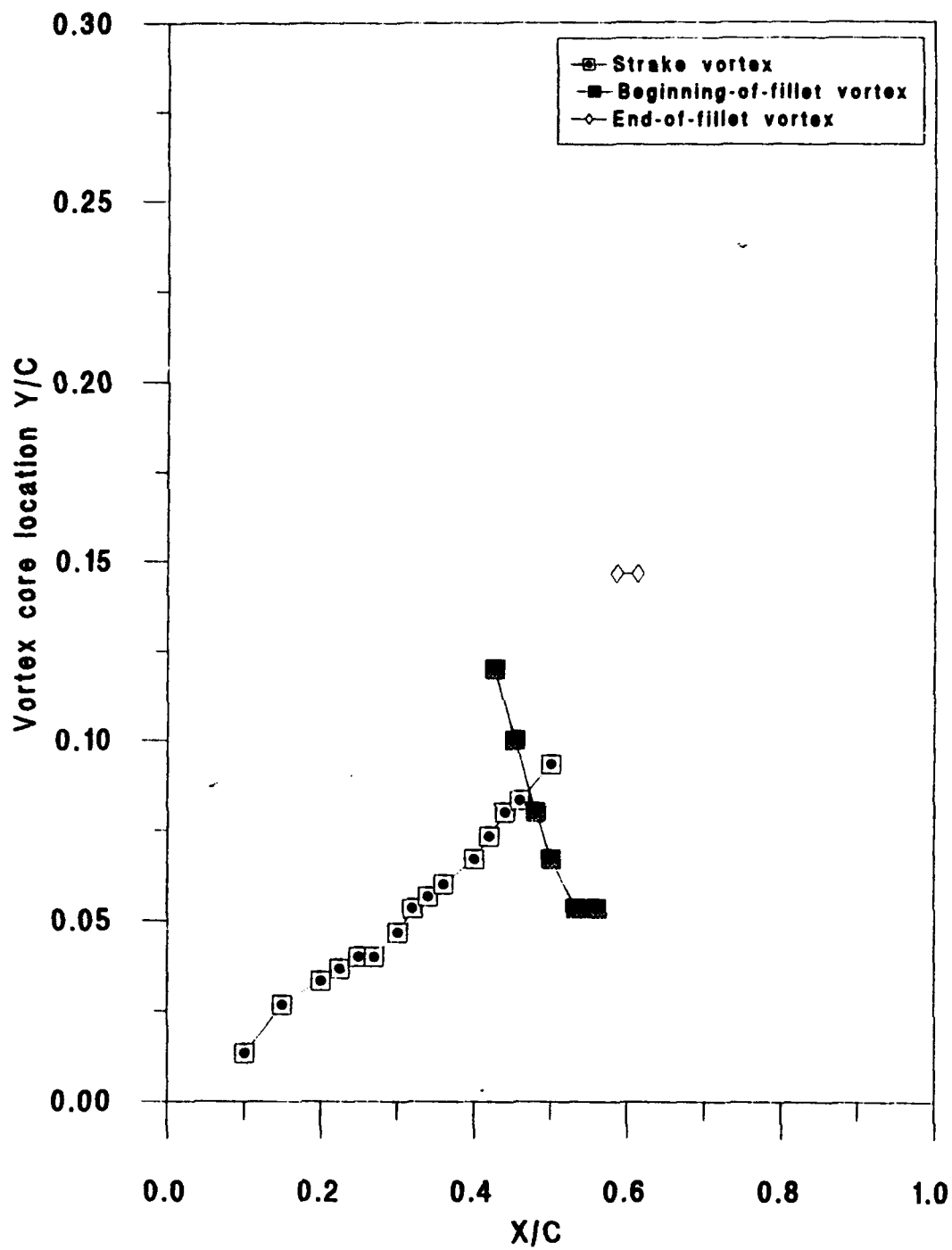


Fig. 85 Vortex core location Y/C for linear-fillet model at $AOA = 22.5$ Deg.

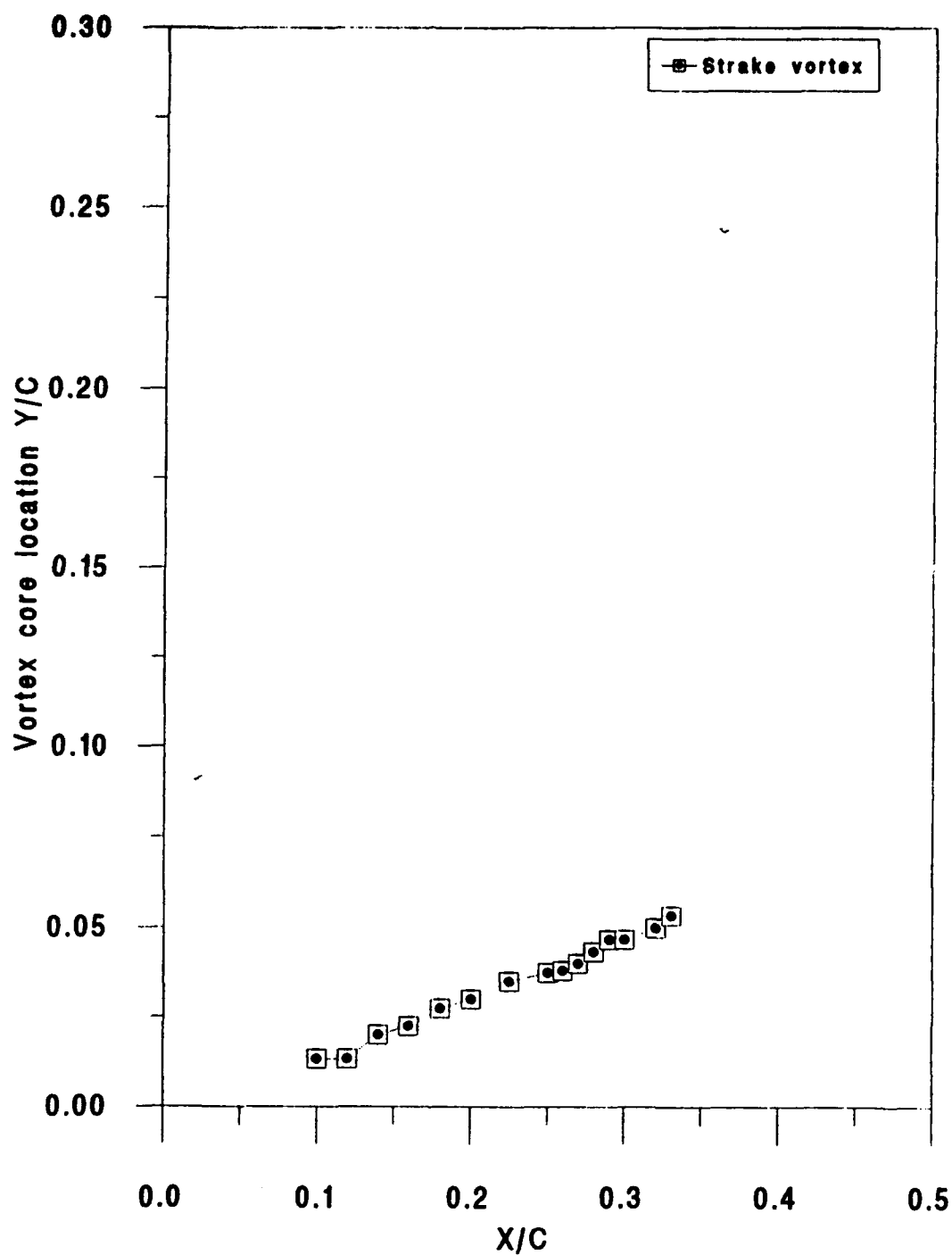


Fig. 86 Vortex core location Y/C for linear-fillet model at
AOA = 30 Deg.

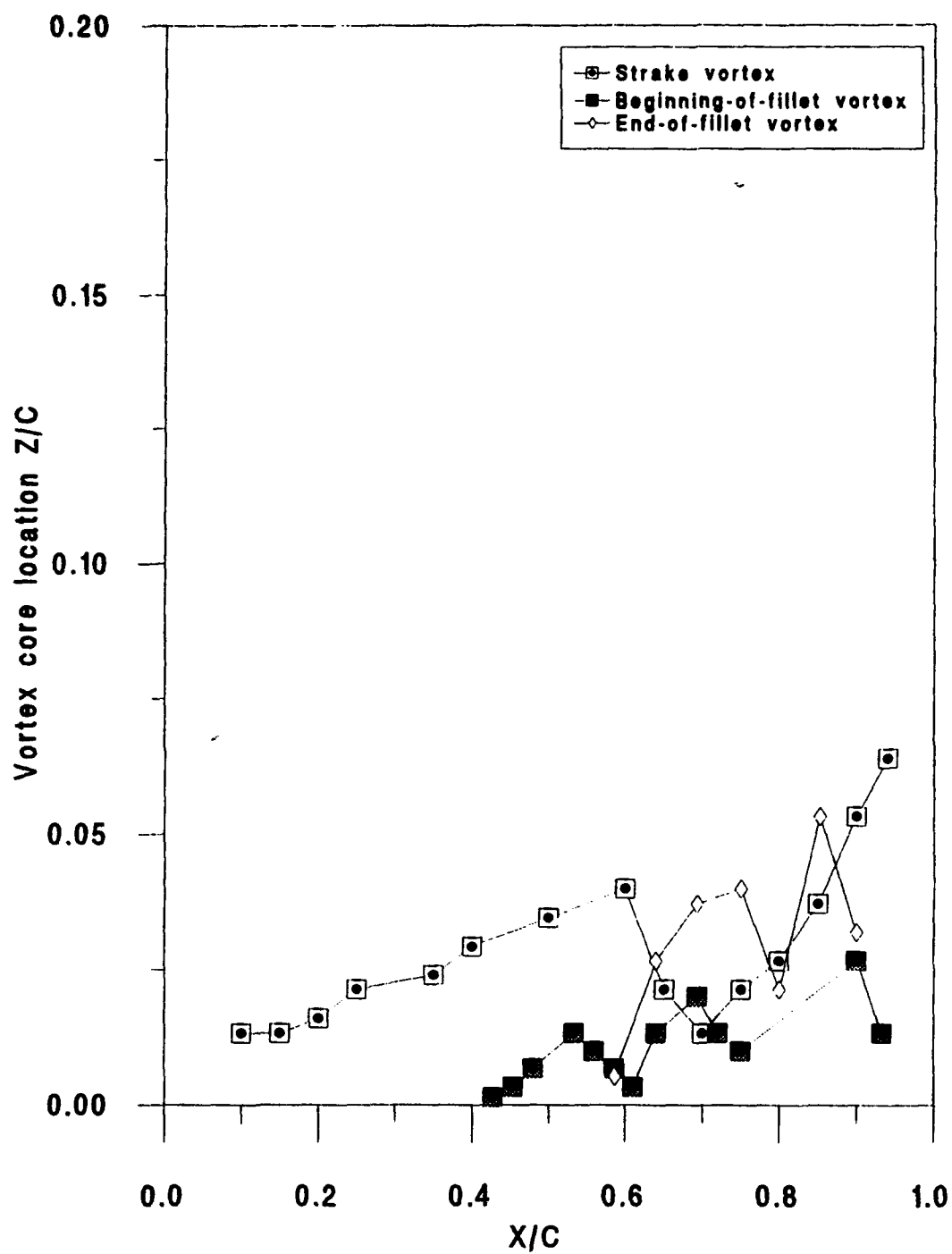


Fig. 87 Vortex core location Z/C for linear-fillet model at $AOA=10$ Deg.

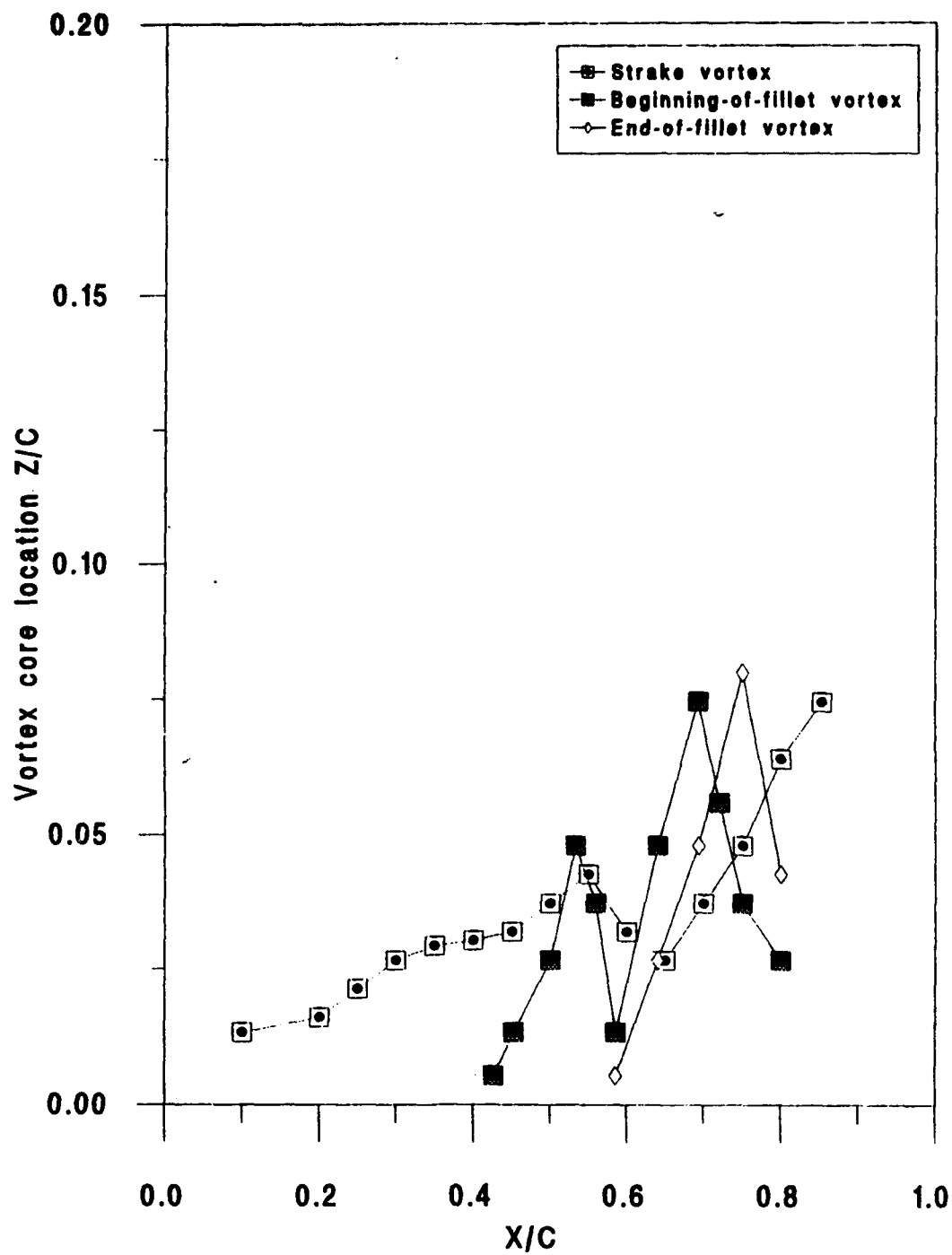


Fig. 88 vortex core location Z/C for linear-fillet model at $AOA=16$ Deg.

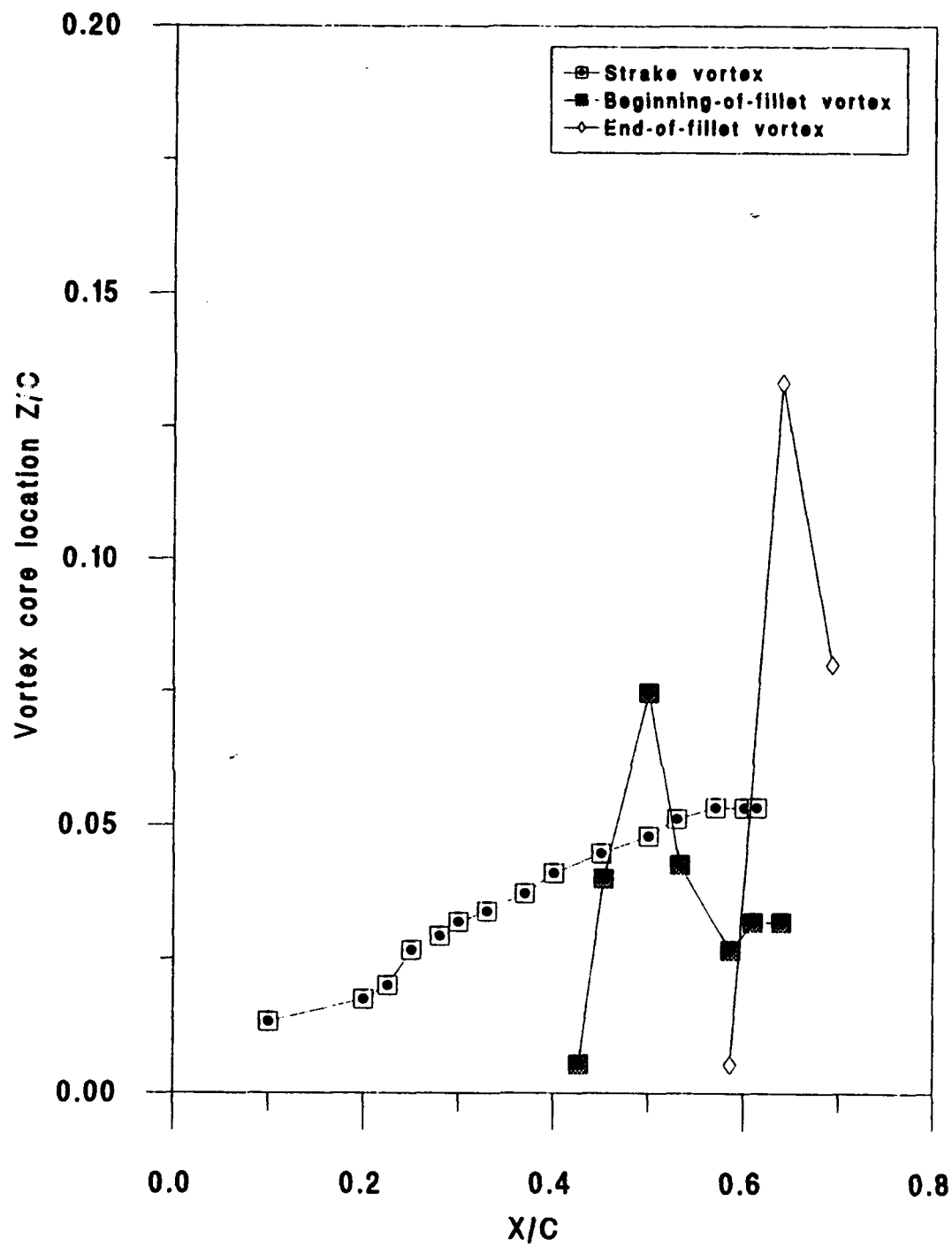


Fig. 89 Vortex core location Z/C for linear-fillet model at AOA = 20 Deg.

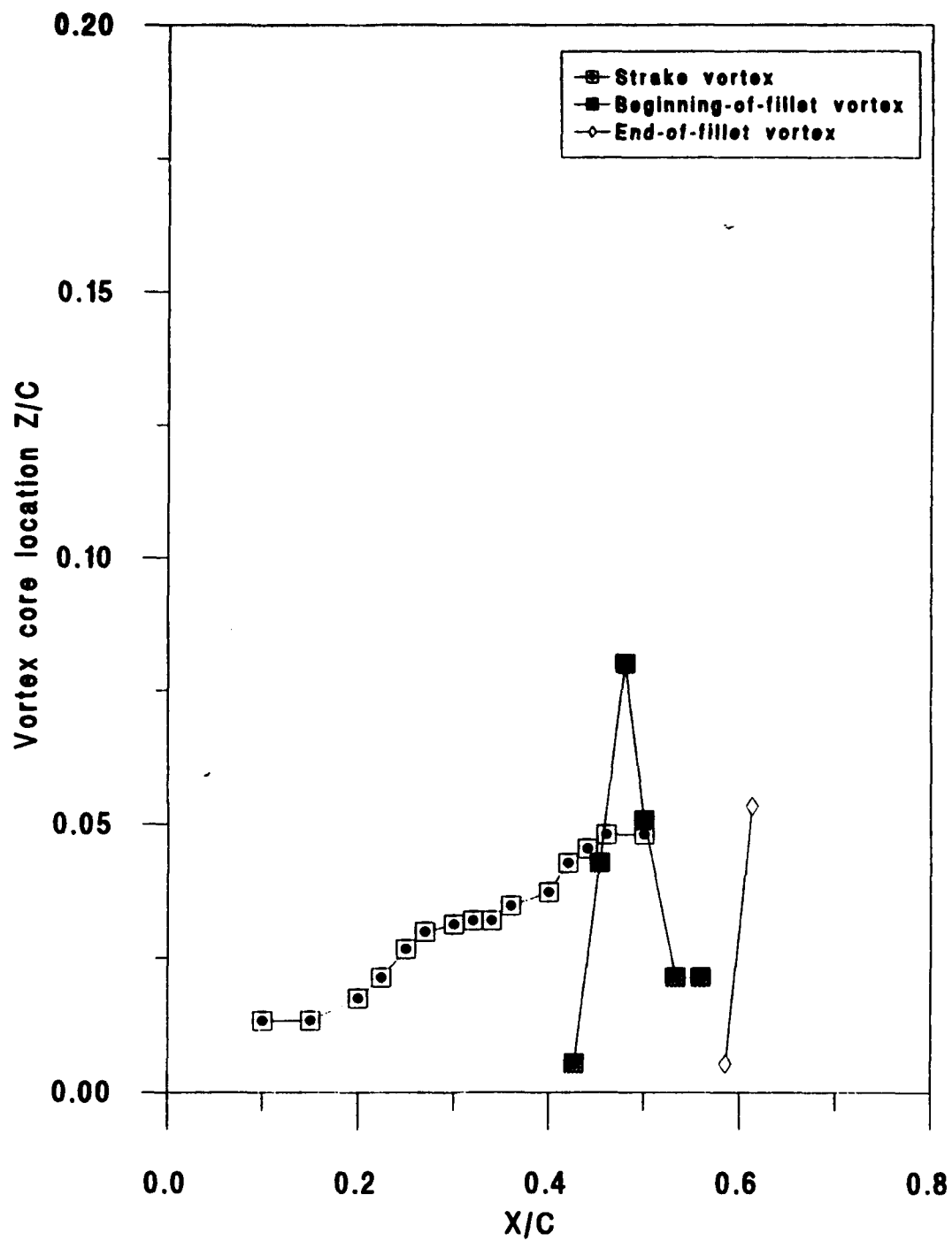


Fig. 90 Vortex core location Z/C for linear-fillet model at $AOA=22.5$ Deg.

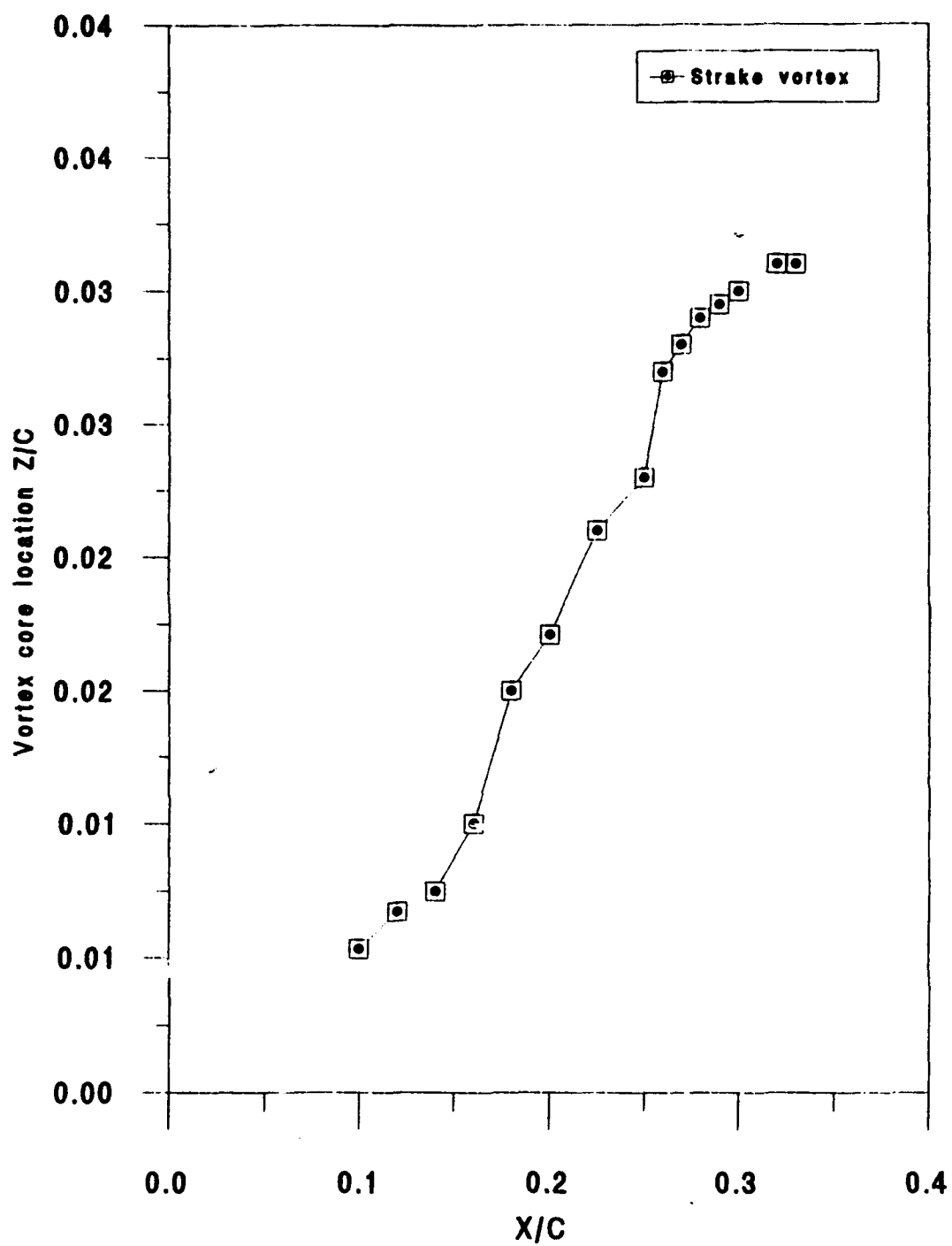


Fig. 91 Vortex core location Z/C for linear-fillet model at AOA=30 deg.

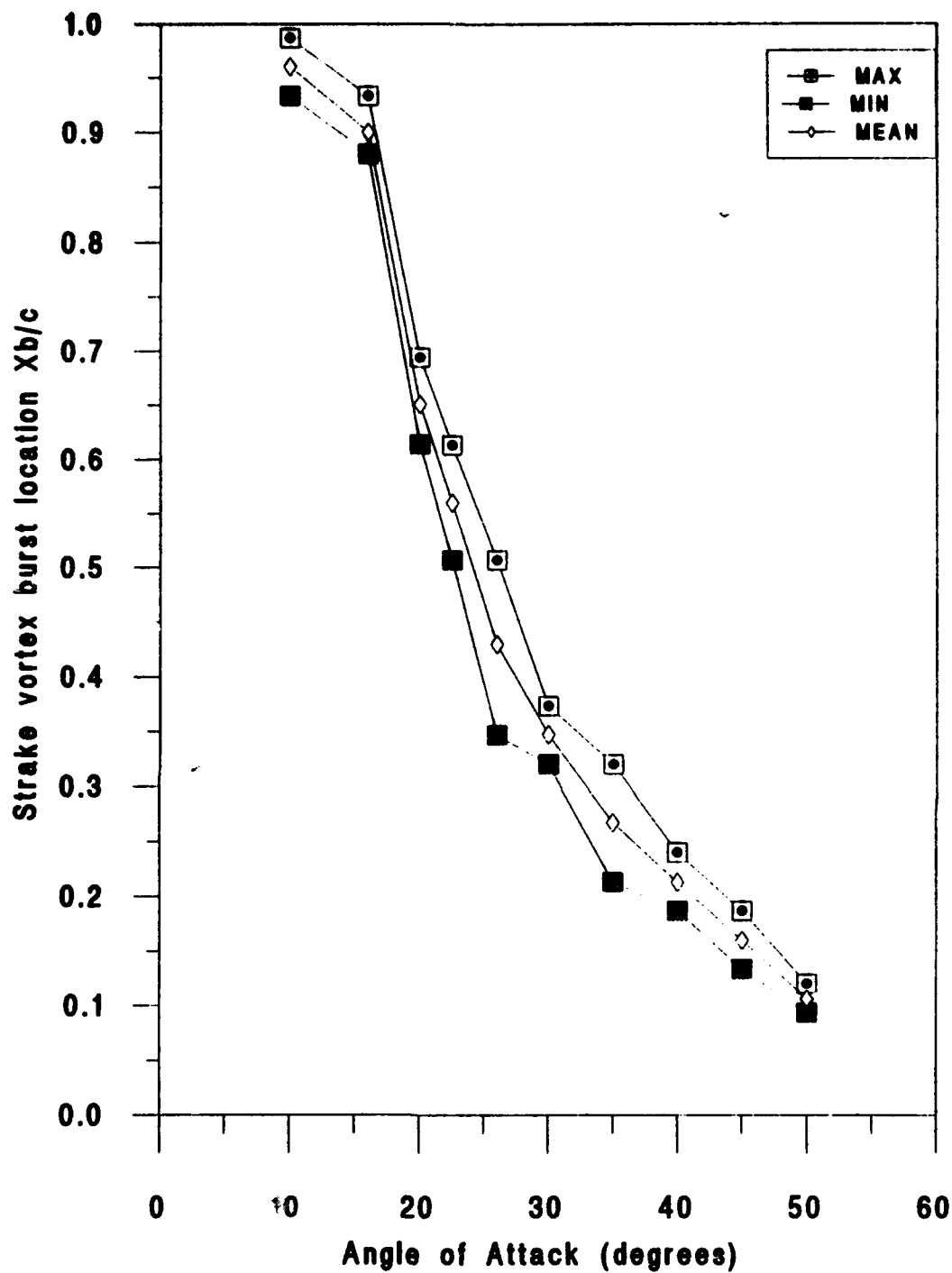


Fig. 92 Vortex burst location Xb/c (maximum, minimum & mean) for linear-fillet model

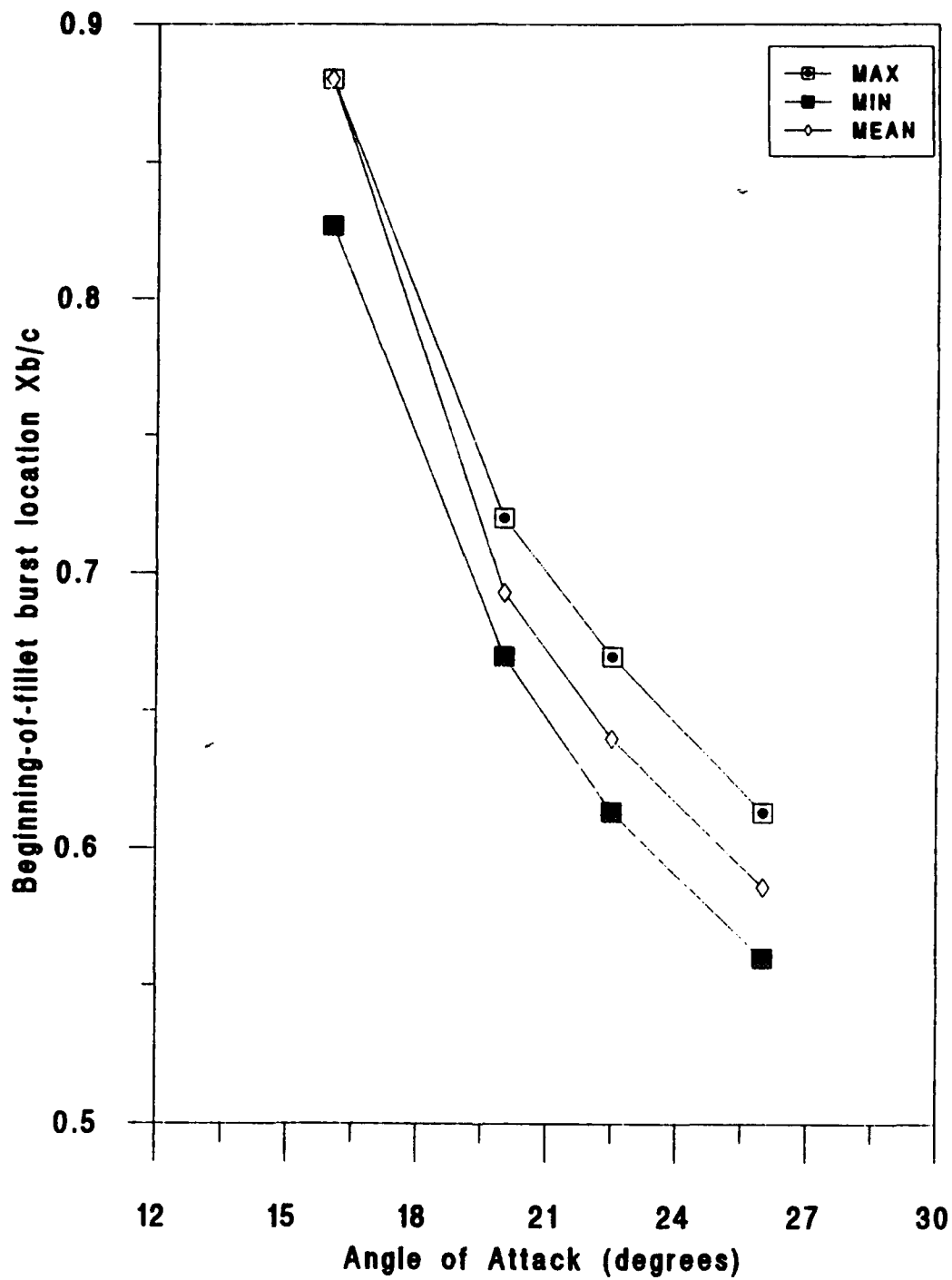


Fig. 93 Vortex Burst Location Xb/c (maximum, minimum & mean) for linear-fillet model

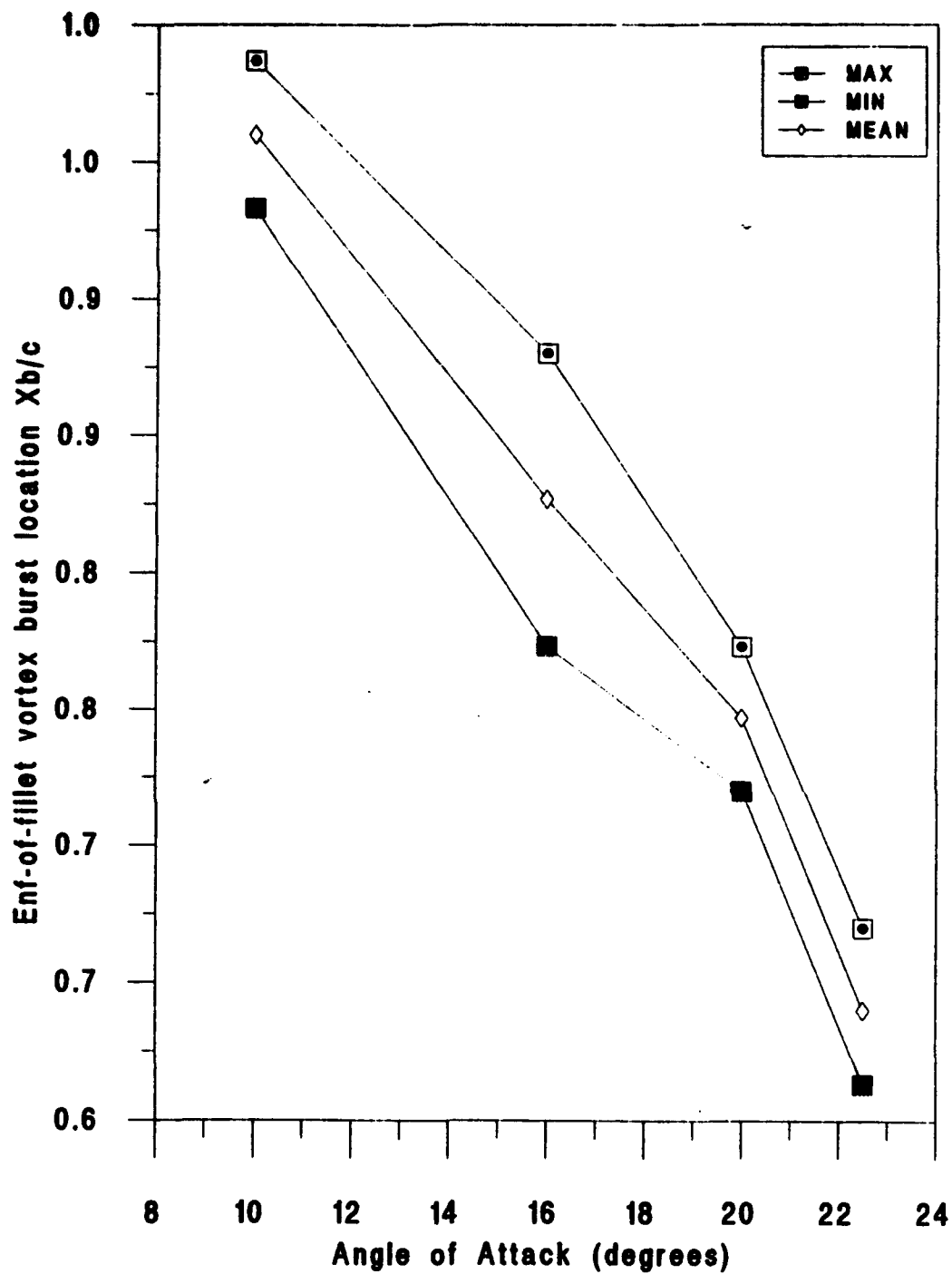


Fig. 94 Vortex Burst Location Xb/c (maximum, minimum & mean) for linear-fillet model

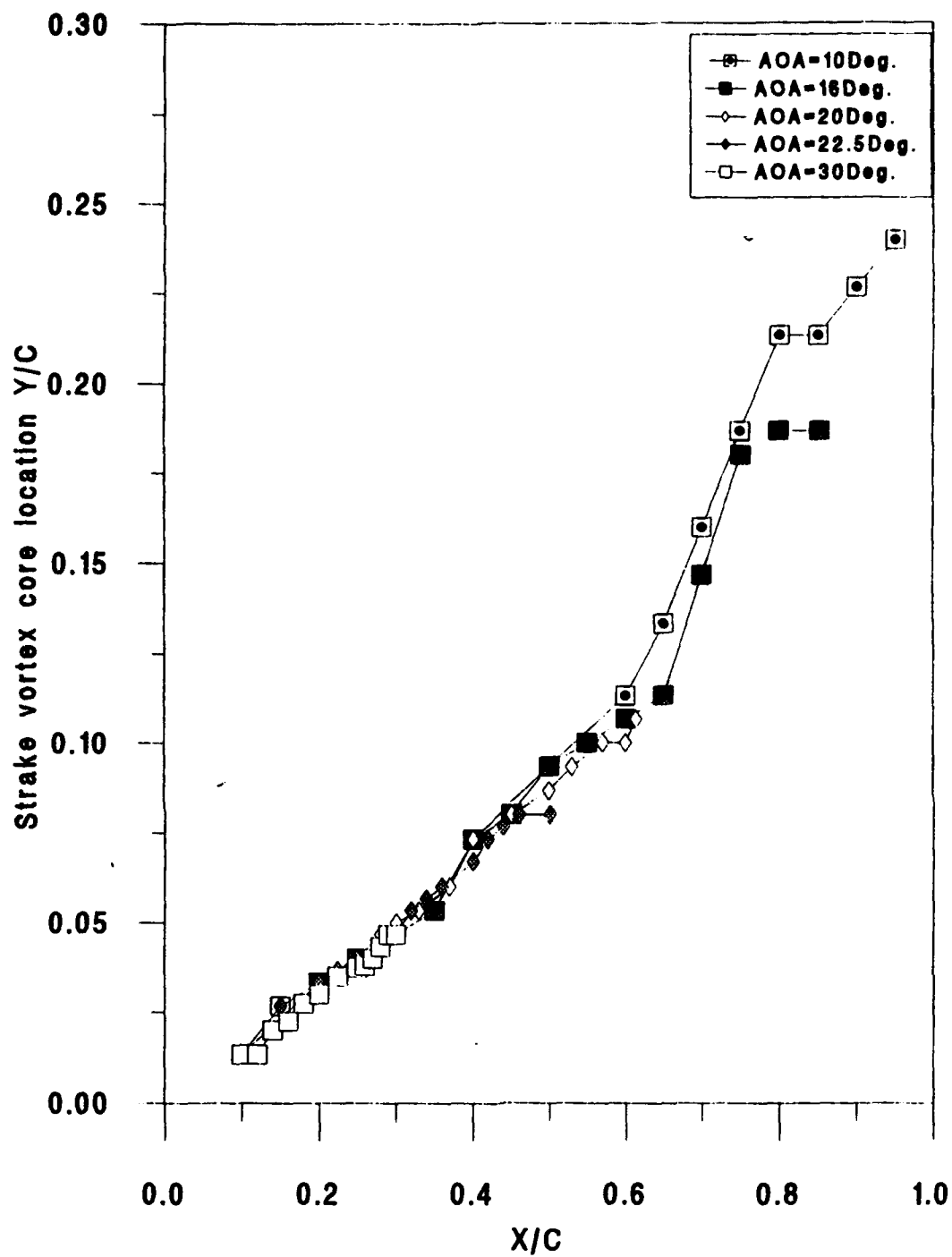


Fig. 95 Vortex core location Y/C for parabolic-fillet model

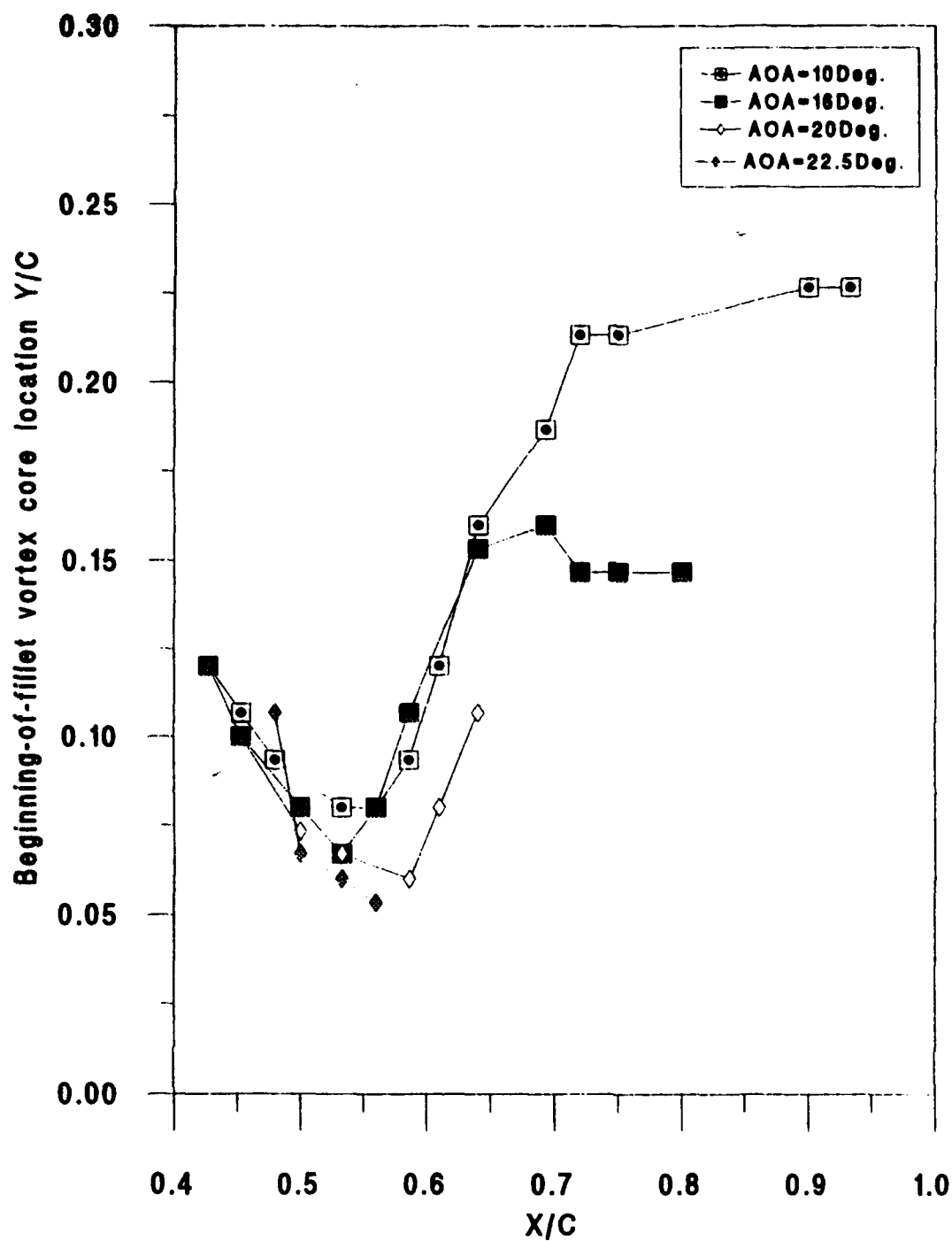


Fig. 96 Vortex core location Y/C for parabolic-fillet model

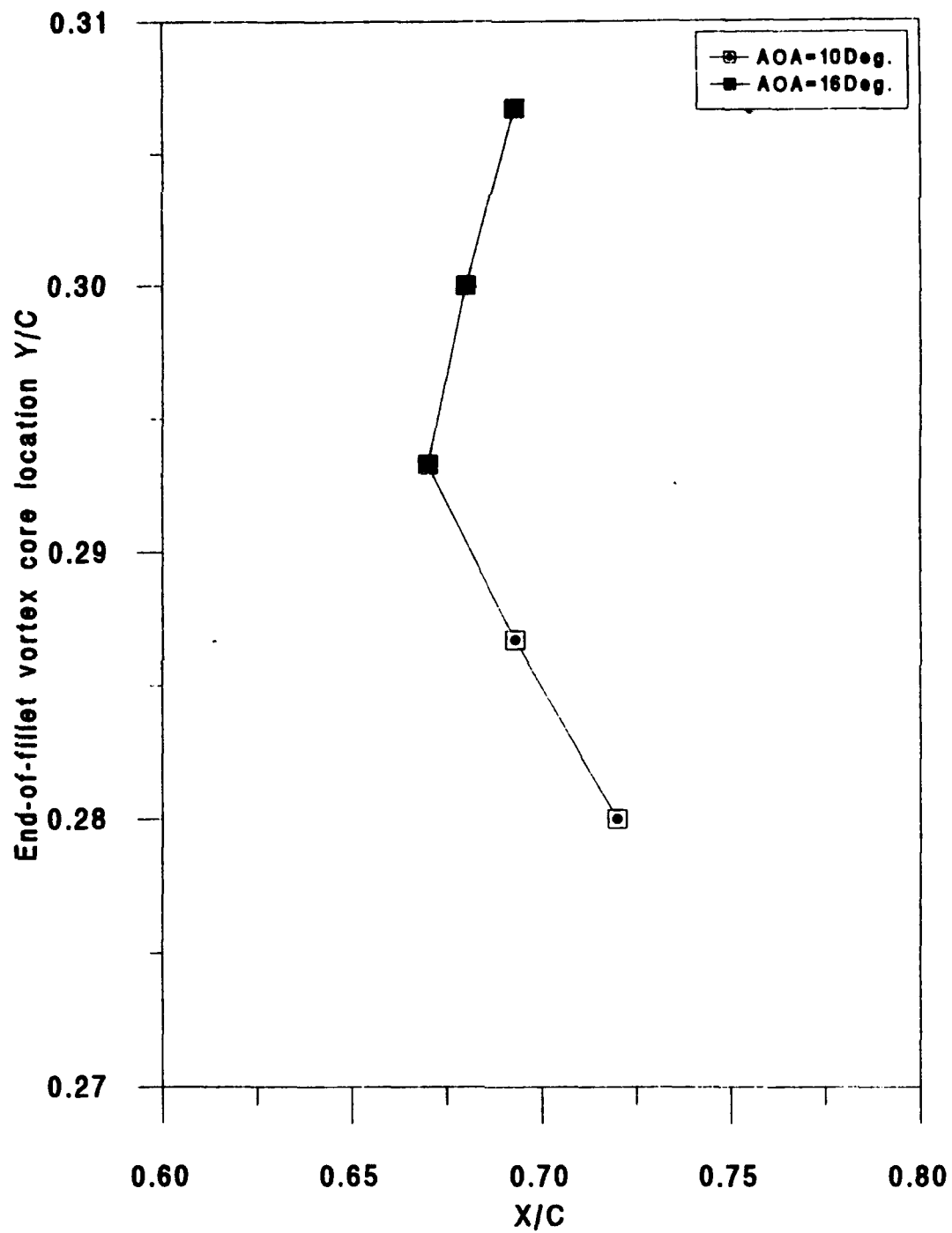


Fig. 97 Vortex core location Y/C for parabolic-fillet model

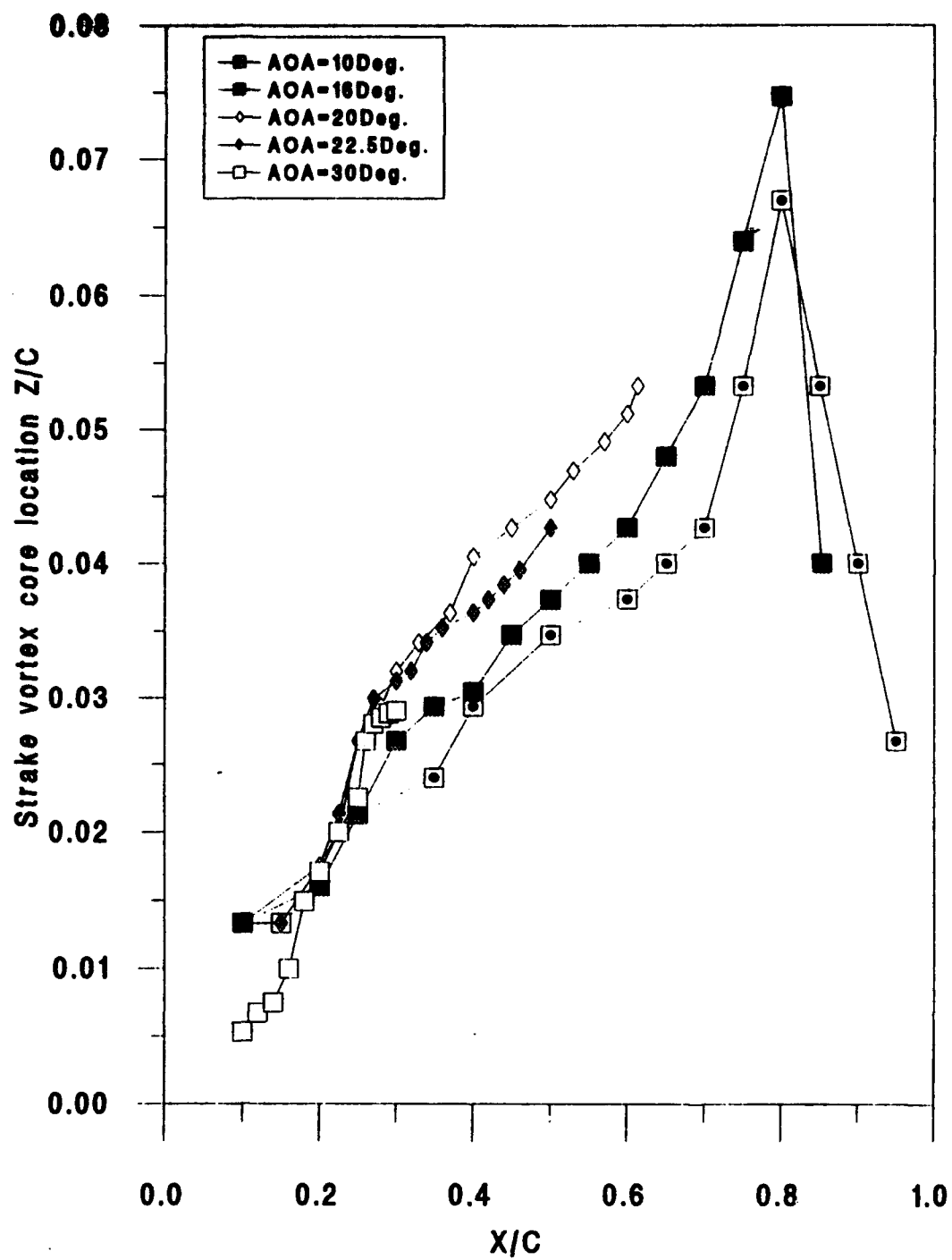


Fig. 98 Vortex core location Z/C for parabolic-fillet model

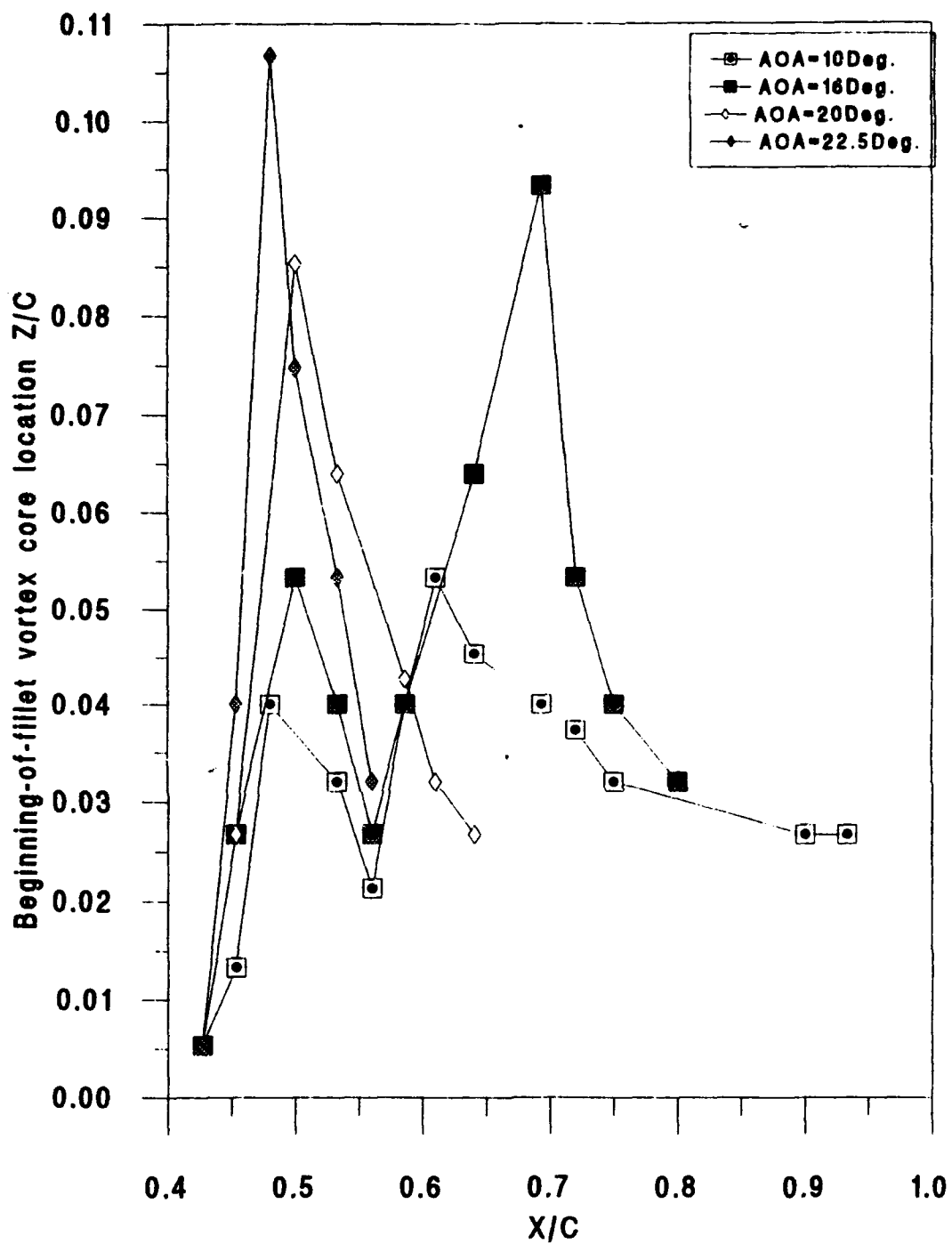


Fig. 99 Vortex core location Z/C for parabolic-fillet model

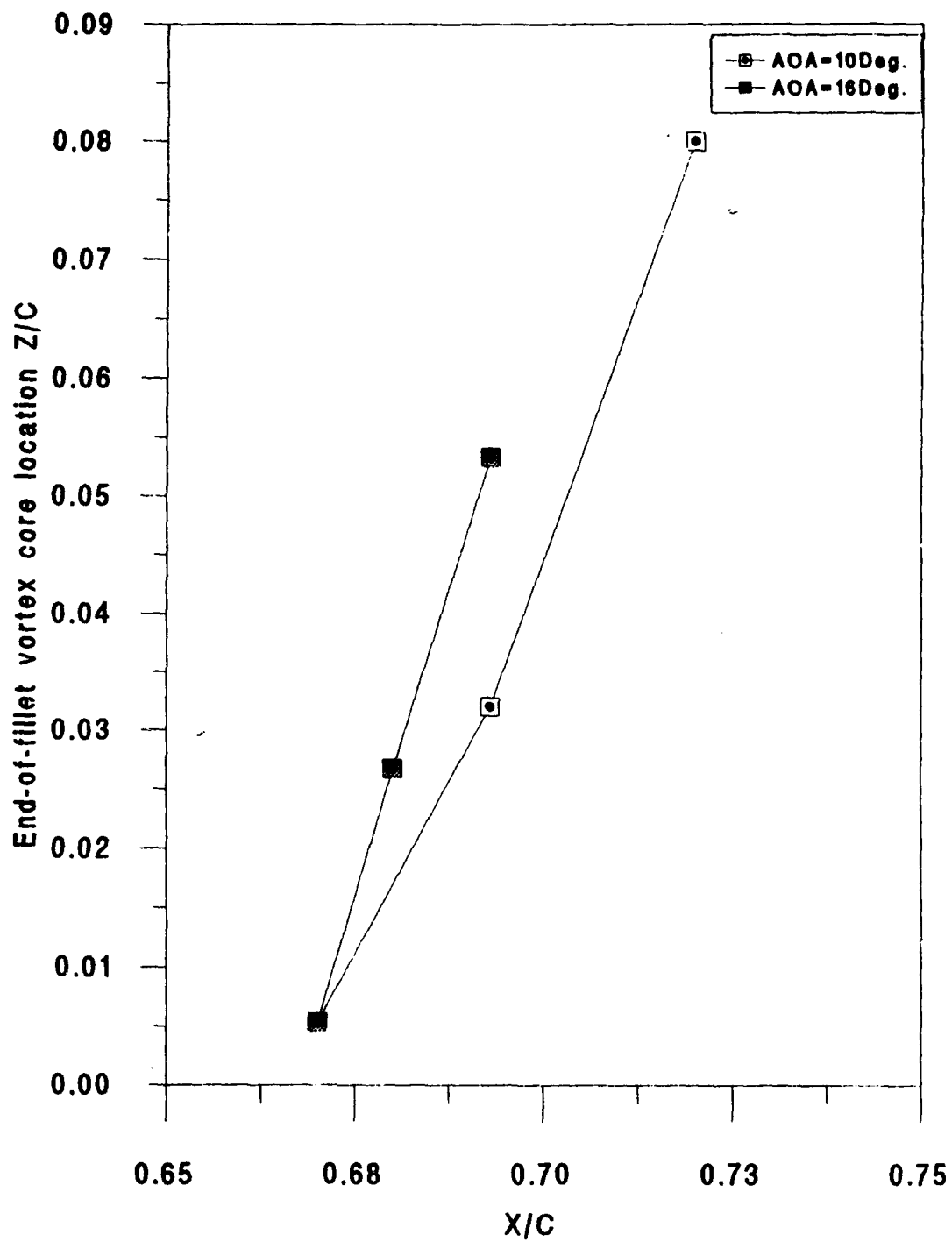


Fig. 100 Vortex core location Z/C for parabolic-fillet model

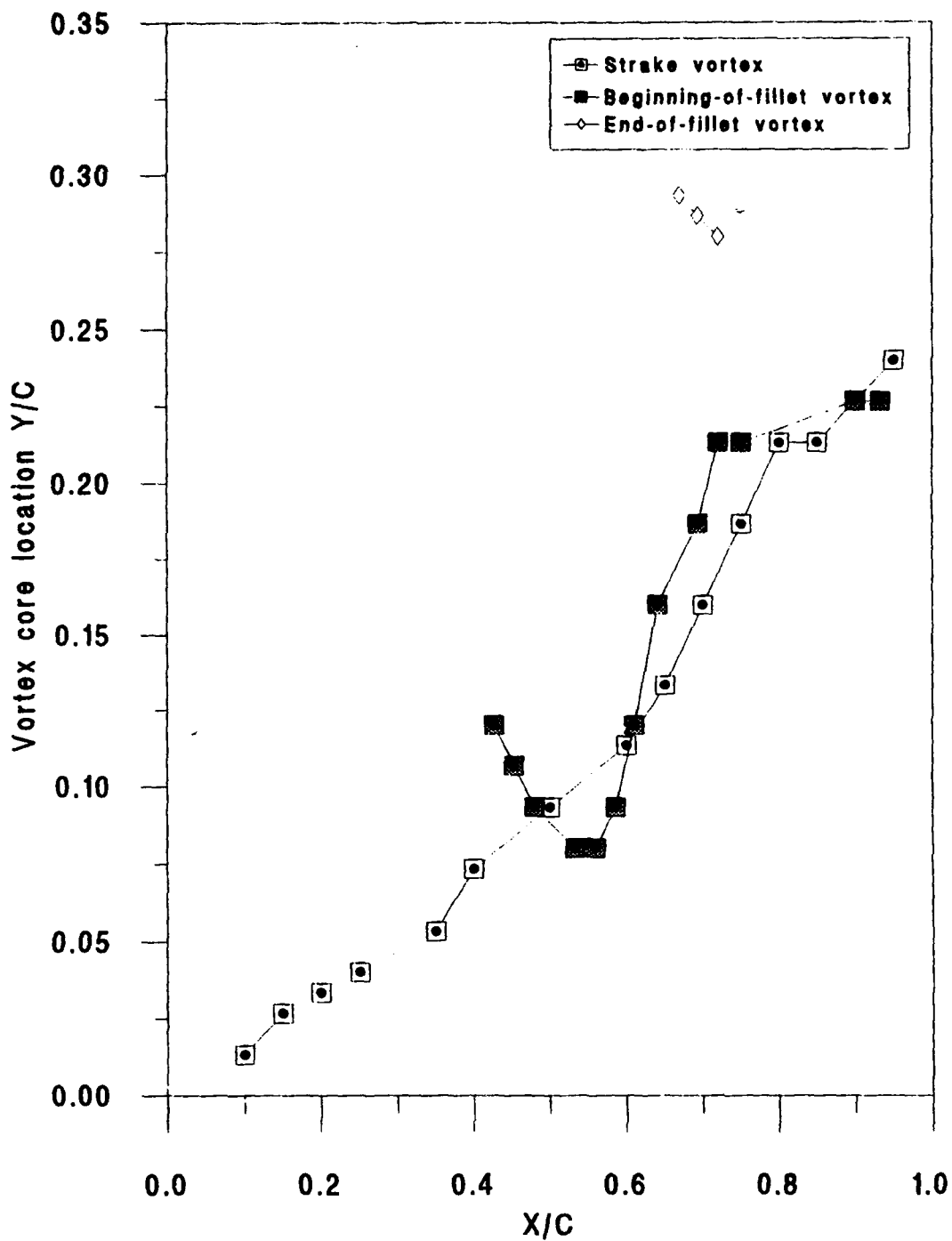


Fig. 101 Vortex core location Y/C for parabolic-fillet model at AOA= 10 Deg.

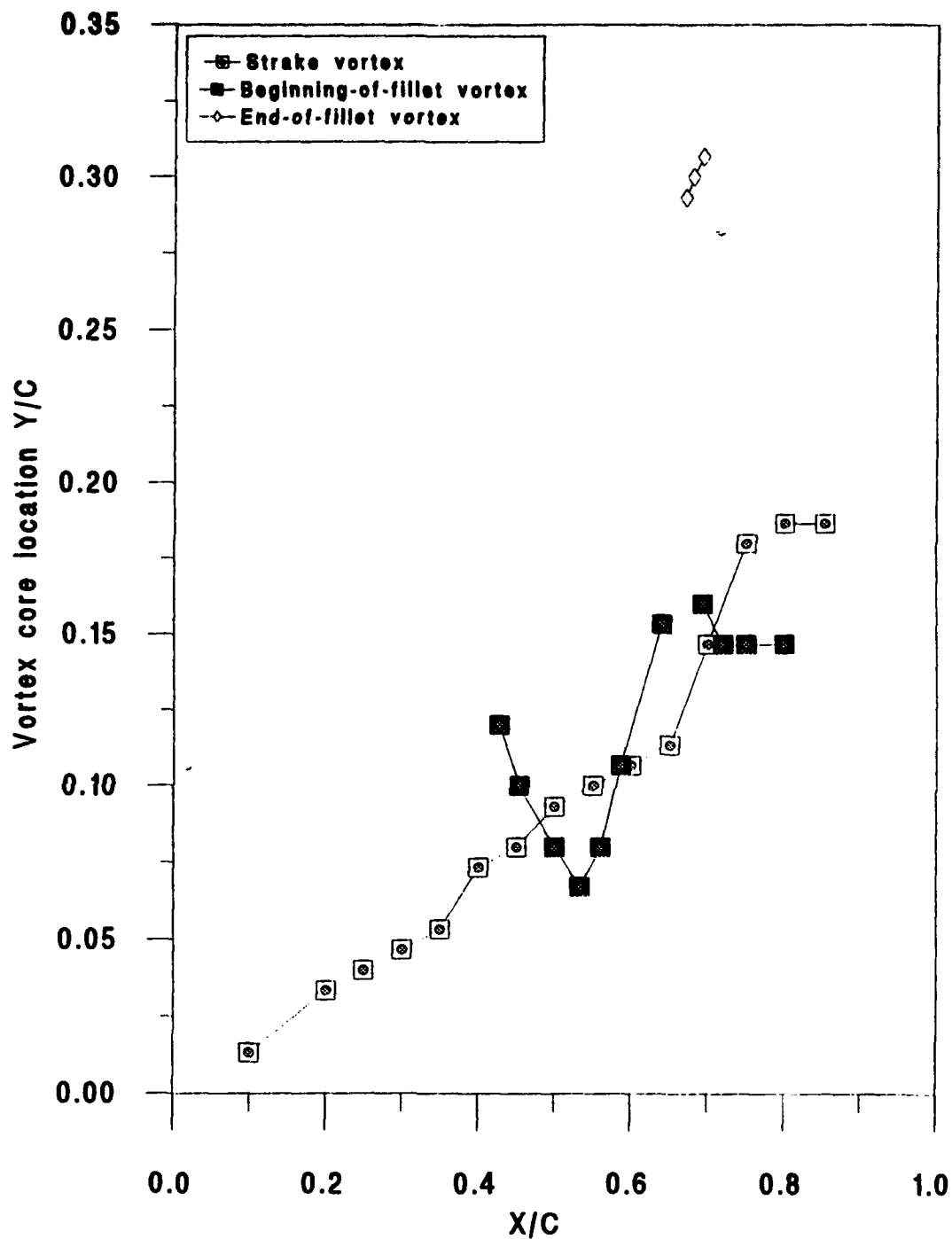


Fig. 102 Vortex core location Y/C for parabolic-fillet model at $AOA = 16$ Deg.

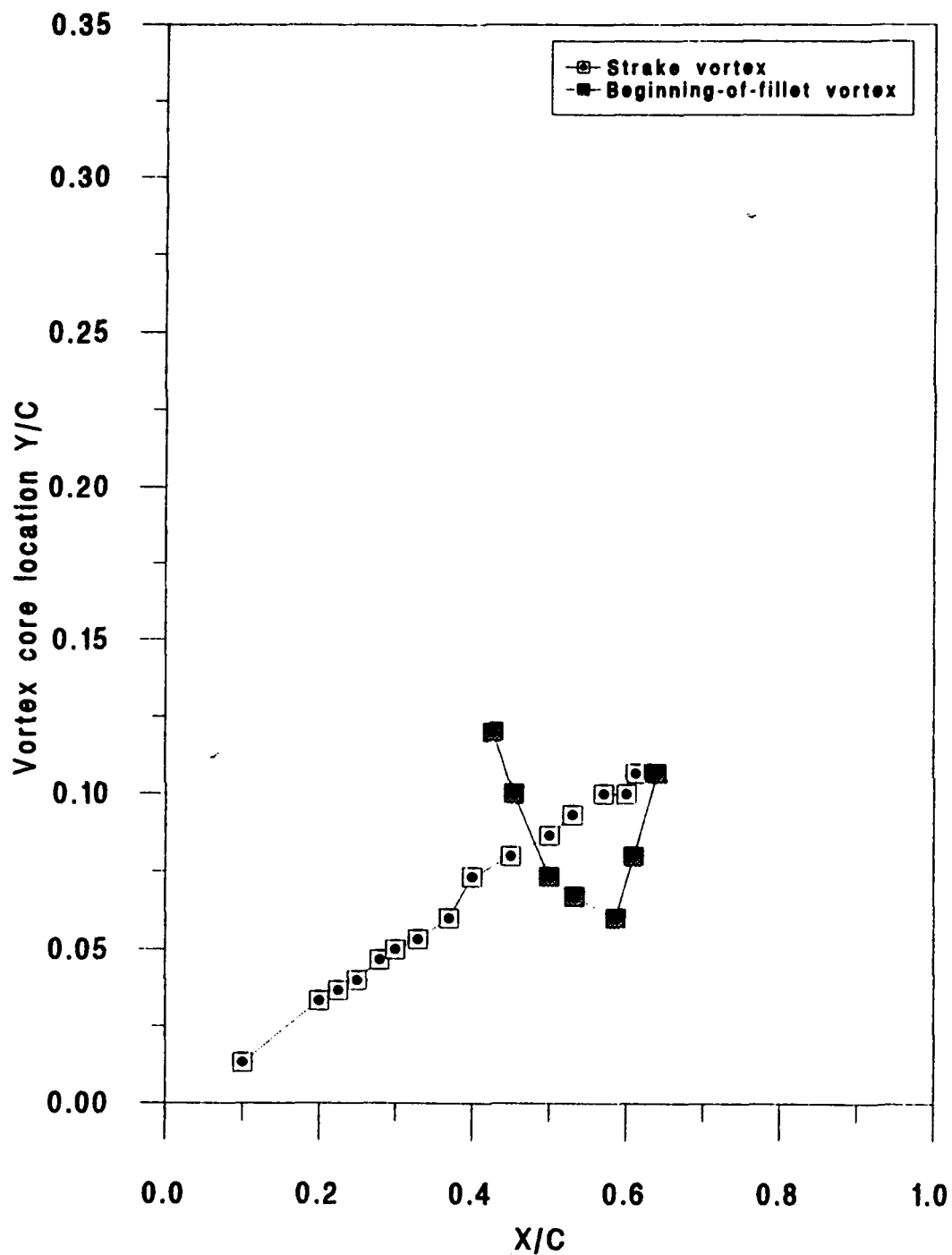


Fig. 103 Vortex core location Y/C for parabolic-fillet model at AOA = 20 Deg.

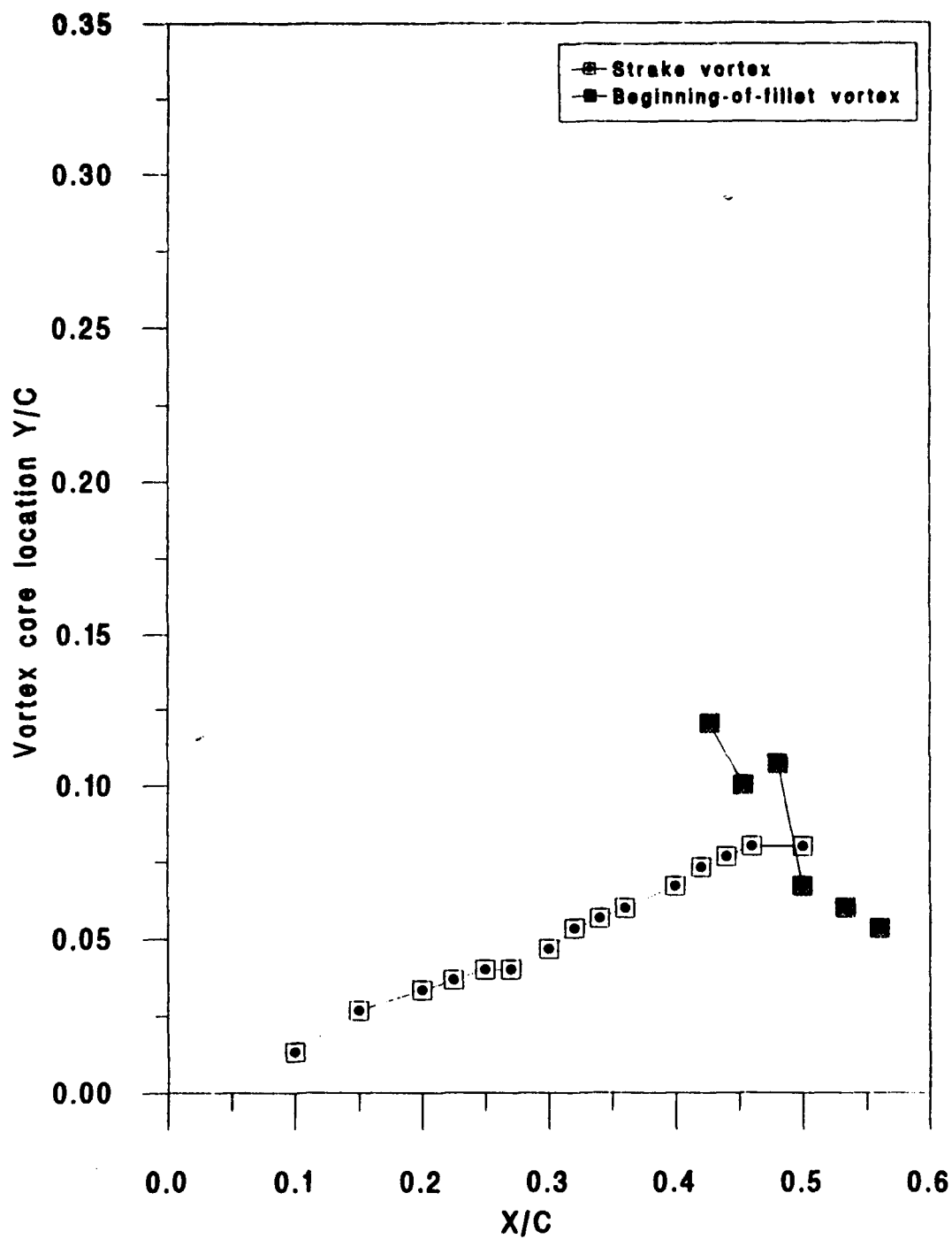


Fig 104 Vortex core location Y/C for parabolic-fillet model at AOA = 22.5 Deg.

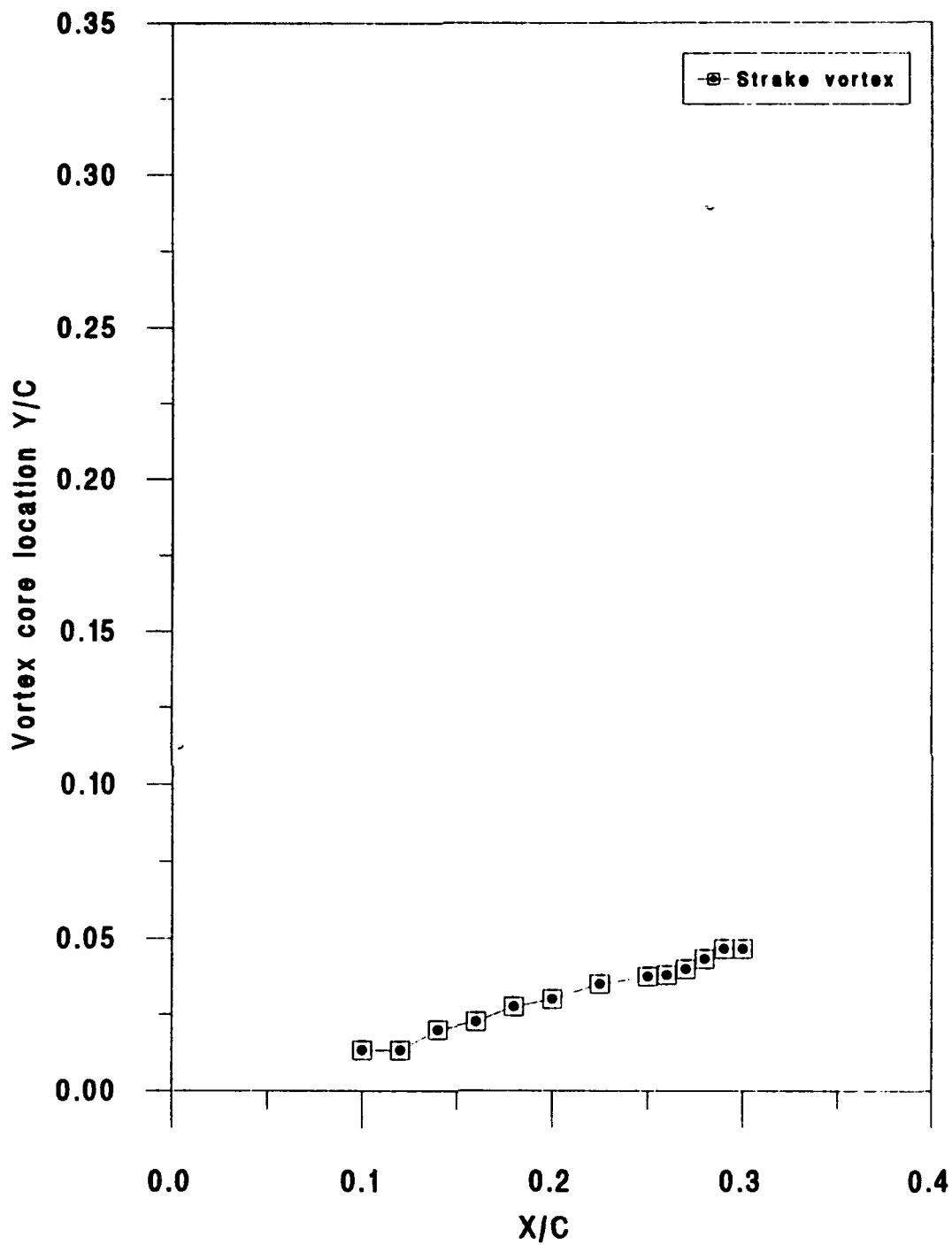


Fig. 105 Vortex core location Y/C for parabolic-fillet model at AOA = 30 Deg.

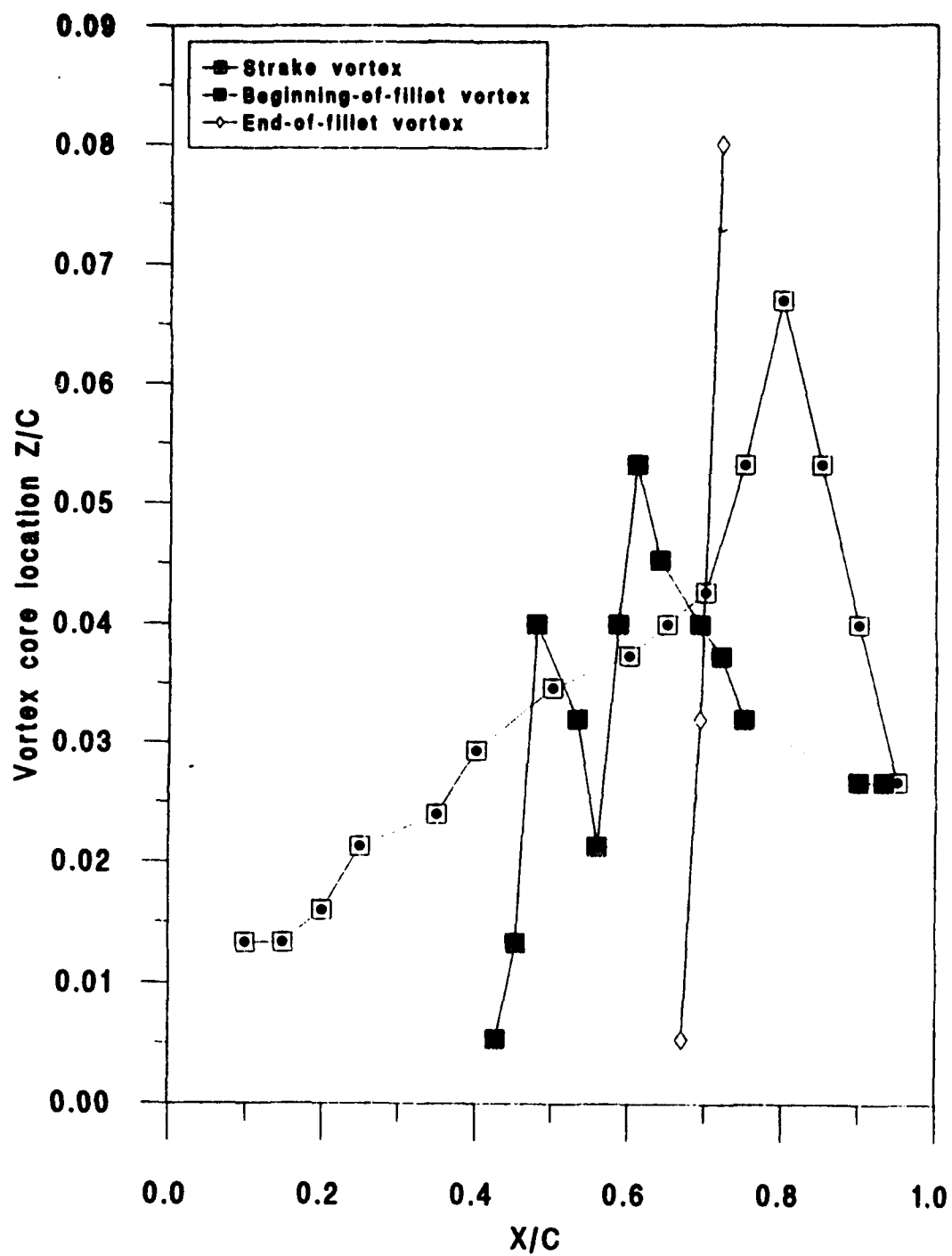


Fig. 106 Vortex core location Z/C for parabolic-fillet model at $AOA = 10$ Deg.

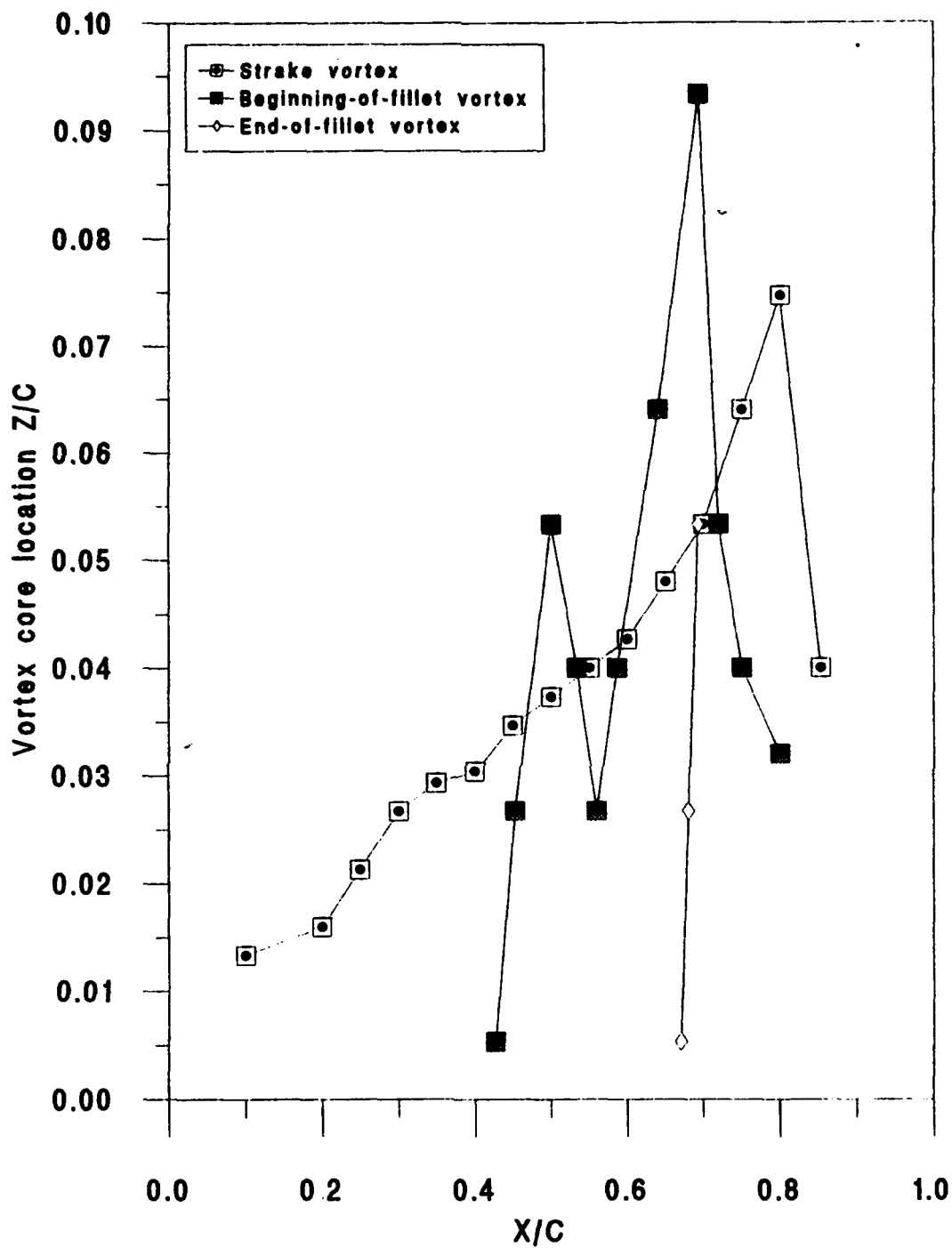


Fig. 107 Vortex core location Z/C for parabolic-fillet model at AOA = 16 Deg.

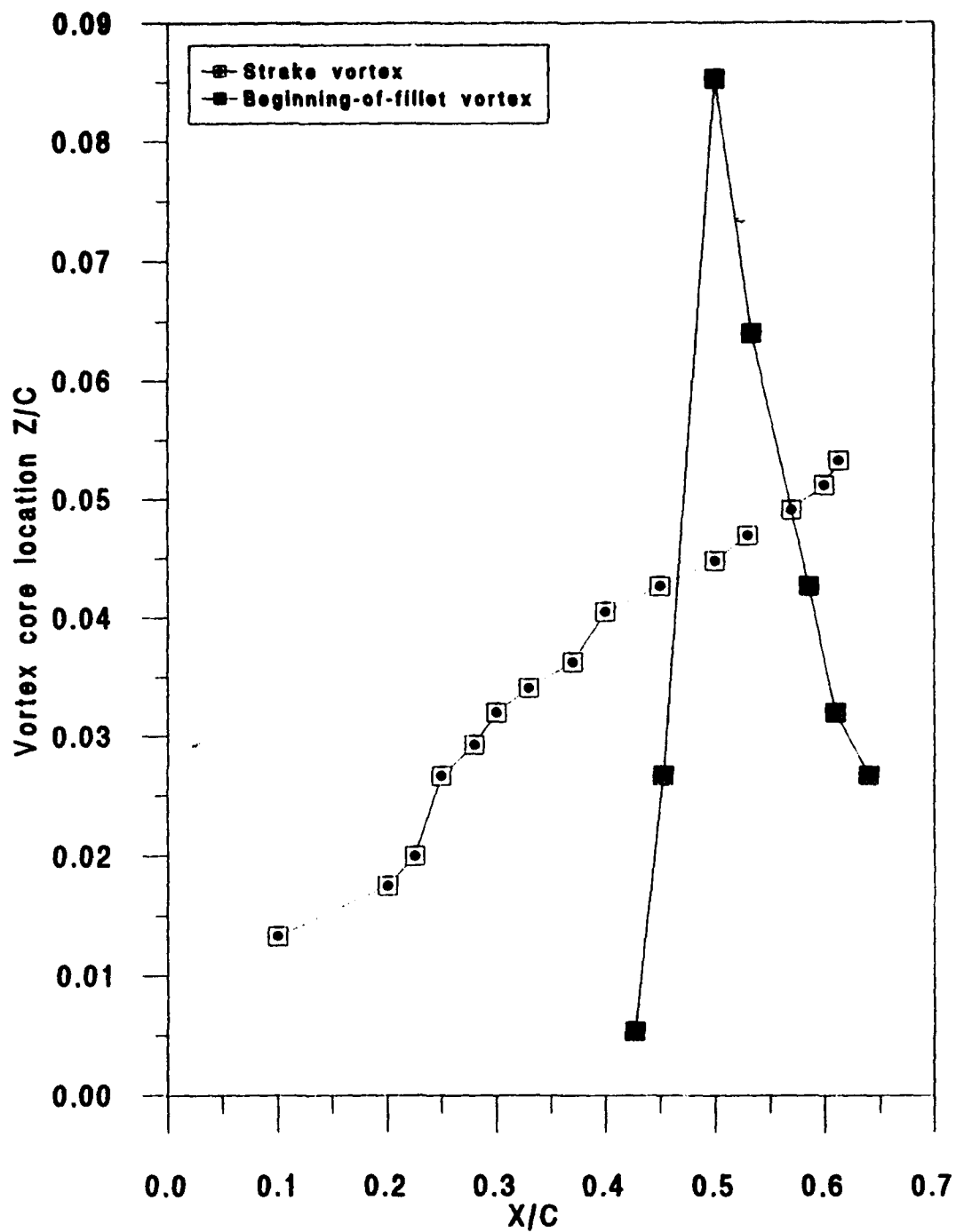


Fig. 108 Vortex core location Z/C for parabolic-fillet model at $AOA=20$ Deg.

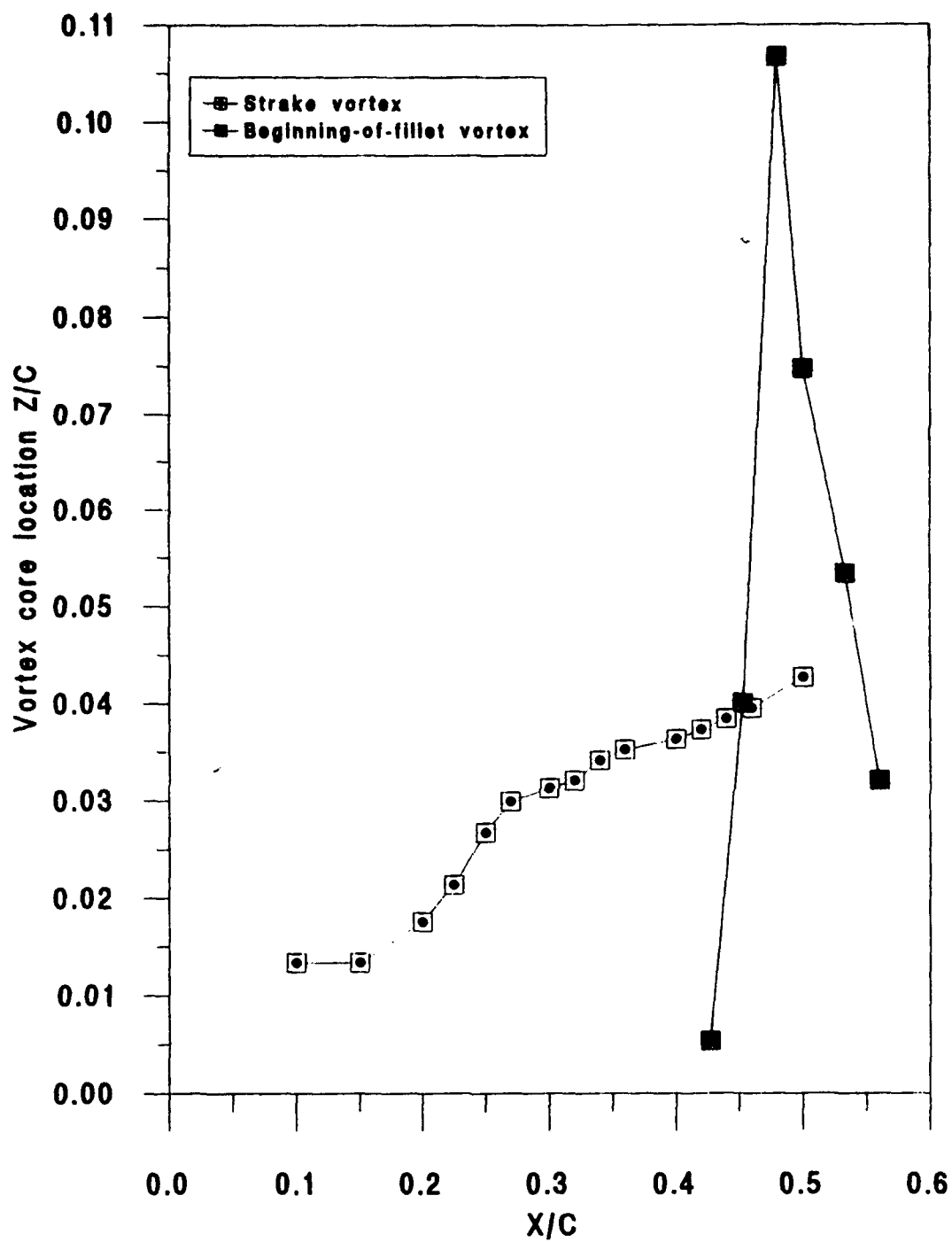


Fig. 109 Vortex core location Z/C for parabolic-fillet model at AOA = 22.5 Deg.

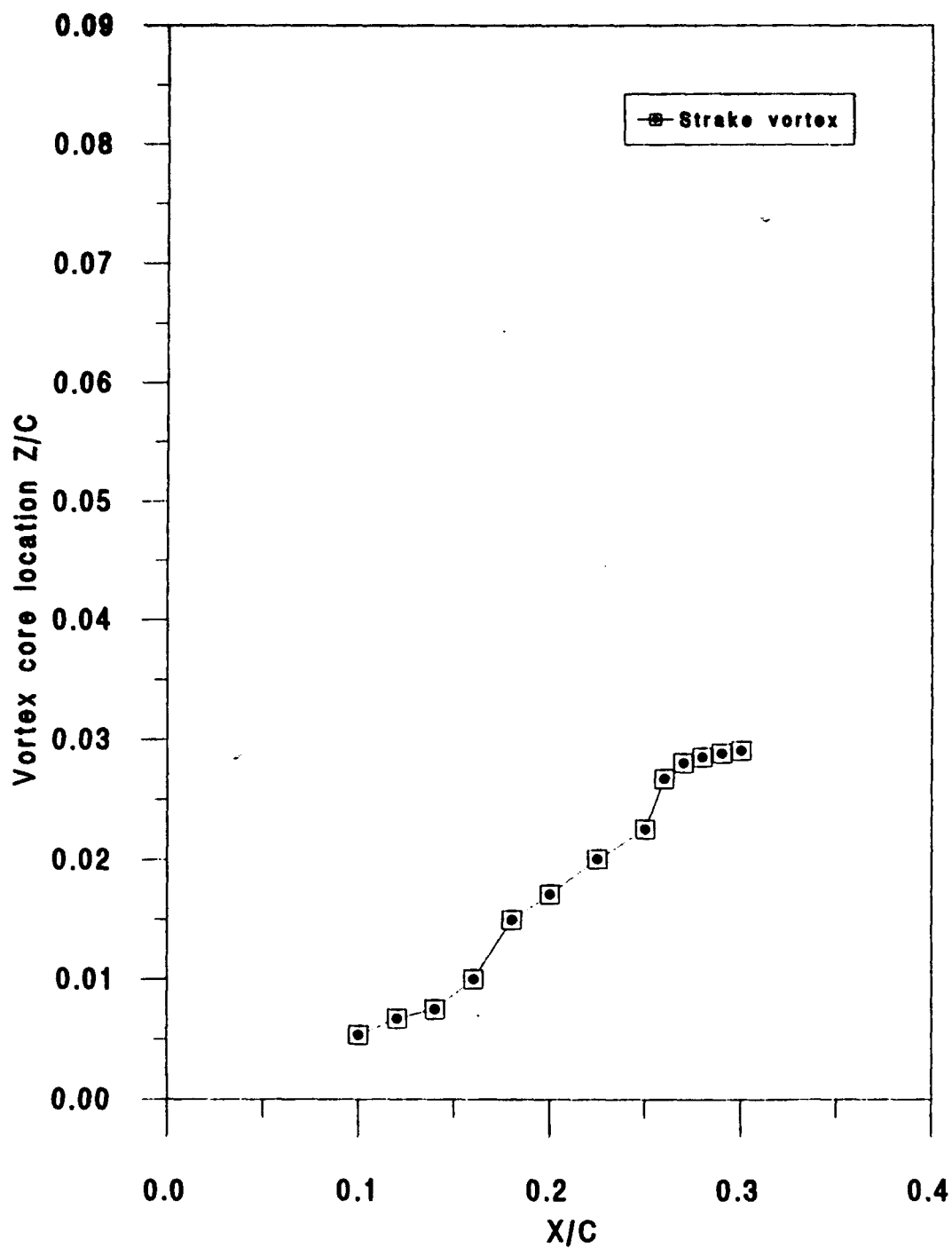


Fig. 110 Vortex core location Z/C for parabolic-fillet model at AOA=30 Deg.

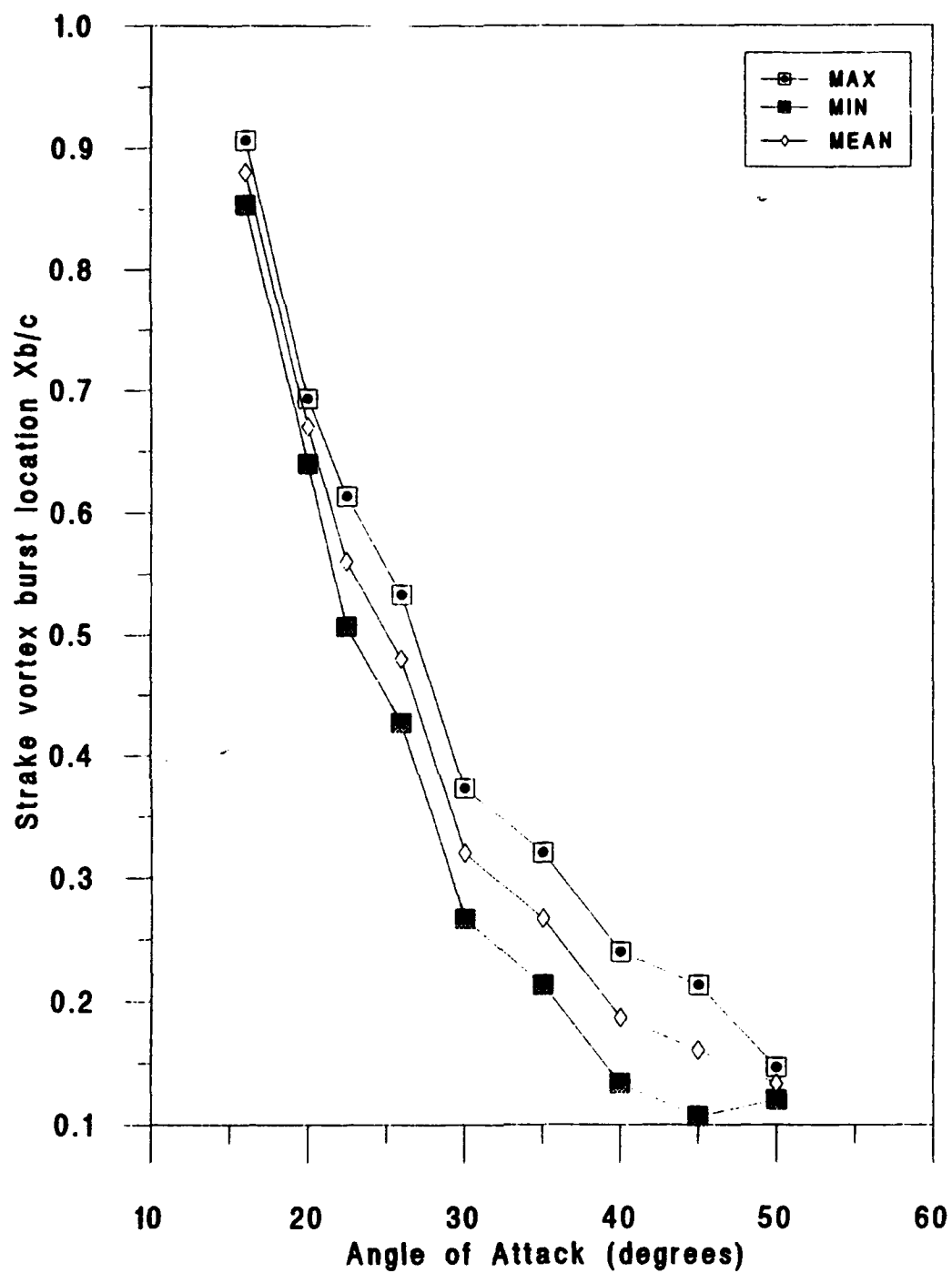


Fig. 111 Vortex burst location Xb/c (maximum, minimum & mean) for parabolic-fillet model

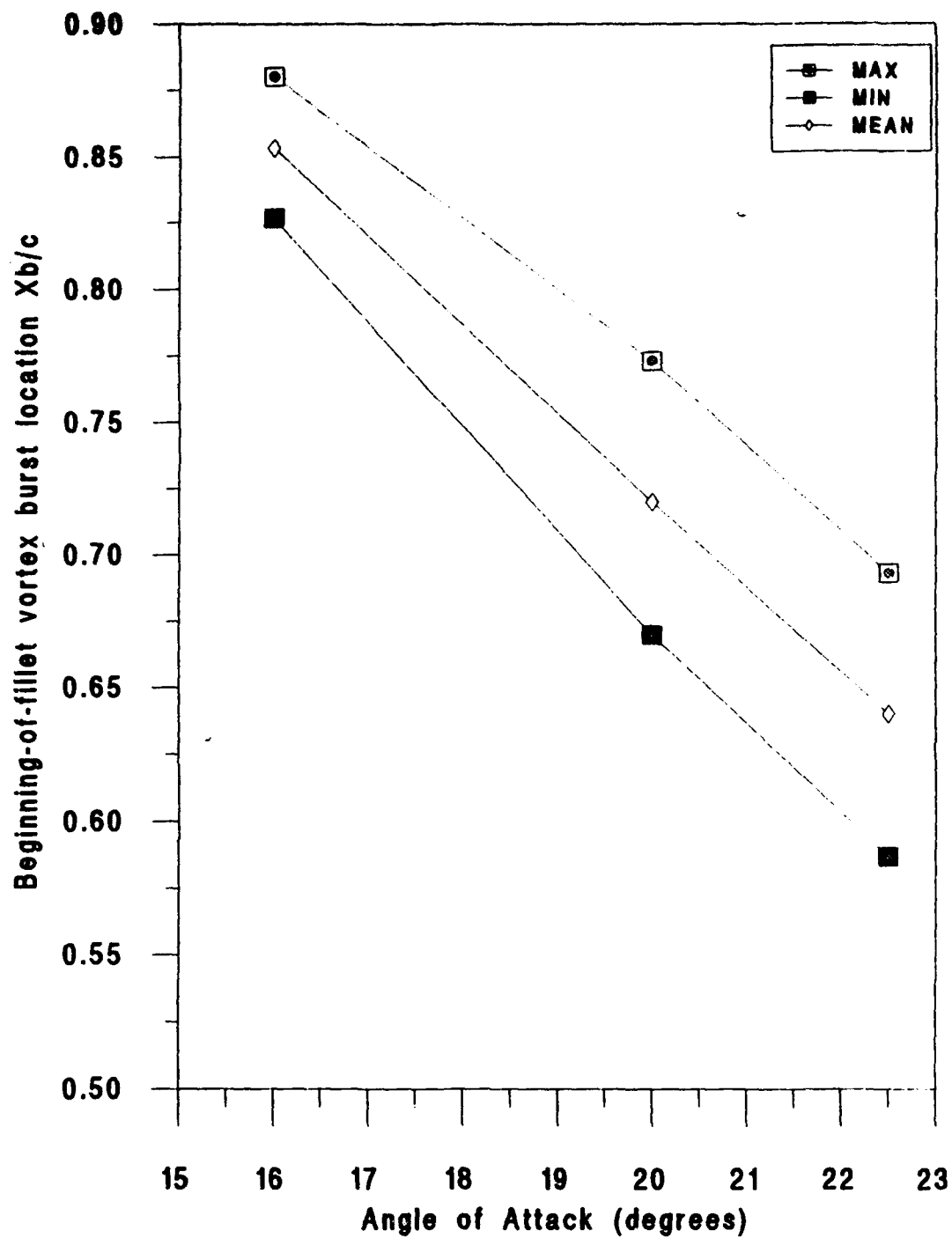


Fig. 112 Vortex burst location Xb/c (maximum, minimum & mean) for parabolic-fillet model.

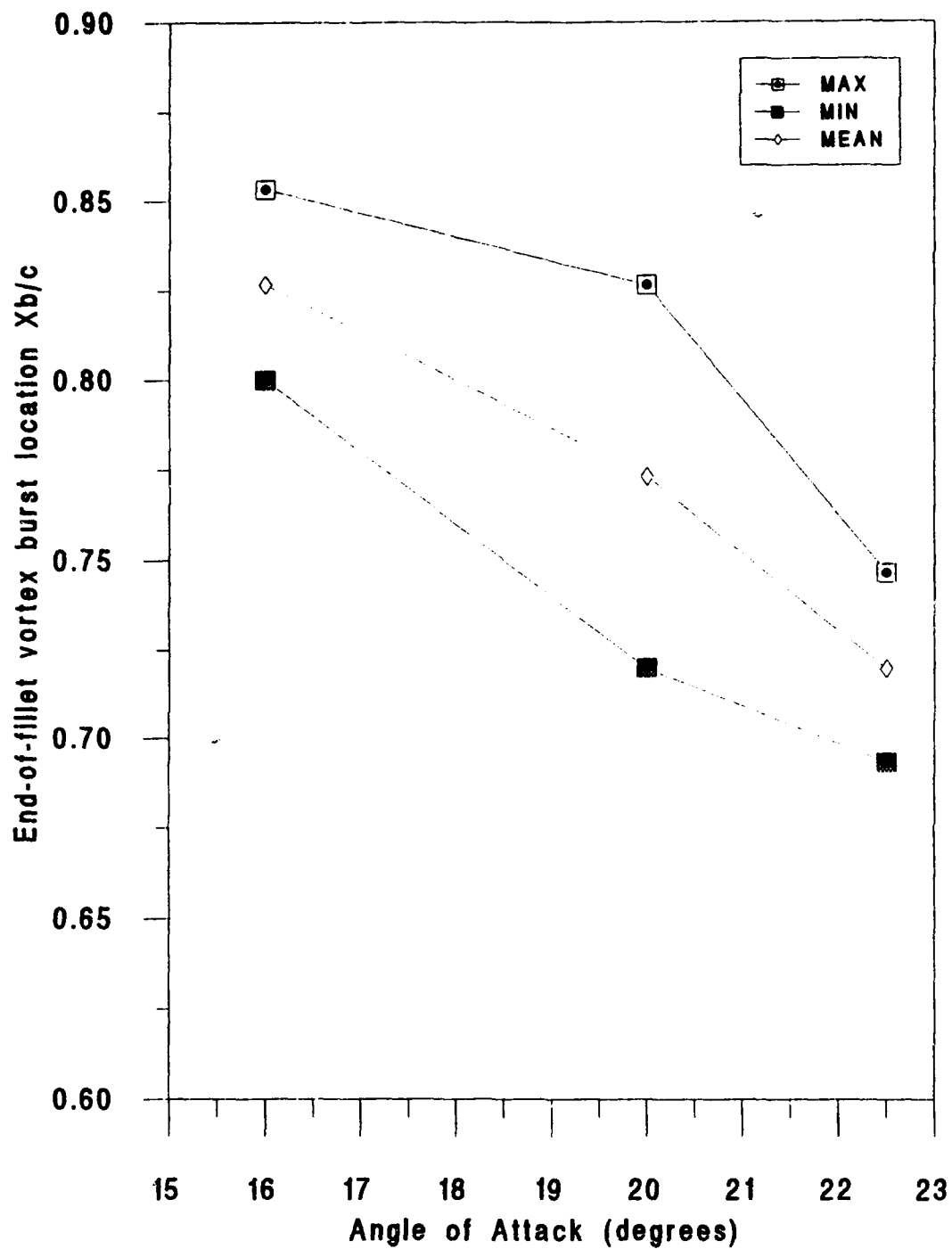


Fig. 113 Vortex burst location Xb/c (maximum, minimum & mean) for parabolic-fillet model

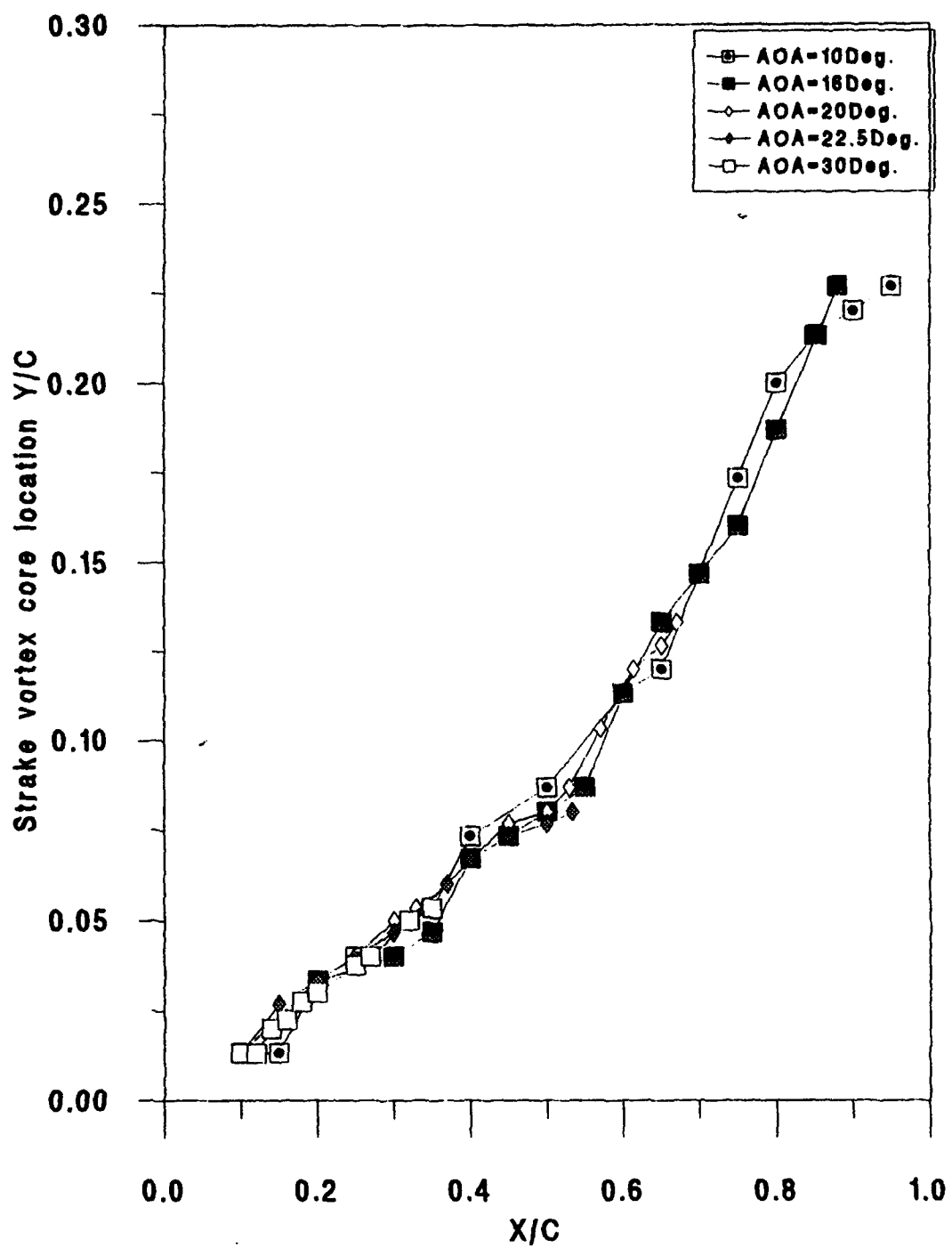


Fig. 114 Vortex core location Y/C for diamond-fillet model

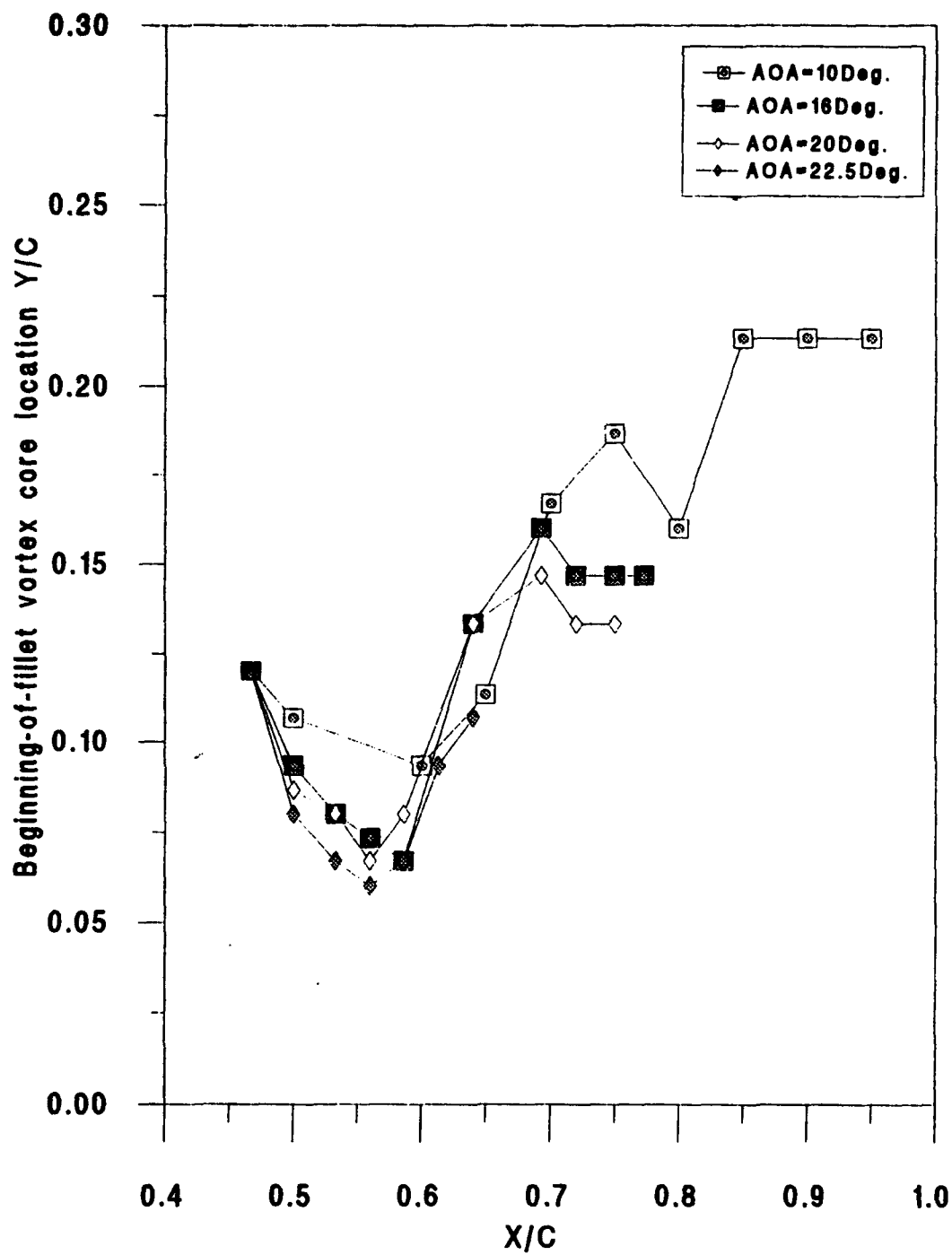


Fig. 115 Vortex core location Y/C for diamond-fillet model

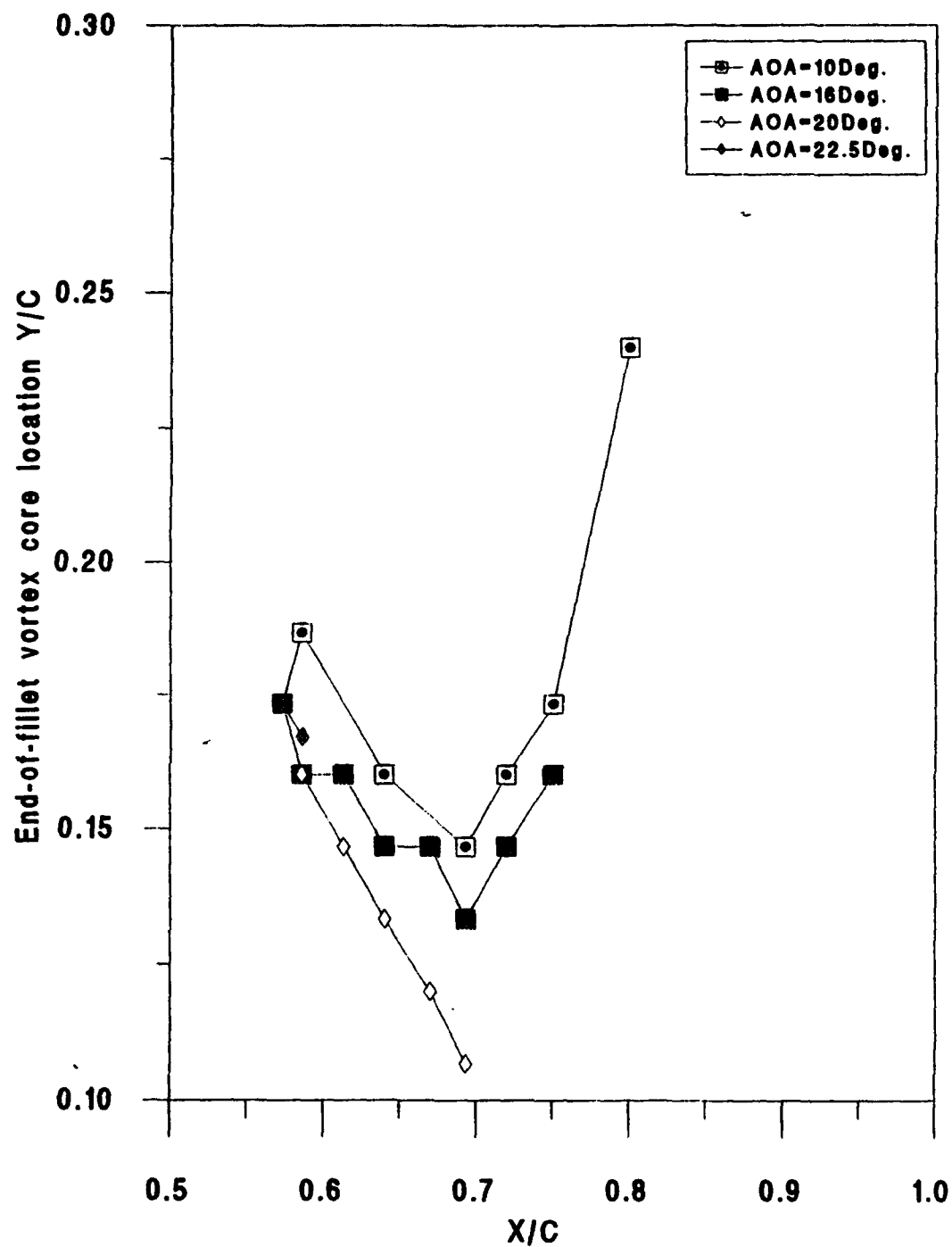


Fig. 116 Vortex core location Y/C for parabolic-fillet model

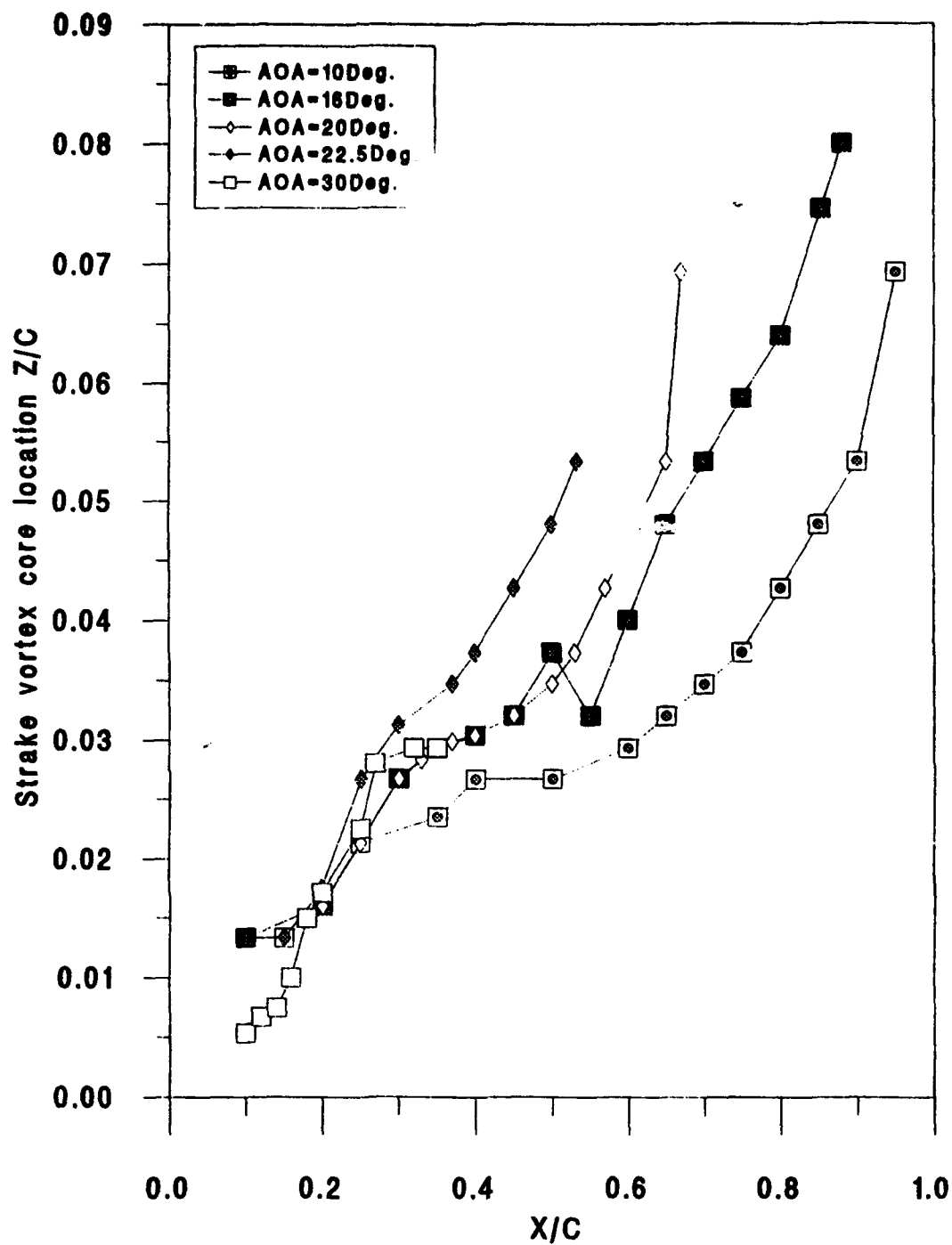


Fig. 117 Vortex core location Z/C for diamond-fillet model

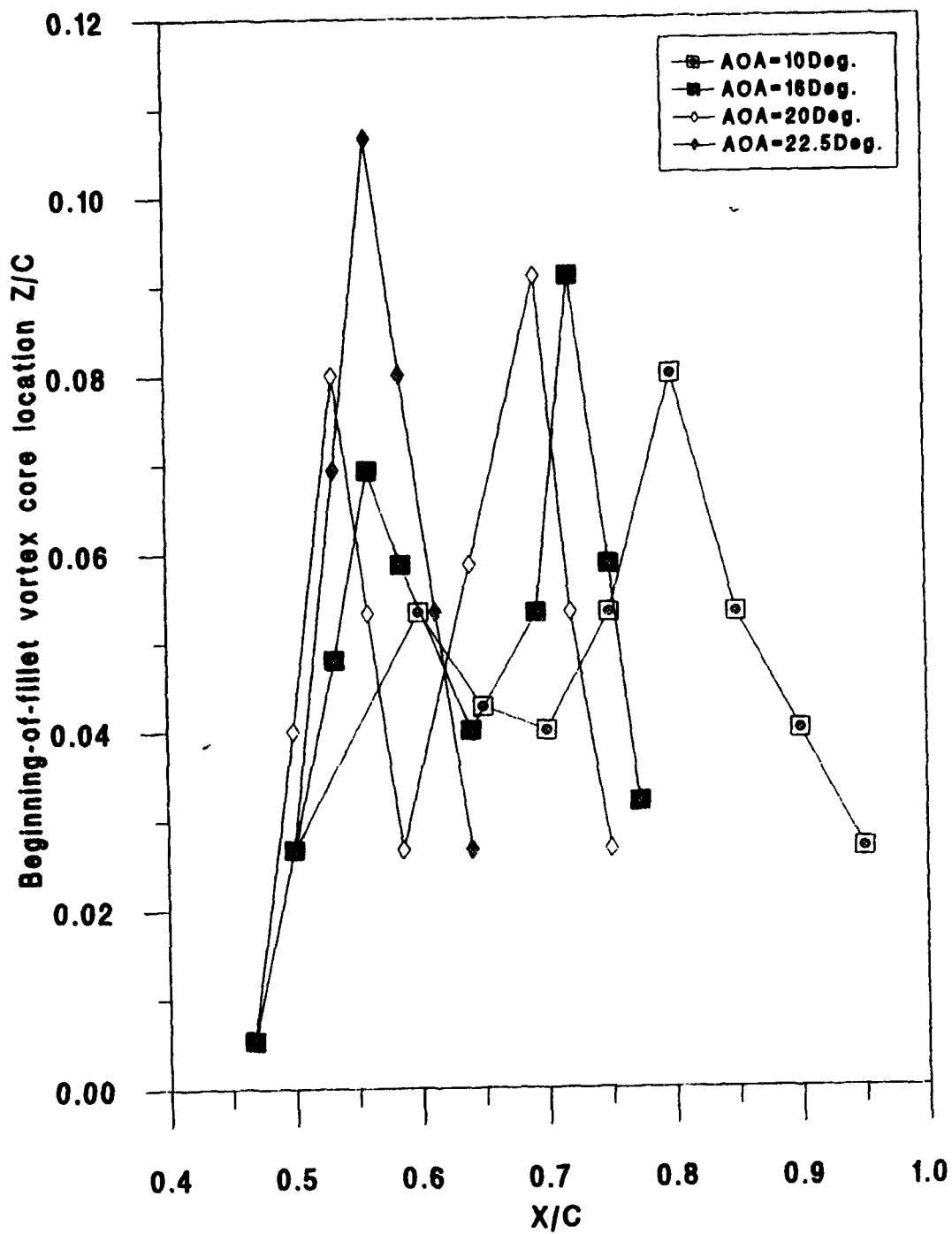


Fig. 118 Vortex core location Z/C for diamond-fillet model

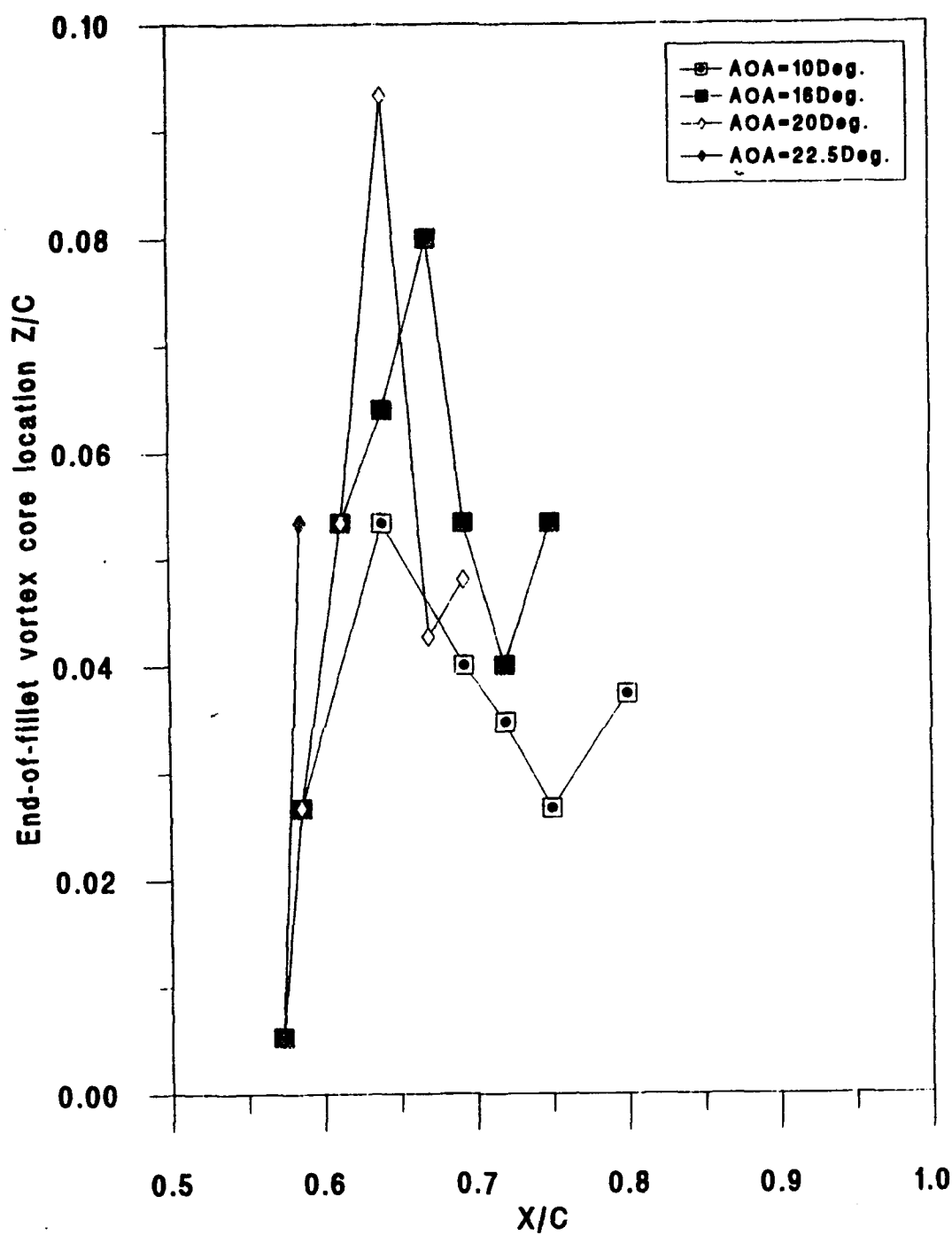


Fig. 119 Vortex core location Z/C for diamond-fillet model

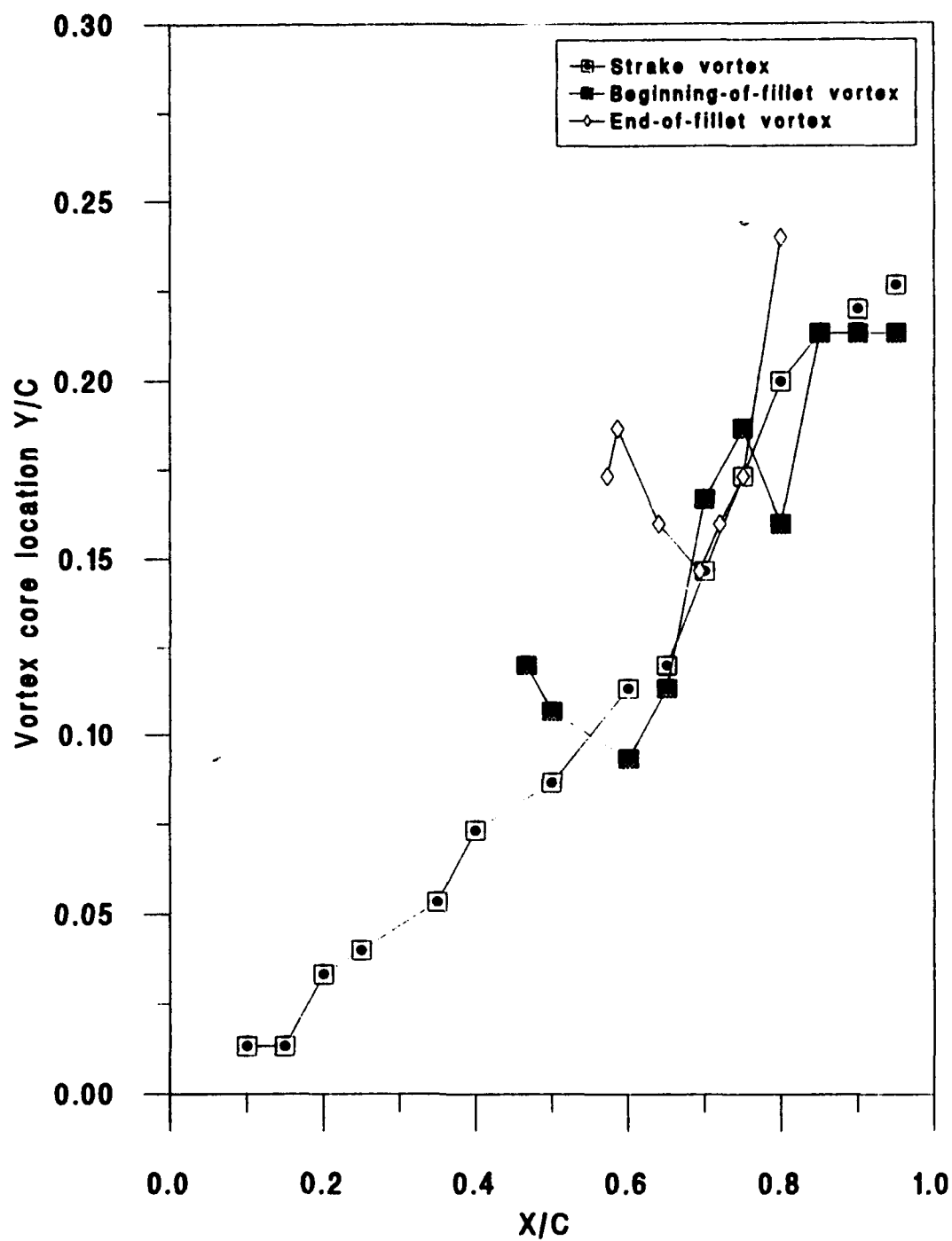


Fig. 120 Vortex core location Y/C for diamond-fillet model at AOA= 10 Deg.

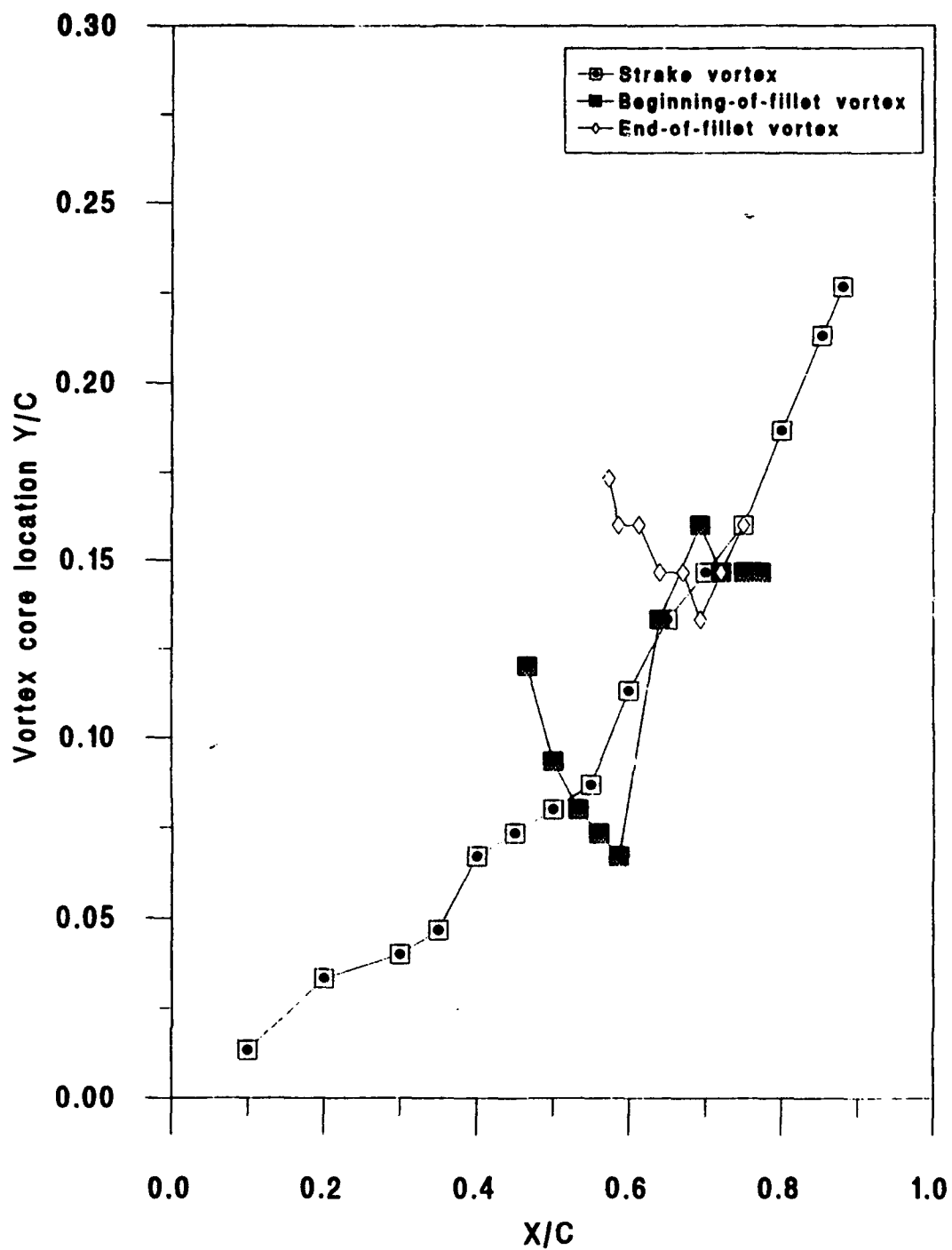


Fig. 121 Vortex core location Y/C for diamond-fillet model at $AOA = 16$ Deg.

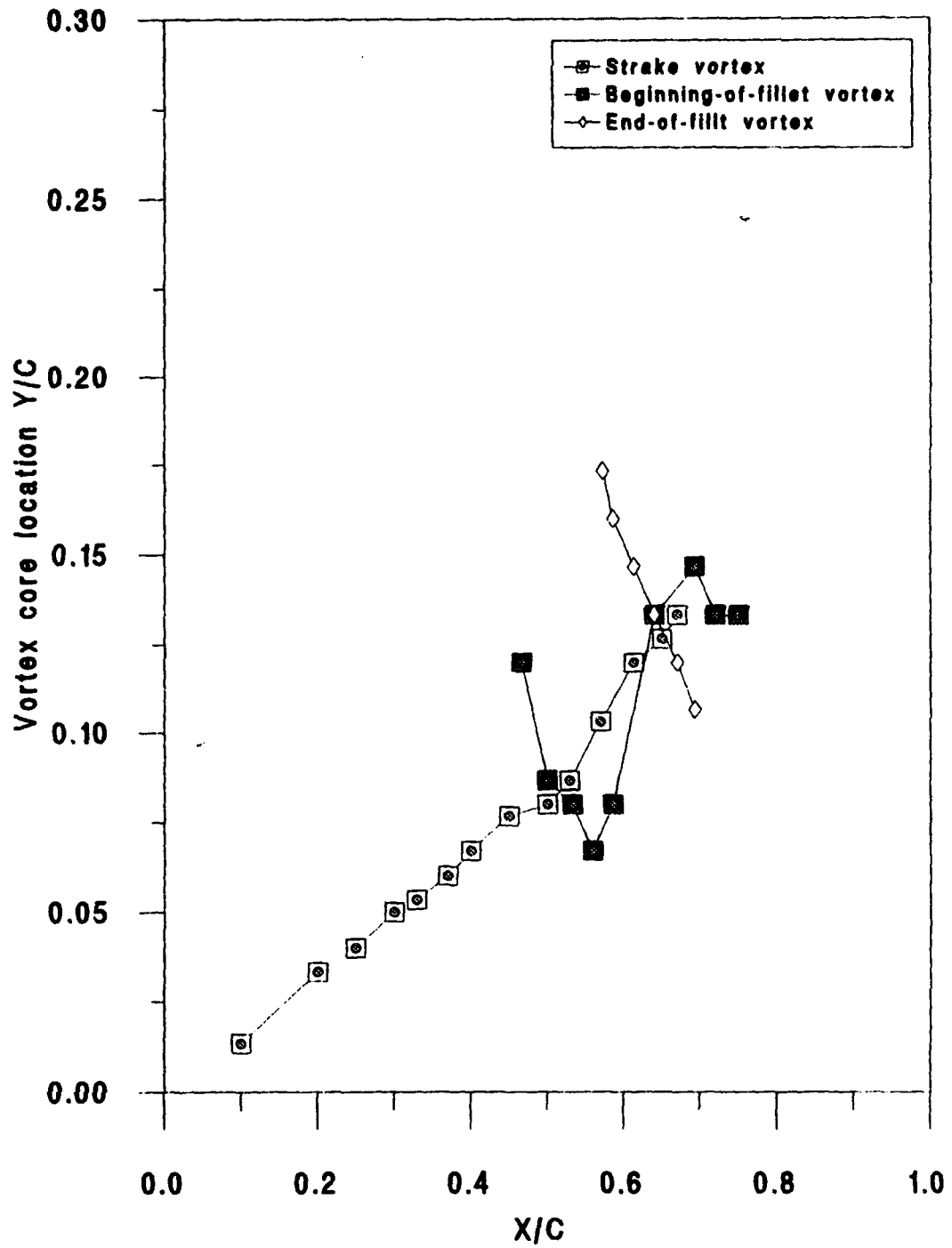


Fig. 122 Vortex core location Y/C for diamond-fillet model at AOA = 20 Deg.

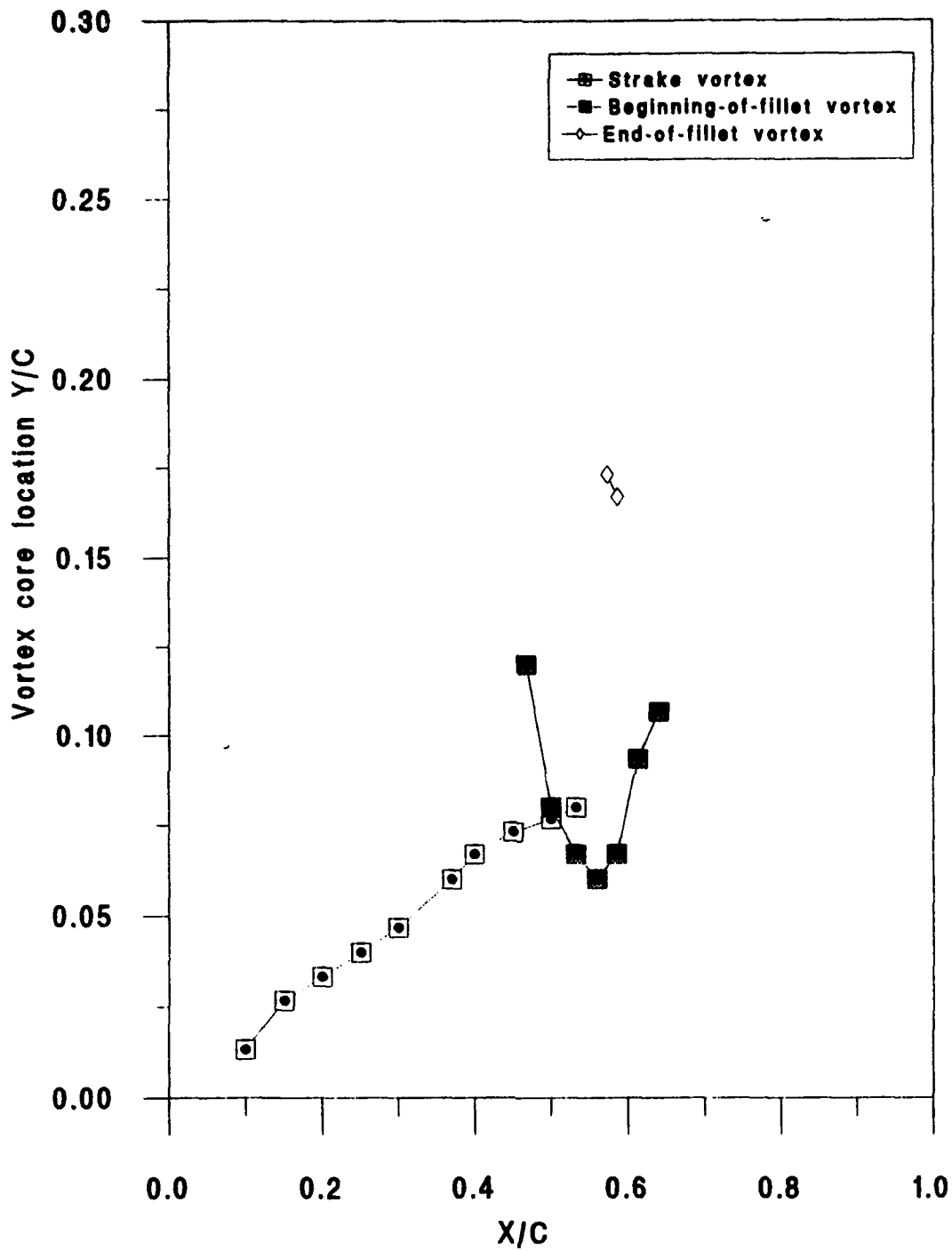


Fig. 123 Vortex core location Y/C for diamond-fillet model at $AOA = 22.5$ Deg.

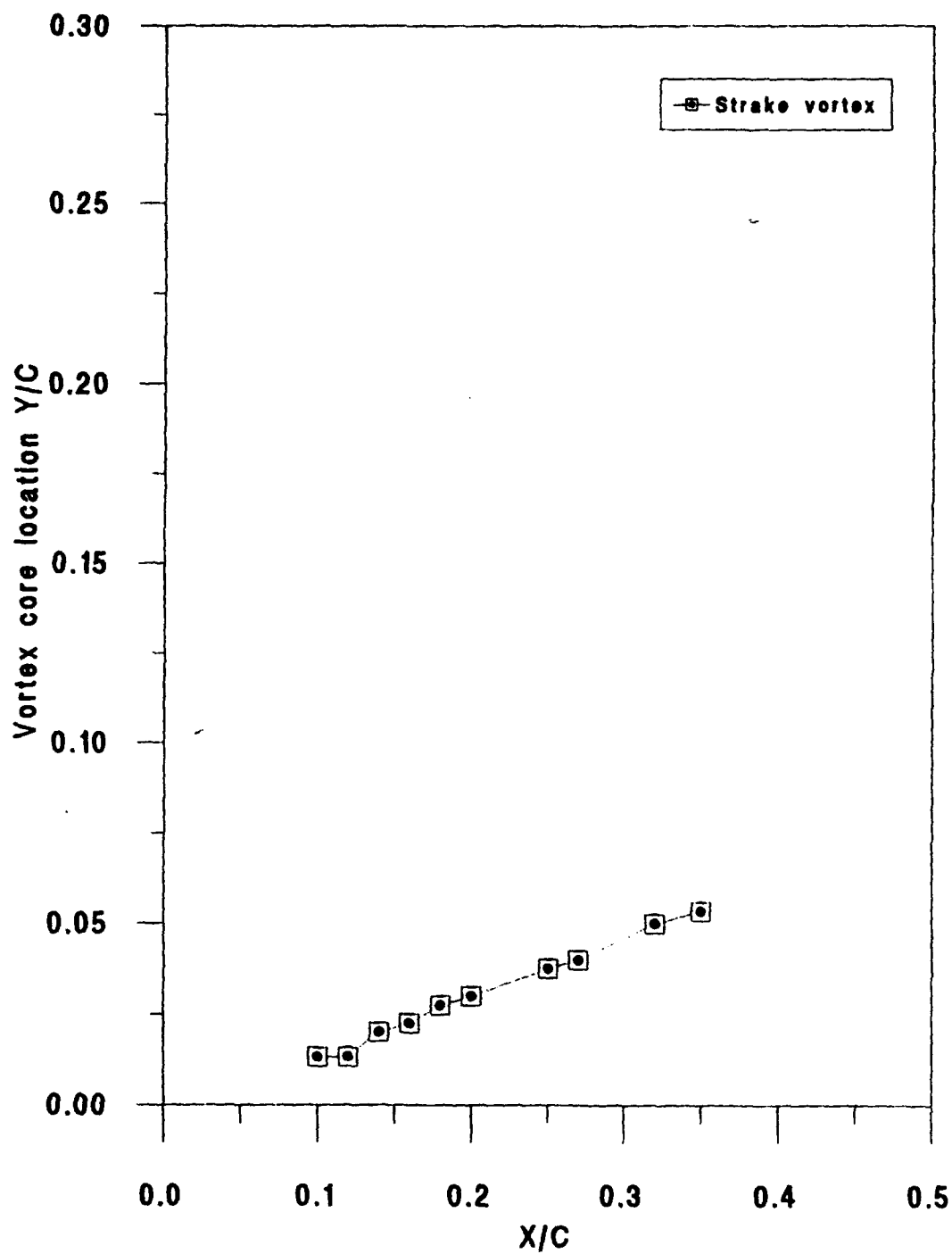


Fig. 124 Vortex core location Y/C for diamond-fillet model at $AOA = 30^\circ$.

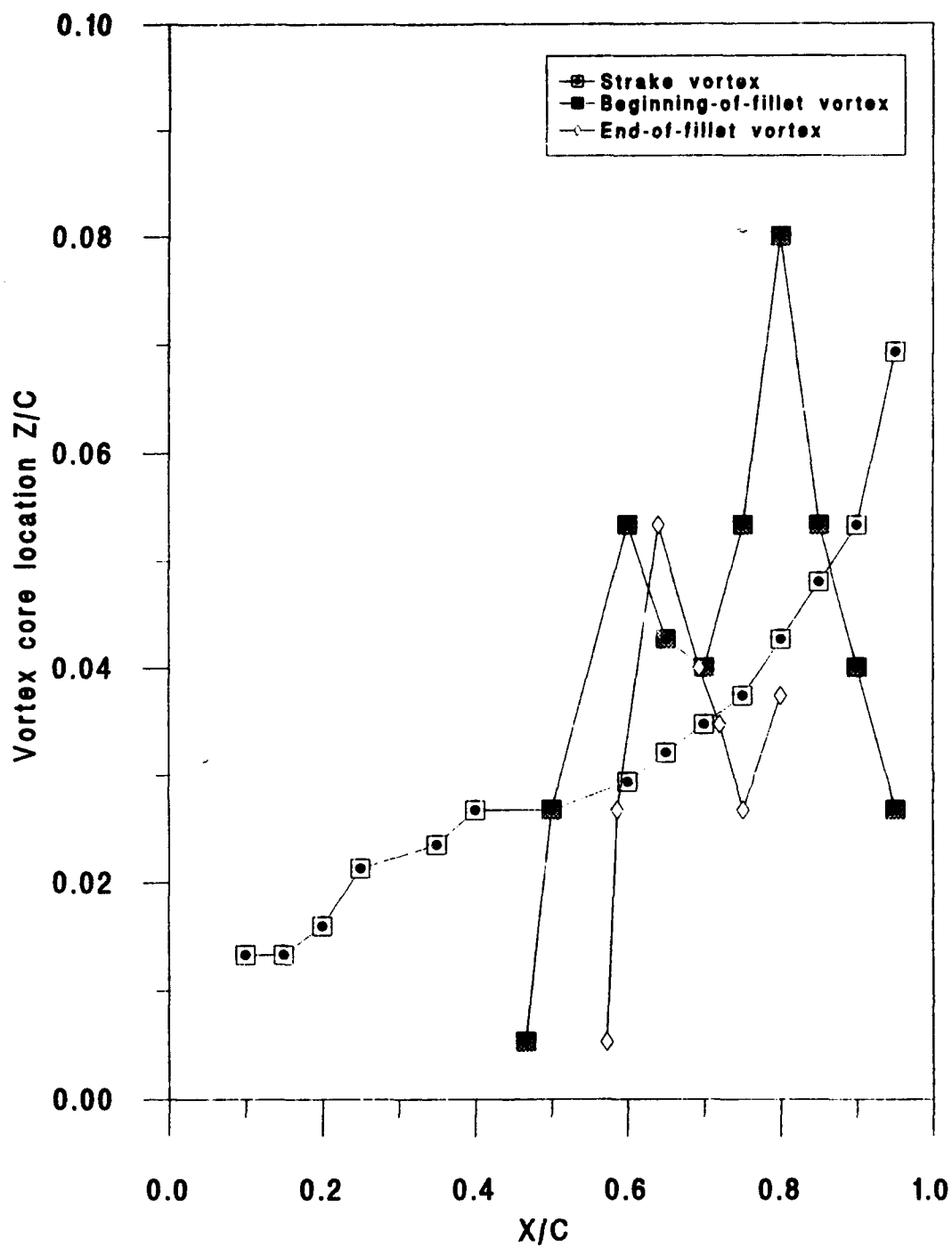


Fig. 125 Vortex core location Z/C for diamond-fillet model at $AOA = 10$ Deg.

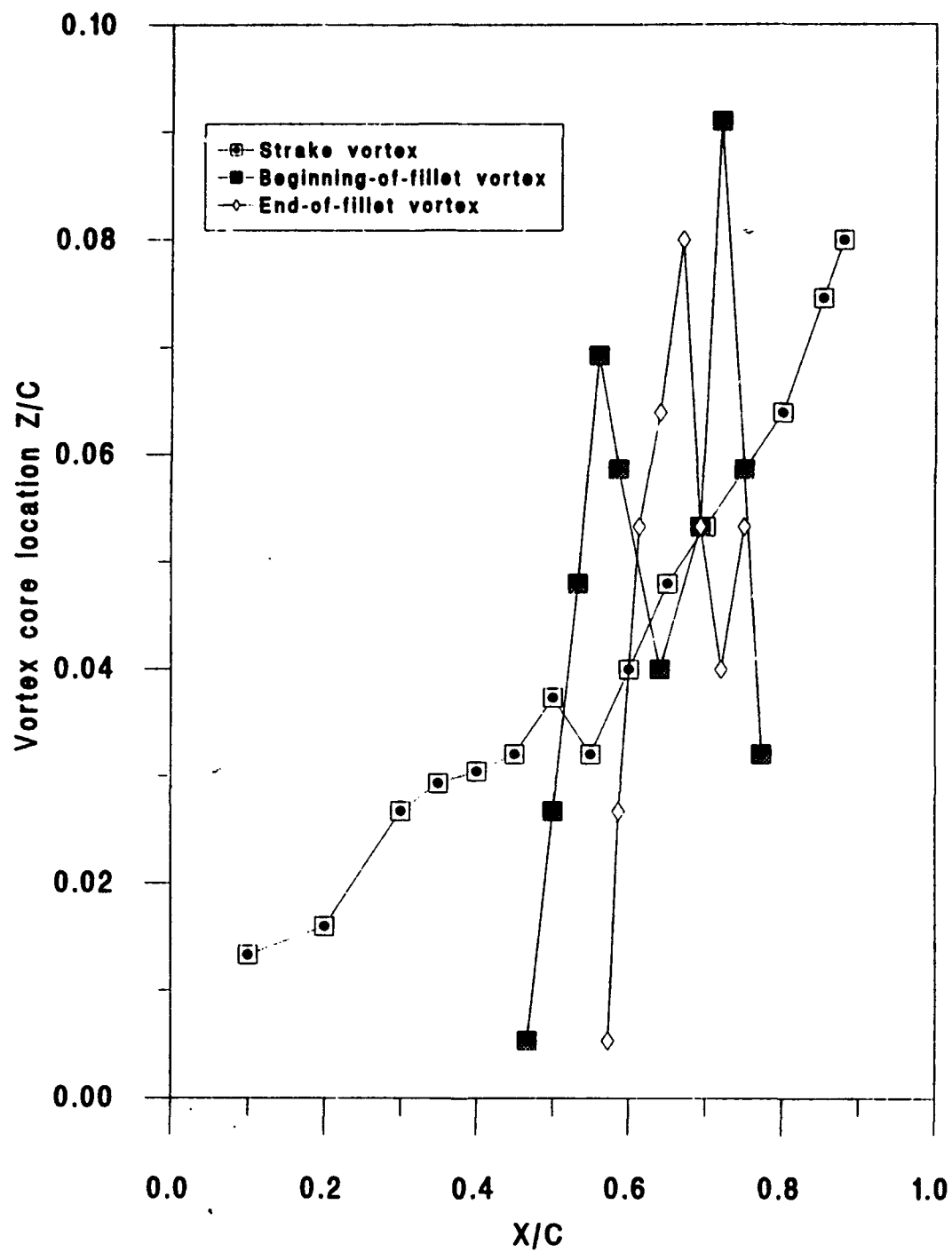


Fig. 126 Vortex core location Z/C for diamond-fillet model at $AOA = 16$ Deg.

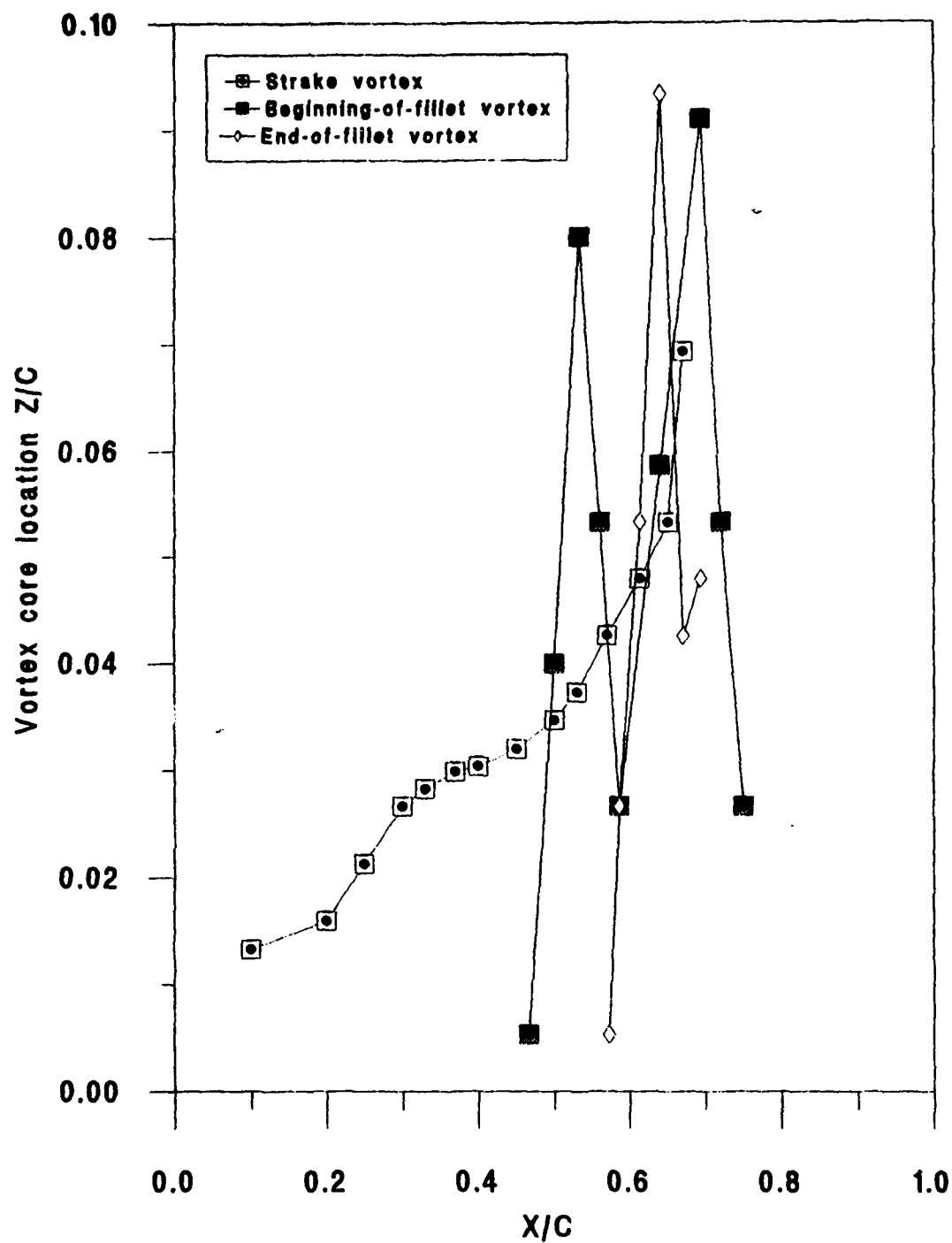


Fig. 127 Vortex core location Z/C for diamond-fillet model at $AOA = 20$ Deg.

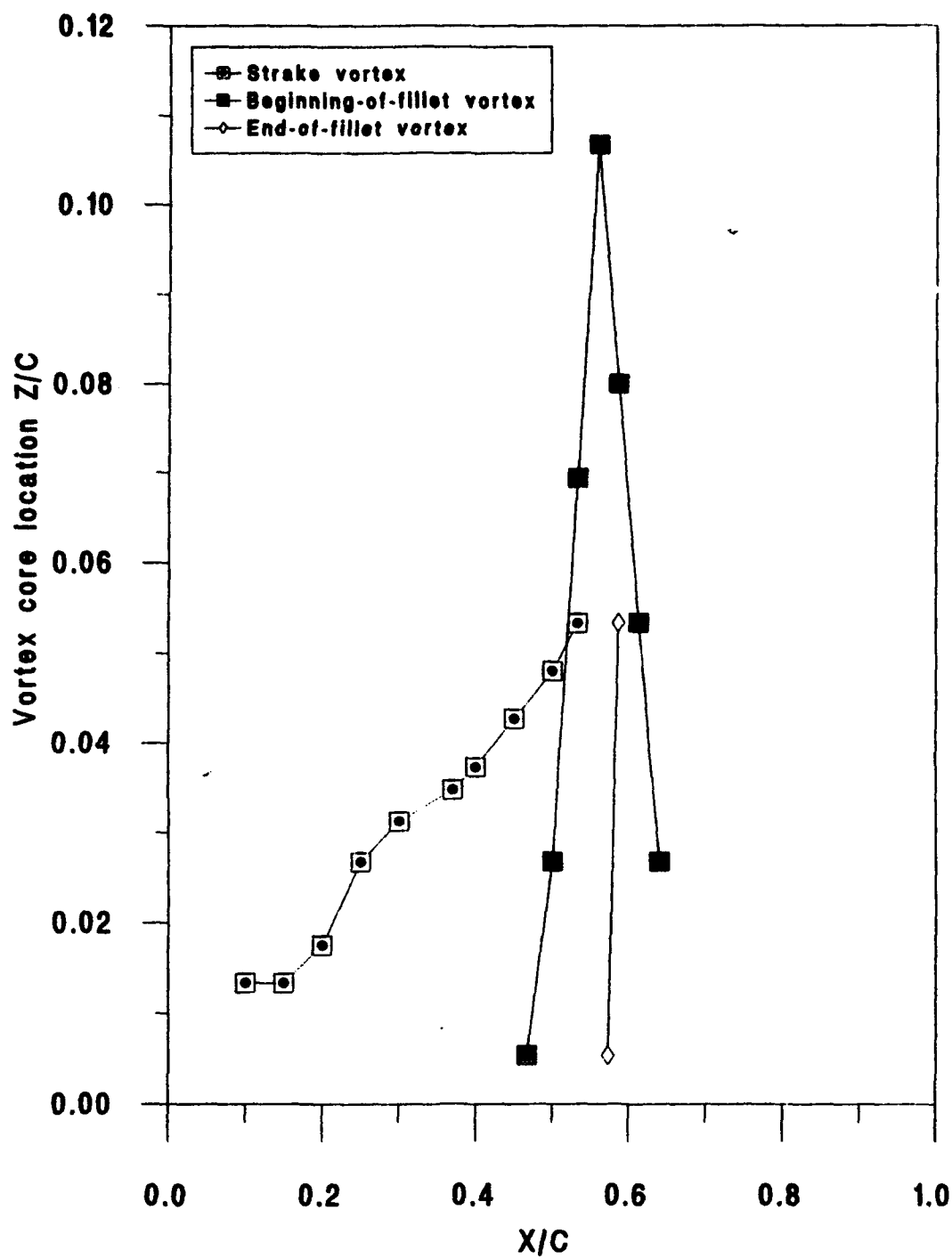


Fig. 128 Vortex core location Z/C for diamond-fillet model at $AOA = 22.5$ Deg.

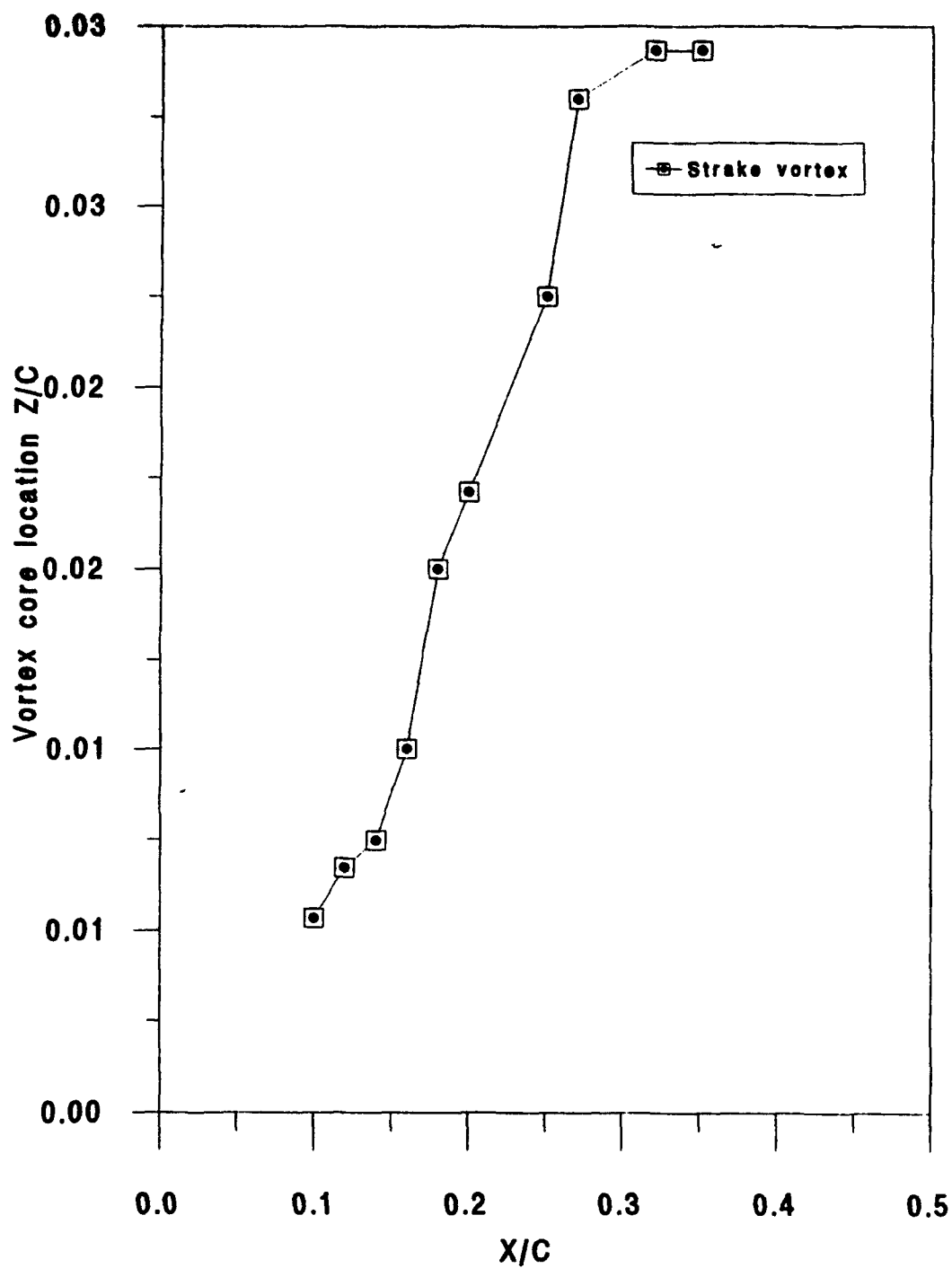


Fig. 129 Vortex core location Z/C for diamond-fillet model at AOA = 30 Deg.

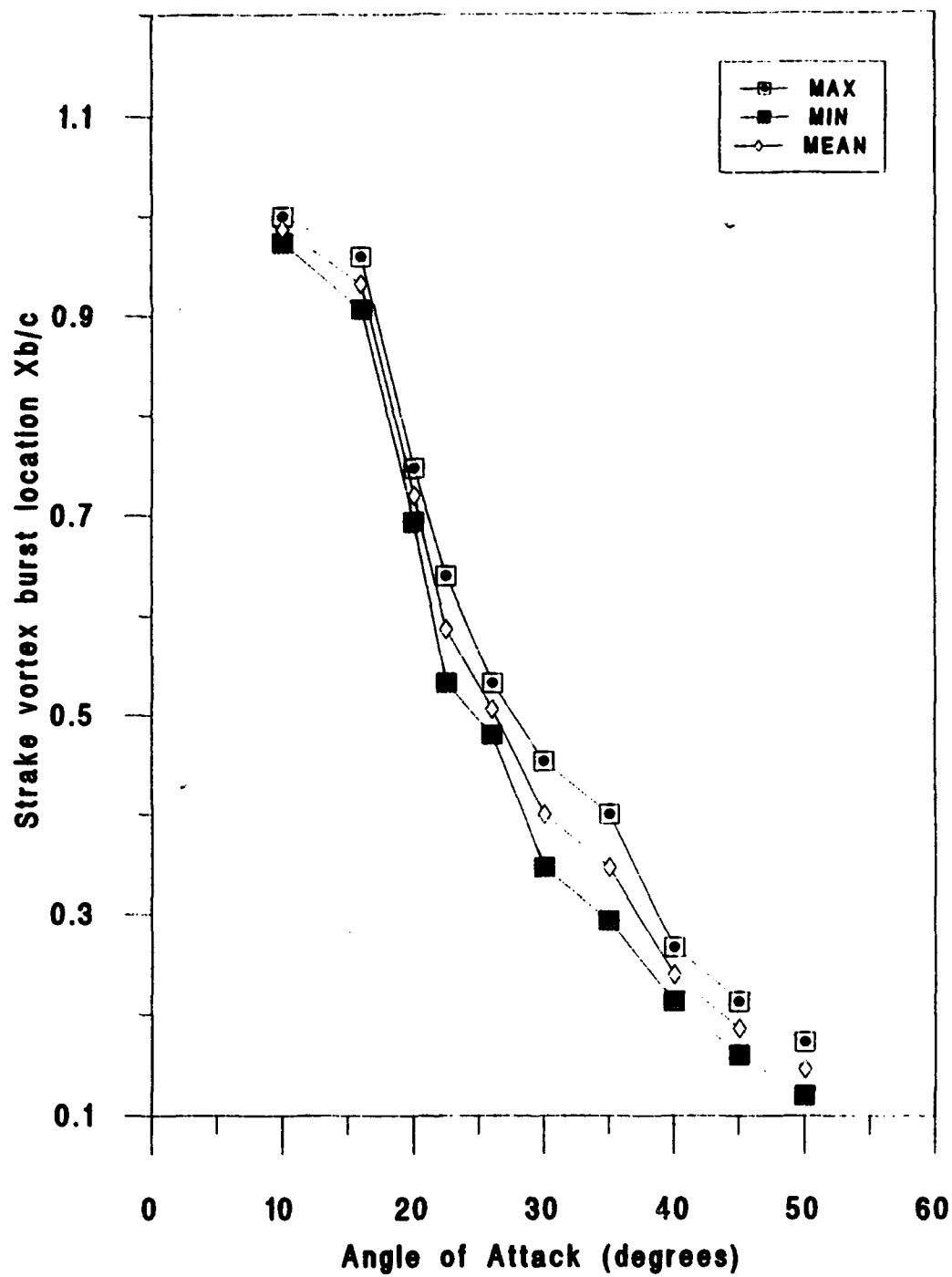


Fig. 130 Vortex burst location Xb/c (maximum, minimum & mean) for diamond-fillet model

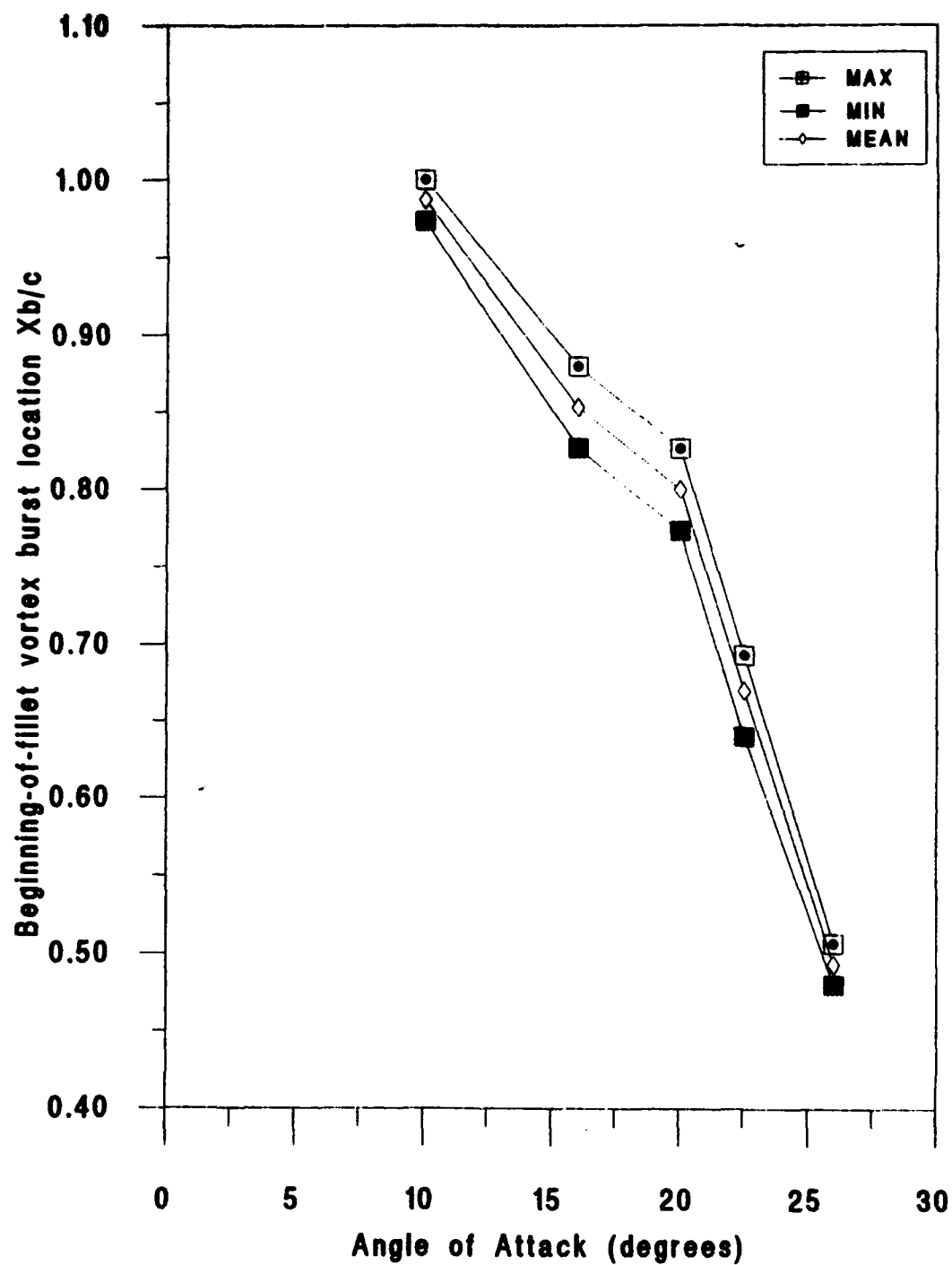


Fig. 131 Vortex burst location Xb/c (maximum, minimum & mean) for diamond-fillet model.

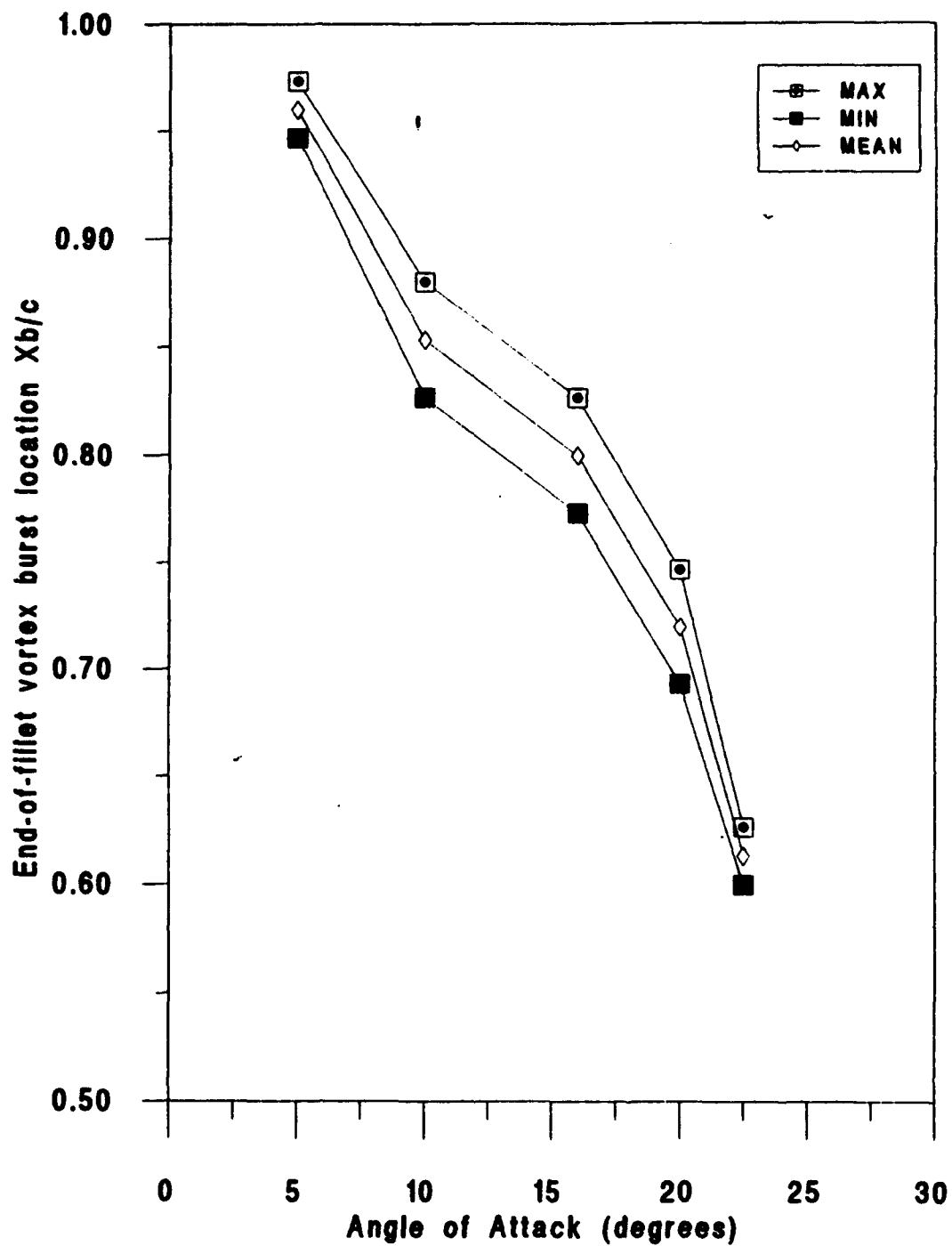


Fig. 132 Vortex burst location Xb/c (maximum, minimum & mean) for diamond-fillet model.

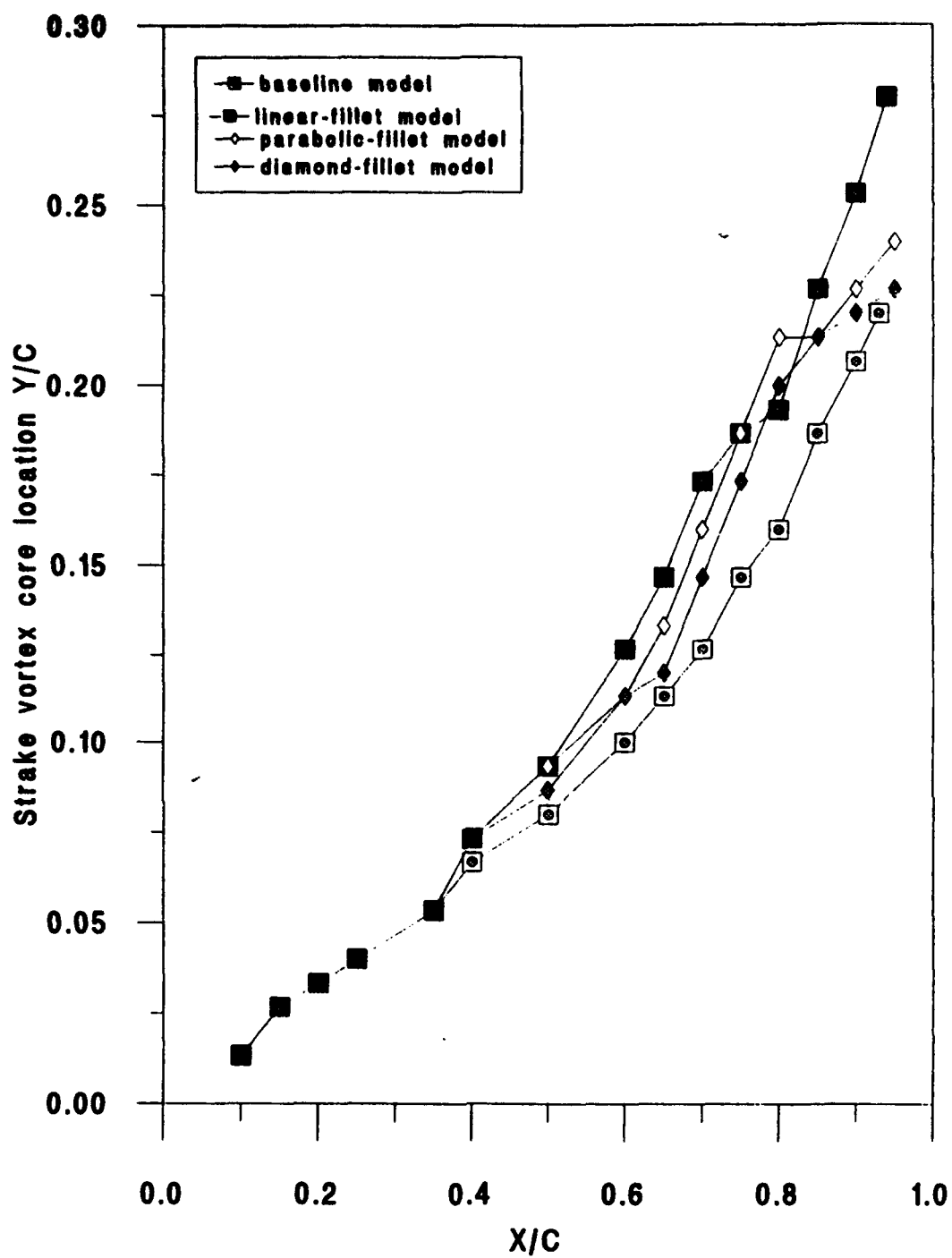


Fig. 133 Vortex core location Y/C for different models at AOA = 10 Deg.

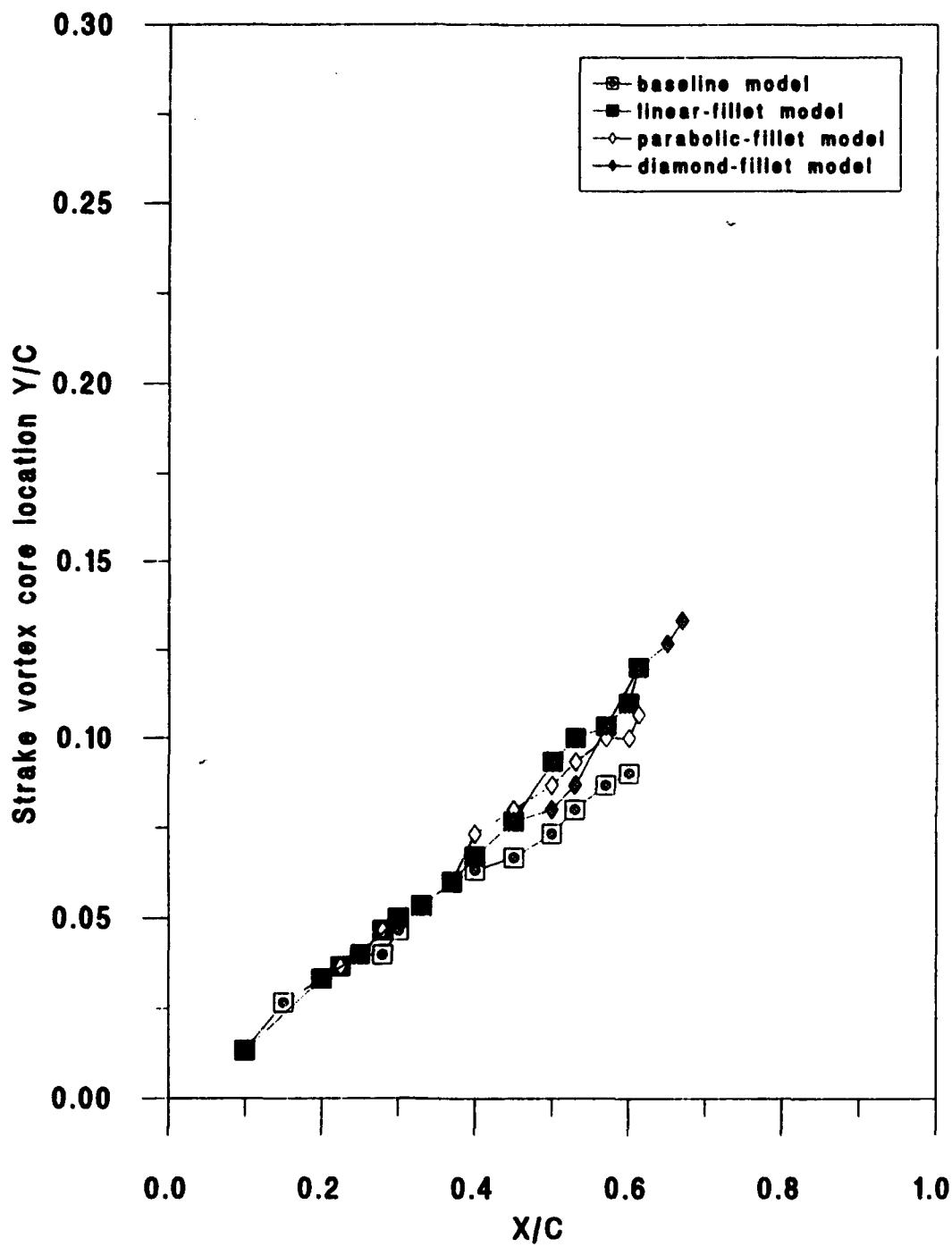


Fig. 134 Vortex core location Y/C for different models at AOA = 20 Deg.

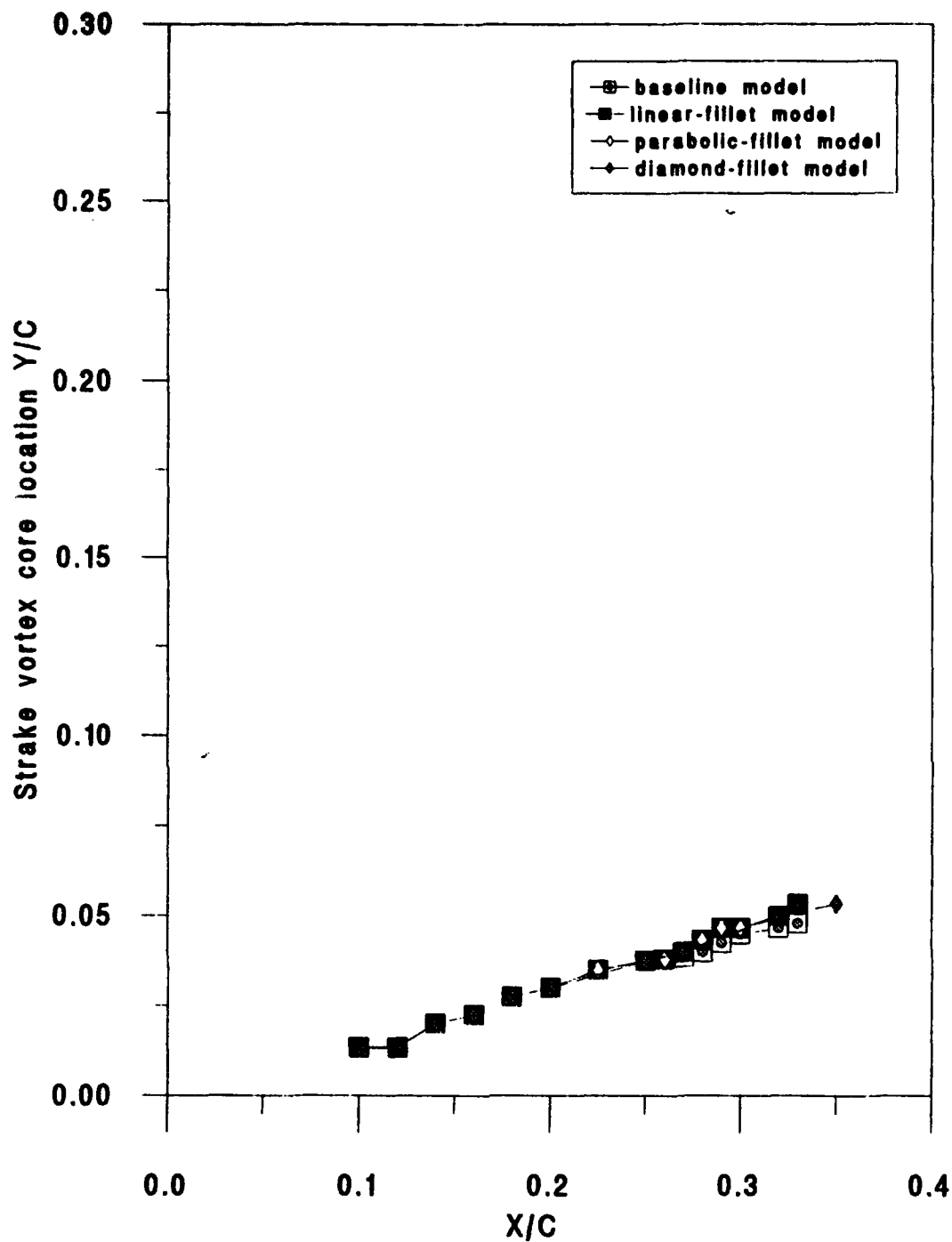


Fig. 135 Vortex core location Y/C for different models at $AOA = 30$ Deg.

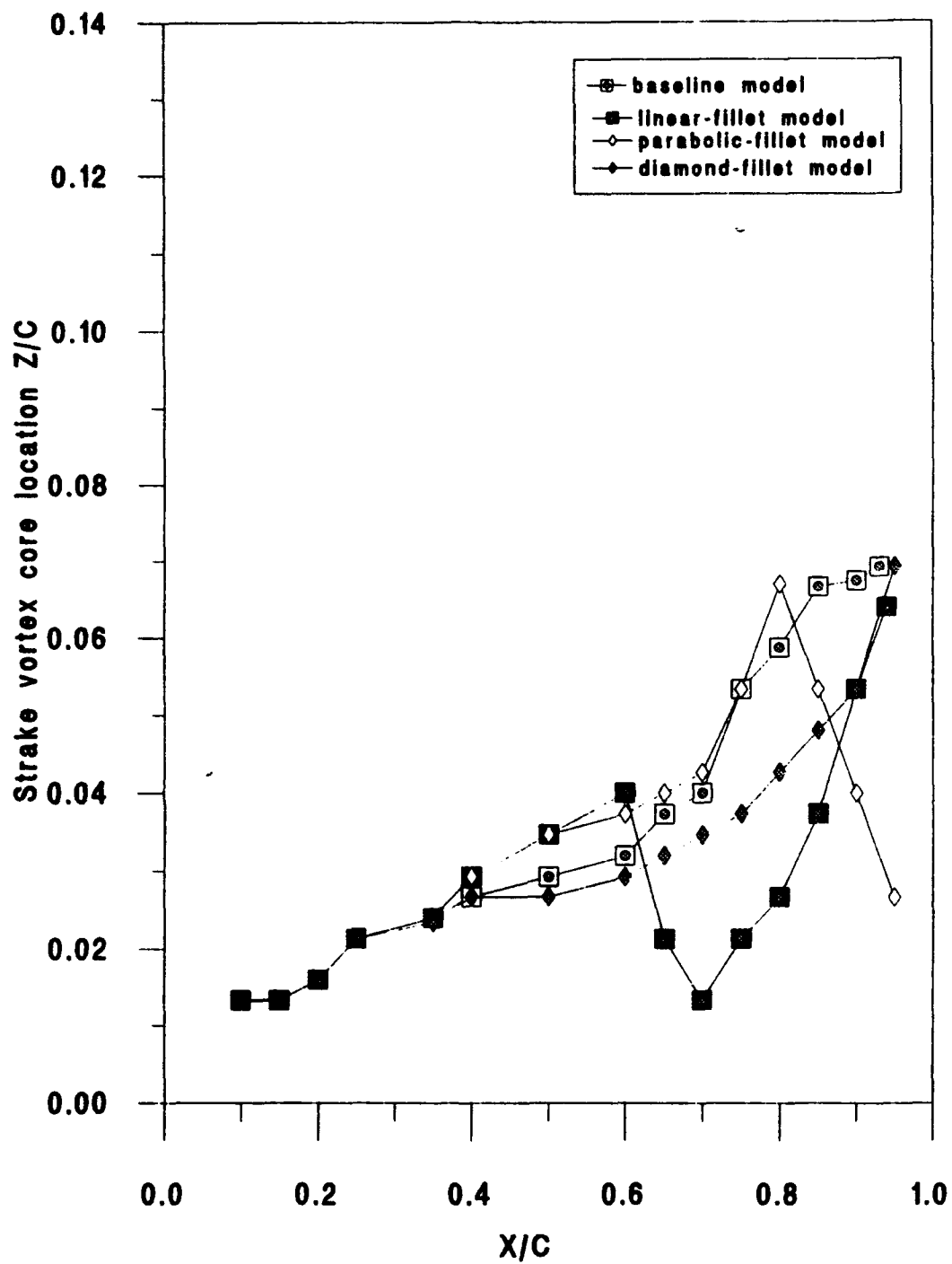


Fig. 136 Vortex core location Z/C for different models at $AOA = 10$ Deg.

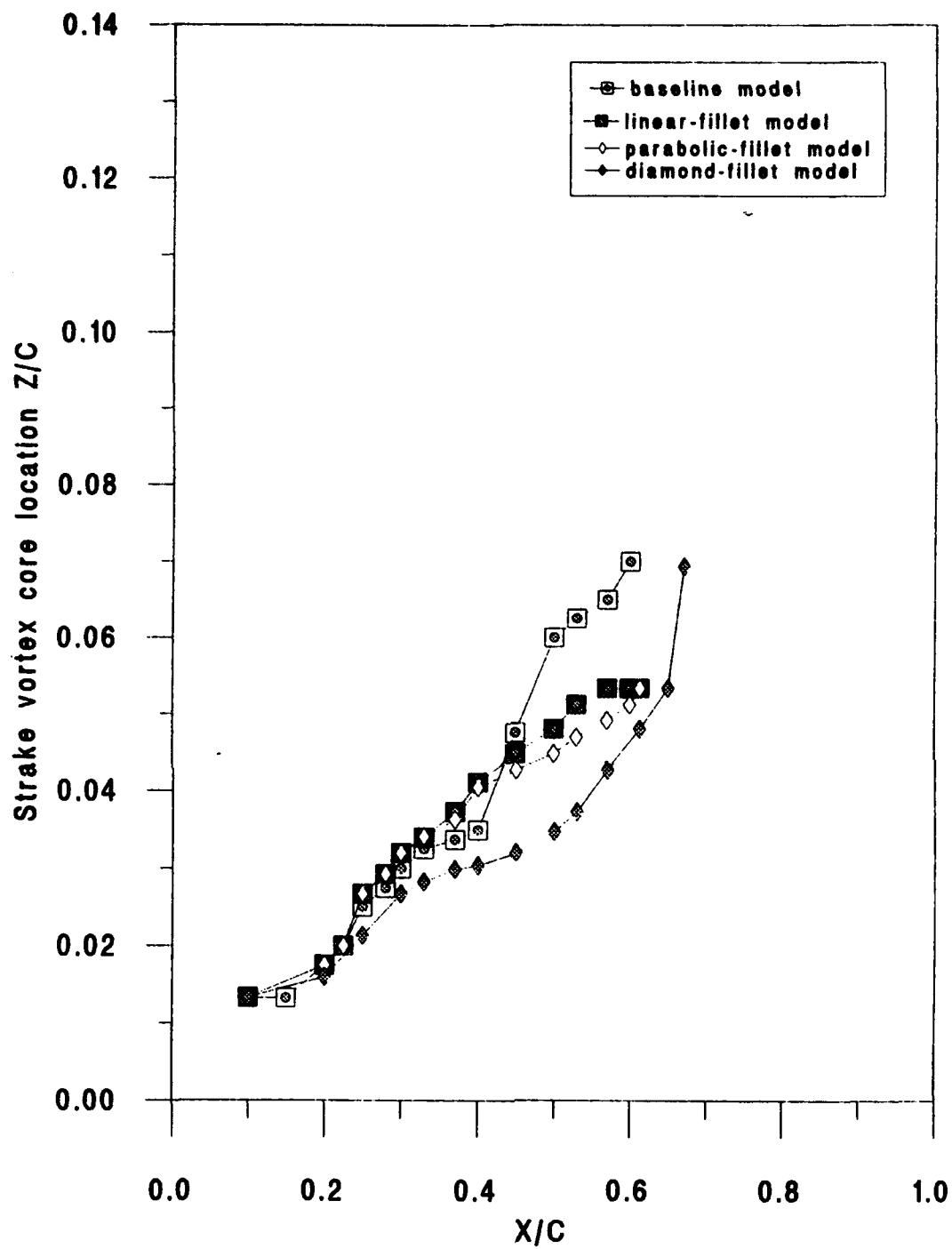


Fig. 137 Vortex core location Z/C for different models at $AOA = 20$ Deg.

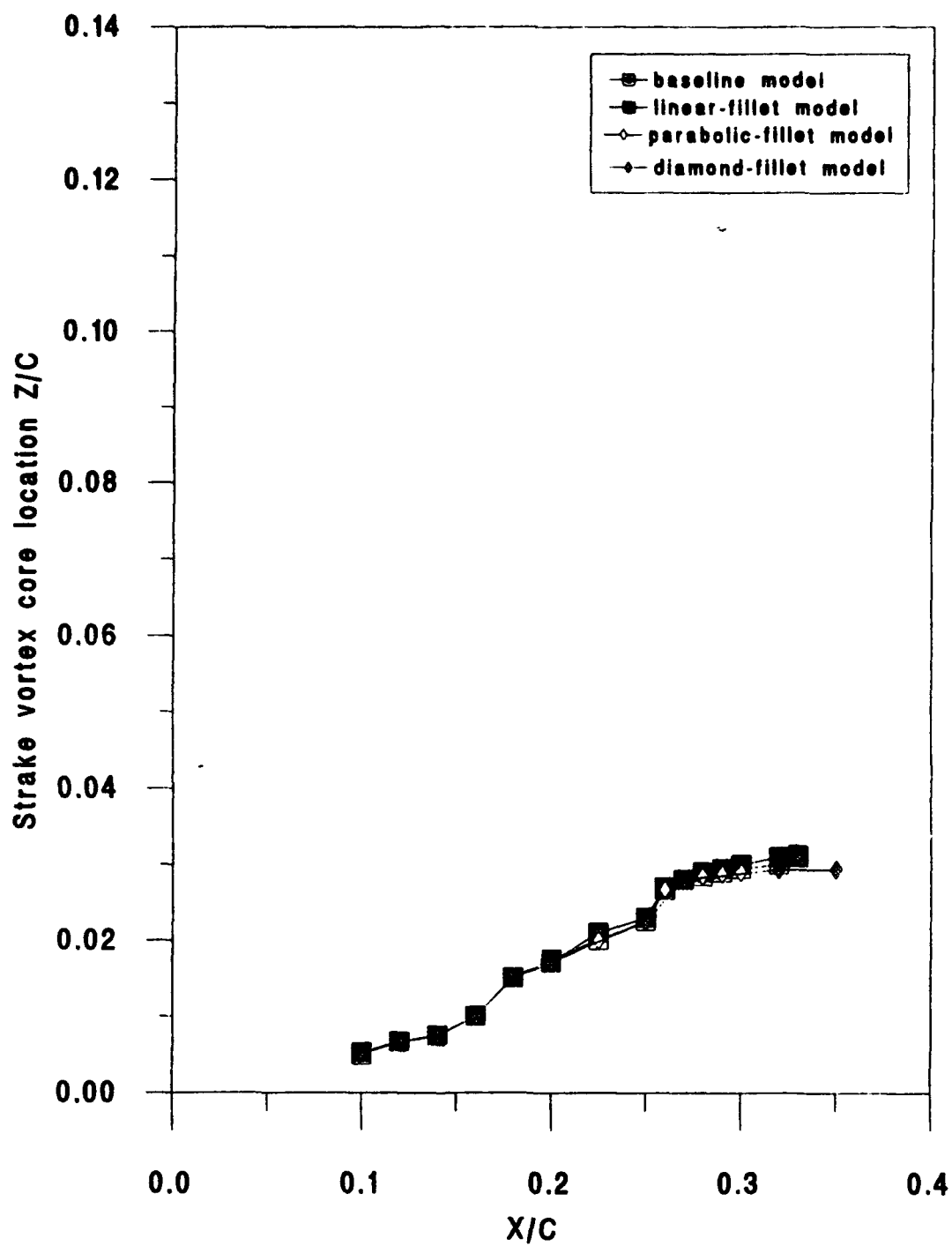


Fig. 138 Vortex core location Z/C for different models at AOA=30 Deg.

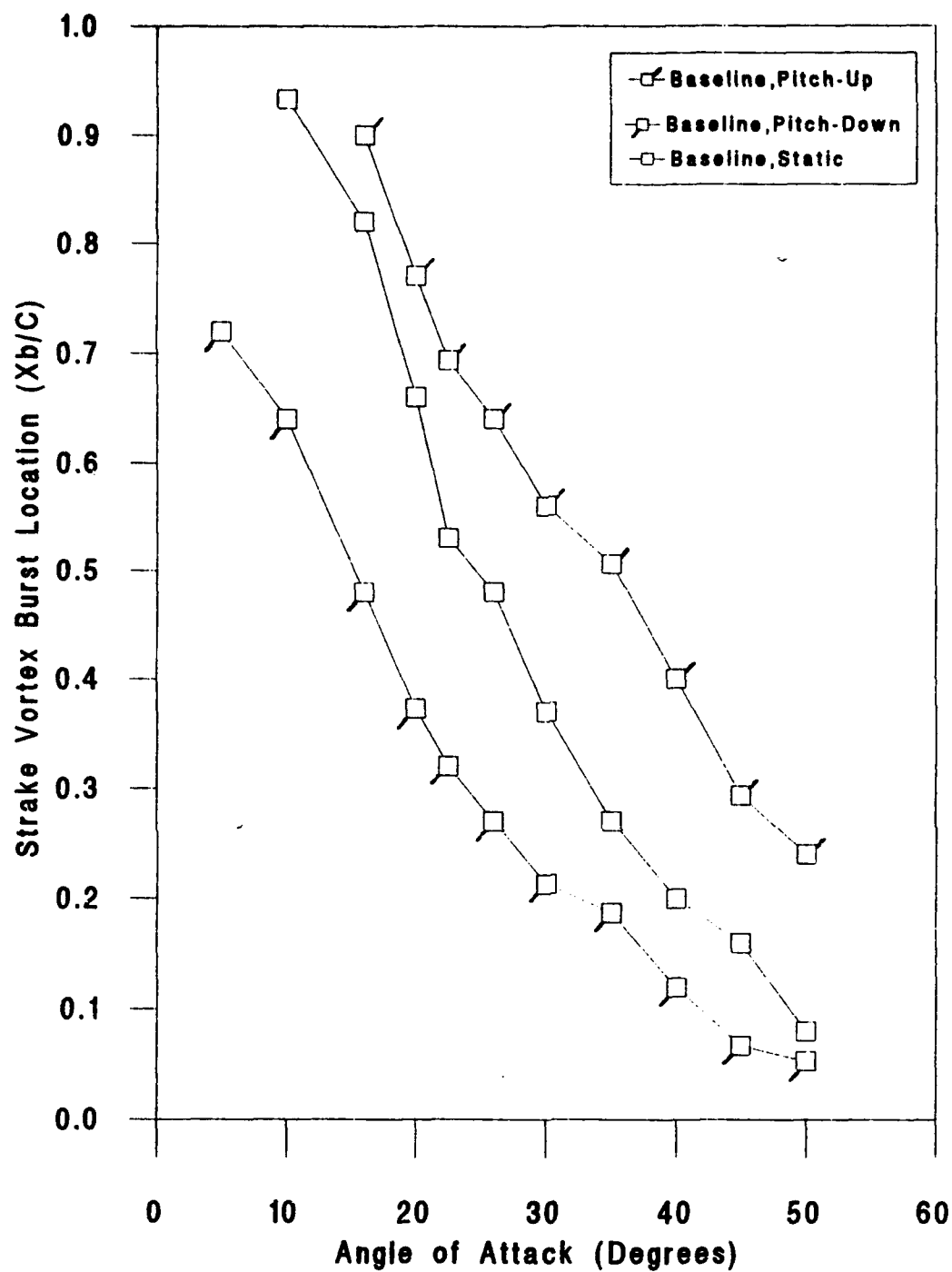


Fig. 139 Strake vortex burst location (Xb/c) for baseline model (static & dynamic cases)

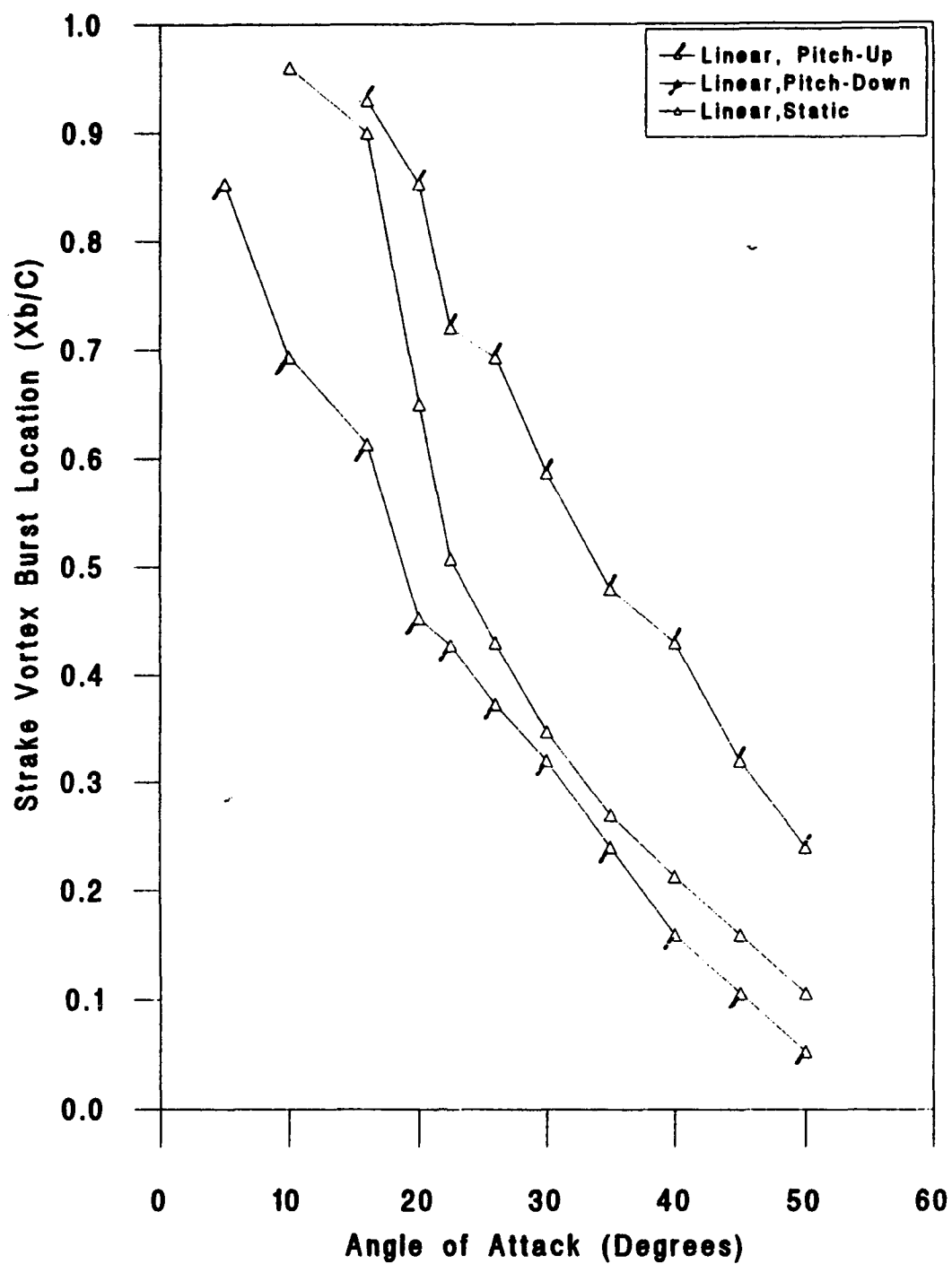


Fig. 140 Strake vortex burst location (Xb/c) for linear-fillet model (static & dynamic cases)

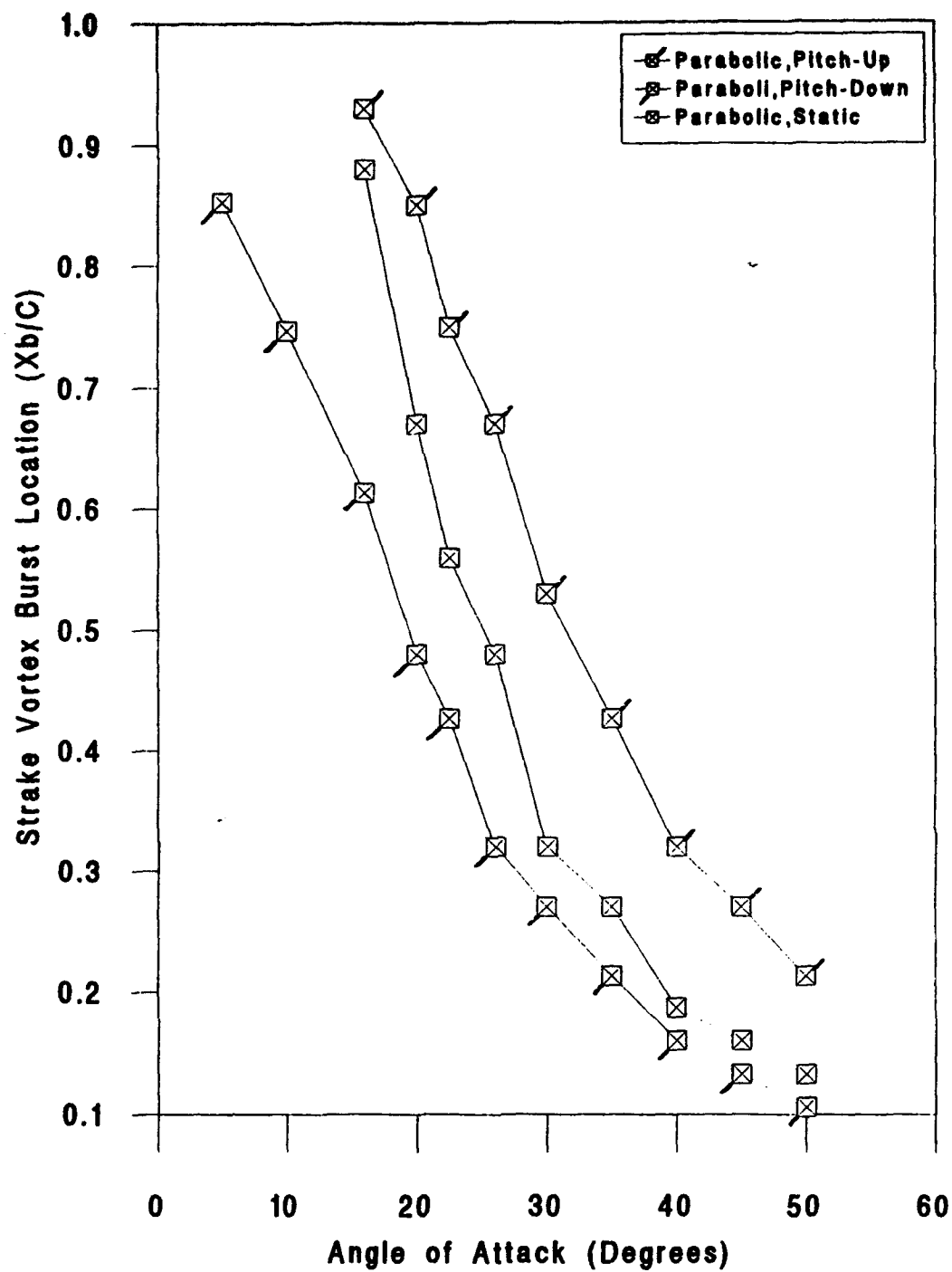


Fig. 141 Strake vortex burst location (Xb/c) for parabolic-fillet model (static & dynamic cases)

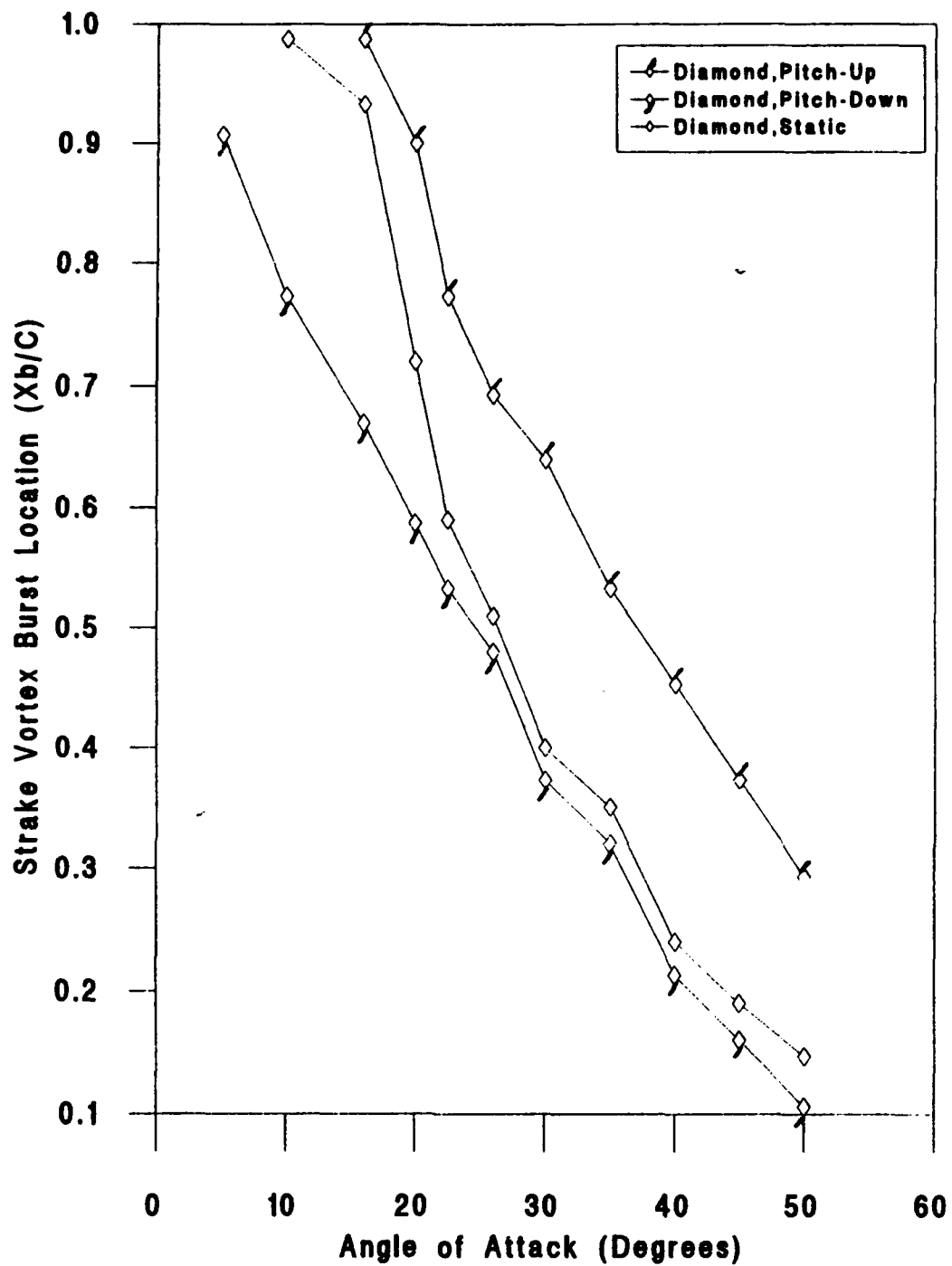


Fig. 142 Strake vortex burst location (X_b/c) for diamond-fillet model (static & dynamic cases)

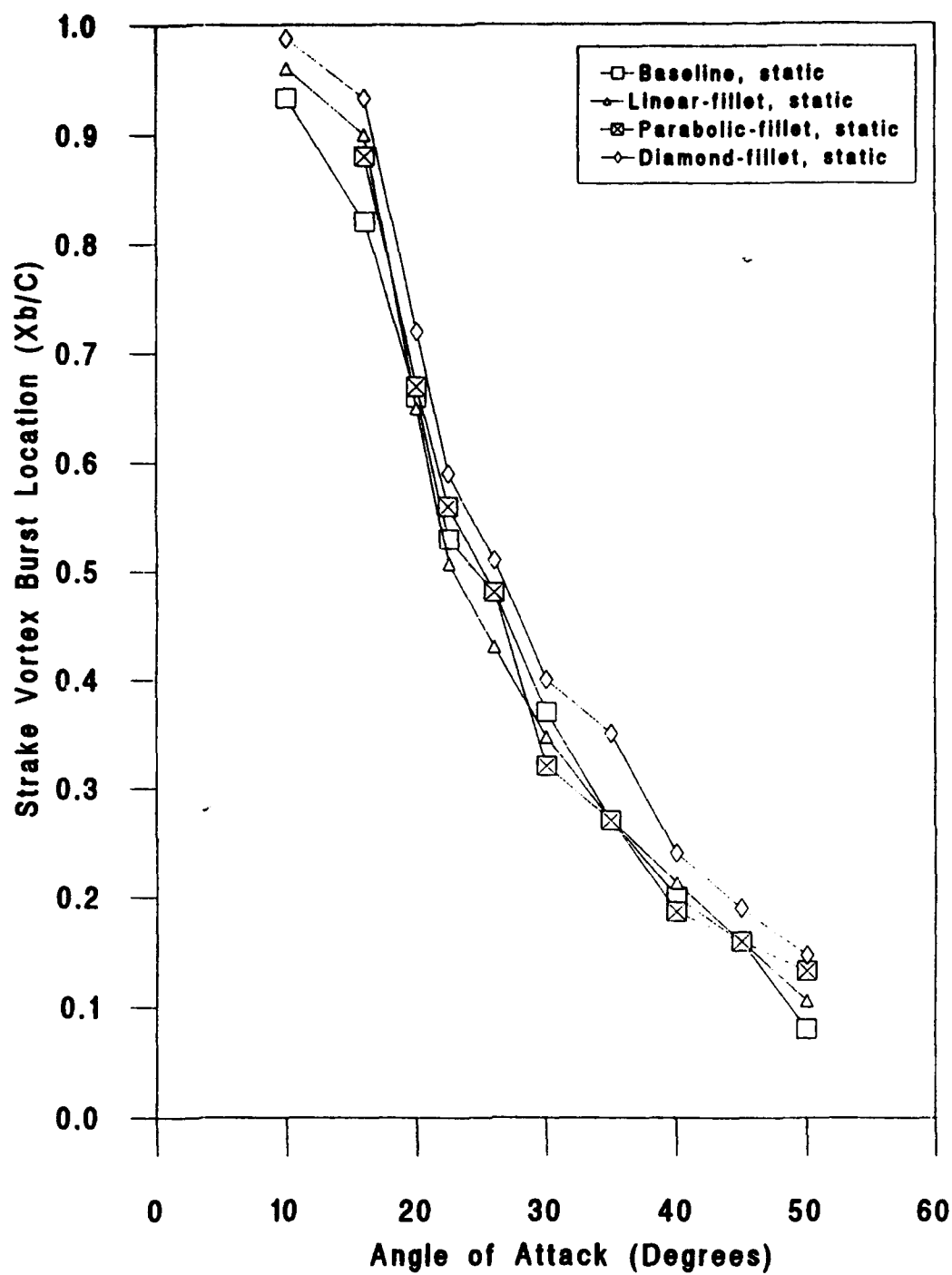


Fig. 143 Strake vortex burst location (Xb/c) for different models (static case)

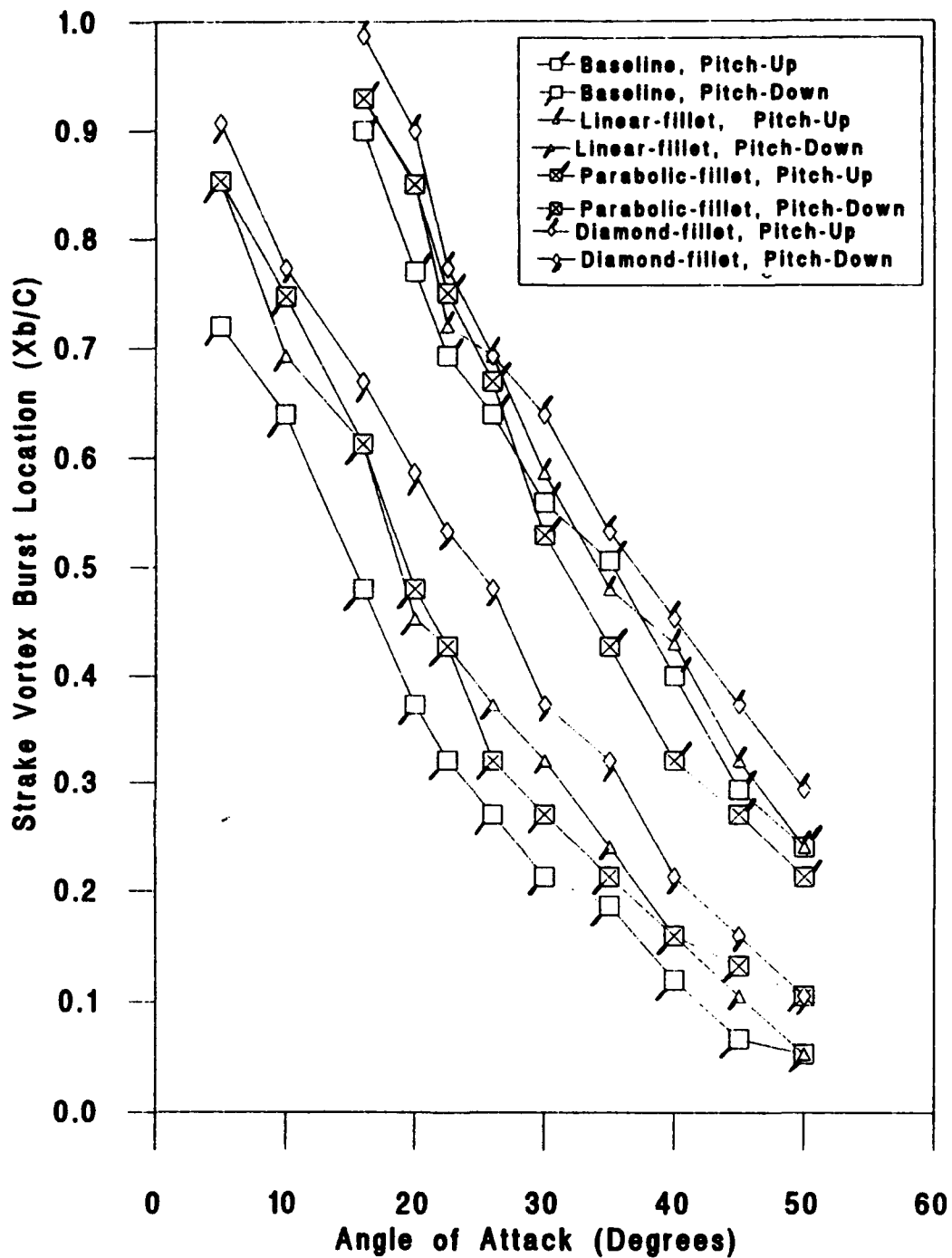


Fig. 144 Strake vortex burst location (X_b/c) for different models (dynamic case)

INTAIL DISTRIBUTION LIST

	No. Copies
1. Defense Technical Information Center Cameron Station Alexandria, VA 22304-6145	2
2. Library, Code 52 Naval Postgraduate School Monterey, CA 93943-5002	2
3. Chairman, Code AA/Co Naval Postgraduate School Monterey, CA 93943-5000	1
4. Professor S.K. Hebbbar, Code AA/Hb Naval Postgraduate School Monterey, CA 93943-5000	5
5. Professor M.F. Platzner, Code AA/P1 Naval Postgraduate School Monterey, CA 93943-5000	3
6. 1ST.LT. A. AL Khozam P.O. Box 1269 Fintas 51013 KUWAIT	2
7. KUWAIT Millitary Attache Office 3500 International Drive, N.W. WASHINGTON, D.C. 20008	2
8. Mr. Marvin Walters Naval Air Warfare Center/Aircraft Division Street Road, Warminster, PA 18974-5000	1
9. Michael J. Harris Aircraft Division Code AIR-931 Naval Air System Command WASHINGTON, D.C., 20361-9320	1
10. Dr. L. B. Schiff Applied Computational Fluids Branch NASA Ames Research Center (M.S. 258-1) Moffet Field, CA 94035	1